University of Venda
Creating Future Leaders

University of Venda

HYDROTHERMAL SYNTHESIS OF CLAY-BASED ADSORBENTS AND THEIR APPLICATION TO FLUORIDE AND PATHOGEN REMOVAL FROM GROUNDWATER

A research thesis submitted to the University of Venda, School of Environmental Sciences, Department of Ecology and Resource Management in fulfilment of the degree of Doctor of Philosophy in Environmental Sciences

By

OBIJOLE Olumuyiwa Adewale

Student number: 16008973

Promoter: PROF W. M. GITARI (University of Venda)

Co-Promoter: PROF P. G. NDUNGU (University of Johannesburg)

February 2021

© University of Venda

DECLARATION

I, OBIJOLE Olumuyiwa Adewale, student number 16008973, hereby declare that this research work titled "**Hydrothermal synthesis of clay-based adsorbents and their application to fluoride and pathogen removal from groundwater"** is my own work and has not been previously in whole or in part submitted to any university for any degree. Moreover, I swear that this is my own work in design and execution and as thus, all reference materials and resources have been duly acknowledged.

Student's Signature: 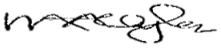 Date: 15th January 2021

© University of Venda

University of Venda
Creating Future Leaders

ACKNOWLEDGEMENT

I wish to express my deep and sincere gratitude to the Almighty GOD for His grace, strength, sound health, wisdom and journey mercies bestowed upon me and my entire family, most especially during the course of studies in South Africa. I give him praise and adoration.

My profound appreciation goes to my promoter and supervisor, **Professor Wilson Mugera Gitari** for thorough and thought provoking comments, financial assistance, and encouragement from time to time and his conceptualization and immense contribution to the success of this research work at the University of Venda despite his busy schedule and travels within and outside South Africa. To my co-promoter, **Professor Patrick Ndungu** of the University of Johannesburg, you are much appreciated for the opportunity. To Dr Rabelani Mudzielwana, thanks so much for painstakingly reading through and correcting the thesis write-up to bring it up to this level.

I am grateful to the Department of Ecology and Resources Management (ERM) and the HoD, Dr Stam. I acknowledge the financial support from NRF, University of Venda Research and Project Committee (RPC) and Professor Gitari's DHET research incentives as well as Miranda Waldron of the University of Cape Town, Remy Bucher of iTemba laboratory, Riana Rossou of Stellenbosch University for their assistance in sample analysis. To all my contemporary postgraduate fellows in Environmental Remediation and Nano Science (EnviReN) research group (Dr Mudzielwana, Dr Ayinde, Oisaemi, Kuziva, Rendani, Rhanzhu, Aluwani, Shumba, Llyod, Humbe, Nsovo, Elisa, Lusani and my mentee, Nkana). I thank you all for every moment shared together in the laboratory, workshops, conferences and leisure times.

Calvary greetings and appreciation to the pastorate, ministers, workers and members of the Redeemed Christain Church of God (RCCG) Sibasa and Siyandinma parishes for their prayers and commitments to the propagation of the gospel in Vendaland, South Africa. To my Daddy and Mummy in the Lord, Pastor and Pastor Mummy R. A Ayoade (PICP, Lagos province 50) for your regular checks, counsels and prayers, I say thank you, more anointing and strength for the work of the ministry of our savior and Lord, JESUS CHRIST.

I should not fail to mention the immediate past Provost, Prof Olukoya Ogen and the current Provost, Dr S. A Akintunde, Adeyemi College of Education (ACE), Ondo, Nigeria, for the opportunity given to me to undergo this study outside Nigeria, Dr Adepoju (School of Education, ACE) for his efforts, support and concerns as well as my colleagues in the department of chemistry,

© University of Venda

Adeyemi College of Education ondo, Nigeria for every little thing. To Dr J. O. Babajide and Dr Mrs Omotola Babajide, you are both appreciated.

My gratitude goes to my parents, **Papa Micheal Oluwafusibi Obijole and Mama Magaret Abiodun Obijole** for their unflinching love, encouragement and prayers. My elder sister, Mrs Olufunmilayo Giwa, her husband, Mr M.A Giwa and their children as well as my in-laws, Uncle Fem Osinaike and Mrs Omolara Oduwaiye, Elijah, Blessing, Deborah and Samuel are also appreciated for always being there for me.

Lastly, my heartfelt gratitude goes to my wife and love, **A/P Bernice Oluremi Obijole** for earnestly standing in the place of prayers, unflinching concerns about my progress and holding forth our home while I was far away in the Republic of South Africa. To our lovely children: **Emmanuel, Favour, Glory and Godswill,** I say a BIG thank you for your agape love, prayers every morning, cooperation and always being there for me. You are all wonderfully and awesomely blessed.

© University of Venda

DEDICATION

This thesis is dedicated to the Almighty GOD who has wisdom and perfect understanding, my amiable wife and the children whose patience during my studies abroad were unequalled.

© University of Venda

University of Venda
Creating Future Leaders

ABSTRACT

Groundwater is the main source of drinking water for majority of rural communities worldwide. This essential resource is often contaminated leading to various medical complications in man. Some groundwater have been found to have high fluoride levels beyond the recommended World Health Organization (WHO) limits of 1.5 mg/L and pathogens leading to fluorosis and waterborne diseases. Over 200 million people are at risk of contracting fluorosis in about 26 countries while waterborne diseases accounts for over 2.2 million deaths annually with most of these occurring in South America, Asia and Africa. Water remediation technologies using different materials have been developed yielding various degree of successes. The quest for fluoride and pathogen free groundwater prompted this work.

First section of this work focused on mechanochemical activation of aluminosilicate clay soils and evaluation in fluoride and pathogen removal. The clays' characterisation was conducted using cation exchange capacity (CEC), Brunauer-Emmett-Teller (BET), scanning electron microscopy-electron dispersion spectroscopy (SEM-EDS), X-ray diffraction (XRD), Fourier transform infra-red (FTIR) and X-ray fluorescence (XRF) techniques. Batch fluoride adsorption studies were conducted, and the antibacterial studies were done using the well diffusion assay method. Mechanochemical activation of the clay samples was conducted. The optimum milling time was obtained by evaluation of the activated clays for fluoride removal at a specific pH using batch mode. The clay soil was rich in aluminosilicate, moderate in cation exchange capacity and mesoporous. The sample with highest percent fluoride removal indicated the optimum contact time for the treatment. The surface area of clay increased with increase in activation time. The mechanochemically activated clay (MAC) showed a maximum adsorption capacity of 1.87 mg/g and 32% fluoride removal, from an initial fluoride concentration of 10 mg/L using 2 g/100 mL dosage, 60 min contact time at, 250 rpm shaking speed and 298 K. Adsorption data fitted well to Freundlich isotherms, hence confirming heterogeneous multilayer adsorption when linearised model was used but fitted well to both Langmuir and Freundlich when non-linear model were employed, thereby confirming both monolayer and multilayer adsorption. Kinetics studies revealed fluoride adsorption fitted well to pseudo-second-order model, indicating the dominance of chemisorption mechanism when linear modelling was used but fitted well to both pseudo-first-order and pseudo-second-order model when non-linear modelling were used, thus indicating

© University of Venda

adsorption mechanisms to be both physiosorption and chemosorption respectively. The sorption of fluoride ions onto the clays' surface followed intra-particle diffusion mode. The clay adsorbent was successfully regenerated for up to five regeneration-reuse cycles. The antibacterial studies revealed no zone of inhibition for all the activated clays, hence, indicating that they are not active against the bacterial strains of *Escherichia coli* (*E. coli)*. Therefore, MAC showed promising adsorptive capabilities but no antibacterial properties, hence, the material cannot be used to remove pathogens from water.

The second section of this work focused on optimisation of synthesis conditions for hydrothermal treatment of the MAC and physicochemical charcterisations. Optimisation of synthesis conditions for hydrothermal treatment of MAC was conducted by varying NaOH concentration and contact time for clay dissolution and followed by concurrent variation of hydrothermal temperature and contact time for the clays' modification. The solid products obtained were characterised using FTIR, BET, SEM-EDS, and XRD. The optimum conditions for Si and Al dissolution occurred at 1.5 M NaOH and 2 h at 298 K while optimum conditions for synthesis were found to be 2 h ageing time, 140 °C hydrothermal temperature, 48 h treatment time and 9 mL of water. The SEM analysis showed changes from external micro rough irregular morphology in MAC to smooth irregular aggregates of gel-like microsphere particles in the HTAC products as conditions were varied. XRD results revealed appearance of several new mineral phases. The optimally synthesised product showed fine crystalline microspheres' gel-like particles having microspheric and spheroidal "cotton ball" morphology with sharp peaks around 2θ = 15, 25, 32 and 35 with new mineral phases corresponding to hydroxy sodalite as confirmed by SEM and XRD respectively. XRD pattern which represents quartz, montmorinollite and mullite in MAC gave way to sharp peaks corresponding to new mineral phases corresponding to hydroxy sodalite in the HTAC products. BET surface area also increases from 17 m^2/g in MAC to 33.56 m^2/g in the products as hydrothermal conditions were varied. However, optimised product with surface area value of 33.56 m^2/g was observed to have the highest percent fluoride removal. The pore distribution of all the products was still within mesoporous range while no significant change was observed in pore volumes and sizes in the products. Five best modified products identified from defluoridation and characterised were HTAC-5, HTAC-6, HTAC-7, HTAC-8 and HTAC-12. Preliminary fluoride removal experiments showed that sample HTAC-8 prepared under optimum

© University of Venda

conditions of 48 h ageing time, 140 °C had highest fluoride adsorption capacity and hence, selected for application in subsequent experiments in the preceeding chapter five.

The third section of this work focused on the application of the synthesised hydrothermally-treated aluminosilicate clay (HTAC) obtained in chapter four for application in fluoride and pathogen removal. Characterisation was carried out using FTIR, BET, XRD SEM-EDS and XRF. Batch adsorption studies were conducted. Antibacterial studies employed the well diffusion assay method. The BET surface area of HTAC was 33.56 mg^2/g while no significant change was observed in pore sizes and volumes. Batch studies showed maximum adsorption capacity of 1.75 mg/g with 53% fluoride removal from initial fluoride concentration of 6.0 mg/L using 0.8 g/40 mL dosage at initial pH 5.8, 5 min contact time and 298 K. The adsorption kinetics data fitted best to pseudo-second order model, while the adsorption data were best described by Freundlich adsorption model. The regeneration and recyclability potential studies with 0.1 M KCl as regenerant showed it can be used for up to six times. Antibacterial activities result of the optimised HTAC towards Escherichia coli (*E. coli*) strains indicated some potency. The outcome of this study showed that the synthesised HTAC has strong potential for application in groundwater defluoridation and pathogen removal.

The fourth section of this work focused on modification of the surface properties of the HTAC in section three by hydrothermal treatment of MAC in the presence of a pore forming agent ($NaClO_3$) (product designated as PHTAC). Operational parameters were optimised for synthesis of porous-hydrothermally-treated aluminosilicate clay (PHTAC) from MAC. They were all characterised using BET, FT-IR, SEM-EDS and XRD. Preliminary adsorption experiments were conducted on all the products with a view to obtain the six best modified PHTAC materials. The results showed operational parameters such as pore former ($NaClO_3$), contact time and temperature were critical in the synthesis and impacted positively on the PHTACs performance. The six best optimised products with highest percent fluoride removal were selected. XRD and SEM analysis showed the optimised product to have new mineral phases corresponding to hydroxyl sodalite with sharp peak intensities around at 2-degree θ = 15, 25, 32 and 35 with fine crystalline piston rod-like particles interlaced with pores. BET results showed increasing surface area for the products from 33 m^2/g to 52.56 m^2/g in optimised PHTAC product. The pore-forming agent ($NaClO_3$) introduced during the hydrothermal treatment increased the surface area, which impacted positively on PHTACs' performance. The best optimised PHTAC-18 was obtained at 6 h treatment

© University of Venda

time with 1.0 g/100 mL adsorbent dosage and 0.20 g/100 mL pore formers in 9 mL water at 300 °C hydrothermal temperature and had the highest fluoride removal of 63% and adsorption capacity of 3.45 mg/g, and was therefore selected for use in batch defluoridation experiments and pathogen removal from groundwater, presented in chapter seven.

The fifth section of this work focused on the application of the optimally synthesised porous-hydrothermally-treated aluminosilicate clay (PHTAC) obtained in section four for fluoride and pathogen removal. The optimised PHTAC was characterised by BET, FT-IR, SEM-EDS, XRD and XRF. Batch adsorption experiments were conducted on the optimised PHTAC and regeneration potential was investigated. Antibacterial studies were conducted using well assay diffusion method and modified liquid culture technique & UV-visible spectrophotometry. Batch defluoridation studies of optimised PHTAC showed maximum adsorption capacity of 3.45 mg/g with 68% fluoride removal at 10 min contact time, 1.0 g dosage/100 mL, 4.0 mg/L initial fluoride concentration, pH ≈ 4.0, 250 rpm at 298 K. The adsorption capacity increased from 1.87 mg/g in MAC to 3.45 mg/g in PHTAC. The fluoride sorption fitted well to both Langmuir and Freundlich models, hence confirming both monogeneous unilayer and heterogeneous multilayer adsorption. The adsorption kinetics data also showed a good fit to both pseudo-first-order and pseudo-second-order models suggesting fluoride sorption proceeded via physiosorption and chemisorption pathways respectively. The synthesised PHTAC could be regenerated for up to eight times when compared to MAC and HTAC. The minimum inhibition zone observed for the bacterial strains was about 15 mm. The percent growth inhibition of the bacterial cell was 89 which is very close to 90 - 95% obtained in most government water treatment plants. The efficiency of PHTAC when further tested in field groundwater containing 2.84 mg/L initial fluoride concentration using 0.9 g/ 100 L adsorbent dosage at 10 min contact time showed its capability to reduce fluoride from initial concentration of 2.84 mg/L to 1.35 mg/L, which is within the permissible WHO limits (1.5 mg/L). In conclusion, the adsorption capacity and antibacterial potency of the PHTAC for fluoride and pathogen removal from groundwater improved. It is recommended that its surface be further modified sonochemically and loaded with suitable antibacterial metal oxides to further enhance its defluoridation and antibacterial potency.

Keywords: Aluminosilicate clay soils, defluoridation, fluoride, groundwater, hydrothermal treatment, mechanochemical activation, pore forming agent, pathogens

© University of Venda

University of Venda
Creating Future Leaders

LIST OF FIGURES

© University of Venda

University of Venda
Creating Future Leaders

© University of Venda

University of Venda
Creating Future Leaders

© University of Venda

© University of Venda

LIST OF TABLES

© University of Venda

University of Venda
Creating Future Leaders

© University of Venda

ACRONYMS AND ABBREVIATIONS

A: Albite

Abs: Absorbance

An: Analcime

BET: Brunauer-Emmett-Teller

Ca: Calcite

Cfu: colony forming unit

Cha: Chabazite

Ch: Chlorite

CDC: Centers for Disease Control and Prevention

CEC: Cation exchange capacity

COD: Co-efficient of determination (R^2)

˚C: Degree Celsius

DWAF: Department of water affairs and forestry

E. coli: *Escherichia coli*

ED: Electrodialysis

EDS: Energy dispersion spectroscopy

F^-: Fluoride

FITR: Fourier transform infra-red

g: gram

h: hour

HS: Hydroxy sodalite

Ho: Horneblende

HTAC: Hydrothermally-treated aluminosilicate clay

ICP-MS: Inductly coupled plasma-mass spectroscopy

ISE: Ion Selective Electrode

K: Kaolinite

^{0}K: Degree Kelvin

L: Litres

LOD: Limit of detection

© University of Venda

MAC: Mechanochemically-activated clay

MDGs: Millennium Development Goals

Mg: milligram

Mi: Microcline

Min: Minutes

Mo: Montmorillonite

ND: Not detectable

OD: Optical density

pH_{pzc}: Point zero charge

pH: Potential Hydrogen

Ph: Phillipsite

PHTAC: Porous-hydrothermally-treated aluminosilicate clay

PFO: Pseudo-first-order

PSO: Pseudo-second-order

Q: Quartz

rpm: revolution per minute

RCS: Reduced chi-square

RMSE: Reduced mean square error

RSS: Residual sum of squares

SABS: South African Bureau of Standards

SANS: South Africa National Standards

SDGs: Sustainable Development Goals

SEM: Scanning Electron Microscopy

TISAB: Total Ionic Strength Adjustment Buffer

UN: United Nations

UNICEF: United Nations International Children Education Fund

XRD: X-Ray Diffraction

XRF: X-Ray Fluorescence

WASH: Water, Sanitation, and Hygiene

WHO: World Health Organisation

WRC: Water research commission

© University of Venda

H_2SO_4: Sulfuric Acid

HCl: Hydrochloric Acid

NaF: Sodium Fluoride

Na_2CO_3: Sodium Carbonate

$NaClO_3$: Sodium Chlorate

$NaNO_3$: Sodium Nitrate

Na_2SO_4: Sodium Sulphate

KCl: Potassium Chloride

© University of Venda

University of Venda
Creating Future Leaders

TABLE OF CONTENTS

© University of Venda

University of Venda
Creating Future Leaders

© University of Venda

University of Venda
Creating Future Leaders

© University of Venda

University of Venda
Creating Future Leaders

© University of Venda

University of Venda
Creating Future Leaders

© University of Venda

University of Venda
Creating Future Leaders

© University of Venda

University of Venda
Creating Future Leaders

© University of Venda

University of Venda
Creating Future Leaders

APPENDIXES

© University of Venda

ACADEMIC OUTPUTS

Published Article

- **Obijole, O. A.,** Gitari, M. W., Ndungu, P. G., & Samie, A. **(2019). Mechanochemically-activated aluminosilicate clay soils and their application for defluoridation and pathogen removal from groundwater.** *International Journal of Environmental Research and Public Health, 16*(4), 654. doi: 10.3390/ijerph16040654.

Book of Proceedings

- **Obijole O.A,** Gitari W. M. & Samie, A **(2018). Application of mechanochemically-activated clay soils for simultaneous fluoride and pathogen removal from groundwater.** Eds; J, Edokpayi., W.M Gitari, E.M Stam and S.E Mhlongo. Proceedings of the first international conference in sustainable management of resources (ICSMNR).

Manuscript accepted

- **Olumuyiwa A. Obijole,** Mugera W. Gitari, Rabelani Mudzielwana, Patrick G. Ndungu, Amidou Samie & Ayinde W. Babatunde **(2020). Hydrothermally-treated aluminosilicate clay (HTAC) for remediation of fluoride and pathogens from groundwater: adsorbent characterisation and adsorption modelling.** *Water Resources and Industry Journal.*

Manuscript under review

- **Obijole, O. A.,** Gitari, M. W., Ndungu, P. G., Mudzielwana, R., Izevbekhai O. I & Samie, A **(2021). Hydrothermal treatment of aluminosilicate-rich clay soils: evaluating optimum condition for synthesis and physicochemical characterisation.**

Manuscript under preparation

- **Obijole, O. A.,** Gitari, M. W., Ndungu, P. G., Mudzielwana, R., Izevbekhai O. I & Samie, A **(2021). Porous-hydrothermally-treated aluminosilicate rich clays (PHTAC): Evaluation of optimum conditions for synthesis, defluoridation and physicochemical characterisation.** Under preparation.
- **Obijole, O. A.,** Gitari, M. W., Ndungu, P. G., Mudzielwana, R & Samie, A **(2021). Application of porous-hydrothermally-treated aluminosilicate clay (PHTAC) adsorbent in defluoridation and pathogen removal from groundwater.** Under preparation.

© University of Venda

- **Obijole, O. A.,** Gitari, M. W., Ndungu, P. G., Mudzielwana, R., Ayinde W. B & Samie, A **(2021). Porous smectite rich-clay adsorbents' defluoridation and pathogen removal potency in groundwater: Comparative adsorption kinetics and isotherms modelling studies.** Under preparation.

Presentation at Conferences

- **Obijole, O. A**., Gitari, M. W., Ndungu, P. G., Mudzeilwana, R & Samie, A. **(2019). Hydrothermally-treated aluminosilicate clays (HTAC) and their Application to water treatment.** 20th Waternet/WARFSA/GWP-SA Symposium on Integrated Water Resources Development and Management: Leaving No One Behind for Water Security in Eastern and Southern Africa, held at Indaba Hotel, Spa & Conference Centre, Fourways, Johannesburg, South Africa 30th October - 1st November 2019.
- **Obijole O.A**, Gitari W. M. & Samie, A. **(2018). Application of mechanochemically-activated clay soils for simultaneous fluoride and pathogen removal from groundwater**. International Conference on Sustainable management and natural resources (ICSMNR). Bolivia lodge, Polokwane, Limpopo, South Africa. 15 - 19 October 2018.

© University of Venda

CHAPTER ONE: INTRODUCTION

1.1 Background

Water is an essential resource for all forms of life. Access to safe drinking water has great influence on health, economic productivity and quality of life of the people. According to World Health Organization (WHO, 2017), there are at least 5 million deaths per year due to unsafe drinking water and about 1.4 billion people do not have access to drinking water (Ganvir *et al.*, 2002; Matthys, 2000). Majority of people in rural areas depend on groundwater which is sometimes contaminated by fluoride and pathogens due to lack of drinking water. Groundwater may be contaminated through natural and anthropogenic sources. Natural sources include fluoride-rich rocks or fluorapatite which found their way into groundwater aquifers via long term weathering, rainwater flow/seeping and leaching from these fluoride rich rocks (Bretzler & Johnson, 2015; Kut *et al.*, 2016). Anthropogenic fluoride and pathogen sources are human activities such as the use of phosphatic fertilizers, coal combustion, industrial effluents, sewage percolating from pit latrines and seeping through soils and unhygienic practices (Brindha & Elango, 2011; WHO, 2015).

Fluoride is a double-edged sword which can be both beneficial and detrimental to human health if ingested at certain levels (Biswas *et al.*, 2007; Waghmare & Arfin, 2015; WHO, 2016). Consumption of water containing fluoride concentration below 1.5 mg/L helps in prevention of dental caries, healthy bone and teeth formation, while consumption of water with lower fluoride contents < 0.7 mg/L results in dental caries. Conversely, prolonged intake of water with fluoride concentrations exceeding 1.5 mg/L gives rise to dental fluorosis and still higher concentrations leads to skeletal fluorosis (Johnson & Bretzler, 2015; Kut *et al.*, 2016; WHO, 2019). In addition to fluorosis, excess fluoride in water has been known to cause non-fluorosis diseases like thyroids, cancer, respiratory problems, damage kidney-liver-nervous systems, thyroids and Alzheimer (Kumar *et al.*, 2017). Statistics showed that over 200 million people from 26 countries are at great risk of contracting fluorosis, with an increasing prevalence in India, China, Cameroon, East African countries such as Ethiopia, Kenya, Uganda and Southern African region including South Africa (Amini, 2008; Momba *et al.*, 2009; Viswanathan *et al.*, 2009b; Shen & Schäfer, 2015; 2016).

Water treatment processes for defluoridation include chemical precipitation (Aldaco *et al.*, 2005), electrocoagulation flotation/electrodialysis (Loganathan *et al.*, 2013), ion exchange (Pan *et al.*, 2018), membrane filtration process (Kumar *et al.*, 2017), nanofiltration (Waghmare

© University of Venda

& Arfin, 2015), and adsorption (Ghorai & Pant, 2004; Mudzielwana *et al.*, 2016). Adsorption is the method of choice due to its effectiveness, low cost, simplicity, environmental friendliness and universal applicability (Ghorai & Pant, 2004; Mudzielwana *et al.*, 2016). Most of the materials applied in defluoridation which include zeolites (Shameli *et al.*, 2011; Musyoka *et al.*, 2012), diatomaceous earth (Izuagie *et al.*, 2016), mesoporous granular materials (Mulugeta *et al.*, 2009), various forms of clay and its modified forms (Mudzielwana *et al.*, 2016, 2017; Gitari *et al.*, 2017), reported in literature are either not effective or ineffective at a narrow pH range and some cannot be regenerated effectively, hence, there is the urgent need to develop a suitable multifunctional and appropriate technology that will be effective at wide pH range for excellent defluoridation and pathogen detoxification and removal from groundwater.

Apart from fluoride, waterborne pathogens such as bacterial contaminants in drinking water are major public health concerns worldwide. Water sources are often contaminated with bacterial agents such as *Escherichia coli*, *Pseudomonas aeruginosa* and *Legionella spp.*, which cause infections traceable to waterborne diseases such as diarrhea, cholera and other acute gastrointestinal/urinary tract infections, acute respiratory illness, severe anemia, hepatitis, dermatitis, kidney failure and a host of other lethal infections leading to death (Sedillo, 2008; Barrett, 2019). Waterborne diseases are responsible for an estimated 2.2 million deaths yearly (Bitton, 2014; WHO, 2017). Generally, pathogens find their ways to water bodies/aquifers through underground seeping of sewages, unwholesome sanitation and hygiene practices, mining activities and through some oxidative processes leading to genetic mutations and penetration through the rocks and soil consequent of weathering and rainfall (WHO, 2019).

There are various methods used for pathogen inactivation and removal from water. These methods range from simple conventional treatments to modern technologies which are physical methods, such as boiling, heating (fuel and solar), sedimentation, chlorination, filtering, solar disinfection, and UV lamps disinfection and chemical methods such as coagulation-flocculation and precipitation, adsorption, ion exchange and chemical disinfection with germicidal agents. The methods have all been proven to improve microbiological quality by reducing bacteria, viruses and some protozoa in drinking water (Lantagne *et al.*, 2006; Potgieter, 2007; WHO, 2010; Connelly & Baeumner, 2012; Ingerson-Mahar and Reid, 2012; Singh *et al.*, 2013; Mwabi *et al.*, 2013; Bridle & Desmulliez, 2014; Al-Gheethi *et al.*, 2019). Most of these methods are not totally effective and not applicable in rural households due to high cost, non-satisfactory performance and inapplicability (Lantagne *et al.*, 2006; Potgieter, 2007; Dunn *et al.*, 2014; Whelan *et al.*, 2014; Ramírez-Castillo *et al.*, 2015).

© University of Venda

Although some of the available technologies for fluoride and pathogen removal from drinking water are effective, some are unsustainable and unsuitable for application particularly at rural household level. Hence, to address the twin challenges of fluorosis and waterborne diseases, a novel approach to deliver fluoride-free and bacteriologically safe drinking water at household (point-of-use) levels should be developed particularly in isolated areas, where centralized systems are not economically feasible. This can be achieved by developing effective, affordable, multifunctional and sustainable materials for simultaneous defluoridation and pathogen removal from groundwater. Thus, this study was an attempt at developing multifunctional, low-cost adsorbents from naturally occurring smectite-rich clay soils for application in simultaneous defluoridation and pathogen removal from groundwater at household level.

1.2 Problem statement

Groundwater is the most widely used source of drinking water for many rural communities worldwide. Fluoride contamination could be through anthropogenic or natural sources while pathogen sources could be through fecal droplet percolating into the soils. Groundwater is often contaminated by fluoride concentration >1.5 mg/L recommended WHO and SANS limits (WHO, 2019) and pathogens resulting into medical conditions of dental, skeletal fluorosis and waterborne diseases respectively (Bitton, 2014). Fluorosis is endemic in 26 countries with about 200 million at great risk while waterborne diseases is a public health concern worldwide particularly in rural communities where pipe-borne water is lacking. Some of the countries greatly affected are India, Bangladesh, China, Mexico, Uganda, Tanzania, Kenya, Ethiopia and South Africa. In South Africa, pilot surveys undertaken by the Department of Water Affairs and Forestry (DWAF, 2001) indicated several boreholes across the country contain high fluoride levels (McCaffrey, 1998). Ncube & Schuttle (2005) in their studies noted high correlation of dental fluorosis in communities with high fluoride levels. Odiyo & Makungo (2018) conducted an assessment of groundwater quality, identified the potential sources of contamination and associated health risks of dwellers in Siloam Village, South Africa. The study revealed high fluoride concentrations in their groundwater. The excessively high fluoride concentrations was discovered to be associated with tooth damage and pronounced skeletal fluorosis. There were also the presence of coliforms and *E. coli* in most of the evaluated borehole groundwater which indicated potential presence of fecal contamination from nearby pit latrines and sewages.

© University of Venda

Due to lack of alternative sources of water in Siloam village, the surrounding Nzhelele rural communities and elsewhere, WHO calls for development of sustainable, low cost and point of use water treatment techniques that can be applied in rural communities. Some of the available technologies for defluoridation are chemical precipitation (Aldaco *et al.*, 2005), electrocoagulation (Loganathan *et al.*, 2013), ion exchange (Pan *et al.*, 2018), membrane filtration (Kumar *et al.*, 2017), nanofiltration (Waghmare & Arfin, 2015), and adsorption (Ghorai and Pant, 2004; Mudzielwana *et al.*, 2016). Some of the affordable materials applied are zeolites (Musyoka *et al.*, 2012), diatomaceous earth (Izuagie *et al.*, 2016), mesoporous granular materials (Mulugeta *et al.*, 2009; 2015), various forms of clay and its modified forms (Mudzielwana *et al.*, 2016, 2017; Gitari *et al.*, 2016). Pathogen removal techniques include boiling, heating (fuel and solar), sedimentation, chlorination, filtering, solar disinfection, ultra violet (UV) lamps disinfection, coagulation-flocculation, precipitation, adsorption, ion exchange and chemical disinfection (Lantagne *et al.*, 2006; Potgieter, 2007; WHO, 2010; Ingerson-Mahar & Reid, 2012; Momba *et al.*, 2012; Bridle & Desmulliez, 2014; Al-Gheethi *et al.*, 2019). While some of the technologies for defluoridation and pathogen removal from groundwater are effective, some are expensive, and unsuitable for rural household application. Hence, this study aims to address the twin challenges of fluorosis and waterborne diseases by developing a pore forming-agent, modified hydrothermally-treated aluminosilicate clay (HTAC) adsorbent which would be multifunctional, affordable and effective in defluoridation and pathogen removal from groundwater at household level.

1.3 Research objective

The main objective of this work was to develop an adsorbent based on locally available aluminosilicate rich clay soils through hydrothermal treatment for application in defluoridation and pathogen removal from groundwater.

1.3.1 Specific research objectives

The specific objectives were to:

- mechanochemically activate raw aluminosilicate clay soils (MAC) and evaluate their physicochemical and mineralogical characteristics and their application for defluoridation and pathogen removal from groundwater;
- optimise the operational parameters for synthesis of hydrothermally-treated aluminosilicate clays (HTAC), evaluate their physicochemical properties and potential for fluoride and pathogen removal from groundwater;

© University of Venda

- hydrothermally treat the mechanochemically-activated clay (MAC) at previously established optimum operational parameters and evaluate their adsorptive capacities for fluoride removal in groundwater and further evaluate their antibacterial efficacy towards selected bacterial strains;
- optimise the operational parameters for modification of MAC through hydrothermal treatment in presence of a pore-forming agent, and evaluation of their physicochemical properties and potential for fluoride and pathogen removal from groundwater;
- synthesise a (porous) pore forming-agent-modified-hydrothermally-treated aluminosilicate clay (PHTAC) at previously optimised conditions and evaluation of its fluoride adsorptive capacities in groundwater and antibacterial efficacy towards selected strains.

1.4 Hypothesis

The novel household, pore forming-agent-modified-hydrothermally-treated aluminosilicate clay (PHTAC) adsorbent has the potential for simultaneous fluoride and pathogens removal from groundwater.

1.5 Assumption

It is assumed that the:

- synthesised pore-forming agent-modified-hydrothermally-treated aluminosilicate clay (PHTAC) adsorbents will effectively and simultaneously remove fluoride and pathogens from groundwater;
- hydrothermal treatment and introduction of pore-forming agent ($NaClO_3$) will improve the efficiency of the synthesised adsorbent in fluoride and pathogens removal from groundwater;
- introduction of the pore-forming agent on the synthesised (PHTAC) adsorbents' surface will not affect the quality of the treated groundwater;
- synthesised (porous) pore-forming-agent-modified-hydrothermally-treated aluminosilicate clay (PHTAC) adsorbents will be multifunctional, affordable for point-of-use and applicable for rural households.

© University of Venda

1.6 Significance of the study

Worldwide, groundwater is the main source of drinking water in majority of rural communities. Excess fluoride and pathogens contamination in water have been known to be detrimental to human health leading to dental, skeletal and crippling fluorosis as well as numerous symptoms associated with water borne diseases respectively. Studies have been carried out to reduce or remove these contaminants in water through development and application of various adsorbents which are effective in some cases but not sustainable and applicable for rural dwellers. Some multifunctional adsorbents capable of removing contaminants in water have also been developed but not economical, sustainable and applicable at point-of-use level. This study therefore hoped to develop multifunctional adsorbents for simultaneous defluoridation and pathogen removal from groundwater. Furthermore, the findings of this study will also assist in addressing the United Nations Sustainable Development Goal 3 which aims at improving human wellbeing and health through provision of pathogen-free groundwater amongst others and the United Nations Sustainable Development Goal 6 which seeks to ensure clean potable water for all by the year 2030.

1.7 Thesis layout

This section presents the layout of the chapters:

Chapter 1: Introduction

Chapter 2: Literature review

Chapter 3: Mechanochemically-activated aluminosilicate clay (MAC) soils and their application in defluoridation and pathogen removal from groundwater.

Chapter 4: Hydrothermal treatment of aluminosilicate rich clay soils: Evaluating optimum conditions for synthesis and physicochemical characterisation.

Chapter 5: Hydrothermally-treated aluminosilicate clay (HTAC) and their application in fluoride and pathogen removal from groundwater.

Chapter 6: Pore-forming-agent-assisted-hydrothermally-treated aluminosilicate clays (PHTAC): Evaluating optimum conditions for synthesis and physicochemical characterisation.

Chapter 7: Application of porous-hydrothermally-treated aluminosilicate clay (PHTAC) in defluoridation and pathogen removal from groundwater.

Chapter 8: Conclusions and Recommendations.

© University of Venda

REFERENCES

Aldaco, R., Irabien, A., & Luis, P. (2005). Fluidized bed reactor for fluoride removal. *Chemical Engineering Journal*, *107*(1-3), 113-117.

Al-Gheethi, A. A. S., Noman, E. A., Mohamed, R. M. S. R., Talip, B. A., Kassim, A. H. M., & Ismail, N. (2019). Disinfection Technologies for Household Greywater. In *Management of Greywater in Developing Countries* (pp. 185-203). Springer, Cham.

Amini, M., Mueller, K., Abbaspour, K. C., Rosenberg, T., Afyuni, M., Møller, K. N., & Johnson, C. A. (2008). Statistical modeling of global geogenic fluoride contamination in groundwaters. *Environmental , 42*(10), 3662-3668.

Barrett, C. E. (2019). Impact of Public Health Interventions on Drinking Water–Associated Outbreaks of Hepatitis A—United States, 1971–2017. *MMWR. Morbidity and Mortality Weekly Report*, *68*.

Bitton, G. (2014). Microbiology of Drinking Water Production and Distribution. 1st ed. John Wiley & Sons, Inc. Hoboken, NJ, USA. 312.

Biswas, K., Gupta, K., Goswami, A & Ghosh, U.C. (2010). Fluoride removal efficiency fromaqueous solution by synthetic iron (III)-aluminum (III)-chromium (III) ternary mixed oxide. *Desalination* 255 (1–3), 44–51.

Bretzler, A., & Johnson, C. A. (2015). The geogenic contamination handbook: addressing arsenic and fluoride in drinking water. *Applied Geochemistry*, *63*, 642-646.

Bridle, H., & Desmulliez, M. (2014). Biosensors for the Detection of Waterborne Pathogens. In *Waterborne Pathogens* (pp. 189-229). Academic Press.

Brindha, K. & Elango, L. (2011). Fluoride in groundwater: causes, implications and mitigation measures. In: Monroy, S.D. (Ed.), Fluoride Properties, Applications and Environmental Management. Nova Science Publishing, New York, pp. 111–136.

Centers for Disease Control and Prevention (CDC). Global Water, Sanitation, and Hygiene (WASH).

CDC, Atlanta, GA. (2013). Surveillance for waterborne disease outbreaks associated with drinking water and other non-recreational water—USA. 2009–2010 62 714–720.

Connelly, J. T., & Baeumner, A. J. (2012). Biosensors for the detection of waterborne pathogens. *Analytical and Bioanalytical Chemistry*, *402*(1), 117-127.

Dunn, G., Harris, L., Cook, C. and Prystajecky, N. (2014). A comparative analysis of current microbial water quality risk assessment and management practices in British Columbia and Ontario, Canada. *Science of the Total Environment.* 468–469 544–552.

© University of Venda

Ganvir, V., Biswas, K. & Kokil, S. (2002): A novel water filter technology for rural areas. 28th WEDC Conference: Sustainable Environmental Sanitation and water services. Kolkata (Calcutta), India.

Ghorai, S & Pant, K. K. (2005). Equilibrium, kinetics and breakthrough studies for adsorption of fluoride on activated alumina. *Separation and Purification Technology*. 42, 265–271.

Gitari, W. M., Ngulube, T., Masindi, V & Gumbo, J. R. (2013). Defluoridation of groundwater using Fe3+-modified bentonite clay: optimisation of adsorption conditions. *Desalination and Water Treatment*. 53 6 1578–1591.

Gitari, M.W., Petrick, L.F & Musyoka, N.M. (2016). Hydrothermal conversion of South African coal fly ash into pure phase zeolite Na-P1. In *Metals and Non-metals 'Zeolites-Useful minerals'* Claudia Belviso (Ed). 25-42.

Gitari, W. M., Izuagie, A. A., & Gumbo, J. R. (2020). Synthesis, characterisation and batch assessment of groundwater fluoride removal capacity of trimetal Mg/Ce/Mn oxide-modified diatomaceous earth. *Arabian Journal of Chemistry*, *13*(1), 1-16.

Ingerson-Mahar, M. & Reid, A. (2012). Microbes in Pipes: The Microbiology of the Water Distribution System. A Report on an American Academy of Microbiology Colloquium; ASM Academy: Boulder, CO, USA. 26.

Izuagie, A. A., Gitari, W. M., & Gumbo, J. R. (2016). Synthesis and performance evaluation of Al/Fe oxide coated diatomaceous earth in groundwater defluoridation: towards fluorosis mitigation. *Journal of Environmental Science and Health, Part A*, *51*(10), 810-824.

Johnson, C. A & Bretzler, A. (2015). Geogenic Contamination Handbook—Addressing Arsenic and Fluoride in Drinking Water. *Eawag: Swiss Federal Institute of Aquatic Science and Technology, Dübendorf, Switzerland*.

Kut, K. M. K., Sarswat, A., Srivastava, A., Pittman Jr, C. U., & Mohan, D. (2016). A review of fluoride in African groundwater and local remediation methods. *Groundwater for Sustainable Development*, *2*, 190-212.

Kumar, M. S., Dhakate, R., Yadagiri, G., & Reddy, K. S. (2017). Principal component and multivariate statistical approach for evaluation of hydrochemical characterisation of fluoride-rich groundwater of Shaslar Vagu watershed, Nalgonda District, India. *Arabian Journal of Geosciences*, *10*(4), 83.

© University of Venda

Lantagne, D., Quick, R & Mintz, E. (2006). Household water treatment and safe storage options in developing countries: a review of current implementation practices. Washington DC: Woodrow Wilson International Center.

Loganathan, P., Vigneswaran, S., Kandasamy, J., & Naidu, R. (2013). Defluoridation of drinking water using adsorption processes. *Journal of Hazardous Materials*, *248*, 1-19.

Mathys, A. (2000): Water supply in under-privileged areas. New World Water 2000. 1st Edition Sterling Publication Limited, London.

McCaffrey, L. P. (1998). *Distribution and causes of high fluoride groundwater in the western Bushveld area of South Africa* (Doctoral dissertation, University of Cape Town).

McCaffrey, L. P., & Willis, J. P. (2001). Distribution of fluoride-rich groundwater in the eastern and Mogwase regions of the Northern and North-West Provinces. Pretoria: Water Research Commission.

Momba, M. N. B., Malakate, V. K & Theron, J. (2006a). Abundance of pathogenic Escherichia coli, Salmonella typhimurium and Vibrio cholerae in Nkonkobe drinking water sources. *Journal of Water and Health.* 4 289-296.

Momba, M. N. B., Tyafa, Z., Makala, N., Brouckaert, B. M & Obi, C. L. (2006b). Safe drinking water still a dream in rural areas of South Africa. Case study: The Eastern Cape Province. *Water South Africa.* 32 5 715-720.

Momba, M. N. B., Obi, C. L & Thompson, P. (2009). Survey of disinfection efficiency of small drinking water treatment plants: challenges facing small water treatment plants in South Africa. *Water South Africa*. 35 4 48-5494.

Mudzielwana, R., Gitari, M. W., & Msagati, T. A. (2016). Characterisation of smectite-rich clay soil: Implication for groundwater defluoridation. *South African Journal of Science*, *112*(11-12), 1-8.

Mudzielwana, R., Gitari, M. W., Akinyemi, S. A., & Msagati, T. A. M. (2017). Synthesis and physicochemical characterisation of MnO2 coated Na-bentonite for groundwater defluoridation: Adsorption modelling and mechanistic aspect. *Applied Surface Science*, *422*, 745-753.

Mudzielwana, R., Gitari, W. M., Akinyemi, S. A., & Msagati, T. A. (2017). Synthesis, characterisation, and potential application of Mn 2+-intercalated bentonite in fluoride removal: adsorption modeling and mechanism evaluation. *Applied Water Science*, *7*(8), 4549-4561.

© University of Venda

Musyoka, N. M. (2009). *Hydrothermal synthesis and optimisation of zeolite Na-P1 from South African coal fly ash.* (Doctoral thesis, University of Western Cape, South Africa).

Musyoka, N. M., Petrik, L. F., Gitari, W. M., Balfour, G., & Hums, E. (2012). Optimisation of hydrothermal synthesis of pure phase zeolite Na-P1 from South African coal fly ashes. *Journal of Environmental Science and Health,* Part A, 47 3 337-350.

Mulugeta, M., & Lelisa, B. (2015). Removal of methylene blue (Mb) dye from aqueous solution by bioadsorption onto untreated Parthenium hystrophorous weed. *Modern Chemistry and Application*. 2, 146.

Mwabi, J. K., Mamba, B. B., & Momba, M. M. B. (2013). Removal of waterborne bacteria from surface water and groundwater by cost-effective household water treatment systems (HWTS): A sustainable solution for improving water quality in rural communities of Africa. *Water South Africa*, *39*(4), 445-456.

Ncube, E. J & Schutte, C. F, (2005). The occurrence of fluoride in South African groundwater: A water quality and health problem, *Water SA*. 31 1 35–40.

Odiyo, J. O & Makungo, R. (2012). Fluoride concentrations in groundwater and impact on human health in Siloam Village, Limpopo Province, South Africa. *Water South Africa*, *38*(5), 731-736.

Pan, J., Zheng, Y., Ding, J., Gao, C., Van der Bruggen, B., & Shen, J. (2018). Fluoride removal from water by membrane capacitive deionization with a monovalent anion selective membrane. *Industrial and Engineering Chemistry Research*, *57*(20), 7048-7053.

Potgieter, N., Becker, P. J & Ehlers, M. M. (2008). Evaluation of the CDC safe water-storage intervention to improve the microbiological quality of point-of-use drinking water in rural communities in South Africa. Water SA, 1816-7950.

Ramírez-Castillo, F. Y., Loera-Muro, A., Jacques, M., Garneau, P., Avelar-González, F. J., Harel, J & Guerrero-Barrera, A. L. (2015). Review: Waterborne Pathogens: Detection Methods and Challenges. *Pathogens* 4 307-334. doi:10.3390/pathogens4020307

SANS 241 (2006). South African National Standard (SANS) 241 Drinking Water Specification. South African Bureau of Standards (SABS) SANS 241. Pretoria, SA.

Sedillo, J. L., Quintana, A., Souza, K., Oshima, K. H & Smith, G. B. (2008). The development of point-of-use water filters as sampling devices in bioforensics: extent of microbial sorption and elution. *Environmetal Monitoring.* 10 6 718-23. doi: 10.1039/b718064k. Epub 2008 Apr 22.

© University of Venda

Sharma, P. P., Yadav, V., Maru, P. D., Makwana, B. S., Sharma, S., & Kulshrestha, V. (2018). Mitigation of fluoride from brackish water via electrodialysis: an environmentally friendly process. *Chemistry Select*, *3*(2), 779-784.

Shameli, K., Ahmad, M. B., Zargar, M., Yunus, W. M. Z. W., Rustaiyan, A., & Ibrahim, N. A. (2011). Synthesis of silver nanoparticles in montmorillonite and their antibacterial behavior. *International Journal of Nanomedicine, 6*, 581.

Shen, J., Richards, B. S., & Schäfer, A. I. (2016). Renewable energy powered membrane technology: Case study of St. Dorcas borehole in Tanzania demonstrating fluoride removal via nanofiltration/reverse osmosis. *Separation and Purification Technology*, *170*, 445-452.

Shen, J., & Schäfer, A. I. (2015). Factors affecting fluoride and natural organic matter (NOM) removal from natural waters in Tanzania by nanofiltration/reverse osmosis. *Science of the Total Environment*, 527, 520-529.

Singh, A., Poshtiban, S & Evoy, S. (2013). Recent advances in bacteriophage-based biosensors for food-borne pathogen detection. Sensors 13 1763–1786.

Tomar, G., Thareja, A., & Sarkar, S. (2015). Enhanced fluoride removal by hydroxyapatite-modified activated alumina. *International Journal of Environmental Science and Technology*, *12*(9), 2809-2818.

Viswanathan, N., Sundaram, C. S & Meenakshi, S. (2009). Removal of fluoride from aqueous solution using protonated chitosan beads. *Journal of Hazardous Materials*. 161 (1), 423–430.https://doi.org/10.1016/j.jhazmat.2008.03.115.

Waghmare, S. S., & Arfin, T. (2015). Fluoride removal by clays, geomaterials, minerals, low cost materials and zeolites by adsorption: a review. *International Journal of Science, Engineering and Technology Research*, *4*(11), 3663-3676.

Whelan, G., Kim, K., Pelton, M. A., Soller, J. A., Castleton, K. J., Molina, M., Pachepsky, Y & Zepp, R. (2014). An integrated environmental modeling framework for performing quantitative microbial risk assessments. *Environmental Modelling & Software*, *55*, 77-91.

World Health Organization (WHO). Water Sanitation and Health. (2015). Available online: http://www.who.int/water_sanitation_health/diseases. Accessed 28th April, 2019.

World Health Organization (WHO), (2010; 2011; 2016). Guidelines for Drinking Water Quality. Fluoride in drinking water. Guidelines for Drinking Water Quality, Geneva.

© University of Venda

World Health Organization. (2017). Progress on drinking water, sanitation and hygiene: 2017 update and SDG baselines.

World Health Organization. (2019). *Preventing disease through healthy environments: inadequate or excess fluoride: a major public health concern* (No. WHO/CED/PHE/EPE/19.4. 5). World Health Organization.

© University of Venda

CHAPTER TWO: LITERATURE REVIEW

2 Introduction

Groundwater is the main source of drinking water in majority of rural communities worldwide. Some aquifers are contaminated with various contaminants from different origins among whom are fluoride and pathogens resulting in medical conditions of fluorosis and various forms of waterborne diseases. This chapter focuses on the literature review of fluoride and pathogen contaminations in groundwater and associated health effects in humans, nature, source and fluorine and pathogen occurrence in groundwater. This chapter also reviewed available technologies and different materials applied in fluoride and pathogen removal from groundwater with a special emphasis on hydrothermal treatment of aluminosilicate materials and gaps identified with a view to developing a sustainable technology using cheap aluminosilicate materials for rural household application.

2.1 Fluorine: Nature and occurrence

Fluorine is a chemical element with the symbol F, atomic number 9. Atomic Mass: 18.998404 Armstrong mass unit. Melting Point: -219.62 °C (53.530006 K, -363.31598 °F), Boiling Point: -188.14 °C (85.01 K, -306.652 °F) with cubic crystal structure (Jaccaud *et al.*, 2000). It has a density of 1.696 g/cm^3 at 293 K. Fluorine is the lightest member of the halogen group and exists as a highly toxic pale yellow diatomic gas at standard conditions. It is the most electronegative element and is extremely reactive. Fluorine is 24th most common in universal abundance and 13th most common element in Earth's crust at 600 - 700 ppm (parts per million) by mass (Jaccaud *et al.*, 2000).

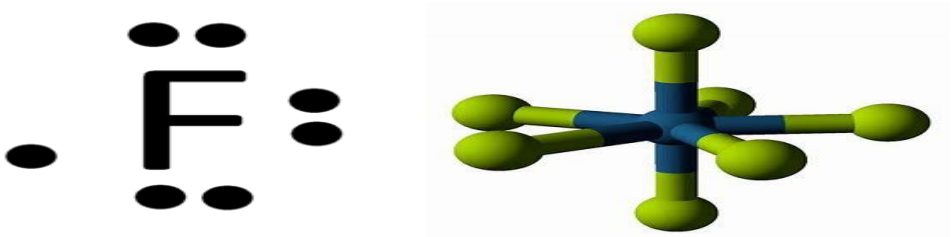

Figure 2.1: (a) Fluorine atom (b) Fluorine atomic model (Jaccuad *et al.*, 2000).

2.2 Fluoride: Origin and occurrence in groundwater

As the 13th most abundant element in the lithosphere and lightest element among Halogen group, fluorine is the most electronegative and reactive element known and hence it

© University of Venda

is rarely found in the elemental state. It usually forms ionic bonds. Fluorine can form complexes such as $(AlF_6)_3$ or AlF_2^+. Fluorite (CaF_2), Fluorapatite ($Ca_5(PO_4)_3F$), Cryolite (Na_3AlF_6) and Topaz $(Al_2(SiO_4)(OHF)_2)$ are the common accessory minerals in which fluorine is an essential element (Greenwood & Earnshaw 1998; Jaccuad *et al.*, 2000; Schmedt *et al.*, 2012).

Major fluorine/fluoride-containing minerals

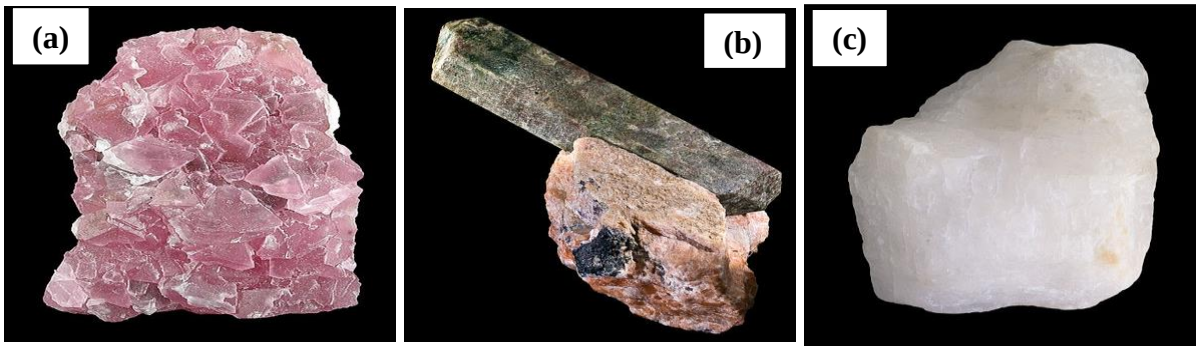

Figure 2.2: Picture of (a) Fluorite (b) Fluorapatite (c) Cryolite.

Fluorite-bearing granitic rocks provide sources of dissolved fluoride in groundwater. Fluorine is one of few potentially toxic elements whose primary path into the human body is via drinking water particularly when present in high concentrations above human body tolerance levels (WHO, 2015; 2017).

2.3 Groundwater contamination by fluoride

Fluoride levels in rocks and soils are linked to geological processes, even though it could also be due to human activities (Brindha & Elango, 2011). Geogenic fluoride sources in groundwater are closely associated to the geological setting of the region. It may also vary from region to region due to type of rocks, geology contact time of aquifer water with the rocks, climate of the region, overall chemical composition, aquifer depth, and weathering intensity (Brahma, 2018). Rock containing fluoride-bearing minerals, including fluorite, fluorspar, fluoride-rich clays or fluorapatite, cryolite, topaz, apatite, biotite, hornblende, mica and their related congregated rocks, including basalt shale, granite and syenite are sources of natural fluoride in groundwater (Brindha & Elango, 2011; Bretzler & Johnson, 2015; Kut *et al.*, 2016). Volcanic rock settings originating from tertiary to current period are usually associated with high fluoride levels in groundwater. Long-term weathering, rainwater flow, and penetration into these rocks have been traced to higher fluoride levels in groundwater. Metasomatic processes have enriched fluorine content of the minerals making up these rock types (Kut *et*

© University of Venda

al., 2016). Further, these fluorine-enhanced minerals have negligible solubility in water. As a result, fluorides will only contaminate groundwater where the water is exposed to conditions which favour their dissolution, or if anthropogenic effluents containing fluoride are disposed of from industrial activities. The final groundwater fluoride concentrations depend on the duration for which water is forced into contact with the aquifer minerals, the local pH, microbial action, and oxygen content. Other fluoride sources in groundwater are from human activities such as the use of phosphatic fertilisers, coal combustion and clays used in ceramic industries (Brindha & Elango, 2011).

Water is life and essential for normal functioning of biochemical systems of our body, for drinking, personal hygiene, domestic use, irrigation and economic development (Braune & Xu, 2010). Many regions of the world have elevated fluoride levels in drinking water which have led to emergence of fluorosis. These include Asia, South America, North America, parts of Europe and Africa. Studies showed that fluorosis is endemic in at least twenty-six counties (Figure 2.3) where fluoride concentrations in drinking water are above the upper limit of 1.5 mg/L set by the World Health Organization (WHO, 2017, 2019).

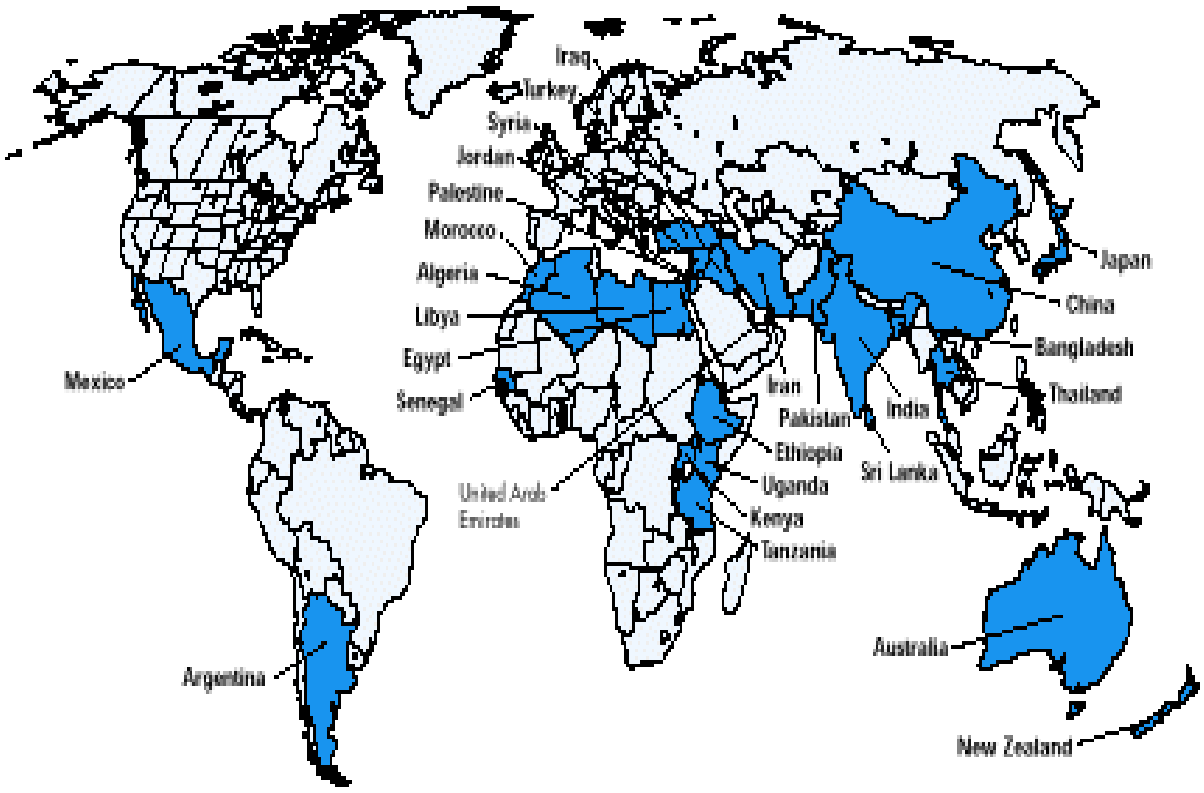

Figure 2.3: Map showing countries in the world with endemic fluorosis.
Source: UNICEF MAP OF FLUOROSIS - Swami Vivekananda Institute of Pharmaceutical Sciences. (SVIPS), Vangapally, Bhongir. http://www.unicef.org/wes/files/wf13e.pdf

© University of Venda

Evidence from India and China indicates high risk of skeletal fluorosis and bone fractures at a total fluoride intake of 14 mg/day and increased risk of skeleton effects at a total intake above 6 mg/day (WHO, 2019).

Incidences of fluorosis have been reported in some regions of Sudan, Cameroon, Morocco, Algeria, Chad, Namibia, South Africa, Mozambique, Zimbabwe, Senegal and the Rift Valley countries of Ethiopia, Kenya, Tanzania, Uganda and Malawi (Fawell *et al.*, 2006; Fantong *et al.*, 2010), (Figure 2.4). About 80% of Ethiopians living in the Rift Valley are exposed to high fluoride levels (Rango *et al.*, 2010; Kut *et al.*, 2016), owing to regular intake of fluoride-infested groundwater exceeding 1.5 mg/L (WHO, 2017). High fluoride levels have been known to occur generally in alkaline volcanic areas of the East African Rift Valley (Bretzler & Johnson, 2015) and Southern Africa.

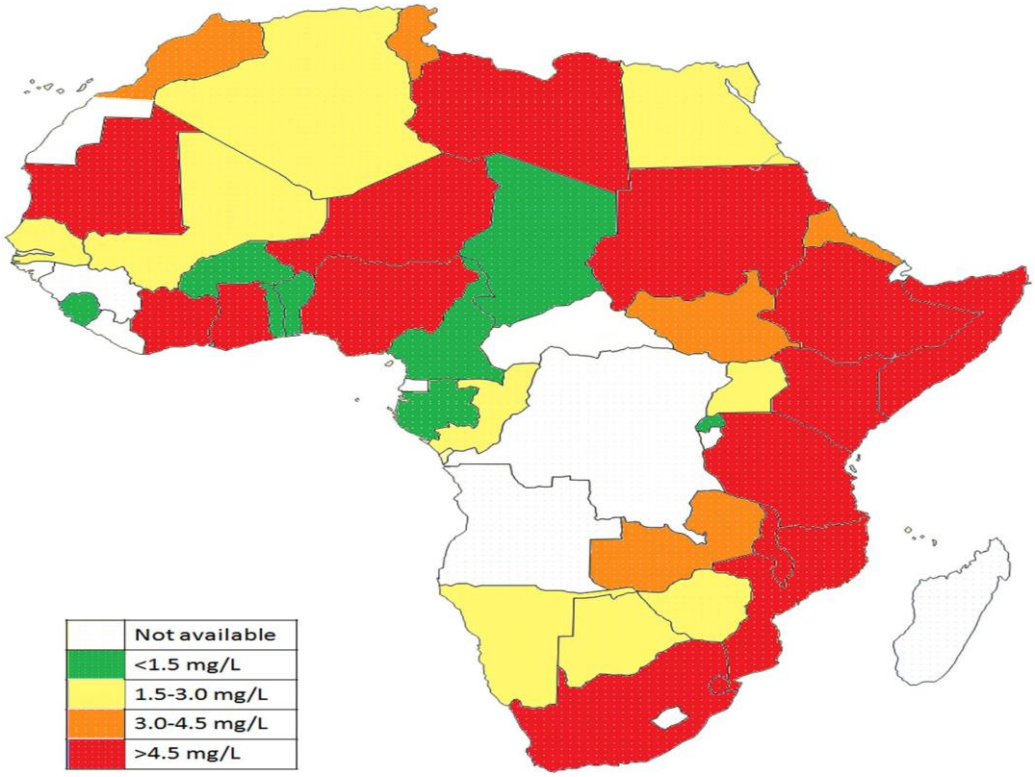

Figure 2.4: Reported fluoride concentrations in selected african groundwaters (Source: Kut *et al.*, 2016).

Different studies on dental fluorosis in the affected areas in South Africa have revealed that the ailment is a function of high fluoride concentrations in groundwater (McCaffrey *et al.*, 2001; Momba *et al.*, 2005; De Chaisemartin *et al.*, 2017). Areas mostly affected are Limpopo (Siloam and Liphalele), Karoo, Northern Cape (Vredendal) and North West province (Mmabatho), Bushveld and Pilanesberg. More than thirty percent of boreholes in Western

© University of Venda

Bushveld and Pilanesberg areas have fluorides levels of between 1mg/L and 30mg/L (Figure 2.5) (McCaffrey & Willis, 2001; Ncube & Schutte, 2005; Odiyo & Makungo 2012). Though the South African government has made remarkable progress in delivering safe drinking water to rural communities, through the centralised systems since 1994, but most of these communities are isolated and dispersed with rough topography, hence, they have not been effectively reached.

Among the challenges being faced with centralised systems are lack of experienced water experts to maintain and upgrade water supply facilities, high financial inputs, inadequate management and violation of drinking water standards (Mackintosh *et al*., 2003; Momba *et al*., 2009; Odiyo & Makungo 2012).

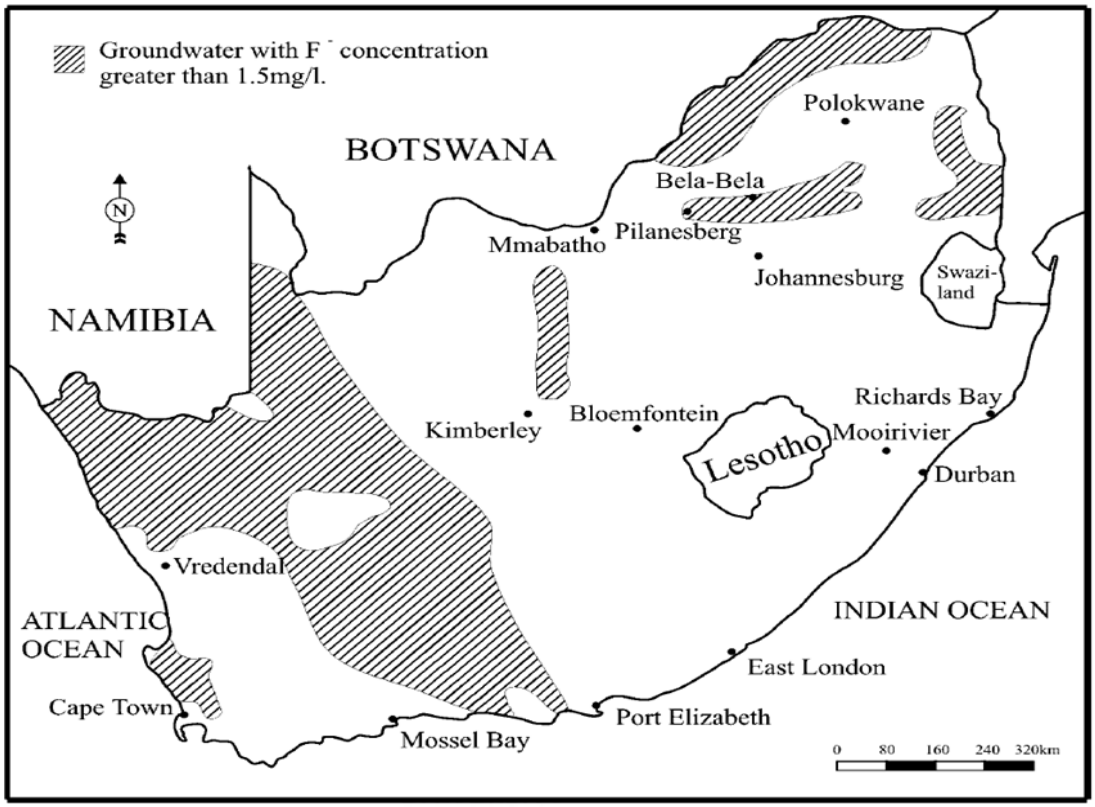

Figure 2.5: Map showing regions in South Africa with groundwater with fluoride concentrations higher than 1.5mg/L (Source: McCaffrey & Willis, 2001).

According to South African National Standard for Drinking Water Quality (SANS 241, 2011), an ideal water treatment system for rural communities should be affordable and be able to reduce contaminants to an acceptable level set by the relevant regulatory bodies. Therefore, there is the need to develop cheap multifunctional household adsorbent for defluoridation of drinking water in these fluorosis prone communities.

© University of Venda

2.3.1 Health effects of ingesting fluoride rich water

Fluoride is often described as a double-edged sword, because inadequate ingestion is associated with dental caries and skeletal fluorosis due to prolonged ingestion at high fluoride concentrations, while excess intake results in fluorosis such as skeletal and dental fluorosis (Table 2.1) (WHO, 2011, 2019). Excess fluoride intake usually occurs through consumption of fluoride-rich groundwater naturally rich in fluoride. Although removal of excessive fluoride from drinking-water may be difficult and expensive, several low-cost technologies are being developed and applied particularly at a local household level.

Table 2.1: Different fluoride doses (long time ingestion through water) and their effects on human body. Source: (WHO, 2011).

Fluoride mg/L	Effect on human body
Below 0.5	Dental caries
0.5 - 1.0	Protection against dental caries. Takes care of bone and teeth
1.5 - 3.0	Dental fluorosis
3.0 - 10.0	Skeletal fluorosis. (adverse changes in bone structure)
Above 10.0	Crippling Skeletal fluorosis and severe Osteosclerosis

Fluoride is often described as a double-edged sword, because inadequate ingestion is associated with dental caries and skeletal fluorosis due to prolonged ingestion at high fluoride concentrations while excess intake results in fluorosis such as skeletal and dental fluorosis (Table 2.1) (WHO, 2011, 2019). Excess fluoride intake usually occurs through consumption of fluoride-rich groundwater naturally rich in fluoride. Although removal of excessive fluoride from drinking-water may be difficult and expensive, several low-cost technologies are being developed and applied particularly at local household level.

Adverse health effects of excess fluoride in water can induce toxic effects by binding with calcium and interfering with the activity of proteolytic and glycolytic enzymes. Fluoride is known to react with gastric acid in the stomach to produce hydrofluoric acid. Acute exposure to high levels of most soluble fluoride compounds results in abdominal pain, excessive saliva, nausea and vomiting, seizures and muscle spasms (Geoff, 2017). The main effect of long-term ingestion of high fluoride levels is fluorosis.

Dental fluorosis can develop owing to intake of water with high levels of fluoride characterised by the appearance of white areas in the enamel. In the more severe form, reduced mineralisation of the enamel results in stained and pitted teeth. In skeletal fluorosis, fluoride accumulates progressively in the bone over a prolonged period of years. Early symptoms are

© University of Venda

pain and stiffness in the joints. Crippling skeletal fluorosis is closely linked with osteosclerosis, calcification of tendons and ligaments and bone deformities (WHO, 2019).

2.4 Available technologies for fluoride removal from water

Generally, there are various water treatment processes for provision of safe drinking water which are chemical precipitation (Aldaco *et al.*, 2005), electrocoagulation flotation and electrodialysis (Loganathan *et al.*, 2013), ion exchange (Pan *et al.*, 2018), membrane filtration process (Kumar *et al.*, 2017), nanofiltration (Waghmare & Arfin, 2015), and adsorption (Ghorai & Pant, 2004; Mudzielwana *et al.*, 2016). Adsorption is the most effective and widely used water treatment process, owing to its effectiveness, low cost, simplicity, environmentally friendliness and universal applicability (Ghorai & Pant, 2004; Mudzielwana *et al.*, 2016).

2.4.1 Defluoridation technologies

Defluoridation is defined as the downward adjustment of fluoride in drinking water to acceptable levels. It is conventional and most acceptable method for delivering safe drinking water to fluorosis endemic communities. Defluoridation technologies are (1) ion exchange (Pan *et al.*, 2018); (2) precipitation-coagulation (Loganathan *et al.*, 2013); (3) electrochemical (Zhu *et al.*, 2007; Bennajah *et al.*, 2009); (4) membrane filtration (Nasr *et al.*, 2013). (5) reverse osmosis (Bennajah *et al.*, 2009; Babu *et al.*, 2011). 6) electrodialysis (ED) (Huang *et al.*, 2007). (7) adsorption (Aldaco *et al.*, 2005; Ghorai & Pant, 2004; Mudzielwana *et al.*, 2016; Kumar *et al.*, 2017; Pan *et al.*, 2018).

© University of Venda

University of Venda
Creating Future Leaders

Table 2.2: Table of defluoridation techniques.

Method	Description	Advantage	Disadvantage	References
(1) Ion exchange	This technique is based on fluoride removal from water with a strongly basic anion exchange resin containing quaternary ammonium functional groups.	Highly efficient at about 99 percent fluoride removal.	Reduced efficiency in the presence of other anions. Large volume of regenerate is required for regeneration of cation and anion exchange resin. Costly and releases fluoride-rich waste. Treated water has a very low pH.	Meenakshi, 2006; Pan *et al.*, 2018.
(2) Precipitation-coagulation	Method is based on the addition of chemicals (coagulants and aids) to water and the subsequent formation of insoluble fluoride precipitates.	The technique is cost effective. No regeneration of media. Design and construction is simple. It has the least disposal problems. No electricity is needed.	Percent fluoride removal is low. Produces hard water. The use of aluminium sulphate as coagulant causes the sulphate ion to increase substantially and exceed the permissible limit of 400 mg/L. The residual aluminium in excess of 0.2 mg/L in treated water causes dementia disease, pathophysiological, neuro behavioural, structural and biochemical changes. It affects cardiovascular, respiratory,	Eswar & Devaraj, 2011; Nayak, 2002; Loganathan *et al.*, 2013.

© University of Venda

			musculoskeletal, endocrine and reproductive systems.	
(3) Electrocoagulation (EC)	This technique involves *in situ* generation of coagulants by dissolving either Al or Fe ion electrically at the anode.	Effective for pollutants removal from water. It does not require addition of chemicals for coagulation. There is no generation of large volumes of sludge.	Expensive technique. Requires technical skills and electricity supply. It is not applicable for rural households.	Zhu *et al.*, 2007 Bennajah *et al.*, 2009.
(4) Membrane filtration	Membrane filtration techniques involves the use of semi-permeable membranes for removing ions from water.	lower operating cost over RO and electrodialysis (ED)	Sensitive to temperature, pH and High maintenance cost. Expensive and very complicated. Removes all the ions present in water. High electrical energy. Not applicable to households in rural areas.	Nasr *et al.*, 2013.
(5) Reverse osmosis (RO)	Reverse osmosis is a physical process whereby the contaminants are removed by applying pressure on the feed water to direct it through	Produces high purity water. High fluoride removal efficiency.	High operating cost. Requires electricity supply. They are not applicable to households in rural areas.	Bennajah *et al.*, 2009. Babu *et al.*, 2011.

© University of Venda

University of Venda
Creating Future Leaders

	a semi-permeable membrane.			
(6) Electrodialysis (ED).	This technique arranges ion exchange. membranes alternately in a direct current field.	Useful in demineralisation.	Higher operating cost than RO. Requires electricity supply. It is not applicable to households in rural areas.	Huang *et al.,* 2007.
(7) Adsorption	Adsorption is a surface phenomenon in which the reactants are of different phases.	Universality, low cost, ease of maintenance, highly effective, simple, environmentally friendly and universally applicable.	Applicable mainly for household water treatment.	Mudzielwana *et al.,* 2016; Izuagie *et al.,* 2017; Obijole *et al.,* 2019; Gitari *et al.,* 2020.

© University of Venda

2.4.1.1 Adsorption

Adsorption is considered the most efficient technology for defluoridation of water. The technology involves filtering of water through a column packed with a strong adsorbent such as activated alumina (Al_2O_3), activated charcoal, or ion exchange resins, bone char and bone, molecular sieves, iron oxides, natural or synthetic zeolites and clay. This method is suitable for both household and community use. When the adsorbent becomes saturated with fluoride ions, the filter material is backwashed with a mild solution of alkali or acid to regenerate and clean it. The household units are more convenient for filtering the small amounts of water intended for drinking only, as better care is taken of them; but an efficient and extensive service system is needed to ensure that the filters are regenerated or replaced at the right time.

Activated Charcoal (AC) is most commonly and widely used for water defluoridation, however, high price of AC makes the cost of operation of this method high, coupled with high flow rate, therefore not suitable for rural household use (Wendimu *et al.*, 2017). Activated Alumina (AA) is also widely used for defluoridation due to its availability and cheapness, however, its disadvantages include low adsorptive capacity and much lower capacity after regeneration (Ghorai & Pant, 2004). Bone char has been found to be a promising adsorbent for defluoridation of water. It easily removes fluoride from water by replacement of its hydroxyl ions by the fluoride ions. Its usage is however discouraging because of socio-cultural factors and because the quality of final water produced after defluoridation is low and often has a rotten meat taste particularly if the bone charring process is not properly carried out (Fawell *et al.*, 2006).

2.4.1.2 Adsorbents for contaminants removal from water

Adsorbents are generally used to remove dissolved contaminants which are not adequately removed by particle-removal processes or destroyed by chemical oxidation during disinfection methods in water treatment (Sobsey, 2002). Among various adsorbents that are widely used are charcoal, activated carbon, natural zeolites as well as bio-sand filters, which have also been used in household water treatment systems (Sobsey, 2002).

2.4.1.3 Charcoal and activated carbon filters as adsorbents

Activated Carbon (AC) is a porous material with a large surface area which is produced by heating of a carbonaceous material such as coal, wood, coconut shells or peat (WHO, 2006). AC is primarily used to remove heavy metals, toxic organic materials, taste and odour from water, including cyanotoxins and pesticides (Sobsey, 2002). AC filters are not effective in microbe removal and can easily become a breeding ground for bacteria, resulting in higher

© University of Venda

bacterial counts in contaminated water. Some commercially available carbon point-of-use filters are impregnated with silver to prevent bacterial colonisation (Sobsey, 2002). AC filters become exhausted over time and will have to be regenerated or replaced, just like any adsorbent. The frequency of regeneration or replacement depends on the adsorptive capacity of the filter and quality of the raw water. In particular, the capacity for specific target contaminants is greatly reduced by the presence of background organic contaminants (WHO, 2011). Frequent replacement of the carbon makes the technique costly, hence making it unaffordable for rural household use. Alternatively, ordinary local charcoal is used as a filter to remove taste, colour and odour (Kayaga & Reed, 2005). Charcoal, though much cheaper than AC, is less effective and must be replaced more frequently. An up-flow granular media filter including a layer of charcoal has been developed by UNICEF (Kayaga & Reed, 2005).

2.5 Water contamination by pathogens

Waterborne diseases outbreak is a global phenomenon despite efforts being made to ensure water safety. The mortality and morbidity arising from drinking pathogen-contaminated water are high and must be controlled by improving the quality of water (Bitton, 2014; Pandey, 2014; WHO, 2015; 2017). The major bacterial contaminants found in water are bacteria, viruses, protozoa, fungi, and helminthes. The worst type of bacterial contaminants in water is *Escherichia coli* (*E. coli*), also known as *E. coli* O157:H7 which causes bloody diarrhea and sometimes cause kidney failure which may also lead to death. Hence, the need for concerted efforts at arresting the situation by developing strategies aimed at inactivating and or removal of these pathogenic contaminants from water.

2.5.1 Health effects of ingesting pathogens-infested water

Waterborne pathogens such as bacterial and microbial contaminants in drinking water are major public health concerns worldwide. This is due to high morbidity and mortality arising from numerous waterborne diseases which are often lethal. Waterborne diseases are responsible for an estimated 2.2 million deaths per year including diarrhea, cholera, urinary tract infections and other gastrointestinal diseases and infections, with over 80% of these deaths occurring in Africa and Asia (Bitton, 2014; WHO, 2015; 2019). About 1.4 million of these deaths are children mostly from the developing world (Bitton, 2014; WHO, 2015; 2019). Studies conducted in South African rural communities which largely depend on groundwater for drinking purposes, showed that the dwellers in these communities have developed medical symptoms traceable to pathogen contaminants in water (Ncube, 2005; Momba *et al.*, 2013). To

© University of Venda

prevent waterborne diseases in these communities, a new approach to deliver bacteriologically safe drinking water to these communities at household (point-of-use) levels should be developed particularly in isolated areas, where centralized systems are not economically feasible and viable.

2.5.2 Available technologies for pathogen removal from groundwater

Although some of the available technologies for pathogen removal from drinking water are effective, some are unsustainable and unsuitable for application particularly in rural communities. The various methods which have been used for pathogen (coliform) inactivation and removal from water are well documented in the literature. This ranges from simple conventional treatments to modern technologies which include physical methods, such as boiling, heating (fuel and solar), settling, filtering, exposing to the UV radiation in sunlight, and UV disinfection with lamps, and chemical methods such as coagulation-flocculation and precipitation, adsorption, ion exchange and chemical disinfection with germicidal agents (Lantagne *et al.*, 2006; Potgieter, 2007; Connelly & Baeumner, 2012; Ingerson-Mahar & Reid, 2012; Singh *et al.*, 2013; Bridle & Desmulliez, 2014). It should be noted that many of these methods are not suitable for rural household applications (Lantagne *et al.*, 2006; Potgieter, 2007; Dunn *et al.*, 2014; Whelan *et al.*, 2014; Ramírez-Castillo *et al.*, 2015).

However, simple water treatment technologies such as boiling, sedimentation, solar disinfection, filtration, chlorination, and the combined treatments of chemical coagulation-filtration have been proven to improve microbiological quality by reducing bacteria, viruses and in some cases protozoa in water samples (Lantagne *et al.*, 2006; WHO, 2010). Adeeyo. (2014) his studies of multi-step strain improvement of L. edodes for exopolysaccharide production, succeeded in improvement of the material towards water remediation.

The antibacterial activities of Ag-zeolite nanocomposites have been reported by many authors which led to their broad applications in diverse fields (Shameli *et al.*, 2012; Shameli *et al.*, 2011; Yuranova *et al.*, 2003). Antibacterial properties of silver nanoparticles prepared via green method were investigated by Shameli *et al.* (2012). This study revealed that the Ag-NPs with different stirring times showed inhibition towards the tested gram-negative and gram-positive bacteria. Silver-nanoparticles have been known to have various activities against bacteria and fungi, some of which are listed as follows: *Escherichia coli* (*E. coli*) (Kim *et al.*, 2007; Li *et al.*, 2011; Raffi *et al.*, 2010; Zhang *et al.*, 2000). *Staphylococcus aureus* (El-Rafie *et al.*, 2012; Kim *et al.*, 2007) Smetana *et al.*, 2008). *Pseudomonas aeruginosa* ((Balogh *et al.*, 2001; Shukla *et al.*, 2012). This study however employed simple technology where the

© University of Venda

antibacterial activities of the developed clay were evaluated with Gram-negative *Escherichia coli* sensitive indicator strains by using well diffusion assay method. The zone of inhibitions was recorded in millimeter (mm). The bacterial suspensions were prepared with the turbidity of 0.5 McFarland. Muller-Hinton agar plates was prepared by suspending 38 g of the medium in 1 liter of milli-Q water and heated with frequent agitation followed by boiling to completely dissolve the medium. The agar was sterilised by autoclaving at 121 °C for 15 min and thereafter cooled to room temperature. The cooled Mueller-Hinton agar (25 mL) was poured into sterile petri plates placed on a level, horizontal surface to give a uniform depth. Allow to cool to room temperature. Check and ensure the final pH is pH is 7.3 ± 0.1 at room temperature and store the petri plates upside down to prevent contamination at 2 - 8 °C. Mueller-Hinton agar plates were inoculated with *E. coli* (ATCC 35218) strains. Wells with a diameter of 6 mm were cut using a cork borer and filled with 30 µL of the activated clay soil samples. Plates were incubated for 24 h at 37 °C. After incubation, the growth inhibition zone diameters were measured in millimeter (mm). All the materials and glassware used in the analysis were sterilised for 30 min at 121°C in an autoclave before each of the experiments was carried out. The plates as well as the samples were carefully packed in sealed disposable plastic bags for destruction immediately after the measurements were made.

2.6 Zeolites adsorbents for contaminants removal from water

Zeolites are hydrated aluminosilicates which have both ion exchange and molecular sieve properties. Zeolites are preferred choice in water treatment owing to their abundance in nature, low cost, ease of modification to remove certain chemical contaminants, and their regenerative properties (Widiastuti *et al.*, 2008).

Synthesis of adsorbents from coal fly ash (CFA) and other aluminosilicates-rich materials for defluoridation have been reported by various authors. These include materials such as clay (Agarwal *et al.*, 2003), CFA (Waghmare & Arfin, 2015; Wang *et al.*, 2008), Red Mud (Tor *et al.*, 2009), activated kaolinites (Meenakshi *et al.*, 2008), china clay (Waghmare & Arfin, 2015), bentonite and montmorillonite (Tor *et al.*, 2006; Mudzielwana *et al.*, 2017), zeolites (Onyango *et al.*, 2004; Musyoka *et al.*, 2011) for defluoridation of groundwater. Others include ceramic adsorbents such as mesoporous granular materials (Chen *et al.*, 2010).

© University of Venda

Table 2.3: Table of adsorbents from CFA and other aluminosilicates-rich materials for defluoridation.

Adsorbents	References
Red Mud	Tor *et al.,* 2009.
Activated Kaolinites	Meenakshi *et al.,* 2008.
Bentonite and Montmorillonite	Tor *et al.,* 2006; Mudzielwana *et al.,* 2017.
Mesoporous granular materials	Chen *et al.,* 2010.
Diatomaceous Earth	Izuagie *et al.,* 2016; 2017.
China Clay	Waghmare & Arfin, 2015.
Clay	Agarwal *et al.,* 2003; Obijole *et al.,* 2019; Gitari *et al.,* 2020
Coal Fly Ash (CFA)	Wang *et al.,* 2008; Waghmare & Arfin, 2015.
Zeolites	Onyango *et al.,* 2004; Musyoka *et al.,* 2009; 2011.

2.7 Clay soils as adsorbents for defluoridation

The search for low-cost, household, simple and an acceptable method for efficient defluoridation of water for rural and household usage lead to the choice of clay materials, since clay soil minerals are widespread and are in great abundance around the world. The term ‘clay minerals’ refers to naturally occurring fine-grained phyllosilicate minerals which impart plasticity to clay and hardened when dried or fired (Guggenheim & Martin, 1995). There are different types of clays which are kaolinite, illite, bentonite and montmorillonite (Guggenheim & Martin, 1995). The knowledge about the chemistry and structure of clay soil minerals has significantly increased and its use has greatly expanded due to recent advances in instrumental analytical methods such as electron microscopy, spectroscopy, and X-ray diffraction. Attention is now focusing on the properties of clay as natural nano-sized particles which find application in adsorption, catalysis, and in nanotechnology research on synthetic materials (Guggenheim & Martin, 1995; Coetzee *et al.,* 2003).

Clay minerals can be broadly classified into two types, 1:1 or 2:1 based on their layered structure. A 1:1-type clay mineral consists of one tetrahedral sheet and one octahedral sheet. Examples are kaolinite, halloysite and serpentine. A 2:1-type clay mineral is composed of an octahedral sheet sandwiched between two tetrahedral silicate (SiO) sheets. Examples include talc, vermiculite, montmorillonite, saponite, and sepiolite. Clays contain the following main elements: aluminum, silicon and oxygen; others are iron, magnesium, alkali metals, alkaline earths, and other cations present either in the interlayer space or in the lattice framework by isomorphous substitution (Konta, 1995). Clays and clay minerals have been used by man since

© University of Venda

the stone-age, primarily due to abundance of clay minerals on the earth's surface and are utilised widely for ceramics, building materials and agriculture.

The South African clay deposits are broadly classified into three dominant clay minerals: (a) kaolin fields with the dominant clay minerals being kaolinite; (b) bentonite fields in which the dominant clay minerals being montmorillonite, which form part of the smectite group; (c) palyorskite fields with dominant clay being palygorskite. Adsorption studies on clays and bauxite show that bauxite has the best adsorption capacities followed bentonite and palygorskite, while kaolin had the lowest adsorption capacities for defluoridation (Coetzee *et al.*, 2003).

Various independent studies carried out by subjecting clay to high temperatures produced clay wares with optimal fluoride binding capacity. The results of these studies showed that clay could be a promising choice as efficient adsorbent for defluoridation of water (Ndegwa, 1980; Zewge & Moges, 1990; Hauge *et al.*, 1994). Other examples of clay materials that are promising adsorbents for defluoridation are laterite (Sarkar *et al.*, 2006), mechanochemically-activated kaolinites (Meenakshi *et al.*, 2008), China clay (Chaturvedi *et al.*, 1988), bentonite and montmorillonite (Tor, 2006).

Srimurali *et al* (1998) reported the use of bentonite, kaolinite, lignite, charfines and nirmali seeds for fluoride removal from water by batch method where 46% removal was observed at optimum conditions. Defluoridation of zirconium-loaded bentonite was carried out by Ma e*t al*. (2005). Ma e*t al*. (2005) established that maximum adsorption of fluoride took place at $pH < 6$ and the fluoride adsorption was preceded by ion exchange mechanism in water. The adsorption potential of magnesium, lanthanum, and manganese oxide-loaded bentonite clay was reported by Kamble *et al.* (2009) for defluoridation of water. The modified metal oxides adsorbent showed better fluoride adsorptive capacities in water than the unmodified adsorbent. Thakre *et al.* (2010) have also carried out bentonite clay modification using magnesium chloride to enhance defluoridation, hence an effective adsorbent for water defluoridation. Vhahangwele, *et al.* (2014) synthesised Al^{3+}-modified bentonite clay adsorbent by ion exchange method. Comparative studies on the adsorbent using batch experiment show that the modified clay adsorbent has a high fluoride adsorptive capacity. An efficient fluoride adsorbent was successfully synthesised by coating Na-activated bentonite with MnO_2 through *in-situ* reduction of $KMnO_4$. The study showed some promising defluoridation capabilities, however, recommendation is made for improvement on the adsorbent stability (Mudzielwana *et al.*, 2017). Mudzielwana *et al.* (2018) developed a low-cost adsorbent from Mn^{2+}-modified

© University of Venda

bentonite clay and applied for defluoridation of groundwater. The results showed optimum F^- uptake occurred within the first 30 min contact time and the percent removal increased with increasing adsorbent dosage. Furthermore, the batch results showed that pH of the solution governed the percent of fluoride removal with the optimum of 75.2% fluoride removal achieved at pH 4. The study demonstrated that Mn^{2+}-intercalated bentonite clay has potential for application in defluoridation of groundwater.

Evaluation of the application of smectite-rich clay soil from Mukondeni, in defluoridation of groundwater showed that 0.8 g/100 mL of the clay removed up to 92% of fluoride from the initial concentration of 3 mg/L at a pH of 2 with a contact time of 30 min (Mudzielwana *et al.,* 2016). Nigiri *et al.,* (2017) investigated cow bone char as sorbent for the defluoridation of aqueous solutions. The cow bone char was characterised in terms of its morphology, chemical composition, and functional groups present on the bone char surface using different analytical techniques: scanning electron microscopy (SEM), energy dispersion spectroscopy (EDS), nitrogen adsorption-desorption Brunauer-Emmett-Teller (BET) (N_2-BET) method and fourier transform infra red (FTIR) spectroscopy. Batch equilibrium studies were performed for the bone chars prepared using different procedures. The sorption capacities for fluoride were q = 6.2 ± 0.5 mg/g and q = 6.4 ± 0.3 mg/g for acid-washed and aluminium-doped bone char sorbents respectively. The potential of mixed Mukondeni clay soils (MMCS) as low-cost adsorbent for defluoridation from groundwater was studied by Ngulube *et al. (*2017). The results indicated that the optimum conditions for the defluoridation of water using MMCS were 60 min, 1.5 g, 9 mg/L, 1.5/100 S/L ratio, pH of 2 and 298K. Although the study showed that locally available MMCS are good defluoridation materials, modification via metal oxide blending was recommended for an enhanced adsorption capacity. Wang *et al*. (2017) in their studies observed a highly efficient fluoride adsorption capacity from aqueous solution by nepheline prepared from kaolinite through alkali-hydrothermal process. Studies conducted by Amor *et al.* (2018), in which Tunisian raw clays were used in defluoridation revealed the optimum defluoridation capacity at 30 min contact time, 20 g/L of clay dose, and pH = 3 to be promising.

Ayinde *et al.* (2018) successfully synthesised a multi-functional 3-layered Ag-MgO/nanohydroxyapatite (Ag-MgOnHaP) composite via a combined microwave and ultrasonically-modified methods towards simultaneous defluoridation and pathogen removal from groundwater. The study showed optimum adsorption capacity of 2.15 mg/g at pH 6 and 298 K, with over 90% fluoride removal at 0.3g dosage. The results showed the nanocomposite

© University of Venda

to be potentially active against *E. coli* and *K. pneumonia* strains and good adsorbent for groundwater defluoridation.

In the study carried out by Gidi *et al.* (2019), a novel cost-effective, eco-friendly clay composite adsorbent was developed from mixtures of clay, grog, bone char, and sawdust, towards fluoride remediation. The maximum of 91.6% fluoride removal efficiency was obtained. The composite clay material exhibited excellent removal efficiency for the real water samples analysed. In the study in which aluminosilicate-rich clay soils were prepared through mechanochemical activation and applied for defluoridation and pathogen removal, the maximum adsorption capacity was found to be 1.87 mg/g with 32% fluoride removal. The results indicated activated clays' potential for defluoridation but not effective in pathogen removal, hence, further modifications of the clays' surfaces were recommended (Obijole *et al.*, 2019). In the study by Gitari *et al.* (2020), a trimetal Mg/Ce/Mn oxide-modified diatomaceous earth (DE) was synthesised at optimal conditions and applied for defluoridation. The optimum fluoride uptake capacity was 12.63 mg/g at the initial fluoride concentration of 100 mg/L. Fluoride removal was > 91 % for solutions with initial pH range of ~4 - 11 (initial fluoride concentration: 9 mg/L, sorbent dosage: 0.6 g/100 mL).

2.8 Hydrothermal technology

The term "hydrothermal" has its origin from geology. British-born geologist, Sir Roderick Murchison (1792 - 1871) used the term to describe the action of water at elevated pressure and temperature on the earths' crust which led to the formation of various minerals and rocks (Byrappa, 1990). The formation of largest single crystal in nature (beryl crystal of > 1,000 kg) and quartz crystals of several thousands kg which is the largest quantity of single crystals created by man in one experimental run has been traced to hydrothermal origin (Byrappa, 1990).

Hydrothermal processing is defined as the reaction of any homogeneous (nanoparticles) or heterogeneous (bulk materials) in the presence of aqueous solvents or mineralisers under high pressure and temperature conditions to dissolve and recrystallise (recover) materials that are relatively insoluble under ordinary conditions. Byrappa & Yoshimura (2012) define hydrothermal as any homogeneous or heterogeneous chemical reaction in the presence of a solvent (whether aqueous or non-aqueous) above the room temperature and at pressure greater than 1 atmosphere in a closed system.

Hydrothermal technology facilitates the fabrication of some of the toughest or the most complex material(s) with desired physicochemical properties. The advantages of hydrothermal

© University of Venda

technology over other conventional processes are energy saving, simplicity, cost-effectiveness, better nucleation control, pollution-free (since the reaction is carried out in a closed system), higher dispersion, higher rate of reaction, better shape control, and lower temperature of operation in the presence of an appropriate solvent, etc (Yoshimura & Byrappa, 2008).

The hydrothermal technology has a lot of advantages like native elements, metal oxides, hydroxides, silicates, carbonates, phosphates, sulphides, tellurides, nitrides, selenides etc. Particles and nanostructures like nanotubes, nanowires, nanorods, and so on have been obtained using the hydrothermal method (Byrappa & Yoshimura, 2012). The method is also popular for the synthesis of a variety of forms of carbon like sp^2, sp^3 and intermediate types (Chu & Li, 2006; Yoshimura & Byrappa, 2008). Hydrothermal method was first used in 1845 by Schafthual in the preparation of fine quartz particles in a papin's digester. This was followed by the synthesis of various silicates, clays, hydroxides and oxides minerals. Over 150 mineral species were synthesised including diamond by 1900 (Morey & Niggli, 1913). Application of hydrothermal technology commercially started in 1908 when leached bauxite mineral was bleached under hydrothermal conditions to obtain aluminum (Bayer, 1887). This were followed by the synthesis of various minerals in the 1940s where bulk crystal growth and phase equilibria studies were conducted (Suto *et al.*, 2007; Yoshimura & Byrappa, 2008).

Hydrothermal method is now used in the processing of a wide range of materials including bulk crystals, nanoparticles and fine nanoparticles with a controlled size and morphology.

2.8.1 Hydrothermal processing of fine particles

The processing of fine particles hydrothermally to nanocrystalline materials could be dated back to 1840s to early 1900s, but the developed materials could not be confirmed due to limitations in the instruments available then, except some chemical techniques (Byrappa *et al.*, 2006). A lot of work were done on the synthesis of fine particles of some silicate, hydroxides, zeolites and clays (Morey, 1953). Barrer's work on hydrothermal synthesis of particles of zeolites in the 1940s, ushered in a new era of molecular sieve technology. The late 1960s brought excellent crystallinity and reproducibility, microstructure control, high reactivity and sinter ability (Byrappa, 2005). Varieties of highly crystalline, fine ceramic materials were synthesised using hydrothermal technology, hence, taking the advantages of hydrothermal method over conventional methods such as moulding, heat treatment, hot pressing and firing (Lobachev, 1973; Mitsuda, 1980; Byrappa, 1990; Somiya, 1990; Somiya, 2006).

© University of Venda

The hydrothermal research has ushered in the processing of fine particles to ultra-fine particles with a controlled size and shape, controlled morphology, high purity, controlled stoichiometry, high quality, narrow particle size distribution, uniformity, lesser defects and dense particles. The hydrothermal technology is most suitable method for growing large bulk crystals of quartz, berlinite, gallium phosphate, and synthesis of zeolites and other clay materials (Byrappa, 1990; Somiya, 2006).

2.8.2 Hydrothermal preparation of nanocomposites

The hydrothermal technology is now emerging as a vital tool in nanocomposites preparation. Different types of nanocomposites have been reported to be developed within few hours at lower temperature in the presence of appropriate solvent and or organic ligands. Examples of nanocomposites are zeolites:CNT, TiO_2:activated carbon, ZnO:activated carbon, TiO_2:CNT, TiO_2:HAp, ferrites:polymer, organic–inorganic composites, polymer and semiconductor composites (Sujaridworakun *et al.*, 2005; Byrappa *et al.*, 2006: Dayananda *et al.*, 2007).

Liu *et al.* (2011) reported highly porous magnesium oxide (MgO) nanoflakes developed by the calcination of magnesium hydroxide nanoflakes via hydrothermal process. The MgO nanoflakes had a high specific surface area with an exceptional As (III) removal performance from aqueous solutions, much higher than most reported values from other metal oxide nanomaterials. Johnson *et al.* (2014) successfully synthesised zeolite A from natural kaolin (metakaolin) and NaOH mixtures by stirring for 30 min before hydrothermal treatment at 100 °C for 8 h. The application of hydrothermally-modified limestone powder in presence of the phosphoric acid (PA) for fluoride adsorption behaviour was reported by Gogoi *et al.* (2016). The hydrothermally-modified limestone product obtained using 0.90 M phosphoric acid (PA), with an adsorption capacity of 6.45 mg/g , was observed to have potential for application in defluoridation of water. Lyu, *et al.* (2016) prepared a cost-effective adsorbent for fluoride removal by loading activated aluminum and lanthanum onto hydrothermally treated palygorskite (HP) (denoted as La-Al-TAP). The materials showed strong potential for defluoridation. Pure zeolite X with remarkable thermal stability and promising defluoridation potential was prepared from aluminosilicate-rich diatomite via a simple hydrothermal method at 5 h contact time, 110 °C crystallisation temperature, 30 °C ageing temperature, 30 min ageing time, H_2O/Na_2O ratio of 40 and Na_2O/SiO_2 ratio of 1.4 by Yao *et al* (2018). Nagaraj *et al* (2018) in their studies successfully developed a mineral-substituted hydroxyapatite (mHAp) nanocomposite adsorbent via a one-pot hydrothermal synthesis method and further evaluated for

© University of Venda

fluoride removal in water samples. The synthesised material was found to have a high fluoride removal capacity.

2.9 Knowledge gaps, summary and conclusion

Groundwater is the main source of drinking water worldwide. Fluoride concentrations at elevated concentrations and pathogens in groundwater have been proven to be pose health risks to human health. Literature reported that fluorosis is endemic in 26 countries with over 200 million people worldwide are at risk of fluorosis while 2.2 million death occur yearly due to ingestion of pathogen-infested groundwater. Some of the countries where incidence of fluorosis has been reported include India, China, Mexico, Uganda, Kenya, Ethiopia, Sudan, Chad, Morocco, Mozambique Tanzania, Malawi, Cameroon and South Africa. Areas most affected in South Africa are Karoo, Bushveld, Limpopo and North-West provinces, particularly in rural communities where groundwater is the main source of water for drinking purposes.

There are various technologies available for defluoridation. These include adsorption, ion exchange, precipitation and coagulation, membrane-based technology and adsorption. Amongst these technological innovations, adsorption is often the preferred choice particularly for application in rural areas since it uses materials that are largely available in nature at little or no cost, easy to operate, simplicity and high fluoride removal efficiency. Most of the proposed materials including zeolites, diatomaceous earth, mesoporous granular materials, various forms of clay and its modified forms, reported in literature are either not effective or effective at a narrow pH range and some cannot be regenerated effectively. Hence there is urgent need to develop a suitable multifunctional and appropriate technology that will be effective at wide pH range for excellent defluoridation and pathogen removal from groundwater. Furthermore, the developed adsorbent should be low-cost and be regenerable to make it more sustainable for use not only in rural areas of African continent but worldwide.

© University of Venda

REFERENCES

Abiye, T., Bybee, G & Leshomo, J. (2018). Fluoride concentrations in the arid Namaqualand and the Waterberg groundwater, South Africa: Understanding the controls of mobilization through hydrogeochemical and environmental isotopic approaches. *Groundwater for Sustainable Development*, *6*, 112-120.

Adeeyo A. O (2014). Multi-Step strain improvement of L. edodes for exopolysaccharide production. Master's Thesis submitted to Ladoke Akintola University of Technology, Nigeria. 1-312.

Agarwal, M., Rai K., Shrivastav, R & Dass, S. (2003). Defluoridation of water using amended clay. *Journal of Cleaner Productions*, 11 439-444.

Ahamad, K. U., Singh, R., Baruah, I., Choudhury, H., & Sharma, M. R. (2018). Equilibrium and kinetics modeling of fluoride adsorption onto activated alumina, alum and brick powder. *Groundwater for Sustainable Development*, *7*, 452-458.

Aldaco, R., Irabien, A., & Luis, P. (2005). Fluidized bed reactor for fluoride removal. *Chemical Engineering Journal*, *107*(1-3), 113-117.

Al-Gheethi, A. A. S., Noman, E. A., Mohamed, R. M. S. R., Talip, B. A., Kassim, A. H. M., & Ismail, N. (2019). Disinfection Technologies for Household Greywater. In *Management of Greywater in Developing Countries* (pp. 185-203). Springer, Cham.

Amor, T. B., Kassem, M., Hajjaji, W., Jamoussi, F., Amor, M. B., & Hafiane, A. (2018). Study of Defluoridation of Water Using Natural Clay Minerals. *Clays and Clay Minerals*, *66*(6), 493-499.

Anthony A. Izuagie., Wilson M. Gitari & Jabulani R. Gumbo. (2016). Synthesis and performance evaluation of Al/Fe oxide coated diatomaceous earth in groundwater defluoridation: Towards fluorosis mitigation. *Journal of Environmental Science and Health, part a.* 51 10 810–824

Ayinde, W. B., Gitari, W. M., Munkombwe, M., & Amidou, S. (2018). Green synthesis of Ag/MgO nanoparticle modified nanohydroxyapatite and its potential for defluoridation and pathogen removal in groundwater. *Physics and Chemistry of the Earth, Parts A/B/C*, *107*, 25-37.

Azari, A., Kalantary, R. R., Ghanizadeh, G., Kakavandi, B., Farzadkia, M., & Ahmadi, E. (2015). Iron–silver oxide nanoadsorbent synthesised by co-precipitation process for fluoride removal from aqueous solution and its adsorption mechanism. *RSC Advances*, *5*(106), 87377-87391.

© University of Venda

Balogh, L., Swanson, D. R., Tomalia, D. A., Hagnauer, G. L., & McManus, A. T. (2001). Dendrimer − silver complexes and nanocomposites as antimicrobial agents. *Nano Letters*, 1 1 18-21.

Barrett, C. E. (2019). Impact of Public Health Interventions on Drinking Water–Associated Outbreaks of Hepatitis A—United States, 1971–2017. *MMWR. Morbidity and Mortality Weekly Report*, *68*.

Bayer, K. J (1887) cited by Habashi. F. In: A textbook of hydrometallurgy. Libraire Universitaire du Quebec, Canada (1993), p 10.

Bennajah, M., Gourich, B., Essadki, A. H., Vial, C. H & Delmas, H. (2009). Defluoridation of Morocco drinking water by Electrocoagolation/Electroflotation in an electrochemical external-loopairlift reactor. *Chemical Engineering Journal*, 148 122-131.

Bukhari, S. S., Behin J., Kazemian H & Rohani S. A. (2014). Comparative study using direct hydrothermal and indirect fusion methods to produce zeolites from coal fly ash utilizing single-mode microwave energy. *Journal of Material Science*, 49 8261–8271.

Brahma, S. (2018). Geogenic Fluoride Contamination in Two Diverse Geological Settings in West Bengal. In *Clean and Sustainable Groundwater in India* (pp. 39-60). Springer, Singapore.

Braune, E., & Xu, Y. (2010). The role of ground water in Sub-Saharan Africa. *Groundwater*, *48*(2), 229-238.

Bretzler, A & Johnson, C. A. (2015). The geogenic contamination handbook: addressing arsenic and fluoride in drinking water. *Applied Geochemistry*, *63*, 642-646.

Brindha, K & Elango, L. (2011). Fluoride in groundwater: causes, implications and mitigation measures. *Fluoride Properties, Applications and Environmental Management*, *1*, 111-136.

Byrappa, K. (Ed) (1990). Hydrothermal growth of crystals. Progressive Crystal Growth Characterisation 21.

Byrappa, K. (2005) In: Kirk-Othmer encyclopedia of chemical technology. John Wiley & Sons, London.

Byrappa, K., Subramani, A. K., Ananda, S., Rai, K. L., Sunitha, M. H., Basavalingu, B., & Soga, K. (2006). Impregnation of ZnO onto activated carbon under hydrothermal conditions and its photocatalytic properties. *Journal of Materials Science*, *41*(5), 1355-1362.

© University of Venda

Byrappa, K., & Yoshimura, M. (2012). *Handbook of hydrothermal technology*. William Andrew Publications, 2nd edition. NJ, USA. eBook ISBN: 9781437778366.

Chen, Nan., Zhang, Z. Y., Feng, C. P., Sugiura, P., M. Li, M & Chen, R. Z. (2010). Fluoride Removal from water by granular ceramic adsorption, *Journal of Colloid and Interface Science*, 348 579-584.

Chu, P. K., & Li, L. (2006). Characterization of amorphous and nanocrystalline carbon films. *Materials Chemistry and Physics*, *96*(2-3), 253-277.

Coetzee, P. P., Coetzee, L. L., Puka, R & Mubenga, S. (2003). Fluoride adsorption modelling and characterisation of clays for defluoridation of natural clays. *Water South Africa*, 29 3 331-338.

Dahi, E. (2016). Africa's U-Turn in defluoridation policy: From the Nalgonda technique to bone char. *Fluoride*, *49*(4), 401.

Dayananda, A. S., Sajan, C. P., Basavalingu, B., Byrappa, K., Soga, K & Yoshimura, M. (2007). Hydrothermal preparation of ZnO:CNT and TiO 2 :CNT composites and their photocatalytic applications. *Journal of Material Science, 42 231.*

De Chaisemartin, M., Varady, R. G., Megdal, S. B., Conti, K. I., van der Gun, J., Merla, A., ... & Scheibler, F. (2017). Addressing the groundwater governance challenge. In *Freshwater Governance for the 21st Century* (pp. 205-227). Springer, Cham.

Dunn, G., Harris, L., Cook, C. and Prystajecky, N. (2014). A comparative analysis of current microbial water quality risk assessment and management practices in British Columbia and Ontario, Canada. *Science of Total Environment*, 468–469 544–552.

El-Rafie, M., Shaheen, T. I., Mohamed, A., & Hebeish, A. (2012). Bio-synthesis and applications of silver nanoparticles onto cotton fabrics. *Carbohydrate Polymers*, *90*(2), 915-920.

Fantong, W. Y., Satake, H., Ayonghe, S. N., Suh, E. C., Adelana, S. M., Fantong, E. B. S., ... & Zhang, J. (2010). Geochemical provenance and spatial distribution of fluoride in groundwater of Mayo Tsanaga River Basin, Far North Region, Cameroon: implications for incidence of fluorosis and optimal consumption dose. *Environmental Geochemistry and Health*, *32*(2), 147-163.

Fawell, J., Bailey, K., Chilton, J., Dahi, E., Fewtrell, L & Magara, Y. (2006). Fluoride in drinking water, Published on behalf of WHO by IWA Publishing, London.

Geoff, Pain, (2017). Pain in the Gut - Fluoride damage to the gastrointestinal tract. 10.13140/RG.2.2.15283.94248.

© University of Venda

Gevera, P., Mouri, H & Maronga, G. (2019). Occurrence of fluorosis in a population living in a high-fluoride groundwater area: Nakuru area in the Central Kenyan Rift Valley. *Environmental Geochemistry and Health*, *41*(2), 829-840.

Gidi, L. D., Amare, E. Z., Murthy, H. A., & Abebe, B. (2019). Application of Novel Clay Composite Adsorbent for Fluoride Removal. *Material Science Research India*, *16*(2), 164-173.

Gitari, M. W., Petrick, L. F & Musyoka, N. M. (2016). Hydrothermal conversion of South African coal fly ash into pure phase zeolite Na-P1. In *Metals and Non-metals 'Zeolites-Useful minerals'* Claudia Belviso (Ed). 25-42.

Gitari, W. M., Izuagie, A. A., & Gumbo, J. R. (2020). Synthesis, characterisation and batch assessment of groundwater fluoride removal capacity of trimetal Mg/Ce/Mn oxide-modified diatomaceous earth. *Arabian Journal of Chemistry*, *13*(1), 1-16.

Gogoi, S., & Dutta, R. K. (2016). Fluoride removal by hydrothermally modified limestone powder using phosphoric acid. *Journal of Environmental Chemical Engineering*, 4 1 1040-1049.

Goswami, P., Sharma, A., Sharma, S., & Verma, S. (2015). Defluoridation of water using low cost adsorbent. *International Journal of Chemical Studies*, *3*(2), 109-112.

Ghorai, S. & Pant, K. K. (2005). Equilibrium, kinetics and breakthrough studies for adsorption of fluoride on activated alumina. *Seperation and Purification Technology*, 42, 265–271.

Guggenheim, S. & Martin, R. T. (1995). Definition of clay and clay mineral: Joint report of the AIPEA and CMS nomenclature committees. Clays and Clay Minerals 43 2 255–256.

Greenwood, N. N & Earnshaw, A. (1998). *Chemistry of the Elements* (2nd ed). Oxford: Butterworth Heinemann. Pp795 ISBN 0-7506-3365-4.

Hauge, S., Österberg, R., Bjorvatn, K., & Selvig, K. A. (1994). Defluoridation of drinking water with pottery: effect of firing temperature. *European Journal of Oral Sciences*, *102*(6), 329-333.

Hollman, G. G., Steenbruggen, G & Janssen-Jurkovicˇova, M. (1999). A two-step process for the synthesis of zeolites from coal fly ash. *Fuel*, 78 1225–1230.

Höller, H., & Wirsching, U. (1985). Zeolite formation from fly ash. *Fortschritte Der Mineralogie*, *63* 1 21-43.

http://www.unicef.org/wes/files/wf13e.pdf

Hunter, P. R., Payment, P., Ashbolt, N. & Bartram, J. (2003). Assessment of risk. In Assessing Microbial Safety of Drinking Water: Improving Approaches and Methods; Dufour, A.,

© University of Venda

Snozzi, M., Koster, W., Bartram, J., Ronchi, E., Fewtrell, L., Eds.; World Health Organization by IWA Publishing: 79–103.

Ingerson-Mahar, M & Reid, A. (2012). Microbes in Pipes: The Microbiology of the Water Distribution System. A Report on an American Academy of Microbiology Colloquium; ASM Academy: Boulder, CO, USA. 26.

Jaccaud, M., Faron, R., Devilliers, D & Romano, R. (2000). "Fluorine". *Ullmann's Encyclopedia of Industrial Chemistry*. Weinheim: Wiley-VCH. pp. 381–395. doi:10.1002/14356007.a11_293.

Jagtap, S., Yenkie, M. K., Labhsetwar, N., & Rayalu, S. (2012). Fluoride in drinking water and defluoridation of water. *Chemical Reviews*, *112*(4), 2454-2466.

Johnson, E. B. G., Arshad, S. E., & Asik, J. (2014). Hydrothermal synthesis of zeolite A using natural kaolin from KG. Gading bongawan sabah. *Journal of Applied Sciences,* 14 23 3282-3287.

Kamble, S. P., Dixit, P., Rayalu, S. S & Labhsetwar, N. K. (2009). "Defluoridation of drinking water using chemically modified bentonite clay," *Desalination,* 249 2 687–693.

Kayaga, S., & Reed, R. (2005). Emergency treatment of drinking water at point-of-use. WHO – Technical Notes for emergencies. Technical Note No. 5. World Health Organization, Water, Sanitation, Hygiene and Health Unit, Geneva, Switzerland.

Konta, J. (1995). Clay and Man: Clay raw materials in the service of man. *Applied Clay Science,* 10 275–335.

Kim, J. S., Kuk, E., Yu, K. N., Kim, J. H., Park, S. J., Lee, H. J & Hwang, C. Y. (2007). Antimicrobial effects of silver nanoparticles. *Nanomedicine: Nanotechnology, Biology and Medicine*, *3*(1), 95-101.

Kumar, M. S., Dhakate, R., Yadagiri, G., & Reddy, K. S. (2017). Principal component and multivariate statistical approach for evaluation of hydrochemical characterisation of fluoride-rich groundwater of Shaslar Vagu watershed, Nalgonda District, India. *Arabian Journal of Geosciences*, *10*(4), 83.

Kut, K. M. K., Sarswat, A., Srivastava, A., Pittman Jr, C. U., & Mohan, D. (2016). A review of fluoride in African groundwater and local remediation methods. *Groundwater for Sustainable Development*, *2*, 190-212.

Lantagne, D., Quick, R., & Mintz, E. (2006). Household water treatment and safe storage options in developing countries: a review of current implementation practices. Washington DC: Woodrow Wilson International Center.

© University of Venda

Li, W. R., Xie, X. B., Shi, Q. S., Duan, S. S., Ouyang, Y. S & Chen, Y. B. (2011). Antibacterial effect of silver nanoparticles on Staphylococcus aureus. *Biometals*, *24*(1), 135-141.

Liu, Y., Li, Q., Gao, S., & Shang, J. K. (2011). Exceptional As (III) sorption capacity by highly porous magnesium oxide nanoflakes made from hydrothermal synthesis. *Journal of the American Ceramic Society*, 94(1), 217-223.

Lobachev, A. N. (Ed) (1973). Crystallization processes under hydrothermal conditions. Consultants Bureau, New York. 225.

Loganathan, P., Vigneswaran, S., Kandasamy, J & Naidu, R. (2013). Defluoridation of drinking water using adsorption processes. *Journal of Hazardous Materials*, *248*, 1-19.

Lyu, Y., Su, X., Zhang, S., & Zhang, Y. (2016). Preparation and characterisation of La (III)-Al (III) co-loaded hydrothermal palygorskite adsorbent for fluoride removal from groundwater. *Water, Air and Soil Pollution*, 227 12 454.

Ma, Y. X., Shi, F. M., Zheng, X. L., Ma, J. and J. M. Yuan, J. M. (2005). "Defluoridation from aqueous solutions by Zr-loaded bentonite," *Journal of Harbin Institute of Technology* (New Series), vol. 12, supplement 1 224–229.

Mitsuda, T. (1980). Hydrothermal reaction and industry of calcium silicates. *Ceramics Japan*, *15*(13), 184.

Molina, A & Poole C. A. (2004). Comparative study using two methods to produce zeolites from fly ash. *Minerals Engineering*, 17 167–173.

Momba, M. N. B., Obi, C. L & Thompson, P. (2009). Survey of disinfection efficiency of small drinking water treatment plants: challenges facing small water treatment plants in South Africa. *Water South Africa*, 35 4 48-5494.

Morey, G. W., & Niggli, P. (1913). The hydrothermal formation of silicates, a review. *Journal of the American Chemical Society*, *35*(9), 1086-1130.

Morey, G. W. (1953). Hydrothermal synthesis. *Journal of American Ceramic Society*, 36 279.

Mudzielwana, R., Gitari, M. W., & Msagati, T. A. (2016). Characterisation of smectite-rich clay soil: Implication for groundwater defluoridation. *South African Journal of Science*, *112*(11-12), 1-8.

Mudzielwana, R., Gitari, M. W., Akinyemi, S. A., & Msagati, T. A. M. (2017). Synthesis and physicochemical characterisation of MnO2 coated Na-bentonite for groundwater defluoridation: Adsorption modelling and mechanistic aspect. *Applied Surface Science*, *422*, 745-753.

© University of Venda

Mudzielwana, R., Gitari, W. M., Akinyemi, S. A., & Msagati, T. A. (2017). Synthesis, characterisation, and potential application of Mn 2+-intercalated bentonite in fluoride removal: adsorption modeling and mechanism evaluation. *Applied Water Science*, *7*(8), 4549-4561.

Mudzielwana, R., Gitari, M. W., Akinyemi, S. A., & Msagati, T. A. (2018). Performance of Mn 2+-modified bentonite clay for the removal of fluoride from aqueous solution. *South African Journal of Chemistry*, *71*(1), 15-23.

Mulugeta, M., & Lelisa, B. (2015). Removal of methylene blue (Mb) dye from aqueous solution by bioadsorption onto untreated Parthenium hystrophorous weed. *Modern Chemistry Applications*, 2, 146.

Musyoka, N. M. (2009). Hydrothermal synthesis and optimisation of Zeolites Na-P1 from South African coal fly ash. University of Western Cape.

Musyoka, N. M., Petrik, L. F., & Hums, E. (2011). Ultrasonic assisted synthesis of zeolite A from coal fly ash using mine waters (acid mine drainage and circumneutral mine water) as a substitute for ultra pure water. *Proceedings of International Mineral Water Association, Aachen, Germany*, 423-428.

Musyoka, N. M., Petrik, L. F., Hums, E., Baser, H., & Schwieger, W. (2012). In situ ultrasonic monitoring of zeolite A crystallization from coal fly ash. *Catalysis Today*, *190*(1), 38-46.

Musyoka, N. M., Petrik, L. F., Gitari, W. M., Balfour, G., & Hums, E. (2012). Optimisation of hydrothermal synthesis of pure phase zeolite Na-P1 from South African coal fly ashes. *Journal of Environmental Science and Health*, Part A, 47 3 337-350.

Nagaraj, A., Munusamy, M. A., Ahmed, M., Kumar, S. S., & Rajan, M. (2018). Hydrothermal synthesis of a mineral-substituted hydroxyapatite nanocomposite material for fluoride removal from drinking water. *New Journal of Chemistry*, 42 15 12711-12721.

Ncube, E. J., & Schutte, C. F. (2005). The occurrence of fluoride in South African groundwater: A water quality and health problem. *Water South Africa*, 31 1 35–40.

Ndegwa, W. M. (1980). Investigations leading to defluoridation of waters in Kenya. Nairobi: University of Nairobi.

Nigri, E. M., Cechinel, M. A. P., Mayer, D. A., Mazur, L. P., Loureiro, J. M., Rocha, S. D., & Vilar, V. J. (2017). Cow bones char as a green sorbent for fluorides removal from aqueous solutions: batch and fixed-bed studies. *Environmental Science and Pollution Research*, *24*(3), 2364-2380.

© University of Venda

Ngulube, T., Gitari, M. W., & Tutu, H. (2017). Defluoridation of groundwater using mixed Mukondeni clay soils. *Water Science and Technology: Water Supply*, *17*(2), 480-492.

Obijole, O. A., Gitari, M. W., Ndungu, P. G., & Samie, A. (2019). Mechanochemically-activated aluminosilicate clay soils and their application for defluoridation and pathogen removal from groundwater. *International Journal of Environmental Research and Public Health*, *16*(4), 654.

Odiyo, J. O & Makungo, R. (2012). Fluoride concentrations in groundwater and impact on human health in Siloam Village, Limpopo Province, South Africa. *Water South Africa*, *38*(5), 731-736.

Onyango, M. S., Kojima, Y., Aoyi, O., Bernardo, E. C., & Matsuda, H. (2004). Adsorption equilibrium modeling and solution chemistry dependence of fluoride removal from water by trivalent-cation-exchanged zeolite F-9. *Journal of Colloid and Interface Science*, *279*(2), 341-350.

Pan, J., Zheng, Y., Ding, J., Gao, C., Van der Bruggen, B., & Shen, J. (2018). Fluoride removal from water by membrane capacitive deionization with a monovalent anion selective membrane. *Industrial and Engineering Chemistry Research*, *57*(20), 7048-7053.

Pandey, P. K., Kass, P. H., Soupir, M. L., Biswas, S. & Singh V. P. (2014). Contamination of water resources by pathogenic bacteria. *AMB Express*. 4 51. doi: 10.1186/s13568-014-0051.

Potgieter, N., Becker, P. J & Ehlers, M. M. (2008). Evaluation of the CDC safe water-storage intervention to improve the microbiological quality of point-of-use drinking water in rural communities in South Africa. *Water South Africa*, 1816-7950.

Raffi, M., Mehrwan, S., Bhatti, T. M., Akhter, J. I., Hameed, A., Yawar, W., & ul Hasan, M. M. (2010). Investigations into the antibacterial behavior of copper nanoparticles against Escherichia coli. *Annals of Microbiology*, *60*(1), 75-80.

Ramírez-Castillo, F. Y., Loera-Muro, A., Jacques, M., Garneau, P., Avelar-González, F. J., Harel, J., & Guerrero-Barrera, A. L. (2015). Waterborne pathogens: detection methods and challenges. *Pathogens*, *4*(2), 307-334.

Rango, T., Bianchini, G., Beccaluva, L., & Tassinari, R. (2010). Geochemistry and water quality assessment of central Main Ethiopian Rift natural waters with emphasis on source and occurrence of fluoride and arsenic. *Journal of African Earth Sciences*, *57*(5), 479-491.

© University of Venda

Sarkar, M., Banerjee, A., Pramanick, P. P & Sarkar, A. R. (2006). Use of laterite for fluoride removal from contaminated drinking water, *Journal of Colloid and Interface Science,* 302 432–441.

Schafthaul, K. F. E. (1845). Gelehrte Anzeigen Bayer. *Akad, 20*, 557-561.

Schmedt, Auf Der Günne., Jörn; Mangstl Martin & Kraus, Florian. (2012). "Occurrence of Difluorine (F_2) in Nature-In Situ Proof and Quantification by NMR Spectroscopy". *Angewandte Chemie International Edition*. 51 31 7847–7849. doi:10.1002/anie.201203515. PMID 22763992.

Shameli, K., Ahmad, M. B., Jazayeri, S. D., Shabanzadeh, P., Sangpour, P., Jahangirian, H., & Gharayebi, Y. (2012). Investigation of antibacterial properties silver nanoparticles prepared via green method. *Chemistry Central Journal*, *6*(1), 73.

Shameli, K., Ahmad, M. B., Zargar, M., Yunus, W. M. Z. W., Rustaiyan, A., & Ibrahim, N. A. (2011). Synthesis of silver nanoparticles in montmorillonite and their antibacterial behavior. *International Journal of Nanomedicine*, *6*, 581.

Shigemoto, N., Hayashi, H & Miyaura, K. (1993). Selective formation of Na-X zeolite from coal fly ash by fusion with NaOH prior to hydrothermal reaction. *Journal of Material Science,* 28 4781–4786.

Shimelis, B., Zewge, F & Chandravanshi, B. S. (2006). Removal of excess fluoride from water by aluminium hydroxide. *Bulletin of Chemical Society, Ethiopia.* 20 17–34.

Shukla, M. K., Singh, R. P., Reddy, C., & Jha, B. (2012). Synthesis and characterisation of agar-based silver nanoparticles and nanocomposite film with antibacterial applications. *Bioresource Technology*, *107*, 295-300.

Singh, A., Poshtiban, S & Evoy, S. (2013). Recent advances in bacteriophage-based biosensors for food-borne pathogen detection. *Sensors*, 13 1763–1786.

Smetana, A. B., Klabunde, K. J., Marchin, G. R., & Sorensen, C. M. (2008). Biocidal activity of nanocrystalline silver powders and particles. *Langmuir*, *24* (14), 7457-7464.

Sobsey, M. D. (2002). Managing Water in the Home: Accelerated Health Gains from Improved Water Supply. Water, Sanitation and Health. Department of Protection of the Human Environment, World Health Organization, Geneva. 1-70.

Somiya, S. (Ed) (1990). Hydrothermal preparation of fine powders, advanced ceramics III. Elsevier Applied Science Publishers, UK.

Somiya, S. (2006). Historical developments of hydrothermal works in Japan, especially in ceramic science. *Journal of Materials Science, 41*(5) 1307.

© University of Venda

Srimurali, M., Pragathi, A., & Karthikeyan, J. (1998). A study on removal of fluorides from drinking water by adsorption onto low-cost materials. *Environmental Pollution*, *99*(2), 285-289.

Suto, Y., Liu, L., Yamasaki, N., & Hashida, T. (2007). Initial behavior of granite in response to injection of CO_2-saturated fluid. *Applied Geochemistry*, *22*(1), 202-218.

Thakre, D., Rayalu, S., Kawade, R., Meshram, S., Subrt, J & Labhsetwar, N. (2010). "Magnesium incorporated bentonite clay for defluoridation of drinking water," *Journal of Hazardous Materials, 180 1–3 122–130.*

Tomar, G., Thareja, A., & Sarkar, S. (2015). Enhanced fluoride removal by hydroxyapatite-modified activated alumina. *International Journal of Environmental Science and Technology*, *12*(9), 2809-2818.

Tor, A. (2006). Removal of fluoride from an aqueous solution by using montmorillonite, *Desalination*, 201 267–276.

Tor, A., Danaoglu, N., Arslan, G., & Cengeloglu, Y. (2009): Removal of fluoride from water by using granular red mud: Batch and column studies. *Journal of Hazardous Materials*, 164 271-278.

Unicef Map of Fluorosis - Swami Vivekananda Institute of Pharmaceutical Sciences. (SVIPS), Vangapally, Bhongir. http://www.unicef.org/wes/files/wf13e.pdf

Vhahangwele, M., Mugera, G. W., & Tholiso, N. (2014). Defluoridation of drinking water using Al3+-modified bentonite clay: optimisation of fluoride adsorption conditions. *Toxicological and Environmental Chemistry*, *96*(9), 1294-1309.

Vilakati, B. R., Sivasankar, V., Nxumalo, E. N., Mamba, B. B., Omine, K., & Msagati, T. A. (2019). Fluoride removal studies using virgin and Ti (IV)-modified Musa paradisiaca (plantain pseudo-stem) carbons. *Environmental Science and Pollution Research*, *26*(12), 11565-11578.

Waghmare, S. S., & Arfin, T. (2015). Fluoride removal from water by various techniques. *International Journal of Innovative Science Engineering Technology*, *2*(9), 560-571.

Waghmare, S. S., & Arfin, T. (2015). Fluoride removal by clays, geomaterials, minerals, low cost materials and zeolites by adsorption: a review. *International Journal of Science, Engineering and Technology Research*, *4*(11), 3663-3676.

Wang, C., Li, J., Wand, L & Sun, X. (2008). Journal of Hazardous Materials 155 58-64.

© University of Venda

Wang, H., Feng Q., Liu, K., Li, Z., Tang, X & Li, G. (2017). Highly efficient fluoride adsorption from aqueous solution by nepheline prepared from kaolinite through alkali-hydrothermal process. *Journal of Environmental Management*, 196 72-79.

Wendimu, G., Zewge, F., & Mulugeta, E. (2017). Aluminium-iron-amended activated bamboo charcoal (AIAABC) for fluoride removal from aqueous solutions. *Journal of Water Process Engineering*, *16*, 123-131.

Whelan, G., Kim, K., Pelton, M. A., Soller, J. A., Castleton, K. J., Molina, M., Pachepsky, Y & Zepp, R. (2014). An integrated environmental modeling framework for performing quantitative microbial risk assessments. *Environmental Modelling and Software*, *55*, 77-91.

World Health Organization (WHO). (2010). Millennium Development Goals: Progress towards the Health-Related Millennium Development Goals. Geneva, Switzerland. http://www.who.int/topics/millennium_development_goals/en/

World Health Organization (WHO), (2011). Guidelines for Drinking Water Quality. Fluoride in drinking water. Guidelines for Drinking Water Quality, Geneva.

World Health Organization (WHO). Water Sanitation and Health. (2015). Available online: http://www.who.int/water_sanitation_health/diseases.

World Health Organization. (2017). Progress on drinking water, sanitation and hygiene: 2017 update and SDG baselines. *Progress on drinking water, sanitation and hygiene: 2017 update and SDG baselines.*

World Health Organization. (2019). *preventing disease through healthy environments: inadequate or excess fluoride: a major public health concern* (No. WHO/CED/PHE/EPE/19.4. 5). World Health Organization.

Widiastuti, N., Wu, H., Ang, M & Zhang, D. (2008). The potential application of natural zeolite for groundwater treatment. *Desalination*, 821 271-280.

Yao, G., Lei, J., Zhang, X., Sun, Z., & Zheng, S. (2018). One-Step Hydrothermal Synthesis of Zeolite X Powder from Natural Low-Grade Diatomite. *Materials* (Basel, Switzerland), *11* 6 906. Doi:10.3390/ma11060906).

Yoshimura, M., & Byrappa, K. (2008). Hydrothermal processing of materials: past, present and future. *Journal of Materials Science*, *43*(7), 2085-2103.

Yuranova, T., Rincon, A., Bozzi, A., Parra, S., Pulgarin, C., Albers, P., & Kiwi, J. (2003). Antibacterial textiles prepared by RF-plasma and vacuum-UV mediated deposition of silver. *Journal of Photochemistry and Photobiology A: Chemistry*, *161*(1), 27-34.

© University of Venda

Zewge, F., & Moges, G. (1990). Investigation of brick and pot chips as defluoridating media. Water Supply and Sewerage Authority, Southern Regional Office, Awassa, and Department of Chemistry, Addis Ababa University, Addis Ababa.

Zhang, Y., Muyrers, J. P., Testa, G., & Stewart, A. F. (2000). DNA cloning by homologous recombination in Escherichia coli. *Nature Biotechnology*, *18*(12), 1314.

© University of Venda

CHAPTER THREE: MECHANOCHEMICALLY-ACTIVATED ALUMINOSILICATE CLAY SOILS AND THEIR APPLICATION IN DEFLUORIDATION AND PATHOGEN REMOVAL FROM GROUNDWATER

3 Abstract

In this chapter, aluminosilicate rich clay soils were mechanochemically-activated and further tested for fluoride and pathogen removal. Physicochemical and mineralogical properties of the material were determined using CEC, BET, SEM-EDS, XRD, XRF and FTIR techniques. The fluoride removal efficiency was evaluated using batch experiments while the antimicrobial efficacy of the material was evaluated using well diffusion assay method. The BET results showed sample activated for 30 min had the largest surface area (17.19 m^2/g), pore volume (10.07 cm^3) and pore size (14.93 nm) and was found to perform optimally when applied to defluoridation with about 32% fluoride removal compared to samples activated at different times. The mechanochemically-activated clay showed a maximum adsorption capacity of 1.87 mg/g and percent fluoride removal of 32%, from the initial fluoride concentration of 10 mg/L using 2 g/100 mL dosage, 60 min contact time at 250 rpm shaking speed and temperature of 298 K. Fluoride adsorption was found to reduce in the presence of Cl^-, PO_4^{2-} and CO_3^{2-} while it increased in the presence of SO_4^{2-} and NO_3^-. Adsorption data fitted well to Freundlich isotherms, indicating that adsorption occurred on a multilayer surface when linearised model was used but fitted well to both Langmuir and Freundlich when non-linear model were employed, hence suggesting adsorption occurred on both monolayer and multilayer surfaces. Adsorption kinetics data showed a better fit to pseudo-second order model, indicating the dominance of chemisorption mechanism when linear modelling was used but fitted well to both pseudo-first order and pseudo-second order model when non-linear modelling were used, thus indicating adsorption mechanisms to be both physiosorption and chemosorption respectively. The adsorbent was successfully regenerated for up to five regeneration-reuse cycles. The antibacterial studies revealed no zone of inhibition for all the treated activated clays, hence, indicating that they were not active against the bacterial strains of *Escherichia coli*. Therefore, the material cannot be used to inactivate or remove pathogens from water. The adsorptive capacity of the clay materials could be improved upon by subjecting the clay to hydrothermal treatment, introduction of pore-forming agents to increase the surface area, pore volumes and sizes.

© University of Venda

Keywords: Adsorptive capacity, Bacteria, Clay soils, Defluoridation, Fluoride, Mechanochemical activation

3.1 Introduction

Water is an essential resource necessary for human health and survival. Groundwater is one of the major sources of potable water which is becoming increasingly contaminated as a result of natural and anthropogenic activities worldwide. Fluoride is one of the various water contaminants. High fluoride levels above the permissible limit cause fluorosis. The presence of pathogens in water leads to various types of water-borne diseases. Different types of clay and metal oxide-coated aluminosilicate materials have been used in defluoridation and pathogen removal, but they are not totally active against bacterial strains. Clay minerals are naturally occurring fine-grained phyllosilicate minerals which impart plasticity to clay and hardened when dried or fired (Guggenheim & Martin, 1995). Clay types are kaolinite, illite, bentonite and montmorillonite (Guggenheim & Martin, 1995). The knowledge about the chemistry and structure of clay minerals has significantly increased and the use of clay has widened greatly owing to advances in instrumental analytical methods such as X-ray diffraction, electron microscopy and spectroscopy. Attention is now focusing on clay properties as natural nano-sized particles which are applied in adsorption, catalysis, and in nanotechnology research on synthetic materials (Guggenheim & Martin, 1995; Coetzee *et al.*, 2003). Clay minerals can be broadly classified into two types, 1:1 or 2:1 based on their layered structure. A 1:1-type clay mineral consists of one tetrahedral sheet and one octahedral sheet. Examples are kaolinite, halloysite and serpentine. A 2:1-type clay mineral is composed of an octahedral sheet sandwiched between two tetrahedral silicate (SiO) sheets. Examples include talc, vermiculite, montmorillonite, saponite, and sepiolite. Clays contain the following main elements: aluminum, silicon and oxygen. Others are iron, magnesium, alkali metals, alkaline earths, and other cations present either in the interlayer space or in the lattice framework by isomorphous substitution (Konta, 1995). Clays and clay minerals have been used by man since the stone-age, primarily due to the occurrence of clay minerals' abundance on the earth's surface and are utilised widely for ceramics, building materials and agriculture. The South African clay deposits are broadly classified into three according to the dominant clay minerals present. These include (a) kaoline fields where the dominant clay minerals are kaolinite: (b) bentonite fields in which the dominant clay minerals are montmorillonite, which forms part of the

© University of Venda

smectite group; (c) palyorskite fields with dominant clay being palygorskite. Adsorption studies on clay and bauxite show that bauxite has the best adsorption capacities followed by bentonite and palygorskite while kaolinite had the lowest adsorption capacities for defluoridation (Coetzee *et al.*, 2003).

The main objective of this work was to mechanochemically activate and determine the physico-chemical and mineralogical characteristics of the raw clay soil from Mukondeni Village, Limpopo, South Africa, with a view to ascertaining its suitability as adsorbents for simultaneous defluoridation and pathogen removal from groundwater. Mechanochemical treatment is infact the milling process, in which some chemical reactions occured. During the milling process, some of the bonds in Al-O-Al and Si-O-Si bonds in the aluminosilicate clay matrix may have been broken.

This was done by investigating: i) the geological fluoride present in the activated clay, point-of-zero charge and CEC; ii) the chemical and mineralogical properties using XRF and XRD; iii) the functional groups, morphology and the surface area using FTIR, SEM-EDS and BET; iv) the activated clays adsorption capacities by batch mode; v) the effect of co-existing ions on the fluoride uptake; vi) adsorption isotherms modelling from data generated; vii) the adsorption kinetics modelling from generated data; viii) the intra-particle modelling from the data generated; ix) antibacterial activities using the well diffusion method.

3.2 Materials and methods

3.2.1 Sample collection and preparation

Aluminosilicate clay samples were collected from Mukondeni Village, Vhembe District in Limpopo Province, South Africa and stored in a polyethylene plastic bags. Prior to experiment, clay soil were oven-dried for 24 h at 110 ℃ and then milled to fine powder. Thereafter, clay soils were washed at a clay to water ratio of 1:10 in a 2 L beaker. The mixtures were stirred for 2 min and allowed to stand. Thereafter, mixtures were centrifuged at 4000 rpm for 10 min. The residues obtained were then oven dried at 110 ℃ for about 12 h. Thereafter, the dry residues were milled, passed through 250 µm sieve and then stored in a clean corked plastic bottle for future use.

3.2.2 Mechanochemical activation of the aluminosilicate clay samples

To prepare mechanochemically-activated clay (MAC), the optimum milling time was investigated by milling a known mass of finely ground, dried clay at different times of between 5 and 60 min at 700 rpm using a RS200 milling machine (Retsch, Green Bay, WI, USA). The

© University of Venda

resulting clay powder of <250 µm particle size was then oven dried and stored in zip-lock bags. The optimum milling time was obtained by evaluation of the activated clays (samples A - F) for defluoridation at a specific pH using batch mode. A mass of 0.3 g of the mechanochemically-activated aluminosilicate material treated at different contact times were contacted with 50 mL of 5 mg/L fluoride solution to determine the optimal contact time for the treatment. The sample with the highest percent fluoride removal indicated the optimum contact time for the treatment. The optimal mechanochemically-milled clay was then characterised and applied to defluoridation and pathogen removal in fluoride-rich-simulated and groundwater. The process above is a mechanical treatment but during the milling process, some of the bonds in Al-O-Al and Si-O-Si bonds in the aluminosilicate clay matrix may have been broken. This is in fact a form of chemical reaction; hence, the process is called mechanochemical treatment.

3.2.3 Geological fluoride determination

The geological fluoride levels in the activated clays at different contact times of 5 to 60 min were evaluated by using batch mode method and the percent fluoride removal calculated. This was conducted to determine the safe threshold of geological fluoride in the clay soil materials to establish the suitability of the activated clay materials for defluoridation and pathogen removal from groundwater.

3.2.4 Chemicals and reagents

All the chemicals and reagents used in the study were analytical grade, produced by Sigma Aldrich. The list is as follows: Sodium hydroxide (NaOH) pellets-anhydrous > 98%, sodium fluoride (NaF) > 99%, hydrochloric acid (HCl), sodium trioxocarbonate iv (Na_2CO_3) > 99%, sodium trioxonitrate v ($NaNO_3$) > 99%, sodium chloride (NaCl) > 99%, sodium tetraoxophosphate vi (Na_2PO_4) > 99%, sodium tetraoxosulphate vi (Na_2SO_4), TISAB III solution (Sigma Aldrich).

3.2.5 Physicochemical characterisation of the prepared clay samples

Surface area, specific surface area pore sizes and volumes were evaluated by using the Brauner-Emmett-Teller (BET) method. Measurements were carried out using a TriStar II surface area and porosity unit instrument (Micromeritics, Norcross, GA, USA). Mineralogical composition of the activated clay was analysed using a X'Pert Pro powder diffractometer (PANanalytical, Almelo, The Netherlands) in θ–θ configuration with an X'Celerator detector and variable divergence and fixed receiving slits with Fe filtered Co-Kα radiation (λ = 1.789Å). The

© University of Venda

phases were identified using X'Pert Highscore plus software. The relative phase amounts (weight percent) were estimated using the Rietveld method (Autoquan Program). Elemental composition was evaluated by using a PANanalytical Axios X-ray fluorescence spectrometer equipped with a 4 kW Rh tube. The activated clays' morphology (size and shape at the surface) were investigated by sprinkling a small amount of the sample onto a scanning electron microscope (SEM) stub covered with carbon glue. The stubs were then coated with carbon in an evaporation coater. The SEM is a NanoSEM 230 (FEI Nova, Czechoslovakia Republic) with a field emission gun (FEG) (Weber *et al.*, 1974). The elemental analysis was carried out using an X-Max detector (Oxford, Abingdon, UK) equipped with Inca software, at 20 kV. The Fourier transform infrared (FT-IR) analysis of the activated clay, which provides information about the functional groups responsible for fluoride sorption from the groundwater, was carried out using an ALPHA FT-IR spectrophotometer (Bruker, Germany). The point-zero-charge (pH_{pzc}) was determined using titration at 0.1 M, 0.01 M and 0.001 M KCl concentrations (Eggleston, 1998). The concentration of exchangeable cations was determined using flame atomic absorption spectra (600 PerkinElmer, Waltham, MA, USA). The Cation Exchange Capacity (CEC) was evaluated by using ammonium acetate buffers at pH 5.4 and 7.4, respectively (Meimaroglou & Mouzakis, 2019).

3.2.6 Batch adsorption experiments

Batch adsorption experiments were used to assess the activated clays' capacity for defluoridation of fluoride-rich-simulated water: The following parameters were optimised: contact time; adsorbent dosage; pH and fluoride ions concentrations. To evaluate the effect of contact time, 100 mL solution containing 10 mg/L fluoride solution was measured into 250 mL polythene bottles and a mass of 0.5 g was added to make up 0.5 g/100 mL adsorbent dosage. The pH was adjusted to pH 6. The mixtures were agitated in a thermostatic water bath shaker for 10 min. After agitation, the suspensions were filtered to remove the solid. This procedure was repeated for other determinations but with equilibration times of 20, 30, 40, 50 60, 80 up to 200 min respectively. The samples were then refrigerated until analysis. To evaluate the effect of adsorbent dosage, 100mL solution containing 10 mg/L fluoride solution was measured into 250 mL polythene bottles. This was followed by the addition of 0.1, 0.2 up to 10 g of the activated clay into plastic bottles. Mixtures were agitated for 60 min. To evaluate the effect of pH, aliquots of 100 mL of 10 mg/L fluoride solution were measured into seven polythene bottles. A mass 0.5 g of each activated clay sample was weighed into separate bottles and the pH adjusted between 2 and 12 by adding

© University of Venda

0.1 M HCl or 0.1 M NaOH. The mixtures were equilibrated for 60 min. After the equilibration time, the suspensions were filtered and the fluoride ion concentration in each solution was determined using a fluoride ion-selective electrode. To determine the effect of fluoride ion concentration, 100 mL volume of between 1 mg/L to 100 mg/L fluoride solution was measured into ten polythene bottles. A mass of 2 g of each clay sample was weighed into some bottles and the pH adjusted to the optimum pH 6, by adding 0.1 M HCl or 0.1 M NaOH. The mixtures were equilibrated for the optimum contact time of 60 min. After equilibration, the suspensions are filtered. The fluoride ion concentration in each solution was determined. Modelling of adsorption isotherm was done from the data generated using Langmuir and Freundlich equations. Adsorption kinetics studies were also carried out from the generated data. The sorption mechanism of fluoride uptake was investigated by using the pseudo-first-order and pseudo-second-order kinetic models. Studies on the intra-particle diffusion model was also carried out using the data generated to determine if the sorption process during defluoridation is being controlled either by a particle diffusion or a pore diffusion model.

3.2.7 Bench scale testing of fluoride-rich Siloam groundwater with the activated clay

The efficacy of the activated clays for defluoridation was tested with field water containing 5.44 mg/L fluoride concentration collected from boreholes in Siloam Village, Limpopo Province, South Africa. The experiment was conducted at optimum pH 6.0 and natural pH of 8. Aliqouts of 100 mL of field water were pipetted into 250 mL plastic bottles with masses of 2.0 g of adsorbent added to make adsorbent dosage of 2 g/100 mL. Thereafter, mixtures were equilibrated for 60 min at the shaking speed of 250 rpm using a table shaker followed by centrifuging at 4000 rpm. The mixtures were filtered using a 0.45 µm pore membrane filter and the analysis of fluoride in the supernatants was carried out. The percent fluoride removal and adsorption capacity were evaluated using pH meter equipped with ion-selective fluoride electrode. The major cations and anions in the groundwater before and after treatment were analysed using Metrohm 850 professional on chromatography. The cations evaluated were sodium, potassium, calcium and magnesium while the anions were bromide, chloride, nitrate, phosphate and sulphate.

3.2.8 Effect of co-existing anions on fluoride adsorption

Generally, groundwater, including fluoride-rich ones, are most likely to contain several other anions which may compete with fluoride ions uptake in the adsorption process. The effect of co-existing anions on fluoride sorption onto the clays surfaces was evaluated in the presence of

© University of Venda

10 mg/L salt solution of chloride, sulphate, nitrate and phosphate, independently, at an initial fluoride concentration of 10 mg/L. All the solutions for fluoride adsorption experiments and analysis were prepared by appropriate dilution from the stock solution prepared as described earlier in subsection 3.8. Adsorption studies were carried out for each of the prepared 10 mg/L salt solutions of chloride, sulphate, nitrate and phosphate, separately, at an initial fluoride concentration of 10 mg/L in a conical flask by batch method at room temperature. The pH of the fluoride solution was adjusted to 6.9 ± 0.1, using 0.1 M NaOH and HCl solutions. A mass of 2 g of the activated clay was introduced into each of the 100 mL of the blank, chloride, sulphate, nitrate and phosphate solutions and placed in a shaker at a speed of 250 rpm to give homogeneous mixtures. The mixture was centrifuged for 30 min and thereafter, the resulting solution (filtrate) was decanted from the solid particles (residue) which settled at the bottom of the centrifuge tubes. The amount of fluoride in each filtrate was analysed using a pH meter equipped with ion-selective fluoride electrode. The analysis was carried out by using total ionic strength adjustment buffer TISAB III/ Sample Solution ratio of 1:10. A blank experiment was also performed using deionised water with only 10 mg/L fluoride concentration. The percent fluoride removal was then calculated from the result obtained and comparison made.

3.2.9 Regeneration of fluoride loaded adsorbents for re-use

Regeneration of the fluoride-loaded activated clay was carried out by agitating 2.0 g of loaded clay with 100 mL of 0.1 M NaOH for 30 min on a mechanical shaker. After agitation, the mixture was filtered through a 0.45 µm pore membrane filter. The filtrate was diluted to 100 mL and then analysed for desorbed fluoride. The resulting clay adsorbent on 0.45 µm pore membrane filter paper was washed with de-ionised water and then dried in the oven at 110 °C for 4 h. Adsorption studies on the regenerated clay adsorbent were then carried out using batch method. The regenerated clay adsorbent was re-used for defluoridation up to five times.

3.2.10 Antibacterial studies

Antibacterial activities of the six mechanochemically-activated clays were evaluated with *Escherichia coli* (*E. coli*) strains by using well diffusion assay method. The zone of inhibitions was recorded in millimeter (mm). The bacterial suspensions were prepared with the turbidity of 0.5 McFarland. Mueller-Hinton agar plates were inoculated with *E. coli* (ATCC 35218) strains. Wells with a diameter of 6 mm were cut using a cork borer and filled with 30 µL of the six mechanochemically-activated clay soil samples, A - F. The six clay samples were activated at

© University of Venda

varying contact times of between 5 and 60 min. Plates were incubated for 24 h at 37 °C. After incubation, the growth inhibition zone diameters were measured in millimeter (mm). The plates as well as the samples were carefully packed in sealed disposable plastic bags for destruction immediately after the measurements were made.

3.3 Results and discussions

3.3.1 Geological fluoride levels in the mechanochemically-activated clays

The geological fluoride levels in the activated clays at different contact times of 5 to 60 min ranged between 0.04 - 0.06 mg/L (Table 3.1). The fluoride levels in mg/g of the clay were also calculated and found to range between 2.0 $x10^{-3}$ and 3.51 $x10^{-3}$ mg/g (Table 3.1). This showed that clay may not leach fluoride during defluoridation, hence, may not need pre-treatment as fluoride levels in the clay are low. Furthermore, the higher the activation time, the more fluoride released, suggesting the finer the particulate size, the more likely Si-F and Al-F bonds are broken, freeing more fluoride ions. However, batch defluoridation studies on the different activated clays showed increase in percent fluoride removal with increase in activation time which peaked (optimum) at 30 min activation time due to saturation of available sites unto which fluoride are adsorbed. Hence, further increase in activation time did not lead to any increase in percent fluoride removal. The fluoride levels in the raw clay and those activated for 5 min (Sample A) were the same. The fluoride levels in the activated clays were found to be much lower than the World Health Organization's (WHO, 2015) and South African National Standards permissible limits (SANS, 241), whose recommended maximum fluoride limit is 1.5 mg/L. Hence, from Table 3.1, the geological fluoride levels in the activated clay is within safe threshold. Therefore, making the clay materials a safe and promising adsorbent for fluoride removal without compromising the water safety during defluoridation processes.

Table 3.1: Fluoride levels in clay soil samples activated at different contact times.

Samples	Mechanochemically activated time (min)	Fluoride level (mg/L)	Fluoride level (mg/g)
A	5	0.0401	2.0×10^{-3}
B	10	0.0610	3.05×10^{-3}
C	20	0.0605	3.02×10^{-3}
D	30	0.0638	3.19×10^{-3}
E	40	0.0638	3.19×10^{-3}
F	60	0.0703	3.51×10^{-3}

© University of Venda

3.3.2 Defluoridation of simulated fluoride water with mechanochemically-activated clay

The per cent fluoride removal of clays activated at different times of between 5 and 60 min were between 21.81% and 28.49% as presented in Table 3.2. Sample D exhibited highest removal of 28% indicating optimum activation time of 30 min (Table 3.2).

Table 3.2 Percent fluoride removal and adsorption capacities of the activated clays at different treatment time.

Samples	Mechanochemically-activated (minutes)	Initial fluoride concentration C_o (mg/L)	Equilibrium fluoride concentration C_e (mg/L)	Difference between initial and final fluoride concentration (mg/L)	Per cent fluoride removal (%)	Adsorption capacity, q (mg/g)
A	5	8.39	6.45	1.94	23.12	0.970
B	10	8.39	6.51	1.88	22.41	0.940
C	20	8.39	6.43	1.96	23.36	0.980
D	30	8.39	6.00	2.39	28.49	1.195
E	40	8.39	6.22	2.17	25.86	1.085
F	60	8.39	6.56	1.83	21.81	0.915

The plot of adsorption capacity versus activation time is presented in Figure 3.1. The adsorption capacities increased from 0.94 mg/g to 1.195 mg/g at 30 min activation time and reduced thereafter to 0.915 mg/g, hence, indicating that the activation had effect on the adsorption capacity of the clay soils. This was probably due to increase in the surface area which peaked at 30 min activation. The observed decrease in adsorption capacity after 30 min could be attributed to further reduction in pore sizes and volumes as the particle sizes decreased.

© University of Venda

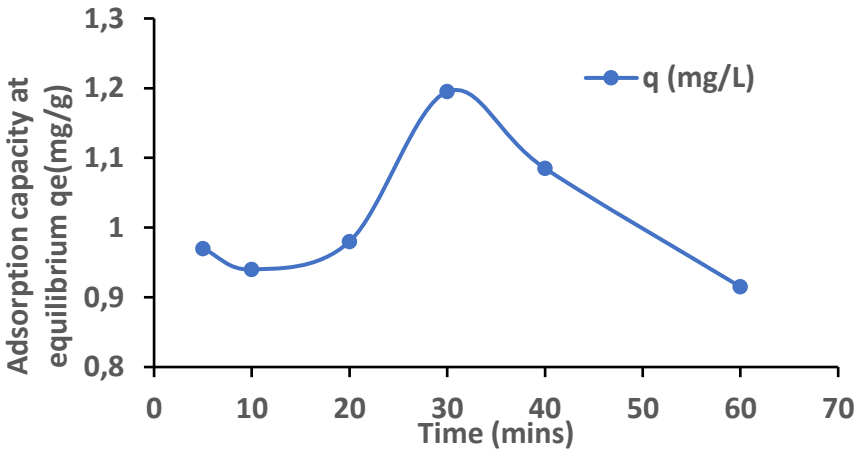

Figure 3.1: Plot of adsorption capacity (mg/g) versus activation time (min).

3.3.3 Physicochemical and mineralogical characterisation

3.3.3.1 Surface area by Brunauer-Emmett-Teller (BET)

The surface area, pore volume and pore size play a significant role in the sorption of the fluoride ions onto the activated clay surface. The results of Brunauer-Emmett-Teller (BET) analysis of the activated clays at different times are presented in appendix 3.3. The clay is mesoporous in nature with pore sizes ranging between 5 -15 nm. Surface area ranged between 13 and 18 m^2/g. Specific surface area ranged between 12 and 17 m^2/g while pore volumes values had an average value of 10 cm^3/g. Clay sample D activated for 30 min had the largest surface area of 17.19 m^2/g, specific surface area of 16.66 m^2/g, pore volume of 10.07 cm^3 and pore size of 14.93 nm, indicating maximum roughness of pore walls and increase of additional active sites for the activated clay while sample F had the smallest surface area (13.23 m^2/g), specific surface area (12.58 m^2/g), a low pore volume (10.05 cm^3/g) and pore size of 14.68 nm respectively, at 60 min treatment time. Since surface area generally plays a significant role in the adsorption of sorbents from the solution, the higher the surface area, the higher the adsorption and vice versa (Spark, 1997). The results also show that activation increased the surface area of the clay from 10 min to 30 min (17.1 m^2/g) and thereafter decreased to about 13 m^2/g at 60 min treatment time. Hence, clay sample D which was activated for 30 min is considered optimum for the modification process since the sample had the highest surface area and pore volume, suggesting that it had more active sites for fluoride uptake, thereby improving the quality of the clay as a good adsorbent for fluoride removal.

© University of Venda

3.3.3.2 Point-zero-charge (pH_{pzc})

Figure 3.2 depicts the pH_{pzc} of the mechanochemically-activated clay soils. pH_{pzc} reflects the pH of solution at which the clay surface will be having a net surface of zero. At pH below the pH_{pzc}, the surface is positively charged while at pH above pH_{pzc} the surface is negatively charged. The pH_{pzc} of the clay soil evaluated was found to be 6.1 ± 0.5 (Figure 3.2) which is close to pH_{pzc} of smectite-rich clay reported by Mudzielwana *et al*. (2016) but lower than that of bentonite clay reported by Gitari *et al*. (2016). Therefore, it is expected that adsorption of fluoride anions is likely to be high at a pH below 6.1 where clay surface is positively charged due to electrostatic attraction forces between negatively charged ions and the surface.

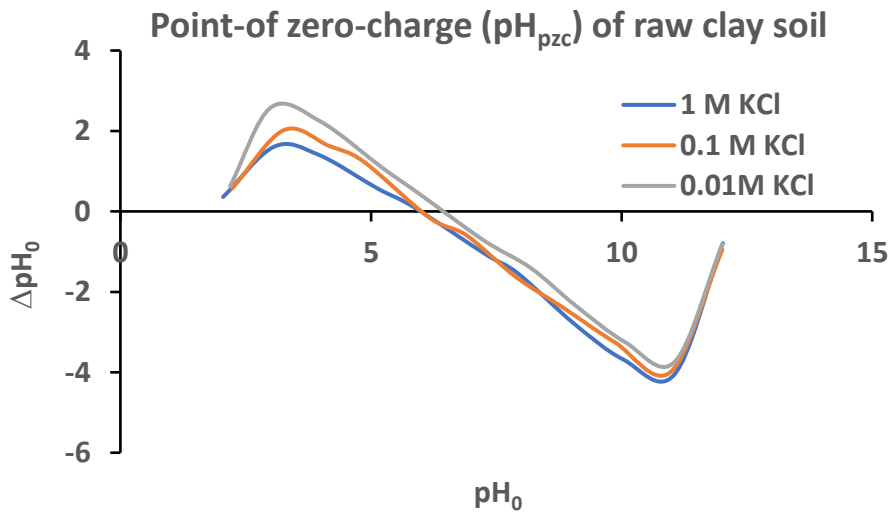

Figure 3.2: pH at point-of-zero charge of mechanochemical-activated aluminosilicate-rich clay soil (adsorbent dosage: 1.0 g/50 mL, contact time: 24 h, agitation speed: 250 rpm, temperature: 298 K: pH varied between 2 and 12).

3.3.3.3 Morphology of the mechanochemically-activated clay.

Figure 3.3 a - d shows the micrographs of the mechanochemically-activated clay at different magnifications. Generally, micrographs show that the clay surface consisted of fine particles of irregular shape and size on external surface with a micro-rough texture. At lower magnifications (Fig 3.3 a - b) micrographs reveals irregular porous structure, nature of the material while at higher magnifications (Fig 3.3 c - d) micrographs show a smooth, irregular surfaces and an expanded flared "cornflake" and platy-like texture. The characteristic images show typical smectite clay surfaces which are consistent with the results obtained by Mudzielwana *et al*. (2016).

© University of Venda

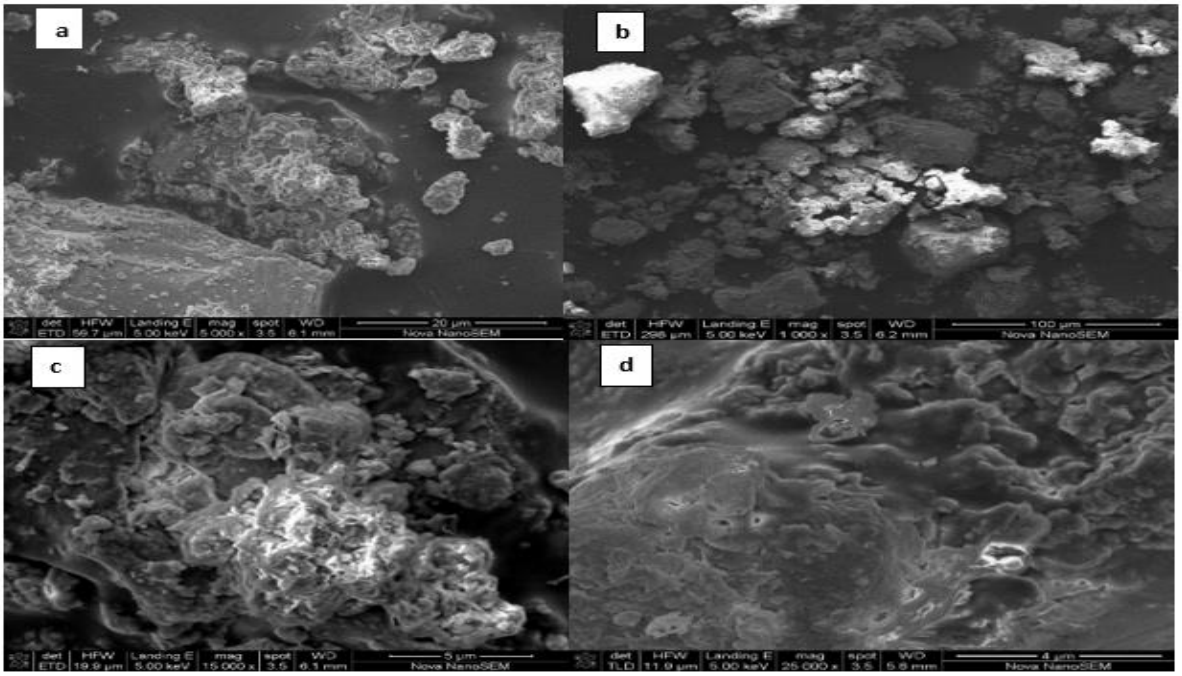

Figure 3.3 a - d: Micrographs of the mechanochemically-activated clay at different magnifications.

Energy dispersal spectroscopy (EDS) of the most mechanochemically-activated clay is presented in Figure 3.4. The elemental concentrations are shown with silicon, iron, aluminium and oxygen having the most elevated concentrations indicating that the clay material is an aluminosilicate material. There is also the presence of base cations of magnesium, sodium, potassium and calcium in the sampled powdered clay, which are the exchangeable fractions and play a vital role in sorption of the fluoride onto the clay surfaces.

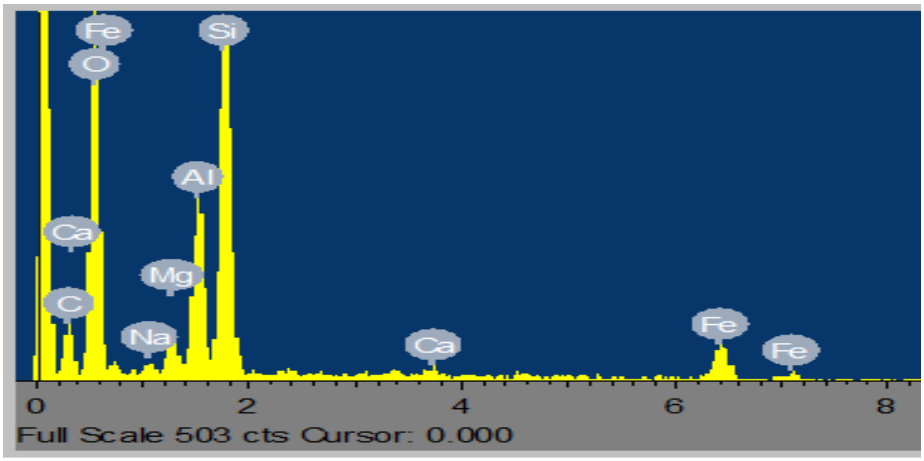

Figure 3.4: Energy dispersal spectroscopy (EDS) of the mechanochemically-activated clay.

© University of Venda

3.3.3.4 Cation exchange capacity (CEC)

Cation exchange capacity (CEC) of the activated clay was determined using standard laboratory methods (Meimaroglou & Mouzakis, 2019). The CEC also reveals that Mg^{2+}, Ca^{2+}, Na^{+} and K^{+} were the exchangeable cations present. The higher the concentrations of these cationic species on the clay surfaces, the higher their adsorptive properties. CEC values of the activated clay soil at pH 7.4 and 5.4 (milliequivalent/100 g) were calculated to be 74.5 and 82.1 respectively (Table 3.3). Thus, indicating that the clay soil is of the high CEC group, that is, they are greater than 10 meq/100g. The CEC is independent of the pH. The fluoride sorption efficiency of the activated clay is enhanced by the moderately high CEC as well as the little difference observed in cation concentations at different pH.

Table 3.3: Concentrations of exchangeable cations in mechanochemically-activated clay.

Metals	Metal concentration (mEq/100 g) at pH:	
	5.4	7.4
Mg^{2+}	34.6	38.1
Ca^{2+}	17.7	19.5
Na^{+}	8.1	9.0
K^{+}	14.3	14.5
	74.7	82.0

3.3.3.5 X-ray diffraction (XRD)

Figure 3.5 depicts XRD spectrum of mechanochemically-activated clay. The Analysis shows that the clay sample is mainly composed of the following mineral phase which are plagioclase, quartz, chlorite, kaolinite, actinolite, muscovite, microcline, calcite and albite. The quantitative results are summarised by the pie chat in Figure 3.5. The results further confirm the presence of plagioclase (smectite-rich clay soil) (31.09%) and quartz (24.55%) as the major minerals and the presence of chlorite (13.71%) and kaolinite (11.62%) as minor minerals.

© University of Venda

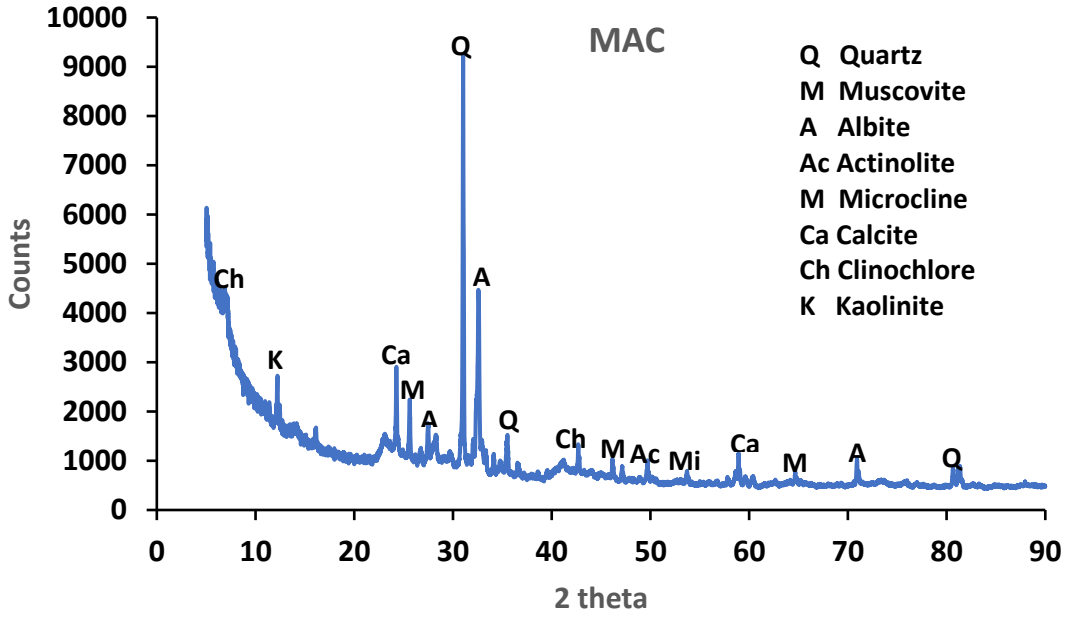

Figure 3.5: X-ray diffraction spectrum of the mechanochemically-activated clay (MAC) soil.

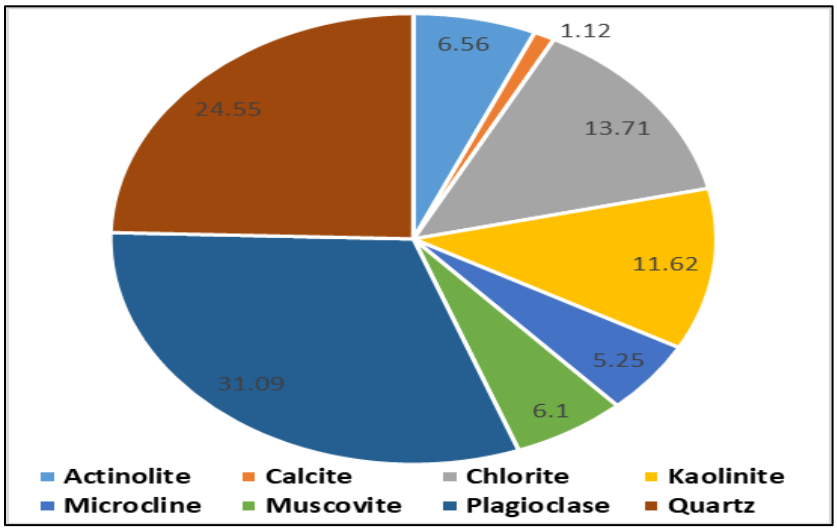

Figure 3.6: XRD quantitative results of the activated aluminosilicate clay sample.

3.3.3.6 X-ray fluorescence (XRF) analysis

Table 3.4 presents the major and minor elemental compositions of the mechanochemically-activated clay. The XRF analysis of the activated clay shows that silica (SiO_2) is the main component at 52.48%, followed by Al_2O_3 at 14.62%. High concentrations of SiO_2 and Al_2O_3 reveal that the black clayey soils are aluminosilicate rich material. Minor elemental compositions are P_2O_5, TiO_2, Na_2O, MnO, K_2O, CaO, MgO and Fe_2O_3 with their compositions ranging between

© University of Venda

0.03 to 6.64 %. Some of these minor elemental compositions form the exchangeable cations which play a vital role in fluoride uptake during defluoridation.

Table 3.4: Elemental composition of the mechanochemically-activated clay (MAC).

Oxides	SiO_2	Al_2O_3	Fe_2O_3	MgO	CaO	K_2O	Na_2O	TiO_2	MnO	P_2O_5
(% w/w)	52.48	14.62	6.64	2.985	1.53	1.24	0.707	0.627	0.125	0.034

3.3.3.7 Fourier transform infra-red (FTIR) analysis

The activated clay samples were scanned in the range between 500 cm^{-1} and 400 cm^{-1} and the spectra obtained are shown in Figure 3.7. The spectra show three main transmittance regions of 3000-3800 cm^{-1}, 1300-1800 cm^{-1} and 500-1200 cm^{-1}. The hydroxyl stretching bands are well established at around 3700 cm^{-1}. The transmittance bands observed at 3400-3500 cm^{-1} and 1600-2700 cm^{-1} could be due to the OH vibrational mode of the hydroxyl molecule, which is observed in almost all the natural hydrous silicates including montmorillonite clay (Toor *et al*., 2014). The transmittance bands between 3400 and 3700 cm^{-1} are attributed to the hydroxyl ions stretching mode. The H-O-H bending of water is observed at 1620-1640 cm^{-1}. In the 500 cm^{-1} - 1000 cm^{-1} region, main functional groups were Si-O-Si and Al-O-H. The IR peak at 970 cm^{-1} may be attributed to Al-OH-Al. The presence of these functional groups and their stretching bands, particularly H-O-H, Al-O-Al and Si-O-Si have been known to play a vital role in fluoride sorption onto the activated clay surfaces. This is mainly through fluoride interaction with the OH groups and direct interactions with metal surface. The observed shifting of these stretching transmittance bands could be closely linked with fluoride uptake (Figure 3.7).

© University of Venda

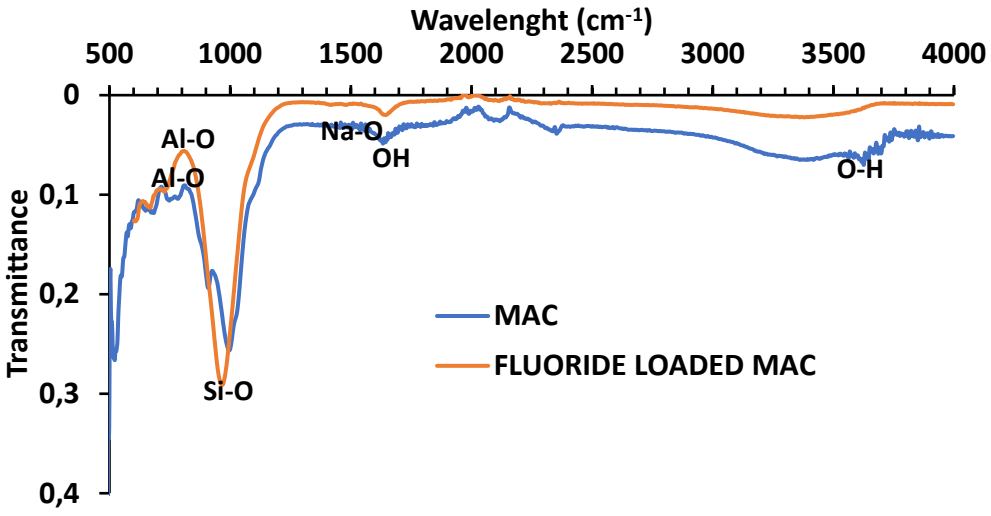

Figure 3.7: FTIR Spectra of the mechanochemically-activated raw clay (MAC) soil.

3.3.4 Optimisation of fluoride adsorption conditions

3.3.4.1 Effect of contact time

Figure 3.8 depicts the variation of contact time with percent fluoride removal. An increase in the per cent fluoride removal with an increase in contact time was observed from 10 min to 60 min due to availability of vacant sites onto which fluoride is adsorbed. The rate of fluoride adsorption or removal from water was very rapid within the first 20 min of contact and thereafter stabilised at ≈ 60 min (24.5% fluoride removal). After 60 min, the fluoride removal rate stabilised, suggesting that the system had reached equilibrium (Figure 3.8). Therefore, 60 min were taken as the optimum contact time and were used for subsequent experiments.

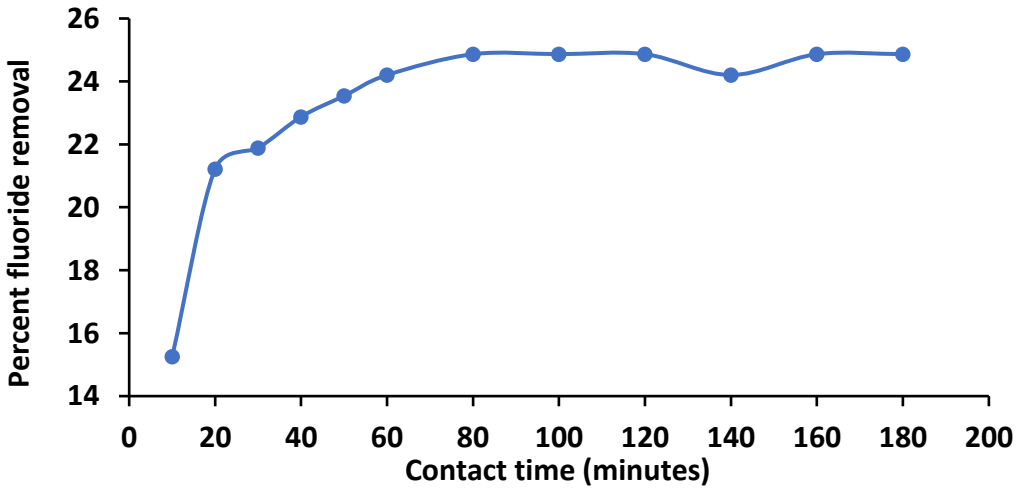

Figure 3.8: Variation of contact time with percent fluoride removal (0.5 g/100 mL adsorbent dosage, 10 mg/L of initial fluoride concentration, pH 6.35, agitation speed of 250 rpm at 298 K).

© University of Venda

3.3.4.2 Effect of adsorbent dosage

Figure 3.9 depicts the variation of percent fluoride removal with dosage. The percent fluoride removal was observed to increase with an increase in the activated clay dosage. This could be attributed to the fact that as dosage increased, more sites and surfaces became available for fluoride uptake. From 0.1 to 2.0 g dosage, the fluoride uptake was observed to increase gradually to about 38% fluoride removal. The adsorption capacity decreased to about 18% as the dosage increased to 10 g/100 mL. Also from 0.1 to 2.0 g dosage, the adsorption capacity decreases sharply with increase in adsorbent dosage and thereafter stabilizes as the adsorbent dosage further increased from to 10 g/100 mL. At low adsorbent dosage, there is a rapid fluoride adsorption since the active sites are more readily available while at high adsorbent dosage, the adsorbate species increasingly find it difficult to access the adsorption sites due to less available sites as a result of the fluoride filling of these sites. Hence there was a gradual stabilisation of the adsorption process. Therefore, it can be concluded that the optimum dosage of the activated clay for defluoridation is 2.0 g/100 mL. Therefore the value was adopted for subsequent experiments.

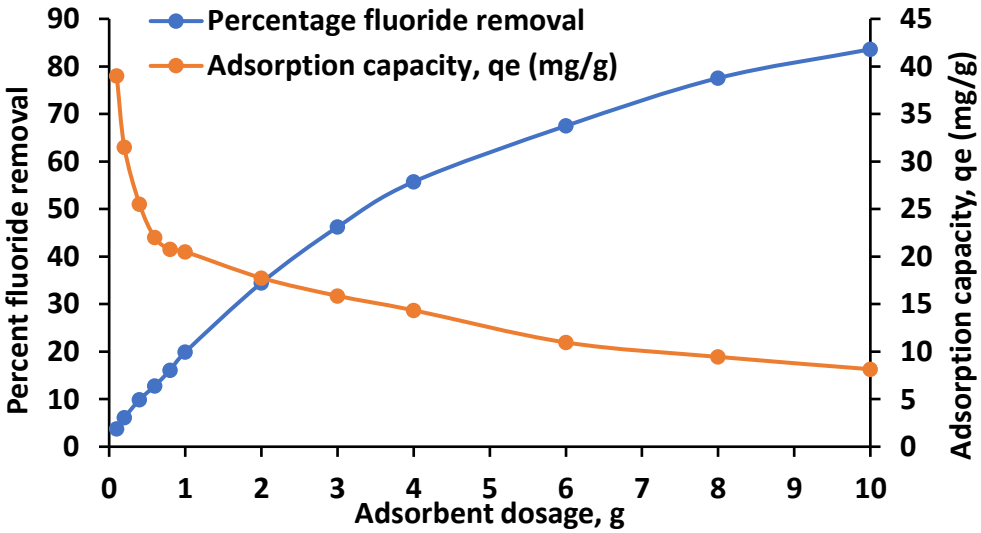

Figure 3.9: Variation of percent fluoride removal and adsorption capacity with adsorbent dosage (pH 6.0, initial fluoride concentration: 10 mg/L, contact time: 60 min, agitation speed: 250 rpm and 298 K).

3.3.4.3 Effect of pH

Figure 3.10 depicts the variation of per cent fluoride removal with initial pH. The maximum per cent fluoride removal of 48% was observed at pH 5. The per cent fluoride removal

© University of Venda

decreased as pH went from acidic to alkaline range. The decrease in percent fluoride removal as the solution became strongly acidic could be attributed to the formation of weak hydrofluoric acid (HF) since there was abundance of H^+ in solution. The significant amount of HF produced could have made fluoride les available for adsorption on the surface. The decrease in percent fluoride removal as the solution becomes more alkaline could be as a result of either competition between the hydroxyl ions and fluoride ions for adsorption sites or due to repulsive forces between negatively charged surface and the fluoride ions.

Equation 3.1 to 3.4 can be used to summarise the interaction between fluoride ions and the surface at different pH levels. At pH below 5, the surface of the clay is positively charged (Equation 3.1), hence, fluoride ions are electrostatically adsorbed to the surface of the clay (Equation 3.2). Moreover, low pH leads to surface protonisation of OH groups to $-OH_2^+$ which facilitates fluoride removal from solution. The clays' surface is electrically neutral at the pH at point of zero charge because the concentration of OH^- is higher than that of H^+ at that pH. Fluoride removal at pH_{pzc} and above would occur by ion exchange between fluoride ions in solution and the hydroxyl ions on the clays' surface as illustrated by Equations 3.3 and 3.4 respectively.

$$\equiv ACOH + H^+ \leftrightarrow \equiv ACOH_2^+ \quad (3.1)$$

$$\equiv ACOH_2^+ + F^- \leftrightarrow \equiv ACOH_2F \quad (3.2)$$

$$\equiv ACOH + F^- \leftrightarrow ACF + OH^- \quad (3.3)$$

$$\equiv AC(OH)_2^- + F^- \leftrightarrow \equiv AC(OH)F + OH^- \quad (3.4)$$

where $\equiv AC$ represents Aluminium and Silicon in the activated clays' surface.

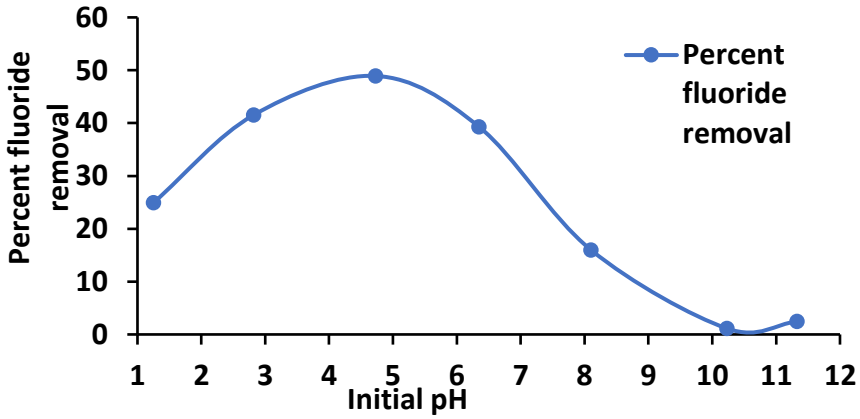

Figure 3.10: Variation of percent fluoride removal with initial pH (2.0 g/100 mL adsorbent dosage, 60 min contact time, 10 mg/L of initial fluoride concentration, agitation speed of 250 rpm at 298 K).

© University of Venda

3.3.4.4 Effect of fluoride ion concentration

Figure 3.11 depicts the variation of percent fluoride removal with initial fluoride concentrations. The percent fluoride removal decreases with increasing initial fluoride concentration. This could be due to more fluoride ions in solution at higher fluoride concentrations, competing for fewer binding sites on the clay surfaces.

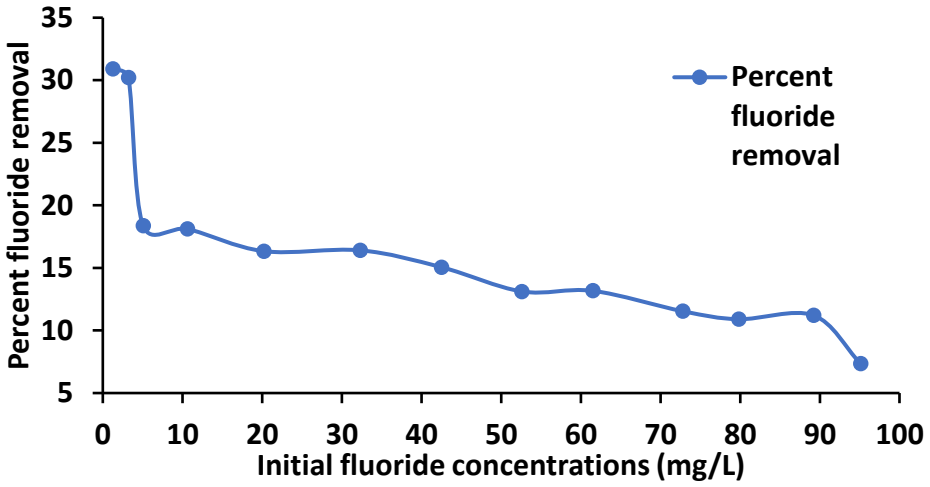

Figure 3.11: Percent fluoride removal with initial fluoride concentration (60 min contact time, 2.0 g/100 mL adsorbent dosage, 10 mg/L of initial fluoride concentration, pH 6.0, agitation speed of 250 rpm and 298 K. Initial fluoride concentration was varied from 1 mg/L to 100 mg/L).

3.3.5 Effect of co-existing anions on the defluoridation process

Groundwater generally may contain other types of anion, in addition to fluoride ions, which may interfere with defluoridation processes. Figure 3.12 shows the results of the effect of some co-existing anions on the adsorption of fluoride ions by activated clay. The presence of Cl^-, SO_4^{2-} and NO_3^- showed little influence on the percent fluoride removal while the presence of PO_4^{3-} and CO_3^{2-} significantly decreased the percent fluoride removal from 36.65% to 30.61% and 17.5%, respectively. Generally, negatively charged ions are naturally attracted to positively charged ions. The extent of attraction is dependent on the magnitude of charge and size of ion. Usually higher (multivalent) charged anions are more strongly attracted to cations for bonding than the univalent anions. This probably explains why PO_4^{3-} and CO_3^{2-} competed more with fluoride for adsorption than other anions.

© University of Venda

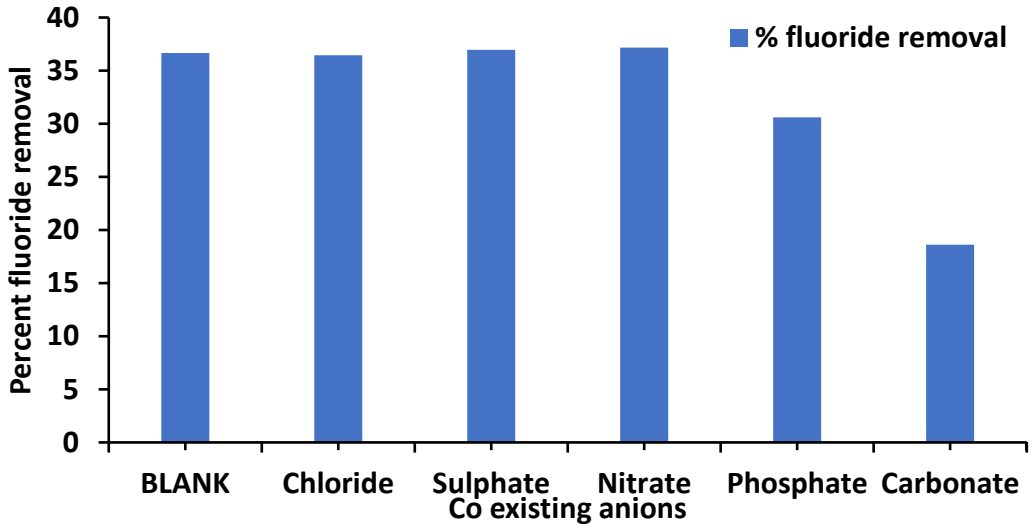

Figure 3.12: The effect of co-existing anions on fluoride removal by the activated clay (10 mg/L initial fluoride concentration, 2.0 g/100 mL adsorbent dosage, 30 min contact time at 250 rpm).

3.3.6 Regeneration of the activated clay adsorbent

Evaluation of the regeneration of activated clay was performed at an initial natural fluoride concentration of 5.44 mg/L, contact time of 60 min at pH 6.0 in five successive adsorption and desorption cycles. The results are presented in Figure 3.13. The percent fluoride removal after the first cycle was observed to decrease slightly after each cycle from 52% to 42%. The same trend was reported by Mudzielwana *et al.* (2016), Jia *et al.* (2015) and Zhang *et al.* (2011). This could be an indication that the surface was inadequately regenerated.

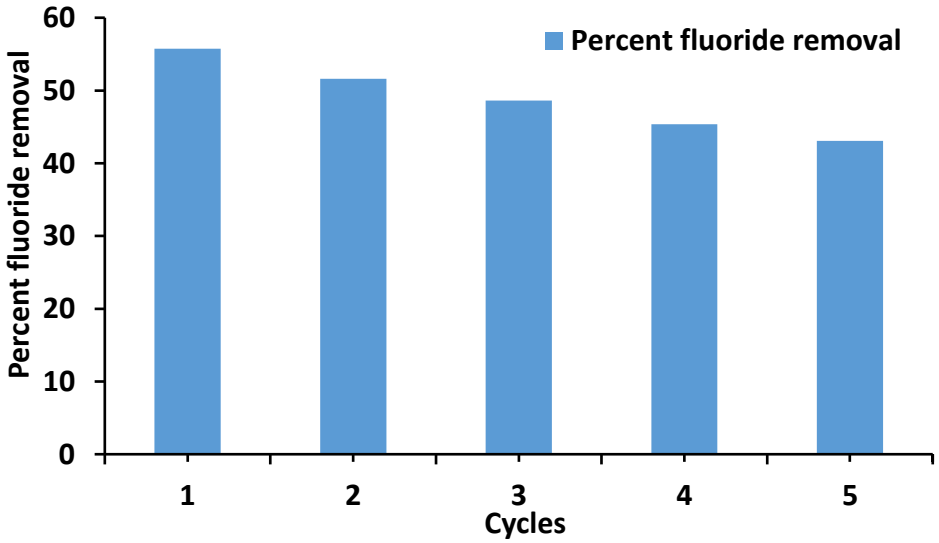

Figure 3.13: Percent fluoride removal by activated clay in successive cycles (at 5.44 mg/L fluoride, 60 min contact time, pH 6.0 at 250 rpm).

© University of Venda

3.3.7 Adsorption isotherms

According to Langmuir (1916) and Freundlich (1906), adsorption isotherms models are equilibrium tests used to model the interaction of adsorbate with adsorbent. Langmuir and Freundlich isotherm models were used to study the distribution of fluoride ions on the adsorbent during adsorption. The sorption isotherms parameters were obtained by using 2.0 g of mechanochemically-activated clay (MAC) adsorbent per 100 mL of fluoride solution (1 - 100 mg/L) for 60 min at 298 K.

Langmuir isotherm models the monolayer coverage of the adsorption surfaces and assumes that adsorption takes place on a structurally homogenous surface of the adsorbent at a given temperature (Firdaous *et al.*, 2017). Equation 3.5 depicts the equation for Langmuir adsorption model.

$$q_e = \frac{q_{max} b C_e}{1 + bC_e} \quad (3.5)$$

Equation 3.6 depicts the linearised Langmuir equation known as Langmuir-1 (Kinniburgh, 1986) is the most used. It is given as:

$$\frac{C_e}{q_e} = \frac{1}{q_{max}} C_e + \frac{1}{bq_{max}} \quad (3.6)$$

where, C_e is the concentration of fluoride at equilibrium, q_e is the adsorption capacity, q_{max} is the maximum theoretical adsorption capacity of the adsorbent and b is the Langmuir adsorption constant. The values of Langmuir parameters, q_{max} and b were calculated from the slope and intercept of the linear plots of $\frac{1}{q_e}$ versus C_e, with regression coefficient (R^2). The minimised deviations from the fitted equation result in the best error distribution (Kinniburgh, 1986).

The higher the b and q_{max} values the better the adsorbent (Tran *et al.*, 2017).

Freundlich isotherm is a modification of the Langmuir isotherm. It models a multi-site adsorption isotherm for rough or heterogeneous surfaces. Freundlich equation is derived to model the multi-site adsorption on heterogeneous surfaces.

The Freundlich isotherm is depicted as:

$$q_e = K_F C_e^{1/n} \quad (3.7)$$

The linearised form of Freundlich model is given as:

$$log\ q_e = log\ K_F + \frac{1}{n\ log\ C_e} \quad (3.8)$$

© University of Venda

where C_e is the equilibrium concentration of fluoride, q_e is equilibrium adsorption capacity, K_F and $\frac{1}{n}$ is Freundlich constants related to minimum adsorption capacity and adsorption intensity respectively. The values of K_F and $\frac{1}{n}$ are obtained from the slope and intercept of the linear Freundlich plot of log q_e versus $log\ C_e$ (Ghorai & Pant, 2004).

Figure 3.14 and Figure 3.15 depict the plots for linearsised Langmuir and Freundlich isotherm respectively, while constant values are presented in Table 3.5.

The plot of C_e/q_e values against C_e for the sorption data at 298 K gave straight lines with correlation coefficients of R^2 = 0.85 (Figure 3.14). The value of *1/n* for Langmuir is between 0 and 1, which is indicative of a favourable adsorption, possibly a monolayer adsorption of fluoride on the smooth surface of the adsorbent.

The plot of *log* q_e against *log* C_e for the sorption data at 298 K gave straight lines with higher correlation coefficients or co-efficient of determination (COD) (R^2 = 0.98) as shown in Figure 3.15. The higher the *b* and q_{max} values the better the adsorbent (Tran *et al.*, 2017). K_F (mg/g) is the Freundlich constant related to adsorption capacity and *1/n* is the dimensionless parameter for Freundlich adsorption isotherm model related to adsorption intensity which is an indication of the magnitude of surface heterogeneity or the adsorption driving force. Adsorption is favourable when *1/n < 1*, unfavourable when *1/n >1*, linear when *1/n = 1* and irreversible when *1/n = 0*. *1/n* value for Freundlich model is between 0 and 1 which is also an indication of favourable adsorption. The plot of *log* q_e against *log* C_e for the sorption data at 298 K gave straight lines with high correlation coefficients (R^2 = 0.98) as shown in Figure 3.15. Therefore, Freundlich isotherm gave a better fit to the sorption data, thereby confirming heterogeneous (multi-site) adsorption process.

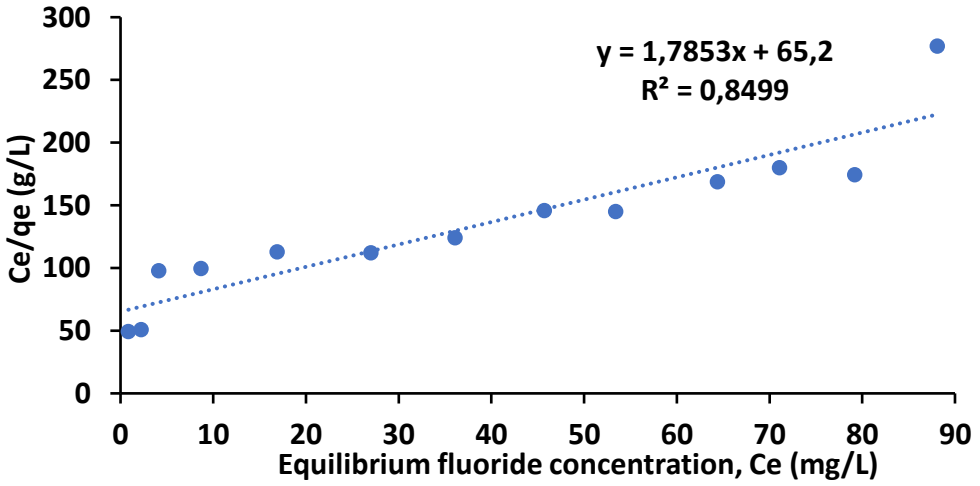

© University of Venda

Figure 3.14: Langmuir adsorption isotherm. (2.0 g activated clay, 60 min contact time, agitation speed of 250 rpm at 298 K. Fluoride concentration was varied from 1 to 100 mg/L).

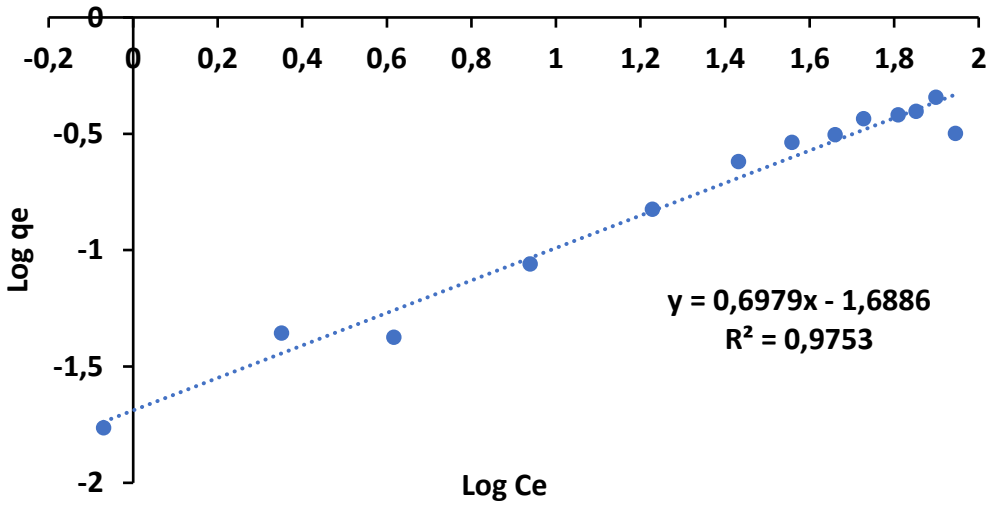

Figure 3.15: Freundlich adsorption isotherm. (2.0 g activated clay, 60 min contact time, agitation speed of 250 rpm at 298 K. Fluoride concentration was varied from 1 to 100 mg/L).

Table 3.5: Constant values for adsorption isotherms (linear).

Langmuir isotherm constants			Freundlich isotherm constants		
Q_m (mg/g)	b (L/mg)	R^2	K_F (mg/g)	$1/n$	R^2
0.62	0.0273	0.85	44.38	0.69	0.98

Langmuir model non-linearised form, which applies to homogeneous adsorption medium describing monolayer systems in a sorbent-sorbate interface is given as (Langmuir, 1916: Karthikeyan *et al.*, 2005: Lee & Tiwari, 2015; Tran *et al.*, 2017: Sahu & Singh, 2019) :

$$q_e = \frac{Q_m K_L C_e}{1 + K_L C_e} \quad (3.9)$$

where C_e is fluoride equilibrium concentration in the solution, q_e (mg/g) is the adsorption capacity or the amount of fluoride ion adsorbed per unit mass of mechanochemically-activated clay (MAC) adsorbent at equilibrium, Q_{max} (mg/g) is maximum adsorbents' monolayer capacity and K_L (L/mg) is Langmiur adsorption equilibrium constant related to the affinity of binding sites.

In addition, the fundamental characteristics of Langmuir isotherm was determined by the use of a dimensionless constant separation factor for the fluoride equilibrium parameter, R_L (Equation 3.10) (Weber & Chakravorti, 1974: Sahu & Singh, 2019). given as:

© University of Venda

$$R_L = \frac{1}{1 + K_L C_i} \quad (3.10)$$

where C_i (mg/L) is the initial fluoride concentration and K_L is the Langmuir equilibrium constant The R_L value is vital in determining if an sorption process is favourable ($0 < R_L < 1$), unfavourable ($R_L > 1$), linear ($R_L = 1$) or irreversible ($R_L = 0$).

The non-linear Freundlich adsorption isotherm is used to describe multilayer sorption on heterogeneous surfaces. Freundlich non-linearised equation is expressed as in Equation 3.11 (Freundlich, 1906: Foo & Hameed, 2010: Sahu & Singh, 2019):

$$q_e = K_F C_e^{1/n} \quad (3.11)$$

where C_e (mg/L) is equilibrium concentration of the fluoride, q_e (mg/g) is adsorption equilibrium capacity of the adsorbent, k_F (mg/g) is empirical Freundlich constant related to capacity of minimum adsorption and 1/n is the dimensionless parameter for Freundlich adsorption isotherm related to the intensity of adsorption which is adsorption driving forces' magnitude or the heterogeneity surface. Adsorption is favourable when 1/n < 1, unfavourable when 1/n >1, linear when 1/n = 1 and irreversible when 1/n = 0 (Ghorai & Pant, 2004: Foo & Hameed, 2010). The values of k_F and 1/n are derived from slope and intercept of log q_e versus log C_e.

Figure 3.16 depicts the non-linear plots for Langmuir and Freundlich adsorption isotherms, respectively while Table 3.6 shows the respective obtained model parameters for fluoride sorption by the mechanochemically-activated clay (MAC) adsorbent at 298 K.

The generated data described by the adsorption isotherms in Figure 3.16 revealed increased adsorption capacities with increasing fluoride concentration, characterised by saturation at high concentration. Based on the high correlation co-efficient (R^2) values and low chi-square (X^2) values in Table 3.6, the adsorption data fitted better to both Langmuir adsorption isotherm model (R^2 = 0.94 and X^2 = 0.001) and Freundlich adsorption isotherm model (R^2 = 0.92 and X^2 = 0.002) at 298 K (Table 3.6). This suggests that adsorption of fluoride onto MAC occurred via both homogeneous and heterogeneous surfaces.

Furthermore, the feasibility of fluoride uptake by both Langmuir and Freundlich models were confirmed by the calculated values of both the dimensionless constant, (R_L) and adsorption intensity (n). Both values range between 0 and 1, thereby affirming the favourable conditions for fluoride sorption by the synthesised MAC.

© University of Venda

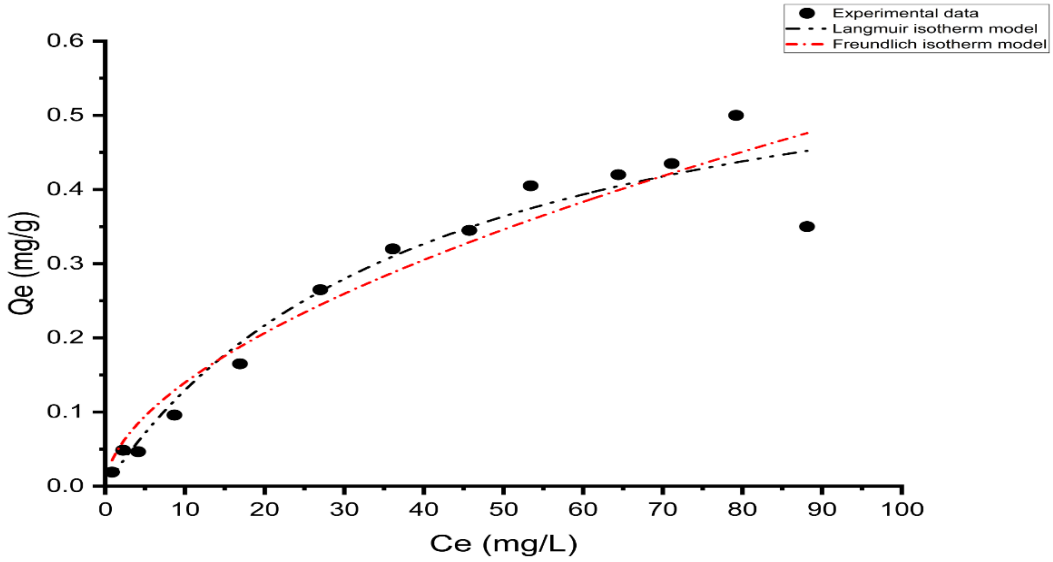

Figure 3.16: Langmuir and Freundlich adsorption isotherm plots of fluoride onto mechanochemically-activated clay (MAC) sorbent. (2.0 g activated clay, 60 min contact time, agitation speed of 250 rpm at 298 K. Fluoride concentration was varied from 1 to 100 mg/L).

Table 3.6: Langmuir and Freundlich isotherm parameters for fluoride sorption onto the mechanochemically-activated clay (MAC).

Model	Langmuir	Freundlich
Equation	(Q_m*K*C_e)(1+(K*C_e)	(K_f*(C_e*(1/n)
Plot	Q_e	Q_e
Q_m	0.6637 ± 1.9851	-
K	0.0242 ± 0.0080	0.0382 ± 0.0129
N	-	1.7752 ± 0.2640
Reduced chi-square (RCS) (X^2)	0.0016	0.0024
COD (R-Square) (R^2)	0.9480	0.9217
Adjusted R-Square (R^2)	0.9433	0.9141

3.3.8 Adsorption kinetic modelling of fluoride sorption

The Lagergren pseudo-first-order and pseudo-second-order of reaction kinetics and the intra-particle diffusion were modelled using the generated adsorption data. Pseudo-first-order kinetic model equation is given as Lagergren pseudo-first-order model (1898):

$$log\ (q_e - q_t) = -\frac{K_1}{2.303}\ t\ + log\ q_e \qquad (3.12)$$

© University of Venda

where q_t is fluoride amount on the clays' surface at time t (mg/g) and K_{1ads} is the equilibrium rate constant of pseudo-first-order sorption (min^{-1}). q_e is the fluoride amount adsorbed at equilibrium and K_1 (min^{-1}) pseudo-first-order adsorption equilibrium rate constant.

The straight-line plots of $log\ (q_e - q_t)$ against t will give the value of the rate constants *(K)*. Linear plots of $log\ (q_e - q_t)$ against t give straight line which shows the applicability of Lagergren equation.

The linear pseudo-second-order kinetic model is given as: (Lagergren, 1898):

$$\frac{t}{q_t} = \frac{1}{h} + \frac{t}{q_e} \qquad (3.13)$$

In equation 3.13, $h = kq_e^2$ (mg/gmin), therefore pseudo-second-order equation becomes

$$\frac{t}{q_t} = \frac{1}{k_2\, q_e^2} + \frac{t}{q_e} \qquad (3.14)$$

where $q_t = q_e^2 kt/(1 + q_e kt)$, fluoride amount on the clays' surface at any time, t (mg/g), K is the pseudo-second-order rate constant (g/mg min), q_e is the amount of fluoride ions sorbed at equilibrium (mg/g) and the initial sorption rate, $h = kq_e^2$ (mg/g min). The value of q_e (1/slope), k (slope^2/intercept) and h (1/intercept) of the pseudo-second-order equation can be obtained experimentally by plotting t/q_t against t (Ho, 2006; AL-Othman *et al.*, 2012)

The fitness of the pseudo-second-order model (Equation 3.14) on the sorption of fluoride on the clays surface was also investigated. The plot of t versus t/q_t gives a straight line with high correlation coefficient R^2 value of 0.99, while pseudo-first order model gave lower value (R^2 = 0.27) indicating that the pseudo-second order model is more applicable (Figures 3.17 and 3.18). From the plot, the values of the rate constant, K_{1ads} (min^{-1}) for first order is 1.1 x 10^{-2} (min^{-1}), while second-order model gave a higher rate constant, K_{2ads} = 2.18 (min^{-1}) (Table 3.7), hence, indicating sorption via chemisorption pathway.

© University of Venda

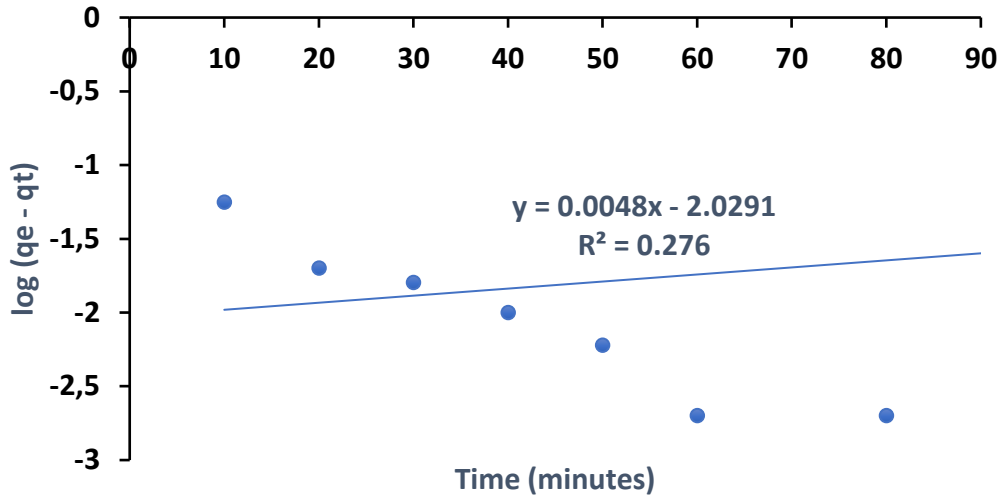

Figure 3.17: Plot of log (qe-qt) against time, t. (Experimental conditions: adsorbate concentration = 5 g/mL; pH = 6.5; temperature = 298 K).

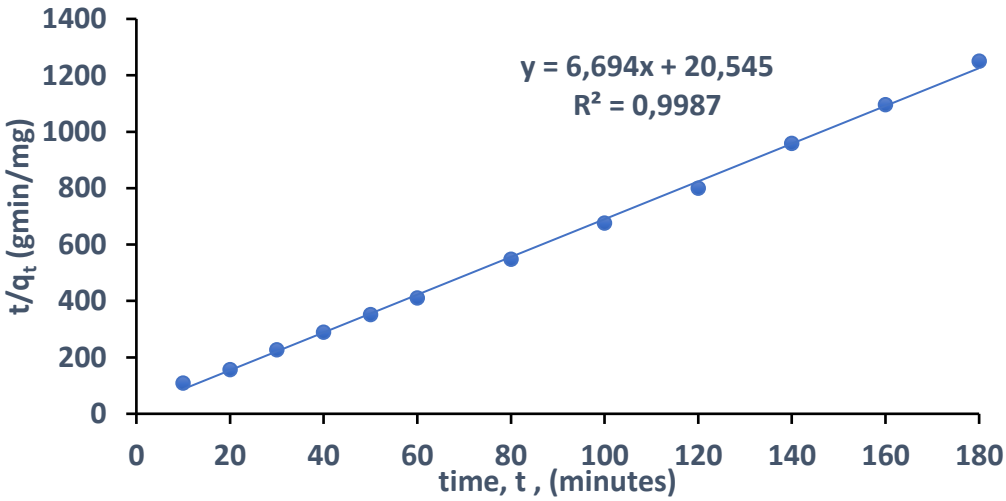

Figure 3.18: Plot of t/q_t against t. (Experimental conditions: adsorbate concentration = 5 g/mL; pH = 6.5; temperature = 298 K).

The constant values for adsorption kinetics model are given in Table 3.7.

Table 3.7: Constant values for adsorption kinetics model.

Pseudo-first-order			**Pseudo-second-order**		
$q_{e(exp)}$ (mg/g)	K_{1ads} (min^{-1})	R^2	K_{2ads} (g/mg.min)	$q_{e(cal)}$ (mg/g)	R^2
$9.8x10^{-1}$	1.1×10^{-2}	0.27	2.18	3.73×10^{-2}	0.99

Adsorption kinetics studies were carried out using pseudo-first-order (PFO) and pseudo-second-order (PSO) models to establish the sorption mechanism and fluoride removal adsorption rate of the synthesised MAC (Lagergren, 1898: Qureshi *et al.*, 1995: Ho *et al.*, 2000: Yoon *et al.*,

© University of Venda

2017: Denga *et al.*, 2018). The pseudo-first-order and second-order models are expressed by the non-linearised mathematical equations 3.15 and 3.16 respectively:

$$q_t = q_e\,(1 - e^{-K_{ad}t}) \quad (3.15)$$

$$q_t = \frac{q_e^2\,K_{2ads}\,t}{1 + K_2 q_e^2\,t} \quad (3.16)$$

Where q_e and q_t are the adsorbed fluoride per unit mass (mg/g) at equilibrium and time, t (min), K_{ad} (min^{-1}) and K_{2ads} ($g.mg^{-1}/min$) are rate constants for pseudo-first-order and pseudo-second-order respectively. Figure 3.19 depicts pseudo-first-order and second-order plots respectively while Table 3.8 presents the derived adsorption modelling parameters values values of pseudo-first-order and pseudo-second-order kinetics respectively.

Adsorption kinetics data in Table 3.8 shows that the co-efficient of determination (R^2) value for pseudo-first-order (PFO) (R^2 = 0.96) and pseudo-second-order (PSO) (R^2 = 0.96) are both high and also have low values of residual root mean square error (RMSE) = 0.003 each while values of X^2 are 0.000068 and 0.000083 in pseudo-first and second-order models respectively, suggesting that adsorption of fluoride onto the MAC interface both occurred via surface interaction between the active binding sites across the MAC and the fluoride ions depended on chemisorption and through physical interaction (physiosorption mechanisms) (Yoon *et al.*, 2017; Ngulube *et al.*, 2017; Denga *et al.*, 2018; Ayinde *et al.*, 2020).). Similar trends were observed and postulated in similar studies (Ngulube *et al.*, 2017; Yoon *et al.*, 2017; Denga *et al.*, 2018: Ayinde *et al.*, 2020).

The solute transfer in a solid-liquid sorption process is usually characterised either by particle or pore diffusion control. Intra-particle diffusion-controlled sorption process equation (Chanda et al., 1983; Meenakshi and Viswanathan, 2007) is given as:

$$In\left(1 - \frac{C_t}{C_e}\right) = -k_p t \quad (3.17)$$

where k_p is the particle rate constant (min^{-1}). The particle rate constant value is obtained by plotting the slope of $ln\,(1-C_t/C_e)$ against t.

The simple intra-particle diffusion model was proposed by Weber and Morris (1964), Gandhi *et al.* (2016), Onal *et al.* (2006) and Ghasemi *et al.* (2014) and the equation is given as:

$$q_t = k_i\,t^{1/2} \quad (3.18)$$

where k_i is the intra-particle rate constant ($mg/g\ min^{1/2}$).

© University of Venda

The slope of the plot of q_t against $t^{½}$ gives the intra-particle rate constant value. The plot of q_t versus $t^{1/2}$ gives an initial curve followed by a straight line which is suggestive of two types of mechanisms involved in the adsorption process. The initial curve represents the boundary layer effect while the linear part corresponds to intra-particle diffusion.

Both particle (Eq. 3.17) and pore (Eq. 3.18) diffusion models have been applied and the values of k_p and k_i shows that $k_p = 1.3 \times 10^{-3}$ min^{-} while $k_i = 2.4 \times 10^{-2}$ mg/min$^{1/2}$ (Table 3.8). Higher co-efficient of determination (COD), $R^2 = 0.84$ indicates the possibility of sorption process being controlled greatly by the particle diffusion while pore diffusion models with ($R^2 = 0.23$) is minimal in the sorption process (Figure 3.20).

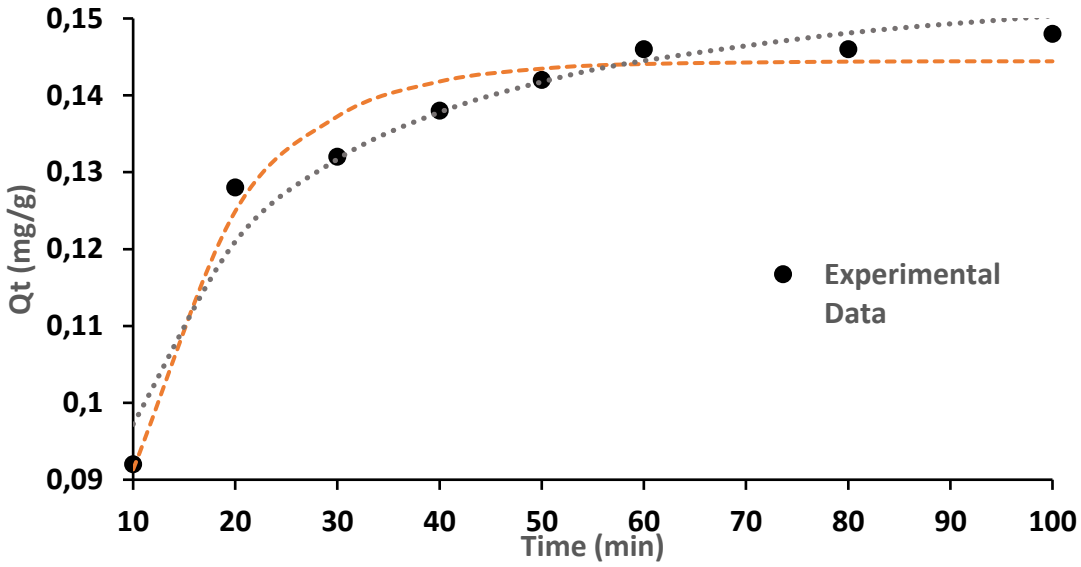

Figure 3.19: Pseudo-first-order (PFO) and Pseudo-second-order (PSO) kinetic model plot of fluoride uptake by the MAC.

© University of Venda

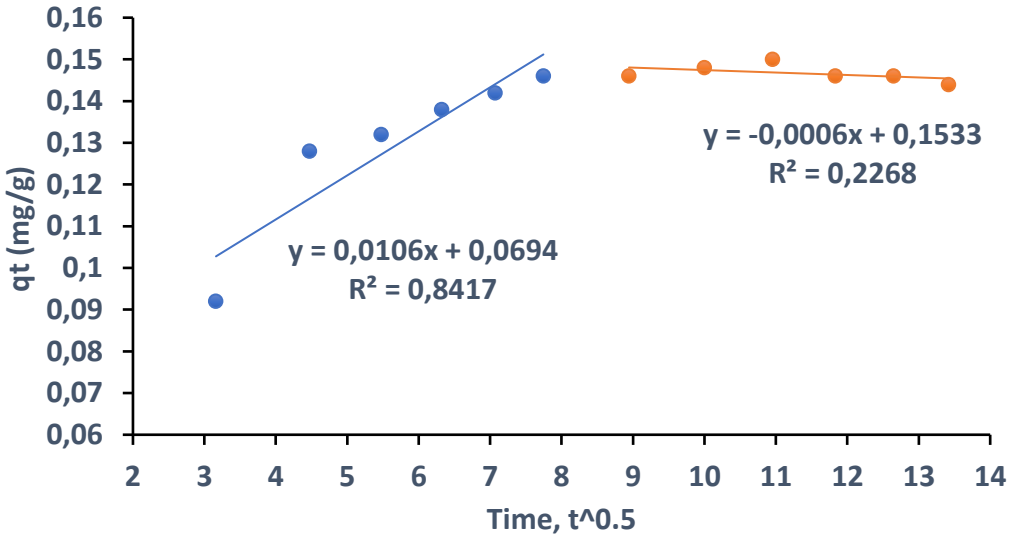

Figure 3.20: Intra-particle diffusion model. (Initial fluoride ion concentration, C_1 = 10 mg/L, pH = 6.5; temperature = 298 K).

Table 3.8: The kinetic parameters for pseudo-first-order (PFO), pseudo-second-order (PSO) and intra-particle diffusion models.

Models	Values
Pseudo-first-order (PFO)	
q_{cal} (mg/g)	0.10
K_{1ad} (min^{-1})	0.14
R^2	0.96
RMSE	0.0032
X^2	0.000068
Pseudo-second-order (PSO)	
q_{cal} (mg/g)	0.16
K_{2ads} (g min^{-1} mg)	0.96
R^2	0.96
RMSE	0.0035
X^2	0.000083
Intra-particle diffusion	
C_1 (mg/g)	0.1
k_1	0.024
C_p (mg/g)	0.2
k_p	0.0013
R_1^2	0.8417
R_2^2	0.2268

3.3.9 Field testing of field (Siloam) groundwater

Table 3.9 depicts the physicochemical properties of field water (pH = 8) before and after treatment. The percentage of fluoride removed from Siloam groundwater was 21%. This is lower

© University of Venda

than the percent fluoride removal of 32% in the simulated fluoride water. The lower value of percent fluoride removal observed for the raw field water might be due to more OH groups at the higher pH 8, which competed. Furthermore, the fluoride concentration in the raw Siloam field water before and after treatments at different pH values of 6.0 and 8.5 are still much higher than the permissible WHO limits. This suggests that the adsorbent was not effective but could be subjected to further modification, thereby increasing its surface area and adsorption capacity. There was no major change in the concentrations of the (major anions) Cl^-, Br^-, and SO_4^{2-} before and after treatment indicating that these co-existing anions did not compete in the defluoridation process, while there was a reduction in the concentration of PO_4^{2-} from 4.84 to 2.19 mg/L, representing 40.4% removal, suggesting that PO_4^{2-} competed with F^- in the defluoridation process. NO_3^- was not detected (ND). Though the concentrations of all the cations were slightly higher after treatment as a result of some cationic exchanges into the media, they are still within WHO permissible limits. Hence, the activated clay is safesafe as far as cation release into water is concerned and therefore recommended for remediation of fluoride from drinking water.

Table 3.9. Physicochemical properties of raw and treated field fluoride rich groundwater.

Parameters	Concentration of parameters in raw field water (mg/L)	Concentration of parameters in defluoridated pH-adjusted field water (mg/L)	Concentration of parameters in defluoridated raw field water (mg/L)	WHO permissible limits (mg/L)
pH	8.0	6.0	8.0	6.5 - 8.5
F^-	5.34	4.18	4.27	1-1.5
Cl^-	5.08	34.15	34.26	250
Br^-	0.41	0.39	0.41	200
SO_4^{2-}	12.22	12.22	12.22	200-400
PO_4^{3-}	4.84	2.19	2.019	20-50
Na+	65.44	102.30	81.50	200-250
K^+	19.40	68.50	66.30	200-250
Ca^{2+}	2.75	3.15	6.80	75
Mg^{2+}	21.25	22.55	51.50	50

3.3.10 Antibacterial experiments using well diffusion assay method

Antibacterial activities of the mechanochemically-activated clay samples were determined by using the well diffusion assay method.

© University of Venda

Figure 3.21 shows a pictorial view of the plates and the six bored holes containing the mixtures of the activated clays and the *Escherichia coli* (*E. coli*) strains that were being investigated for antibacterial activities via zone of inhibition measurements. The six clay samples were activated at varying contact times of between 5 and 60 min. From Figure 3.21, it can be observed that all the six samples within the bored holes did not inhibit the bacterial strains and hence, they had no zone of inhibition, thereby indicating that they might not have any potent activities against the *E. coli* strains used in this study.

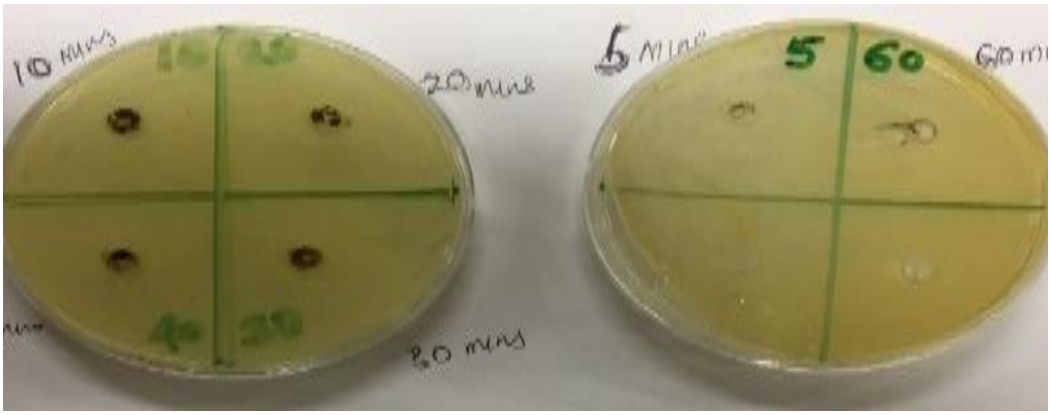

Figure 3.21: Pictorial view of the plates showing mixtures of *E. coli* strains and activated clay samples in the six bored holes.

3.3.11 Conclusion

This chapter evaluated the efficiency of mechanochemically-activated clay soils towards fluoride and pathogen removal from water. The maximum fluoride adsorption capacity of the mechanochemically-activated clay soil was found to be 1.87 mg/g with 32% fluoride removal at 2 g/100 mL adsorbent dosage, initial fluoride concentration of 3.2 mg/L, pH 6.0, 60 min contact time and 250 rpm at 298 K. The presence of Cl^-, SO_4^{2-} and NO_3^- showed little influence on percent fluoride removal while PO_4^{3-} and CO_3^{2-} decreased the percent fluoride removed. The adsorption isotherm data fitted well to Freundlich isotherm model, indicating that adsorption occurred on a multilayer surface when linearised model was used but fitted well to both Langmuir and Freundlich when non-linear model were employed, hence suggesting adsorption occurred on both monolayer and multilayer surfaces. Adsorption kinetics data showed a better fit to pseudo-second-order reaction kinetics when linearised modelling were used indicating the dominance of chemisorption mechanism. The usage of non-linearised modelling which is most recent adsorption modelling showed the isotherms data fitted well to both Langmuir and Freundlich isotherm models while adsorption kinetics data fitted well to both pseudo-first order and pseudo-second order reaction

© University of Venda

kinetics respectively,thus indicating adsorption mechanisms to be both physiosorption and chemosorption respectively.

The mechanochemically-activated clay revealed zero or no inhibition zone against *E. coli* strains, thus suggestive of absence or very low antibacterial properties on the activated clays' surfaces. The mechanochemically-activated clay sorbent showed little adsorption efficiency towards fluoride removal and does not have any potential towards pathogen removal. Therefore, further modification of its surfaces in order to enhance its efficiency through hydrothermal treatment is recommended.

© University of Venda

REFERENCES

AL-Othman, Z. A., Ali, R & Naushad, Mu. (2012). Hexavalent chromium removal from aqueous medium by activated carbon prepared from peanut shell: Adsorption kinetics, equilibrium and thermodynamic studies. *Chemical Engineering Journal*, 1 238-247.

Aram, M., Limaee, N. Y., Mahmoodi, N. M & Tabrizi, N. S. (2005). Removal of dyes from colored textile wastewater by orange peel absorbent: equilibrium and kinetic studies. *Journal of Colloid Interface Science*, 288 371-376.

Chanda, M., O'Driscoll, K. F & Rempel, G. L. (1983). Sorption of phenolics onto cross-linked poly (4-vinylpyridine), *Reaction Polymers*, 1 281–293.

Coetzee, P. P., Coetzee, L. L., Puka, R & Mubenga, S. (2003). Fluoride adsorption modelling and characterisation of clays for defluoridation of natural clays. *Water South Africa*, 29 3 331-338.

Dhillion, A & Kumar, D. (2015). Development of nanoporous adsorbents for the removal of health-hazardous fluoride ion from aqueous systems. *Journal of Materials Chemistry,* A. 3 4215-4228.

Eggleson, C. M & Jordan G. (1998). A new approach to *pH* of point of zero charge mearsurement: Crystal-face specificity by scanning force microscopy (SFM). *Geochimica et Cos. Acta,* 62 11 1919-1923.

Foo, K. Y., & Hameed, B. H. (2010). Insights into the modeling of adsorption isotherm systems. *Chemical Engineering Journal, 156,* 1, 2-10.

Freundlich, H. M. F. (1906). Uber die adsorption in losungen. *Journal of Physical Chemistry,* Leipzig. 57A 385-470.

Gandhi, N., Sirisha, D., Chandra, N & Sekhar, K. B. (2016). Adsorption of Fluoride from Aqueous Solution by Using Pineapple (*Ananas comosus*) Peel and Orange (*Citrus sinensis)* Peel Powders. *International Journal of Environmental Bioremediation & Biodegradation,* 4 2 55-67. doi: 10.12691/ijebb-4-2-4. 05/01/19.

Ghasemi, M., Naushad, M., Ghasemi, N & Khosravi-fard, Y. (2014). A novel agricultural waste-based adsorbent for the removal of Pb (II) from aqueous solution: kinetics, equilibrium and thermodynamic studies. *Journal of Industrial Engineering and Chemistry,* 20 2 454-461. 06/01/19.

© University of Venda

Ghorai, S & Pant, K. K. (2014). Investigations on the column performance of fluoride adsorption by activated alumina in a fixed-bed, *Chemical Engineering Journal*, 98 165–173.

Gitari, W. M., Ngulube, T., Masindi, V & Gumbo, J. R. (2013). Defluoridation of groundwater using Fe^{3+}-modified bentonite clay: optimisation of adsorption conditions. *Desalination, Water Treatment.* 53 6 1578–1591.

Gitari, M. W., Petrick, L. F & Musyoka, N. M. (2016). Hydrothermal conversion of South African CFA into pure phase zeolite Na-P1. In *Metals and Non-metals 'Zeolites-Useful minerals'* Claudia Belviso (Ed). 25-42. Guggenheim, S & Martin, R. T. (1995). Definition of clay and clay mineral: Joint report of the AIPEA and CMS nomenclature committees. *Clays and Clay Minerals*, 43 2 255–256.

Guggenheim, S & Martin, R. T. (1995). Definition of clay and clay mineral: Joint report of the AIPEA and CMS nomenclature committees. *Clays and Clay Minerals*, 43 2 255–256.

Hauge, S., Osterberg, R., Bjorvatn, K. & Selvig, K. A. (1994). Defluoridation of drinking water with pottery: Effect of firing temperature. *Scandinavian Journal of Dental Research,* 102 329-333.

Ho, Y. S. (2006). Second-order-kinetic model for the sorption of cadmium onto tree fern: a comparison of linear and non-linear methods, *Water Research,* 40 119–125.

Ismail, A., Mekky, H & Elmaghraby M. S. (2014). Assessment and Utilization of Some Egyptian Clay Deposits for Producing Lightweight Concrete, *International Journal of Materials Science and Applications,* 3 3 79-83. doi: 10.11648/j.ijmsa.20140303.11

Jia, Y., Zhu, B. S., Zhang, K. S., Jin, Z., Luo, T., Yu, X. Y., *et al.*, (2015). Porous 2-line ferrihydrite/byerite composite (LFBC): Fluoride removal performance and mechanism. *Chemical Engineering Journal.* 268 325–336.

Karthikeyan, G., Pius, A & Alagmuthu, G (2005). Fluoride adsorption studies of montmorillonite clay. *Indian Journal of Chemical Technology*, 12 263-272.

Kinniburgh, D. G. (1986). General purpose adsorption isotherms. *Environmental Science and Technology*,20 9 895-904.

Konta, J. (1995). Clay and Man: Clay raw materials in the service of man. *Applied Clay Science,* 10 275-335.

Lagergren, S. (1898). Zur Theorie der sogenannten adsorption geloster stoffe, K. Sven. Vetenskapsakademiens. *Handlingar*. 24 1–39.

© University of Venda

Langmuir, J. (1916). The properties of solids and liquids. *Journal of America Chemical Society*, 38 2221-2295.

Lee, S. M., & Tiwari, D. (2015). Porous hybrid materials in the remediation of water contaminated with As (III) and As (V). *Chemical Engineering Journal, 270*, 496-507.

Mahramlioglu, M., Kizilicilii, I & Bicer, I. O. (2002). Adsorption of fluoride from aqueous solution by acid treated spent bleaching earth. *Journal of Fluorine Chemistry*, 115 41-47.

Masindi, V., Gitari, M. W & Ngulube, T. (2015). Defluoridation of groundwater using Cryptocsrystalline magnesite. *Journal of Water Reuse and Desalination*, 05.3, 283-292.

Meenakshi, S & Viswanathan, N. (2007). Identification of selective ion exchange resin for fluoride sorption, *Journal of Colloid Interface Science,* 308 438–450.

Meenakshi, S., Sairam, Sundaram, C & Sukumar, R. (2008). Enhanced fluoride sorption by mechanochemically activated kaolinites, *Journal of Hazard Materials,* 153 164–172.

Meimaroglou, N., & Mouzakis, C. (2019). Cation Exchange Capacity (CEC), texture, consistency and organic matter in soil assessment for earth construction: The case of earth mortars. *Construction and Building Materials*, *221*, 27-39.

Mudzielwana, R., Gitari, M. W & Msagati, T. A. M. (2016). Characterisation of smectite-rich clay soil: Implication for groundwater defluoridation. *South African Journal of Science,* 112 11/12 1-8.

Onal, Y., Akmil-Basar, C., Eren, D., Sarıcı-Ozdemir, C & Depci, T. (2006). Adsorption kinetics of malachite green onto activated carbon prepared from Tunc¸ bilek lignite, *Journal of Hazard Materials*, 128 150–157.

Sahu, O., & Singh, N. (2019). Significance of bioadsorption process on textile industry wastewater. In *The Impact and Prospects of Green Chemistry for Textile Technology*, (367-416). Woodhead Publishing.

Sarkar, M.., Banerjee, A., Pramanick, P. P & Sarkar, A. R. (2006). Use of laterite for fluoride removal from contaminated drinking water, *Journal of Colloid Interface Science,* 302 432–441.

SANS 241. South African National Standard (SANS) 241 (2006). Drinking Water Specification. South African Bureau of Standards (SABS) SANS 241. Pretoria, South Africa. 187-205.

Spark, D. L. (1997). Environmental soil chemistry. 2nd ed. Amsterdam: Academic Press.

© University of Venda

Tor, A., Danaoglu, N., Arslan, G & Cengeloglu, Y. (2009). Removal of fluoride from water by using granular red mud: Batch and column studies. *Journal of Hazardous Materials,* 164 271-278.

Toor, M., Jin, B., Dai, S & Vimonoses, V. (2014). Activating natural bentonite as cost effective adsorbent for removal of Congo red in wastewater. *Journal of Industrial Engineering Chemistry*, 1979 1–9.

Tran, H. N., You, S.-J., Hosseini-Bandegharaei, A., & Chao, H. P (2017). Mistakes and inconsistencies regarding adsorption of contaminants from aqueous solutions: a critical review. *Water Research, 120,* 88-116.

Vhahangwele, M., Mugera, G. W., & Tholiso, N. (2014). Defluoridation of drinking water using Al^{3+}-modified bentonite clay: optimisation of fluoride adsorption conditions. *Toxicological and Environmental Chemistry*, *96*(9), 1294-1309.

Waghmare, S. S., & Arfin, T. (2015). Fluoride removal by clays, geomaterials, minerals, low cost materials and zeolites by adsorption: a review. *International Journal of Science, Engineering and Technology Research*, *4*(11), 3663-3676.

Weber, T. W., & Chakravorti, R. K. (1974). Pore and solid diffusion models for fixed-bed adsorbers. *American Institute of Chemical Engineers* (*AlChE*) *Journal*, *20*(2), 228-238.

Weber, W. J & Morris, J. C. (1964). Equilibria and capacities for adsorption on carbon, *Journal of Sanitary Engineering Division,* 90 79–107.

World Health Organization. (2001; 2011; 2013). Water quality: Guidelines, standards and health. Assessment of risk and risk management for water-related infectious disease.

World Health Organization (WHO). Water Sanitation/Health. 2015: http://www.who.int/water_sanitation_health/diseases. 25/08/18

Zhang, Z., Tan, Y & Zhong, M. (2011). Defluoridation of wastewater by calcium chloride modified natural zeolite. *Desalination,* 276 246–252.

© University of Venda

CHAPTER FOUR: HYDROTHERMAL TREATMENT OF ALUMINOSILICATE-RICH CLAY SOILS: EVALUATING OPTIMUM CONDITION FOR SYNTHESIS AND PHYSICOCHEMICAL CHARACTERISATION

4 Abstract

Clay minerals are widespread and abundant on the earth's surface. Clay adsorptive and surface properties have enabled it to be applied as adsorbent for removing contaminants from water. In the previous chapter, the mechanochemically-activated clay (MAC) was applied in batch adsorption study and pathogen removal from water. The maximum adsorption capacity was found to be 1.87 mg/g with 32% fluoride removal at 2 g/100 mL dosage, initial fluoride concentration of 3.2 mg/L, pH 6.0, 60 min and 250 rpm at 298 K. However, the material showed no antibacterial properties. In a quest to improve the efficiency of MAC towards fluoride and pathogen removal, in this chapter, MAC was hydrothermally treated. Two-step process involving silica and alumina dissolution followed by hydrothermal treatment was adopted. For silica and alumina dissolution from the clay, the parameters considered were NaOH concentration and reaction time while for hydrothermal treatment, the parameters considered were hydrothermal treatment temperature, time and water content. Characterisation techniques such as FTIR, XRD, SEM and BET were employed to establish optimum conditions for synthesis of hydrothermally-treated aluminosilicate clay (HTAC ≈ HTMAC). The optimum conditions established for silica and alumina dissolution were 1.5 M NaOH concentration and 2 h contact time at 298 K, based on previous hydrothermal treatment experiments. It was observed that other major and minor metal species were released into the aqueous phase, in addition to natural aluminosilicate precursors found in soil crusts. These metal species impacted on the physical and chemical properties of the clay materials. This study showed that irrespective of the treatment time, increase of treatment temperature enhanced the adsorptive properties of the zeolitic clay products. The optimum conditions for synthesis of hydrothermally-treated aluminosilicate clay (HTAC ≈ HTMAC) were found to be, 48 h hydrothermal treatment time, 140 °C hydrothermal treatment temperature and 9 mL water content. The XRD analysis showed that sample synthesised at these conditions forms aggregated microsphere-like particles. Several new mineral phases corresponding to hydroxy sodalite were confirmed by characteristic sharp peaks around at 2-degree θ = 15, 25, 32 and 35, while SEM micrographs showed clear gel-like geopolymer having microspheric and spheroidal "cotton ball"

© University of Venda

particle morphology after treatments. BET showed an increase in surface area from 25 m^2/g to 33.56 m^2/g after treatment thereby confirming successful activation. The pore diameter distribution as a function of pore volume indicates that all samples had highest volume further confirming that these materials are mesoporous. Preliminary defluoridation experiment showed that the sample prepared under the aforementioned conditions has higher defluoridation capacity over the other samples and was therefore selected for application in subsequent experiments.

Keywords: Clay dissolution; Characterisation; Crystallization; Hydrothermal treatment; Optimisation

4.1 Introduction

Hydrothermal treatment is the reaction of any form of material in the presence of aqueous solvents or mineralisers under high pressure and temperature conditions to dissolve and recrystallise materials that are relatively insoluble under ordinary conditions (Byrappa & Yoshimura, 2006; 2012). It is a multiphase reaction in which dissolution and crystallisation processes occur and involve at least one liquid phase and both amorphous and crystalline solid phases (Cundy & Cox, 2005). This technique offers advantages such as energy-saving, simplicity, cost effectiveness, better nucleation control, pollution-free, higher dispersion, higher rate of reaction, better shape control, and lower temperature of operation in the presence of an appropriate solvent over other conventional treatment methods (Byrappa *et al.*, 2006). Hydrothermal synthesis has been used to improve the surface area and crystallinity of aluminosilicate materials for better adsorption performance (Holler & Wirsching, 1985; Yoshimura & Byrappa, 2008; Byrappa & Yoshimura, 2012; Cundy & Cox, 2005; Luo *et al.*, 2018). Moreover, the technique is also used to synthesis zeolites from parent aluminosilicate materials. Hollman *et al.* (1999) synthesised zeolite Na-P1 through direct hydrothermal treatment from coal fly ash (CFA) and NaOH solution. Apart from direct synthesis procedure used by Hollman *et al.* (1999), Musyoka *et al.* (2009) and Gitari *et al.* (2016) used a two-step process involving aluminosilicate dissolution followed by hydrothermal treatment to synthesise different types of zeolites and other crystalline materials from coal fly ash. In addition, various materials have been previously developed through hydrothermal treatment of alumunosilicate materials including clays and further applied in water treatment (Dhillon *et al.*, 2015; Khandare & Mukherjee, 2019). These materials showed better performance than the parent materials.

© University of Venda

To date, the multi-functionality of the hydrothermally-treated smectite clay feedstock (which mainly contains phillipsite homblende, analcime, calcite, hydrosodalite and cancrinite mineral phases) towards simultaneous removal of fluoride and pathogen from groundwater has not been reported. Hence, this work focuses on hydrothermal treatment of aluminosilicate-rich clay with NaOH and further evaluates its applicability in fluoride and pathogen removal from groundwater. The specific objectives of this chapter were to i) optimise the operational parameters for hydrothermal treatment of aluminosilicate clay soils using NaOH by a two-step process and ii) examine the physicochemical characteristics of the synthesised products and lastly, iii) to conduct preliminary defluoridation experiment to establish conditions that yield higher fluoride removal.

4.2 Materials and methods

4.2.1 Sample collection and preparation

The clay samples were obtained from Mukondeni Village, Vhembe District, Limpopo, South Africa. The clay was pretreated and activated mechanochemically following the procedure described in subsection 3.2.2. All chemical reagents used in this study were as follows: NaOH pellets-anhydrous > 98% (Sigma Aldrich), NaF > 99% (Sigma Aldrich), HCl, Na_2CO_3 > 99% (Sigma Aldrich), $NaNO_3$ > 99% (Sigma Aldrich), NaCl > 99% (Sigma Aldrich), Na_2PO_4 > 99% (Sigma Aldrich), Na_2SO_4, TISAB III solution (Sigma Aldrich). These were all analytical grade chemicals.

4.2.2 Hydrothermal treatment of aluminosilicate clay (HTAC)

A two-step process adopted from Hollman *et al.* (1999), Musyoka *et al.* (2009) and Gitari *et al.* (2016) was used for the synthesis of HTAC. Briefly, the treatment process involved dissolution of the mechanochemically-activated aluminosilicate clay through ageing in NaOH solution followed by hydrothermal treatment. For dissolution of alumina and silica from clay mineral, the optimum NaOH concentration and contact time were evaluated. For hydrothermal treatment, the hydrothermal temperature, time and water content were optimised.

4.2.2.1. Effect of NaOH concentration

To evaluate the effect of NaOH concentration, solutions of 250 mL of 0.5, 1, 1.5 and 2 M NaOH were prepared by dissolving 5, 10, 15 and 20 g of NaOH pellets in 250 mL volumetric flask using Milli-Q water (18.2 mΩ.cm). The flasks were stoppered and shaken thoroughly for effective mixing of solution. Thereafter, 100 mL each of NaOH solution were transferred into 250 mL heat-

© University of Venda

resistant-high-density polyethylene bottles with 5 g clay dispersed into each bottle. Mixtures were stirred for 2 h at a temperature of 47 °C and stirring speed of 800 rpm (Gitari *et al.*, 2016). The mixtures were then filtered using 0.45 µm pore polypropylene membrane filters in a filter flask assemblage connected to a vacuum pump. The residues were washed with 500 mL Milli-Q water, transferred into petri dishes and dried in the oven at 110 °C for 8 h. After drying, residues were placed in desiccators to cool and before weighing.

To further confirm the optimum concentration of NaOH solution for clay dissolution, the filtrates were analysed for silicon and aluminium using an Inductively-Coupled-Plasma Mass-Spectroscopy (ICP - MS) instrument, Agilent 7900 ICP-MS, made in Santa Clara, USA. The NaOH concentration which leached higher Si and Al concentration was then used for subsequent clay soils dissolution (Grutzeck & Siemer, 1997; Catauro *et al.*, 2014; Aldabsheh *et al.*, 2015).

4.2.2.2 Optimisation of contact time

To evaluate the effect of contact time in dissolution of silica and alumina, the solution containing 1.5 M NaOH concentration was used. Aliquots of 100 mL of 1.5 M NaOH were pipetted into four 250 mL heat resistant plastic bottles with 5 g of clay transferred into each bottle. Mixtures were stirred at a speed of 800 rpm for 1, 2, 3, 4, 5 and 6 h at 47 °C. After stirring, the procedure described in subsection 4.2.2.1 was followed by treatment of the mixtures to determine the optimum time for silica and alumina dissolution from the clay.

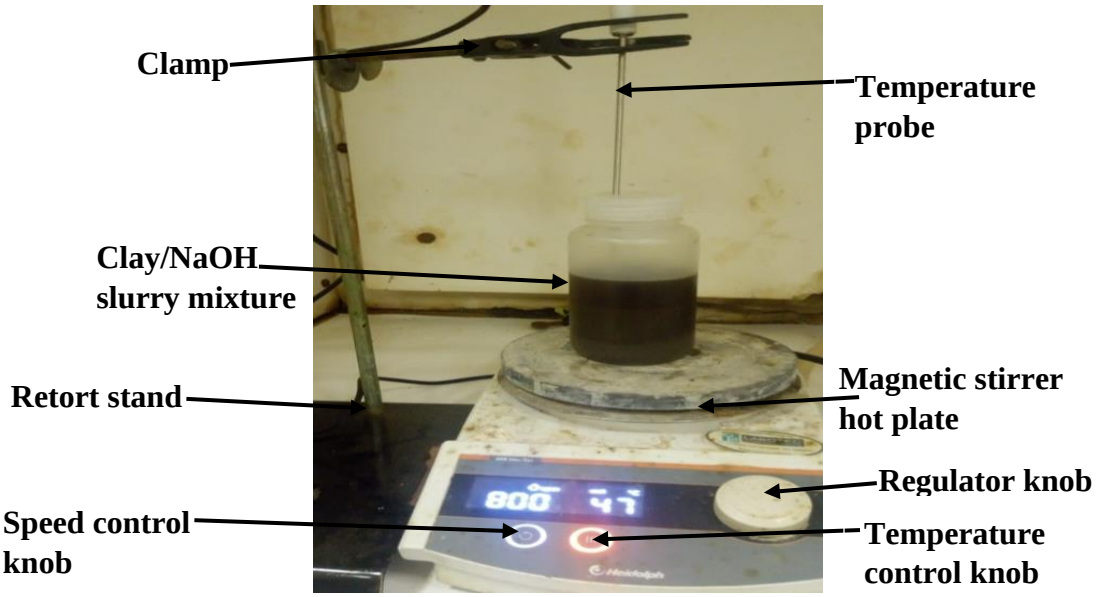

Figure 4.1: Experimental set up during dissolution and ageing process showing the alkaline clay slurry mixture on the magnetic stirrer hot plate.

© University of Venda

4.2.2.3 Optimisation of hydrothermal treatment

In this second step, the mixtures prepared under the condition obtained in subsections 4.2.2.1 and 4.2.2.2 (i.e., using 5 g clay, 1.5 M NaOH and 2-hour contact time) were subjected to hydrothermal treatment. The optimum conditions evaluated for hydrothermal treatment included temperature, treatment time, and water content. Table 4.1 depicts the number of experimental runs conducted for hydrothermal treatment of the clay as well as the experimental variables. Briefly, the hydrothermal treatment was carried out as follows: aliquots of the aluminosilicate slurry obtained from step 1 was mixed with the desired volume of water indicated in Table 4.1 and transferred into a Parr bomb vessel (Figure 4.2), placed in an oven at a desired temperature for a specific time (Table 4.1). After the treatment, the recovered solid residues were dispersed in 500 mL of Milli-Q water to reduce the effect of high alkalinity of solution on the adsorbent formed. The suspensions were then passed through 0.45 µm pore polypropylene membrane filters. The residues were further rinsed with Milli-Q water until near neutral pH. Thereafter, the clean residues were oven-dried at 110 °C for 6 h and then milled to pass through 250 µm test sieve using a mortar and pestle and then stored in plastic bottles to prevent moisture ingress.

© University of Venda

University of Venda
Creating Future Leaders

Table 4.1: Experimental conditions for optimum synthesis of hydrothermally-treated aluminosilicate clay.

Parameter Investigated	Run	H_2O added after Ageing process (mL)	Ageing temperature (°C)	Ageing time (h)	Hydrothermal temperature (°C)	Hydrothermal time (h)	Sample
Hydrothermal	1	9	47	2	100	12	HTAC-1
treatment	2	9	47	2	100	24	HTAC-2
temperature	3	9	47	2	100	36	HTAC-3
and time	4	9	47	2	100	48	HTAC-4
	5	9	47	2	140	12	HTAC-5
	6	9	47	2	140	24	HTAC-6
	7	9	47	2	140	36	HTAC-7
	8	9	47	2	140	48	HTAC-8
	9	9	47	2	160	12	HTAC-9
	10	9	47	2	160	24	HTAC-10
	11	9	47	2	160	36	HTAC-11
	12	9	47	2	160	48	HTAC-12
	13	9	47	2	200	12	HTAC-13
	14	9	47	2	200	24	HTAC-14
	15	9	47	2	200	36	HTAC-15
	16	9	47	2	200	48	HTAC-16
Water content	17	0	47	2	140	48	HTAC-17
during	18	3	47	2	140	48	HTAC-18
	19	6	47	2	140	48	HTAC-19

© University of Venda

University of Venda
Creating Future Leaders

Hydrothermal	20	9	47	2	140	48	HTAC-20
treatment step	21	12	47	2	140	48	HTAC-21

Hydrothermal treatment time and temperature were varied concurrently in order to obtain optimal conditions for HTAC synthesis (Adapted from Musyoka, 2009; 2012).

Footnote: Hydrothermally-treated aluminosilicate clay samples = HTAC ≈ HTMAC samples.

© University of Venda

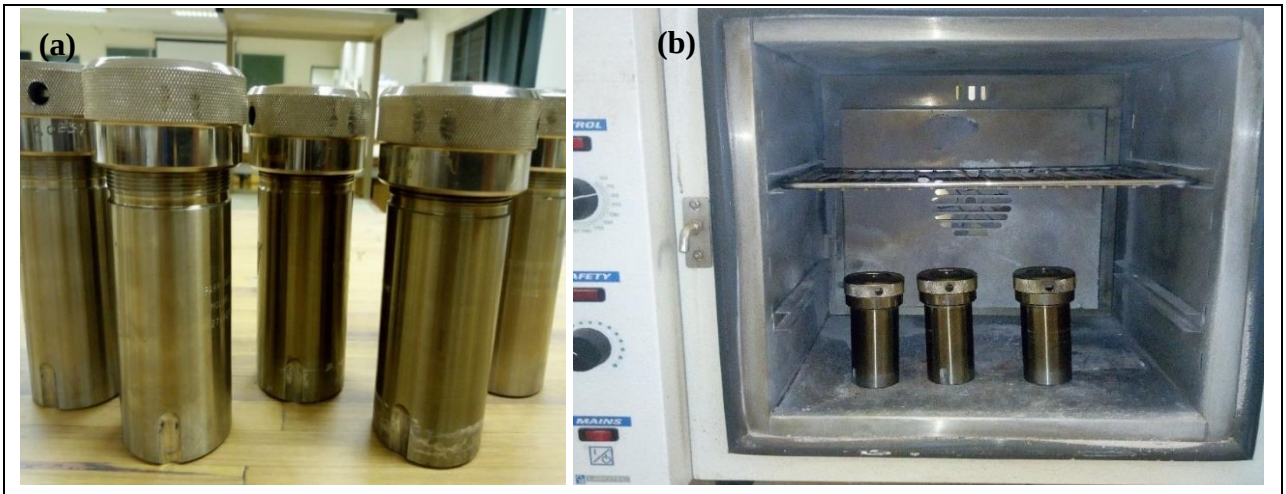

Figure 4.2: (a) 40 mL cups Parr bomb vessels. **(b)** Parr bomb vessels inside the oven.

4.2.3 Defluoridation experiments

All hydrothermally-treated samples were subjected to batch defluoridation in order to determine the sample with highest fluoride removal efficiency. The experiments were conducted using 0.2 g/40 mL HTAC dosage, 13 mg/L fluoride solution in 250 mL bottles at initial pH of 6.5. The mixtures were shaken at 200 rpm speed for 30 min at 298 K. The mixtures were then centrifuged for about 60 min at a speed of 4000 rpm and the supernatants analysed for residual fluoride by using a four-standard-calibrated ORION fluoride ion-selective electrode. TISAB III solution was added to both standards and samples at volume ratio of 1:10 to de-complex fluoride ions. All the experiments were done in duplicates and the mean values were reported.

4.2.4 Physicochemical and mineralogical characterisation

The hydrothermally-treated aluminosilicate clay (HTAC) products were evaluated for functional groups using Fourier Transform Infrared spectroscopy (Bruker, Germany: ATR-Diamond FT-IR spectro-photometer). The treated clay surface and specific area, pore volumes and pore sizes were measured with Micromeritics TriStar II Surface Area and porosity unit instrument (Micromeritics, Norcross, GA, USA) using Brunauer-Emmett-Teller (BET) method. Scanning electron microscope was used to investigate the clays' morphology by using JEOL - 2100 Electron Microscope. Examination of the qualitative and quantitative mineral phase composition was done by using a D8 advance X-ray diffraction (Bruker, Germany) equipped with Cu- Kα source radiation.

© University of Venda

4.3 Results and discussions

4.3.1 Chemical composition of the raw and mechanochemically activated clay soils

X-ray fluorescence analysis of mechanochemically-activated clay (MAC) has been reported in the previous chapter and publication (Obijole *et al.*, 2019). The results showed that MAC had SiO_2 (52.48%) and Al_2O_3 (14.62%) as the major components. This high concentration of SiO_2 and Al_2O_3 is typical of aluminosilicate materials. Other minor components observed were Fe_2O_3 (6.64%), MgO (2.98%), CaO (1.53%) and K_2O (1.24%) in addition to other trace components of TiO_2, Na_2O and P_2O_5. This confirms that MAC is a potential suitable precursor for hydrothermal conversion into zeolitic or geopolymeric products which could improve the surface and adsorptive properties of the clay soils.

4.3.2 Optimisation of silicon and aluminium dissolution from mechanochemically-activated clay (MAC)

4.3.2.1 Optimisation of NaOH concentrations

Figure 4.3 presents the residual Silicon and Aluminium concentrations obtained in filtrates generated from mechanochemically-actvated clay using different NaOH concentrations. It was observed that Silicon concentrations were higher than Aluminium concentrations, which could be partly due to higher content of Silicon than Aluminium in the precursor minerals and higher intrinsic extent of Silicon dissolution than Alluminium (Xu & Deventer, 2000; Obijole *et al.*, 2019). It was also observed that increasing NaOH concentration from 0.5 to 1.5 M led to increasing dissolution of Silicon and Aluminium from the clay soils. Further increase in NaOH concentration to 2 M decreased the dissolution of Silicon and Aluminium significantly. This could be due to the formation of Al-Si gels at the high alkaline regime generated leading to reduction of Aluminium and Silicon in solution at NaOH concentrations higher than 1.5 M (Nikolov *et al.*, 2017). Therefore, 1.5 M NaOH was selected as the optimum concentration for subsequent experiments.

© University of Venda

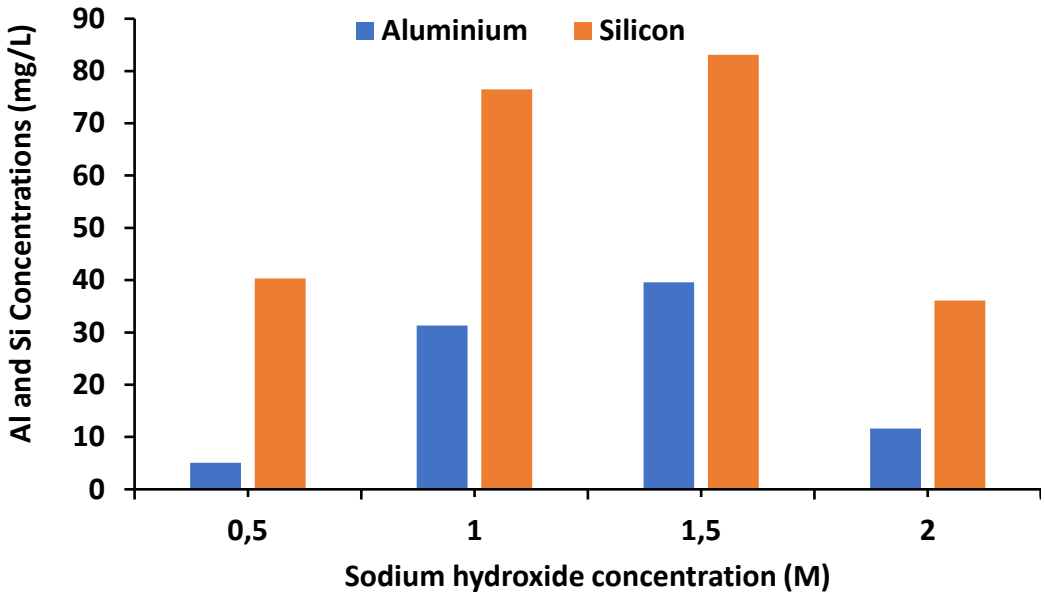

Figure 4.3: Silicon and aluminium concentration (mg/L) in filtrates as a function of NaOH concentration.

4.3.2.2 Optimisation of ageing time

Ageing time was optimised by varying the contact time for the ageing process from 1 to 6 h at 1.5 M NaOH optimum concentration. Figure 4.4 presents residual concentrations of Al and Si obtained in filtrate at different contact times. There was increased dissolution of Aluminium from the aluminosilicate clay soils as the ageing time was increased from 1 to 6 hours. However, no much change was observed after 2 h with a maximum concentration of ≈ 500 mg/L being recorded in the slurry. Highest concentration of Silicon were observed at 1 h of ageing, with subsequent decrease as the ageing time was increased. The silicate species in solution are known to form silica gels on increased exposure to highly alkaline media as is in this case. It's believed that the decrease in Silicon species in solution was due to the formation of silica gels in the highly alkaline media. Nevertheless, based on our previous hydrothermal activation experiments (Musyoka *et al.*, 2012), an ageing time of 2 h was adopted in this work.

It was also observed that other major and minor metal species were released into the aqueous phase, these included Fe (0.59 - 70.5 mg/L) B (100 - 31254 µg/L), V (568 – 1659 µg/L), Cr (550 - 1410 µg/L), Mn (80 - 857 µg/L), Ni (362 – 599 µg/L), Cu (672 - 1213 µg/L), Co (62 - 1924 µg/L), Zn (229 - 5995 µg/L), Ca (0.42 - 6.8 mg/L) and K (11.38 - 24.80 mg/L) (Obijole *et al.*, 2020). It should be noted the clay soils are natural aluminosilicate precursors and hence, would contain other elements found in soil crusts. These metal species are bound to be included in the

© University of Venda

crystal structure of the synthesised products and will have impact on their physical and chemical properties. The alkali species such as Ca, K and Na are important as charge balancing cations in zeolitic structures. The elevated concentrations of metal species such B, V, Cr, Mn, Co, Ni and Cu as well as their interaction with the Aluminium and Silicon in the solution may be responsible for the colour shades of reddish brown coloration in all the filtrates. The concentration of Aluminium dissolved from the mechanochemically-activated clay was comparatively higher than that of Silicon at all contact times. During the dissolution of Aluminium and Silicon, when OH^- from the NaOH solution attacks the aluminosilicates, the Aluminium is the first to be displaced into solution as $Al(OH)_4^-$ complexes resulting in the detached Si-tetrahedral becoming much easier for OH^- attack forming silicon acids and oligomers containing Si–O groups in solution with Na^+ neutralising the negative charges (Duxson & Provis, 2008; Nikolov *et al.*, 2017). Conclusively, contact time of 2 h was therefore selected as the optimum ageing time.

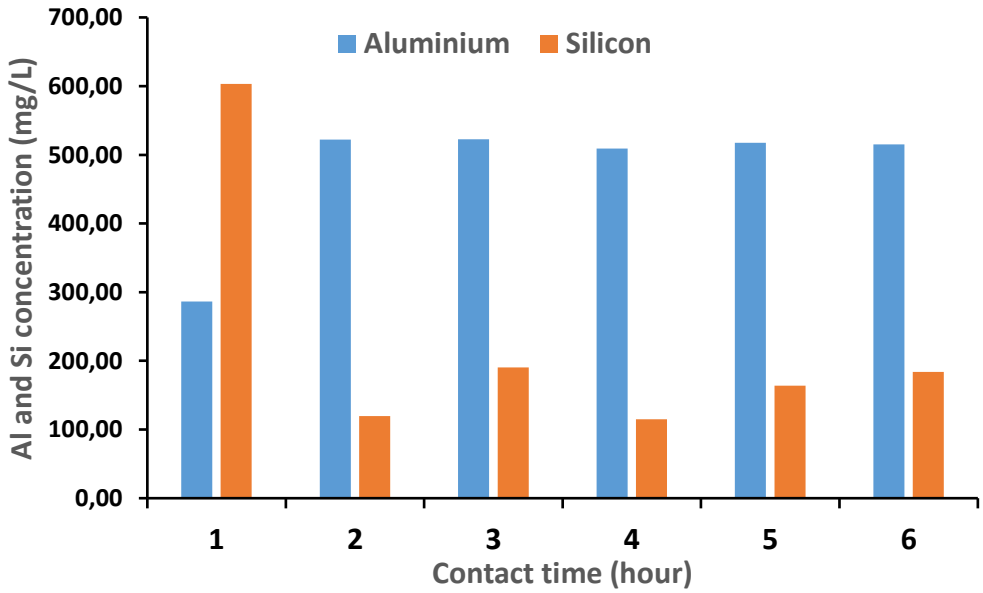

Figure 4.4: Aluminium and silicon concentration (mg/L) in the filtrates as a function of contact time.

4.3.2.3 Colour variations of the hydrothermally-treated aluminosilicate clay products

Figure 4.5 a and 4.5 b presents all the hydrothermally-treated aluminosilicate clay samples CA-1 to CA-21 [HTAC-1 to HTAC-21] respectively obtained at different experimental runs. From the figure, it is observed that hydrothermal treatment of clays yielded samples with different colour variations which is an indication of varying degrees of modification. The light brown colour

© University of Venda

of the raw aluminosilicate activated clay progressively changed to different shades of dark brown, light brown and brownish black colouration under different hydrothermal conditions of temperature, reaction time and water content respectively. These colour variations could be attributed to changes in the structural iron oxidation state within the clay matrix and hydroxylation which occurred as temperature increased (Eissa *et al.*, 1994; Soulé *et al.*, 2020).

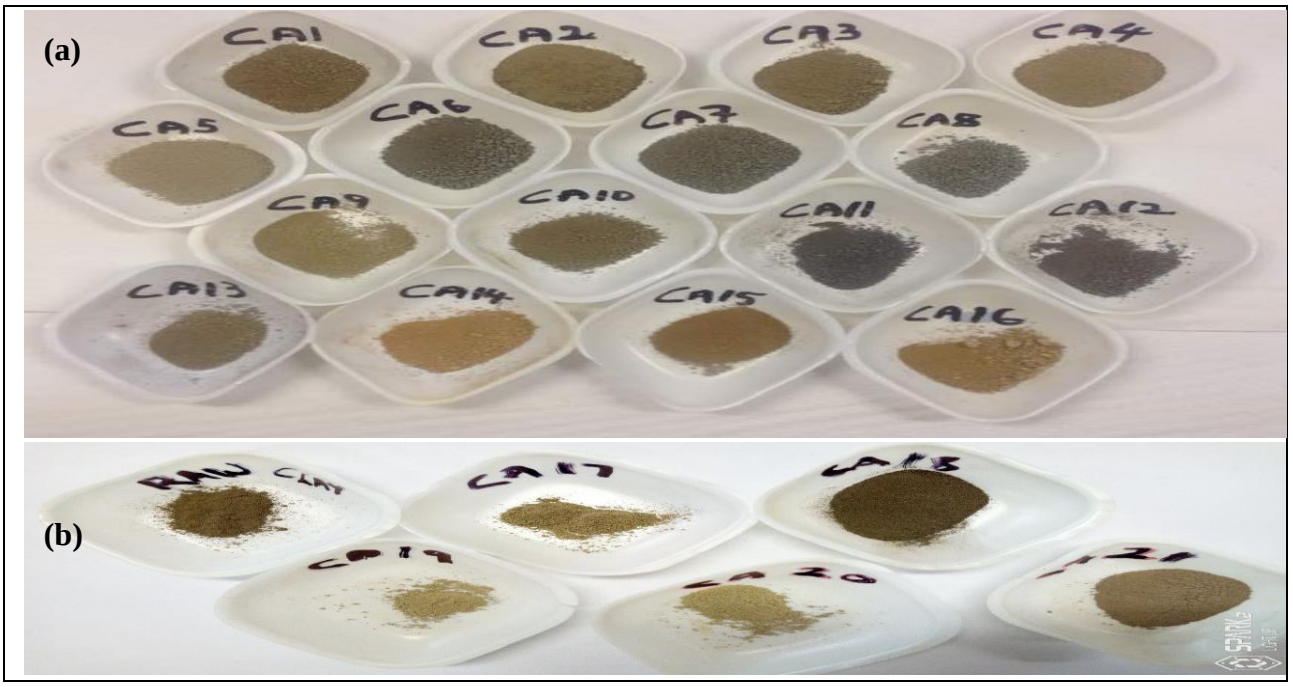

Figure 4.5: (a) Images of hydrothermally-treated clay samples [HTAC-1 to HTAC-16)], treated at varying hydrothermal treatment temperatures and contact times. **(b)** Images of hydrothermally-treated clay samples [HTAC-17 to HTAC-21)], treated at varying water content during hydrothermal treatment step. **Note:** CA≈ HTAC ≈ HTMAC.

4.3.3 Defluoridation of simulated fluoride solutions with the synthesised HTAC samples

Table 4.2 presents the percent fluoride removal and adsorption capacities of all the hydrothermally-treated aluminosilicate clays (HTAC) obtained under different experimental conditions. The adsorption capacity and fluoride removal potential of all the synthesised materials were tested to evaluate the materials' defluoridation potential in the simulated fluoride-rich water. It is observed from Table 4.2 that the lowest percent fluoride removal (32 - 36%) and adsorption capacity (0.902 - 0.978 mg/g) was observed for samples HTAC 1 - 4 (Table 4.2). It should be noted that these samples were hydrothermally treated at 100 °C. Samples (HTAC 5 - 8) (Table 4.2) exhibited higher percent fluoride removal (42 - 48%) and adsorption capacity (1.14-1.24 mg/g) were all treated at 140 °C. Samples treated at 160 °C (HTAC 9 - 12) (Table 4.1 and 4.2) exhibited

© University of Venda

percent fluoride removal (41 - 44%) and adsorption capacity (1.08 - 1.156 mg/g) which was comparable to the performance of the samples treated at 140 °C. This observation indicated that irrespective of the treatment time, increase of treatment temperature enhanced the adsorptive properties of the clay soils. This was attributed to the activation of the aluminosilicates in the clay soils by the alkaline solutions and subsequent formation of new materials with enhanced active adsorption sites.

Previous work on mukondeni clay soils in adsorption of fluoride and arsenic have shown that alkali activation of the clays improves their adsorptive properties (Mudzielwana *et al*., 2018 a, 2019 a, 2019 b and 2019 c). Moreover, several authors (Musyoka *et al*., 2012; Menzi *et al*., 2011; Gougazeh & Buhl, 2014) have observed conversion of aluminosilicate precursors into mixtures of zeolites and geopolymer products on hydrothermal treatment at temperatures ≥ 140 °C. It was further observed that the XRD peak intensities of these minerals increased with hydrothermal treatment time. The alteration of the aluminosilicate feedstock to new mineral phases and increase in surface area with increasing treatment temperature could explain the higher adsorption capacity for fluoride. Samples treated at 200 °C (HTAC 13 - 16) (Table 4.1) showed reduced percent fluoride removal and adsorption capacity (0.798 - 1 mg/g) as compared to samples treated at 140 °C and 160 °C but higher than for samples treated at 100 °C. This indicated that increasing treatment temperature beyond 160 °C led to loss of the adsorptive properties of the products. In previous work in which Musyoka *et al* (2012) observed that, coal fly ash (CFA) subjected to hydrothermal treatment at 100 °C led to no alteration of the aluminosilicate precursors. Samples HTAC 17 - 21 were treated at 140 °C and 48 h, but amount of water added before hydrothermal treatment was varied from 0 - 12 mL (Table 4.1). It's observed that, the percent fluoride removal (37 - 46%) and adsorption capacity (0.69 - 1.238 mg/g) increased with increased amount of water to a maximum at 9 mL for sample HTAC-20. Musyoka *et al* (2012) observed that addition of water after ageing step enabled the formation of pure phase zeolite Na-P1 from coal fly ash. Casci (2005) points out that, the water content during zeolite synthesis improves the purity and type of zeolite material produced. Moreover, addition of excess amount of water can restrict zeolite crystallisation process due to change in degree of supersaturation of the SiO_4^- and AlO_4^- precursor species. Addition of 12 mL of water (HTAC-21) (Table 4.1 and 4.2) seemed to decrease the adsorptive properties of the zeolitic products. All samples treated at the same temperature but increasing treatment time showed improved percent fluoride removal and adsorption capacity

© University of Venda

(Table 4.1 and 4.2). This indicated that time was an important factor in producing optimum zeolitic products. From the above, it can be tentatively concluded that, samples synthesised at 140 °C, 48 h with addition of 9 mL of water after ageing step would give the optimum zeolitic products.

Moreover, samples HTAC-5, HTAC-6, HTAC-7, HTAC-8 and HTAC-12 were selected for characterisation using FTIR, XRD, SEM and BET techniques for better understanding of their surface chemistry as they yielded better fluoride removal efficiency.

Table 4.2: Adsorption capacities and percent fluoride removal of the HTAC samples.

Samples	Percent fluoride removal (%)	Adsorption capacity, q, (mg/g)
CA1(HTAC-1)	32.34	0.902
CA2 (HTAC-2)	33.86	0.940
CA3 (HTAC-3)	35.65	0.955
CA4 (HTAC-4)	35.92	0.978
CA5 (HTAC-5*)	44.38	1.154
CA6 (HTAC-6*)	43.84	1.140
CA7 (HTAC-7*)	45.25	1.176
CA8 (HTAC-8*)	47.69	1.240
CA9 (HTAC-9)	41.23	1.088
CA10 (HTAC-10)	42.25	1.120
CA11 (HTAC-11)	43.55	1.134
CA12 (HTAC-12*)	44.23	1.156
CA13 (HTAC-13)	37.52	0.798
CA15 (HTAC-15)	34.35	0.907
CA16 (HTAC-16)	35.84	0.914
CA17 (HTAC-17)	37.41	0.690
CA18 (HTAC-18)	37.45	0.946
CA19 (HTAC-19)	38.38	0.974
CA20 (HTAC-20)	46.29	1.238
CA21 (HTAC-21)	38.23	0.958

Note: Sample CA8 (HTAC-8) and CA20 (HTAC-20) were prepared under the same condition.
Footnote: * represents the selected samples that were characterised. **Note:** HTAC ≈ HTMAC.

© University of Venda

4.3.4 Physicochemical characterisation

4.3.4.1 Fourier transform infra-red (FTIR)

Figure 4.6 a, b and c presents the FTIR spectrum of MAC and selected hydrothermally-treated aluminosilicate clay (HTAC ≈ HTMAC) samples. The characteristic dominant band in MAC and synthesised hydrothermally-treated crystalline gel-like microspheric alkali aluminosilicate phases is an asymmetric Si-O-Al stretching vibration in the region of 950 - 1100 cm^{-1} (Mikuła *et al.,* 2015; Marsha *et al.,* 2019). The MAC showed major transmission bands and wavelength region of 3400 - 3600 cm^{-1}, 1600 - 2600 cm^{-1} and 500 - 1100 cm^{-1}. The bands at the region of 3100 to 3670 are ascribed to the O-H stretching of the H-OH, Si-OH, Al-OH groups of the absorbed moisture and hydroxyl groups within the clay interlayers (Toor *et al*., 2014). This region appear as bands and increases in intensity in samples HTAC 5 - 14, this could be due to increased adsorption water due to water added during the hydrothermal treatment (Table 4.1). The bands at 500 to 1100 cm^{-1} are linked to the vibration and stretching of Al-O, Si-O and Al-O-Si groups. The bands in the region 1648 - 1680 cm^{-1} are attributed to adsorbed water in aluminosilicate gels and zeolitic minerals in treated clays or the bending O-H vibrations of water molecules retained in the silica matrix (Gougazeh & Buhl 2014). The MAC and the hydrothermally treated clay soils shows similar bands at 3100 - 3670 cm^{-1}, 1648-1680 cm^{-1}, 918 - 995 cm^{-1} and 2 - 4 peaks in the region 650 - 799 cm^{-1} regions. Two new peaks were observed in the region 1423 - 1480 cm^{-1} for samples HTAC-5, 6, 7, 8 and 12 but disappeared in sample HTAC-14 (Table 4.1, Figure 4.6 a and b). The new peaks have been ascribed to Na-O bands resulting from increased sodium aluminosilicate precursor in the hydrothermally-treated materials at 48 h. After hydrothermal treatment, transmission intensity of the bands at 3400 - 3600 and 1600 - 2600 cm^{-1} decreased (Figure 4.6 c). This could be ascribed to loss of moisture via evaporation during treatment as temperature increased. Moreover, the intensity of the bands designating Al-O, Si-O and Al-O-Si from wavelength region of 500 cm^{-1} to 1100 cm^{-1} increased after hydrothermal treatment. The observed increased intensity leading to formation of strong Al-O, Si-O and Al-O-Si bond occurred consequent upon moisture loss as hydrothermal treatment temperature increased (Luo *et al.,* 2018) (Figure 4.6 a).

In alkali activated clays, the peaks in this region 1423 - 1480 cm^{-1} indicates presence of amorphous geopolymeric gels which transformed into crystalline zeolitic products as the treatment temperature was increased. They could also be assigned to carbonates that forms in the highly

© University of Venda

alkaline conditions due to ingress of carbon dioxide (Mezni *et al.,* 2011). Vibration bands at 918 - 995 cm^{-1} and 650 - 799 cm^{-1} are attributed to the stretching Si-O bonds in SiO_2 and Al-O bonds in Al_2O_3 respectively (Kim *et al.,* 2010). In the region 650 - 799 cm^{-1}, four peaks were observed in MAC (658 cm^{-1}, 689 cm^{-1}, 754 cm^{-1}, 799 cm^{-1}) these peaks seemed to merge into 2 peaks as the hydrothermal treatment time and temperature was increased (Table 4.1, Figure 4.6 a and b). These four peaks in MAC are attributed to Al-O bonds in aluminosilicate precursor.

The merging of the peaks indicated activation of the aluminosilicate matrix with subsequent formation of new bonds. Gougazeh *et al* (2014) and Flaningen *et al* (1971) observed that the bands at 650 - 745 cm^{-1} could be attributed to symmetric T-O-T (T = Si or Al) vibrations of the sodalite framework. The peaks (654 - 691 cm^{-1}, 705 - 713 cm^{-1}, 720 - 728 cm^{-1}) observed for samples HTAC 6, 7, 8, 12 and 14 would suggest presence of hydroxy sodalite in the treated clays. MAC sample exhibited a peak at 1005 cm^{-1} and shoulder peak at 918 cm^{-1}, the shoulder peak was observed to disappear with hydrothermal treatment (Table 4.1, Figure 4.6 a and b), moreover the peak at 1005 cm^{-1} shifted to lower wavenumber (958 - 995 cm^{-1}) for all the treated clay samples (Figure 4.6 a and b). The shoulder peak at 918 cm^{-1} in MAC is attributed to Al-O in Al_2O_3 and doesn't appear in the treated clay. The peak at 1000 cm^{-1} shifted to (958 - 995 cm^{-1}) is attributed to antisymmetric stretching of Si-O and Al-O in aluminosilicates with zeolite structures (Gougazeh *et al.,* 2014; Zhang *et al.,* 2012). Nesse (2000) observed that SiO_2 and Al_2O_3 in aluminosilicates are transformed and replaced by a single band at 1000 cm^{-1} which is characteristic of Si-O-Al bonds in TO_4 (T = Si or Al) tetrahedral. Moreover there was increased intensity of this shifted peak (958 - 995 cm^{-1}) in the treated clays as compared to MAC. The increased intensity of this peak could indicate increased formation of Si-O, Al-O bonds mostly attributed to the Si-O-Al in the new mineral phases. Sample HTAC-8 showed the sharpest and most profound peaks for Si-O and Al-O bonds and showed higher fluoride capacity compared with other treated samples. The increased intensity of these bands indicated the conversion of the aluminosilicate gels into crystalline phases. Alonso *et al* (2001) observed increased intensity of these bands in metakoalin based gepolymers.

© University of Venda

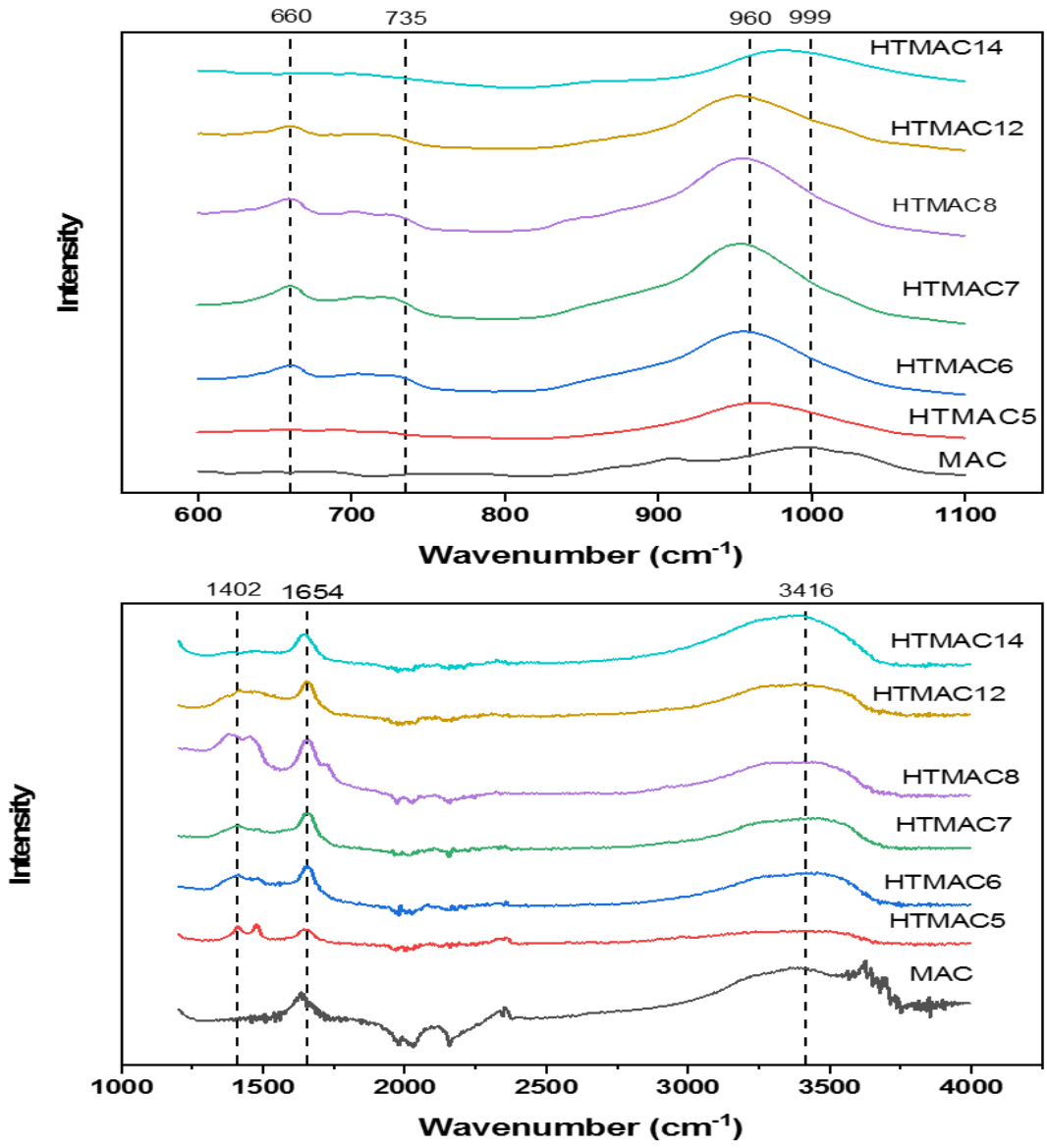

Figure 4.6 a and b: FTIR spectra of mechanochemically-activated clay (MAC) soils and hydrothermally-treated aluminosilicate clay (HTAC) soils. **Note:** HTAC ≈ HTMAC.

© University of Venda

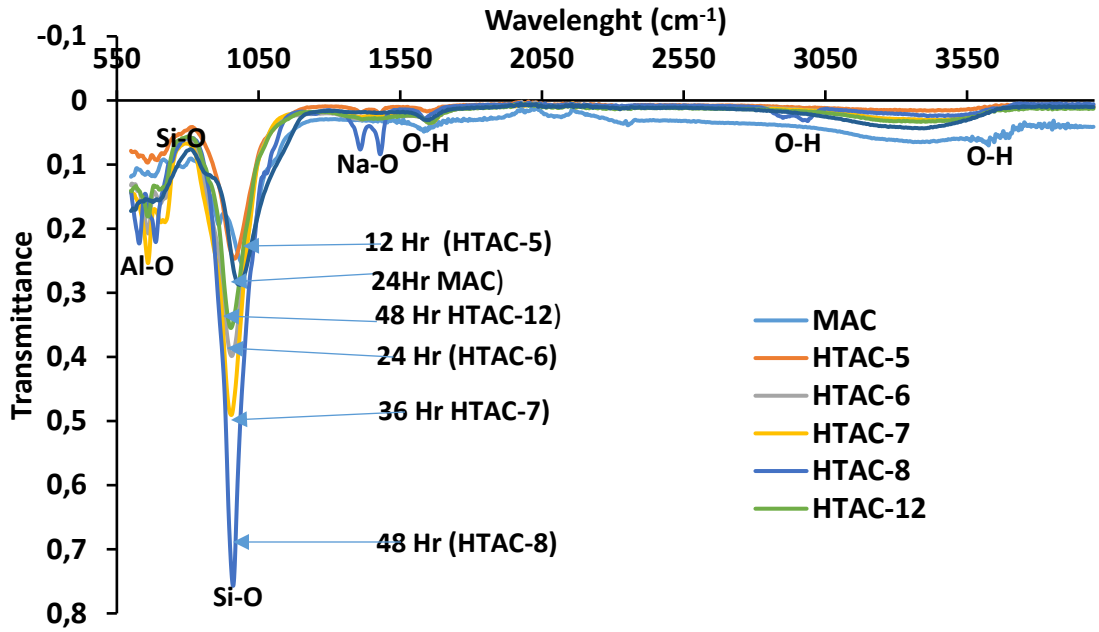

Figure 4.6 c: FTIR Spectra of mechanochemically-activated clay (MAC) soils and the selected hydrothermally-treated aluminosilicate clay (HTACs) soils. **Note:** HTAC ≈ HTMAC.

4.3.4.2 X-ray diffraction (XRD)

Figure 4.7 presents the X-ray diffraction spectra of MAC and selected HTAC 5, 6, 7 and 8 hydrothermally-treated aluminosilicate clay samples using 1.5 M NaOH solutions at 140 °C and at varying times of 12, 24, 36 and 48 h respectively. Sample HTAC-12 was treated at 160 °C and 48h. The principal phase present in all the samples are zeolitic materials with some slight differences. The XRD spectra of MAC shows presence of montmorillonite, kaolinite, quartz, albite and muscovite. The prominent peak of montmorillonite would indicate the dominance of this mineral in the clay soils. Dacosta *et al* (2013) reported concentrations ranging from 38 - 55 weight % of smectite in these mukondeni clay soils. Montmorillonite was identified through its prominent peaks at 6.5°, 12°, 18° and 28° two theta. Samples treated at 140 °C for various times exhibited new peaks. HTAC-5 exhibited new peaks which were matched to zeolite A (Gougazeh *et al.*, 2014; Heller-Kallai & Lapides, 2007). The montmorillonite, quartz, albite and muscovite peaks disappeared in all the hydrothermally treated samples. This indicates that, the conditions employed provided were optimum for dissolution of aluminosilicate matrix to release Al and Si species for the formation of the new zeolitic phases. As the treatment time was increased to 36 and 48 h, new phases appeared different from those of HTAC-5 and MAC. The new peaks were matched to hydroxyl sodalite (Musyoka *et al.*, 2012. Menzi *et al* (2011) reported that, hydrothermal treatment

© University of Venda

of illite clay using 3.52 M NaOH solution, at higher reaction times (> 24 h), the dominant synthesis product was hydroxyl sodalite. Moreover, Heller-Kallai and Lapides (2007) reports that kaolin and metakaolin clays treated with NaOH solutions at 93 °C at varying times (3 h, 26 h, 72 h, 168 h), all samples treated at 3 h and 26 h had zeolite A as the dominant product, while for 72 h, it was a mixture of zeolite A and hydroxyl sodalite. At 168 h the products were predominantly hydroxyl sodalite. Breck (1974) observed that zeolite A is unstable at highly alkaline environment and converts to zeolite P or hydroxy sodalite at longer reaction times. It could be deduced that the absence of any impurity peaks in the products, indicates the zeolites product were highly pure. At 48 h treatment time, increase in temperature (HTAC-8 and HTAC-12) didn't have any impact on the products.

New mineral phases were formed owing to recrystallisation of the HTAC materials. Generally, some slight changes observed in the main peaks, to some extent, could be related to the different water molecules content in the zeolitic materials formed. These were all based on sodium aluminium silicate hydroxide hydrates formed in the various zeolitic products. The degree of recrystallisation increases with increase in hydrothermal treatment temperature and time. HTAC-8 showed more mineral phases and intense crystalline peaks which were corroborated by the SEM micrographs with clear gel-like geopolymer having microsphere particles compared to other materials where the microspheres overlain on a gel-like structures indicated partial transformation of the gels into crystalline microspheres. The FTIR and SEM showed the uniqueness of sample HTAC-8 as the best modified sample. This was confirmed by FTIR which revealed the most intense and sharp peaks while SEM micrographs showed gel-like formation more like geopolymer gel with aggregated microsphere-like particles, which transformed into crystalline microsphere morphology with increased surface area, which imparted positively on the sample defluoridation potentials.

© University of Venda

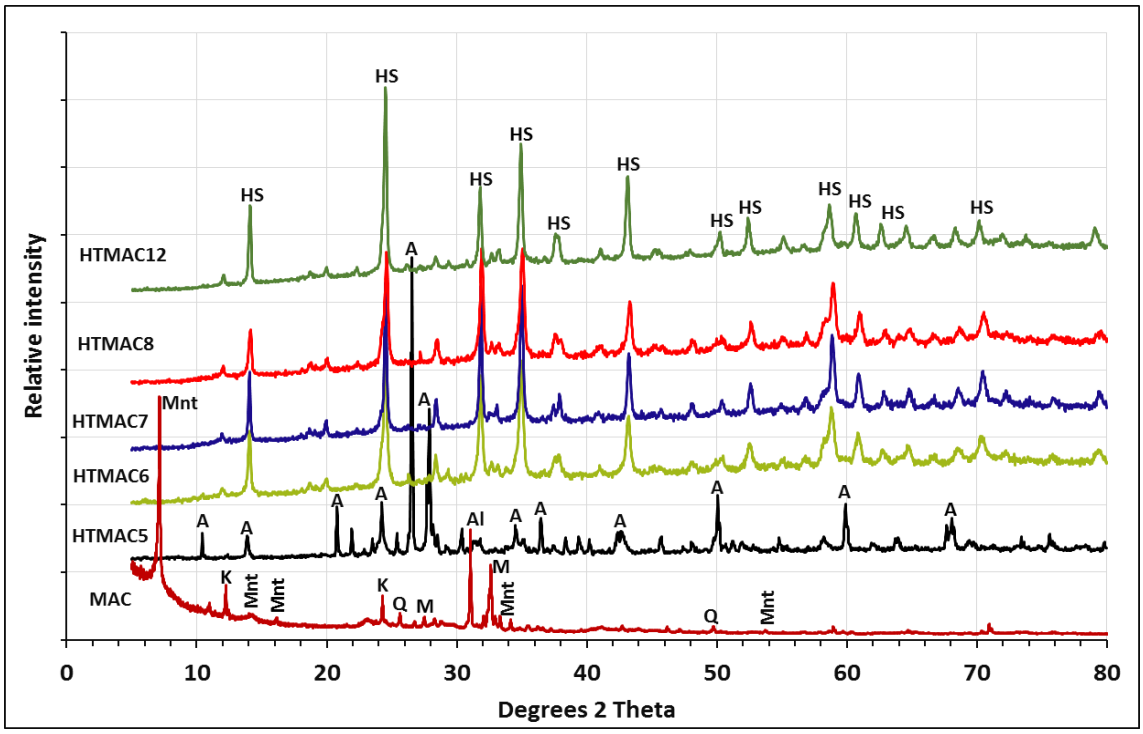

Figure 4.7: XRD spectra of MAC, HTAC 5, 6, 7, 8 treated at 140 °C and times of 12, 24, 36 and 48 h respectively and sample HTAC 12 treated at 160 °C at 48 h using 1.5 M NaOH. **Note:** HTAC = HTMAC. (Mnt-montmorillonite, Al-albite, M-muscovite, Q-quartz, A-zeolite A, HS- Hydroxy sodalite hydrate).

Figure 4.8 presents the X-ray diffraction spectra (XRD) of MAC and samples HTAC 19, 8 hydrothermally treated using 1.5 M NaOH solutions at 140 °C and 48 h with addition of 6 mL and 9 mL of milli Q water before hydrothermal treatment and HTAC 21 treated at 160 °C, 48 h with addition of 12 mL of milli Q water before hydrothermal treatment. Addition of water before hydrothermal treatment at temperatures above 140 °C didn't seem to have any impact of the type of zeolite product.

© University of Venda

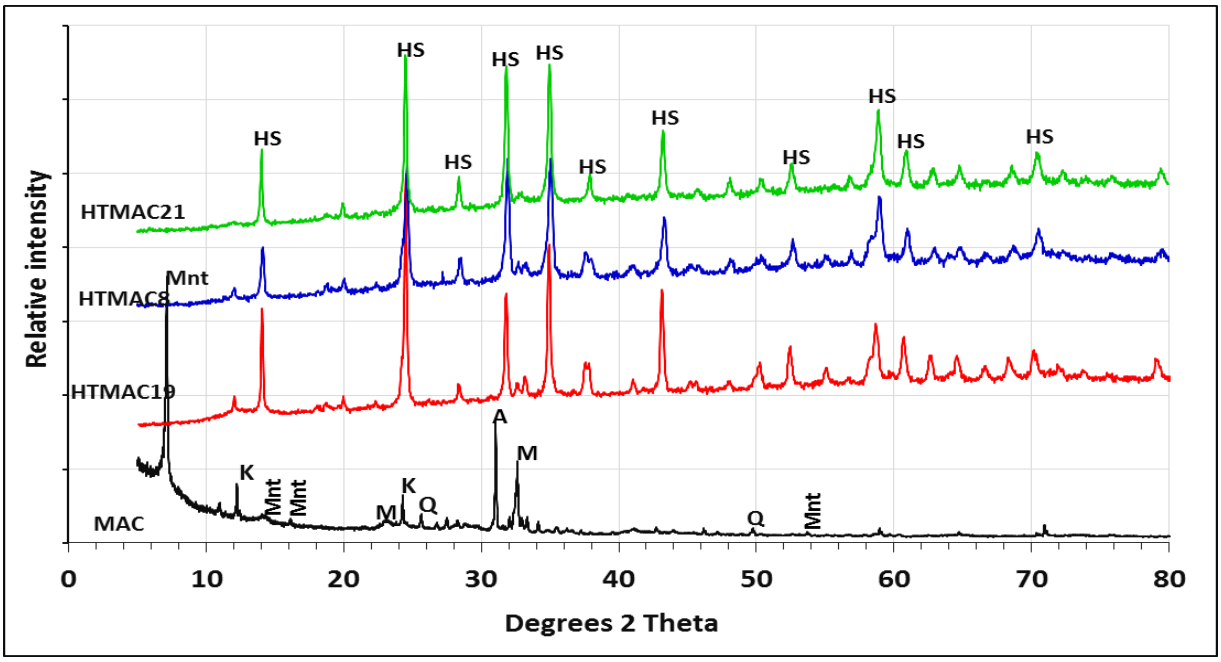

Figure 4.8: XRD spectra of MAC, HTAC 19 and 8 treated at 140 °C and 48 h with addition of 6 and 9 mL Milli-Q water before hydrothermal treatment respectively and sample HTAC-21 treated at 160 °C and 48 h with addition of 12 mL Milli-Q water before hydrothermal treatment.
Mnt - montmorillonite, Al - albite, M - muscovite, Q - quartz, A - zeolite A, HS - Hydroxy sodalite hydrate. **Note:** HTAC ≈ HTMAC

Footnote: X-ray diffraction (XRD) spectra of MAC and the selected hydrothermally-treated aluminosilicate clay (HTAC ≈ HTMAC) samples are in the appendix 4.3 a - g.

4.3.4.3 Morphology of the hydrothermally-treated aluminosilicate clay samples

Figure 4.9 shows the SEM micrographs of the zeolitic products (HTAC1, 2, 4, 5, 6, 7, 8 10, 11, 12, 13 and 16) after hydrothermal treatment of the mechanochemically activated clay soils (MAC) at various reaction time and temperature with 1.5 M NaOH solution and addition of water prior to hydrothermal treatment. A substantial change in morphology of the clay soils is observed.

Generally, hydrothermal treatment duration affects the morphology and size of the materials. Increased hydrothermal treatment time favours the crystals growth while increase in temperature increases evaporation of solvent which leads to a state of supersaturation (evaporation) which is favourable to increased crystal growth (Petrik *et al.*, 2005; Nicholas *et al.*, 2012).

The platy morphology of the clay soils is replaced by spheroidal particle “cotton ball” morphology. In all the treated clay samples, the spheroidal “cotton ball” particle morphology is observed is observed in all the treated samples. The particles appear to be aggregating together or

© University of Venda

partly singly and appear like they are popping from a gel-like substance underneath. Samples HTAC, 6, 7, 8 and 12 exhibited a gentle hump extending from 11 - 72 degrees two theta. This kind of hump is normally associated with amorphous geopolymer-like gel. It would appear the gel formation is the initial step before zeolitisation, this is more clearly depicted in samples HTAC-5 and HTAC-13 treated for 12 h, where the spherical particles appear to be still attached to the gel and have not fully popped out. Menzi *et al* (2011), Gougazeh & Buhl, (2014) and Heller-Kallai & Lapides (2017) reported this spheroidal "cotton ball" particle morphology on hydrothermal treatment of illite and kaolin clay at various NaOH concentrations. X-ray diffraction (XRD) analysis of treated samples (Figure 4 and 5) identified these spheroidal particles to be hydroxyl sodalite. At lower treatment time, i.e 12 h, zeolite A was initially formed and transformed into hydroxyl sodalite as the treatment time was increased (≥ 24 h, Figure 4). Heller-Kallai & Lapidas (2007) reported formation of zeolite A at lower reaction times of 3 - 26 h and hydroxyl sodalite at reaction times of 72 - 168 h on hydrothermal treatment of kaolin clay with 4.25 - 10.75 N NaOH solutions. It is clear from figure 6 that all the conditions employed for the hydrothermal treatment in this work led to the formation of predominantly hydroxy sodalite. This is clear through the dominant microspheric and spheroidal "cotton ball" particle morphology in all samples.

However at lower reaction times (HTAC-1, 2, 4), angular structures which could be attributed to unreacted aluminosilicate materials are observed. These materials are not observed for treated samples above 140 °C indicating temperatures high than 100 °C would be necessary for complete conversion of the aluminosilicate gels into zeolites.

© University of Venda

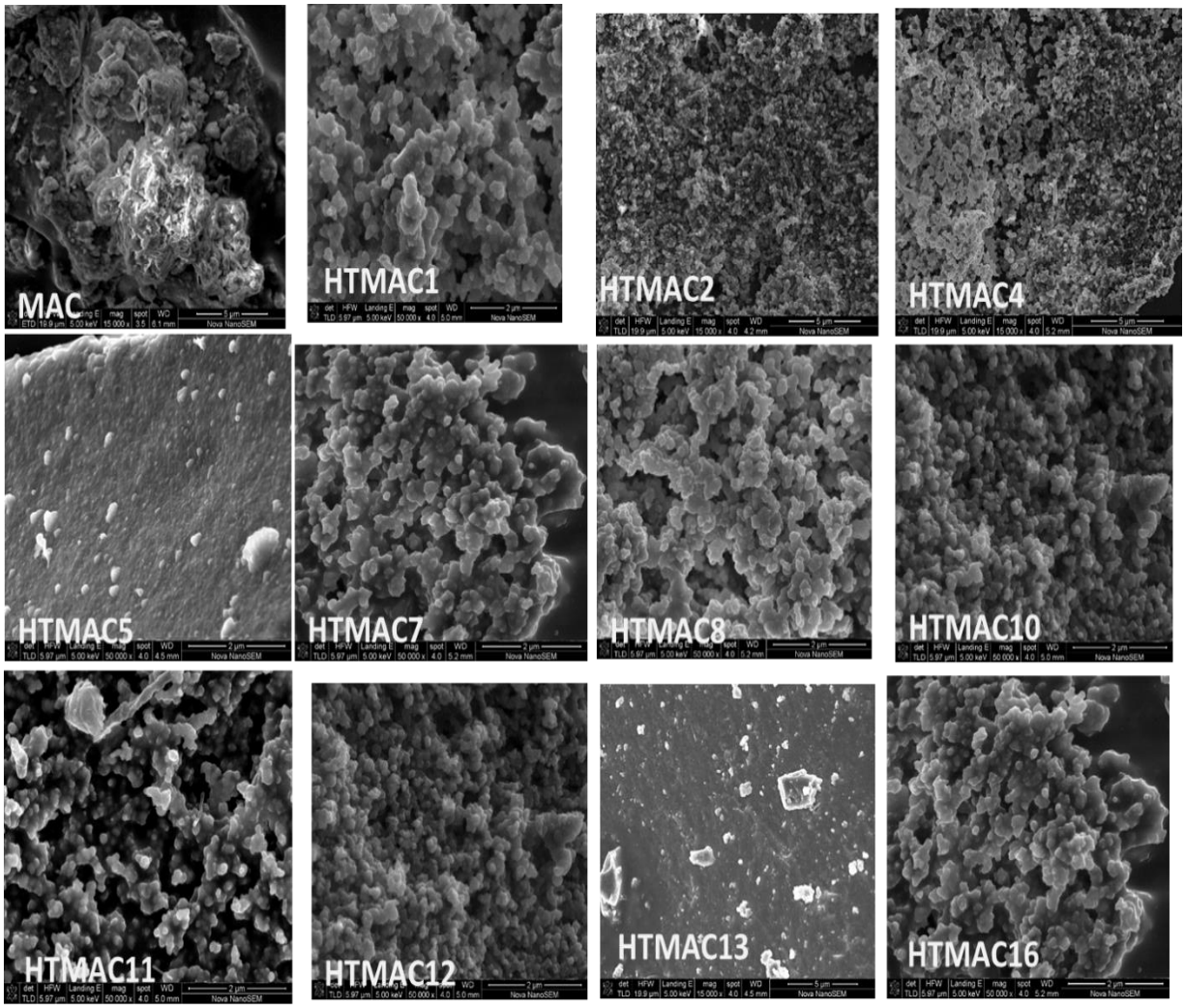

Figure 4.9: SEM micrographs of raw clay (MAC), clays HTAC1, 2, 4 treated at 12 h, 24 h, 48 h at 100 °C and 9 mL of water, HTAC, 5, 7, 8 treated at 12 h, 26 h, 48 h at 140 °C and 9 mL of water, HTAC10, 11, 12 treated for 24 h, 36 h, 48 h at 160 °C and 9 mL of water and HTAC13, 16 treated for 12 h, 48 h at 200 °C. Magnifications at X50,000. All samples were hydrothermally treated with 1.5 M NaOH. **Note:** HTMAC ≈ HTAC

4.3.4.4 Brunauer-Emmett-Teller (BET) surface area and porosity

Table 4.3 presents the BET surface area, surface area single point, pore volume and size of selected hydrothermally-treated aluminosilicate clay (HTAC) and mechanochemically-activated clay (MAC) samples. All the twenty-one synthesised HTAC samples were tested for preliminary fluoride batch adsorption potentials. Based on their defluoridation performance and capacity, the best five performing samples were selected for surface area and other properties characterisation. All samples have pore sizes within 2 - 50 nm range and were therefore mesoporous in nature. There were no significant changes in the pore volumes of the MAC and all the hydrothermally-

© University of Venda

treated samples, suggesting that hydrothermal treatment did not alter the pore volumes of the materials. On the other hand, the surface area increased substantially after hydrothermal treatment from 17.19 m^2/g in MAC to 33.25 m^2/g in HTAC-8. The increase in surface area could be attributed to increasing hydrothermal temperature and time which resulted in the particles' kinetic mobility and breakdown to produce smaller active particles with larger surface area. The increase in surface area further indicated increase in microporosity of the material after hydrothermal treatment. This collaborates the observed increase in adsorptive capacity of fluoride from aqueous media by samples HTAC5 - 8 and HTAC-12 as compared to MAC (Table 4.2). Moreover, the increasing water content from 0 to 9 mL during synthesis was observed to lead to increase in surface area while further increase retarded surface area (Table 4.3). This could be due to enhancement of degree of supersaturation until the material was fully saturated as noted on the optimised material (HTAC-8) after which the degree of supersaturation slowed down with an attendant slow down in the crystallisation kinetics and hence, reduction in surface area as observed in other materials (Petrik, *et al.*, 2005; Casci, 2005; Musyoka *et al.*, 2012).

The BET surface area is calculated with the whole surface such as surface of pores, external surface of material using the adsorption of nitrogen gas on the surface of materials. It is generally higher than the total surface area but is relative to the total surface area and hence more reliable while single point surface area is usually used to determine surface area when quick testing is desired on a single point on the materials surface, but there is no big difference between the two (Hu *et al.*, 2001).

The surface area, N_2 adsorption and desorption isotherms for MAC, HTAC 5 - 8 and HTAC-12 are presented in Figure 4.10 a - f. The pore diameter distribution obtained according to the Adsorption Barrett-Joyner-Halenda (BJH) method are presented in figure 4.10 g - h. There is intense evolution of pore area in the mesoporous range and this is more noticeable for samples HTAC-5 and HTAC-8. Sample HTAC-8 exhibits a trimodal pore size distribution (9, 43 and 98 nm) as compared to MAC which shows a bimodal pore size distribution (9, 43 nm). The pore size distribution results indicates that both MAC and treated samples are mesoporous (Figure 4.10 g). The pore area assigned to the pore diameters (9 and 43 nm) increased in the following order MAC > HTAC7 > HTAC6 > HTAC8. These samples were identified as hydroxyl sodalite by XRD (Figure 4.7).

© University of Venda

Moreover, these samples were treated at increasing time from 24 - 48 h. This would indicate that increasing treatment time increased evolution of mesoporosity. Sample HTAC-12 treated at 48 h and 160 °C exhibited a lower pore area of 28.4 m^2/g, although XRD still indicated its hydroxyl sodalite (Figure 4.7). This would indicate that increasing treatment time beyond 48 h would probably decrease the porosity of the products. The increase in porosity and surface area can be attributed to the conversion of the aluminosilicate precursors in the clay soils to zeolitic products. The N_2 adsorption-desorption isotherms can be classified as type IV with a hysteresis loop type H3 which at high relative pressure is associated with mesoporous structure and at low relative pressure with a microporous structure (Luo *et al.*, 2018) (Figure 4.10 a - f). Increase in pore volume is normally associated with increase in mesoporous structure since the mesopores are easily accessed by N_2 at high relative pressure. The pore diameter distribution as a function of pore volume indicates that all samples had highest volume within the range of 43 - 98 nm further confirming that these materials are mesoporous (Figure 4.10 h).

Table 4.3: The surface area, pore volume and pore size of MAC and the HTAC materials

Samples	BET surface area. (m^2/g)	Surface area single point. (m^2/g)	Pore volume(cm^3/g)	Pore size (nm)
MAC	17.19	16.66	10.06	14.92
CA5 (HTAC-5)	25.46	24.32	10.09	14.93
CA6 (HTAC-6)	26.41	25.27	10.08	12.77
CA7 (HTAC-7)	27.26	26.48	10.08	15.29
CA8 (HTAC-8)	33.25	32.02	10.12	14.16
CA12 (HTAC-12)	28.44	27.14	10.13	17.60

Note: HTAC ≈ HTMAC

© University of Venda

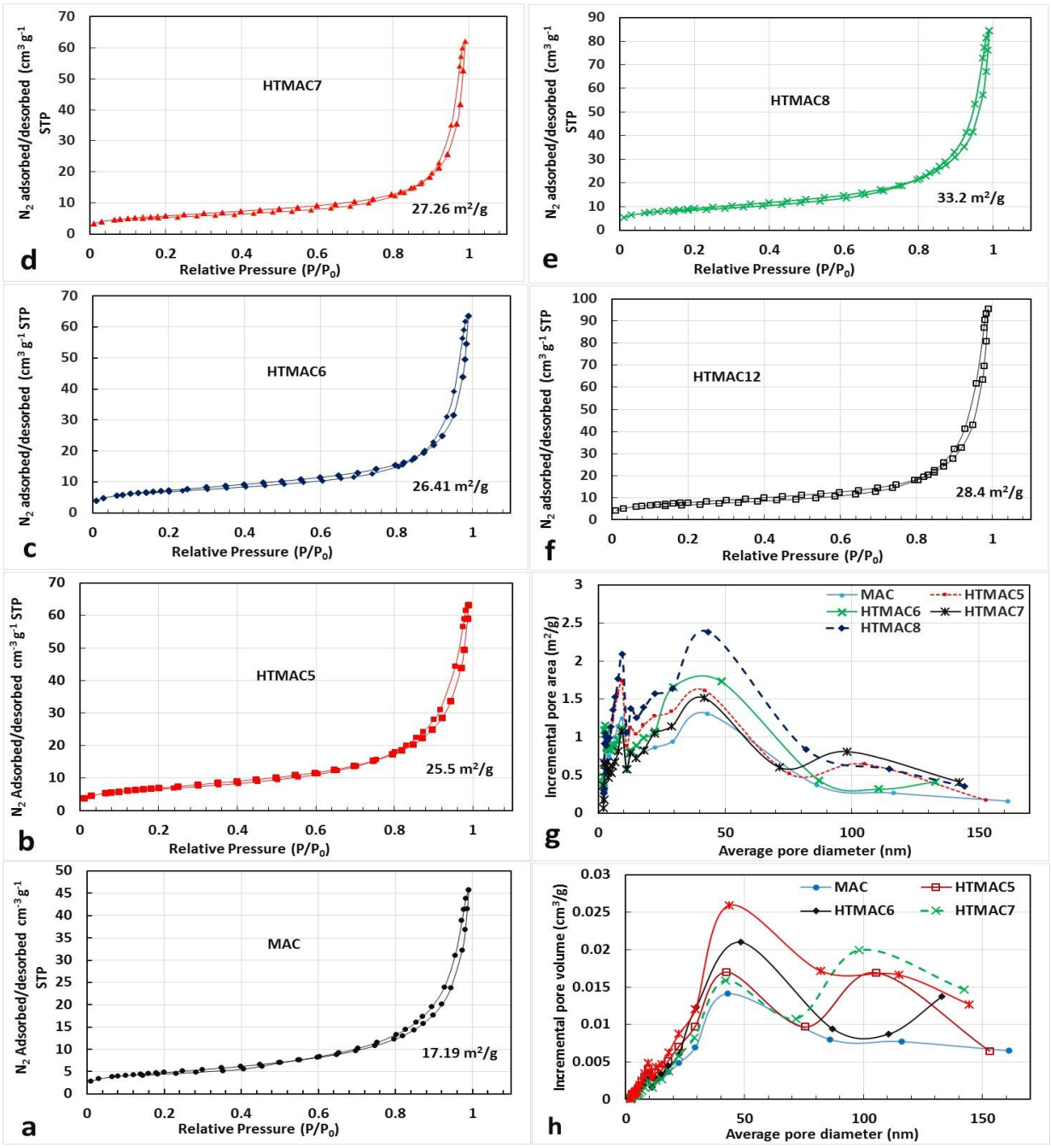

Figure 4.10 a - f: Surface area and N_2 adsorption-desorption isotherms at -195.8 °C for MAC, HTAC5 - 8 and HTAC12. **Figure 4.10 g – h**: BJH pore diameter distribution as a function of pore area and volume respectively for MAC and treated clays HTAC5 - 8. **Note:** HTAC ≈ HTMAC.

4.3.5 Conclusions

In this chapter, the hydrothermal treatment of aluminosilicate clay soils (HTACs) was successfully carried out via a two-step process involving Al and Si dissolution, followed by recrystallisation via hydrothermal treatment. The optimum conditions for dissolution of Al and Si

© University of Venda

from the mechanochemically-activated clay (MAC) were found to be 1.5 M NaOH concentration and 2-hour ageing time. This study also showed that irrespective of the treatment time, increase of treatment temperature enhanced the adsorptive properties of the clay soils, due to the aluminosilicates' activation in the clay soils by the alkaline solutions and subsequent formation of new materials with enhanced active adsorption sites.Optimum conditions for synthesising HTAC were found to be 48-hour ageing time, hydrothermal treatment temperature of 140 °C and 9-mL water content. The increased intensity of the bands indicated the conversion of the aluminosilicate gels into crystalline phases in the zeolitic products.

The XRD analysis shows that a sample synthesised at these conditions (HTAC-8) has higher crystalline particles and several new minerals which was observed as hydroxyl sodalite and confirmed by characteristic sharp peaks around at 2θ = 15, 25, 32 and 35. It was further observed that the XRD peak intensities of these minerals increased with hydrothermal treatment time, while absence of any impurity peaks in the products indicated the zeolites products were highly pure. SEM micrographs show gel-like formation more like a geopolymer gel, which was formed during hydrothermal treatment of aluminosilicate materials (MAC) with NaOH. Platy-like features and amorphous geopolymeric gels of the clays in MAC was also transformed into aggregated microsphere-like particles and crystalline zeolitic products as the treatment temperature increased. Furthermore, some of these microspheres and or spheroidal particle "cotton ball" morphology were seen to overlay on a gel-like structures, indicating partial transformation of the gels initially formed into crystalline microspheres. Hydrothermal treatment led to the formation of predominantly hydroxyl sodalite noted through the dominant spheroidal "cotton ball" particle morphology in all products. Moreover, BET showed an increase in surface area from 25 m^2/g to 33.56 m^2/g after treatment, indicating successful hydrothermal treatments. The pore diameter distribution as a function of pore volume indicated that all samples had highest volume further confirming that these materials are mesoporous. All samples treated at the same temperature but increasing treatment time showed improved percent fluoride removal and adsorption capacity. This indicated that time was an important factor in producing optimum zeolitic products. Preliminary defluoridation experiment showed that HTAC-8 sample (zeolitic product) synthesised under the aforementioned conditions had higher defluoridation and adsorption capacity over other synthesised samples (zeolitic products) and was therefore selected for application in subsequent experiments in the preceding chapter five.

© University of Venda

REFERENCES

Aldabsheh, I., Khoury, H., Wastiels, J., & Rahier, H. (2015). Dissolution behavior of Jordanian clay-rich materials in alkaline solutions for alkali activation purpose. Part I. *Applied Clay Science, 115*, 238-247.

Breck, D. W., & Sieves, Z. M. (1974). Structure, chemistry and use. *Zeolite Molecular Sieves. Wiley, New York.*

Byrappa, K., Subramani, A. K., Ananda, S., Rai, K. L., Sunitha, M. H., Basavalingu, B., & Soga, K. (2006). Impregnation of ZnO onto activated carbon under hydrothermal conditions and its photocatalytic properties. *Journal of Materials Science*, *41*(5), 1355-1362.

Byrappa, K., & Yoshimura, M. (2012). *Handbook of hydrothermal technology*. William Andrew Publications, NJ, USA.

Casci, J. L. (2005). Zeolite molecular sieve: Preparation and scale up. *Microporous and Mesoporous Material,* 2005, 82, 217–226.

Catauro, M., Bollino, F., Papale, F., & Lamanna, G. (2014). Investigation of the sample preparation and curing treatment effects on mechanical properties and bioactivity of silica rich metakaolin geopolymer. *Materials Science and Engineering: C, 36*, 20-24.

Cundy, C. S., & Cox, P. A. (2005). The hydrothermal synthesis of zeolites: Precursors, intermediates and reaction mechanism. *Microporous and Mesoporous Materials*, *82*(1-2), 1-78.

Dacosta, F. A., Muzerengi, C., Mhlongo, S. E., & Mukwevho, G. F. (2013). Characterisation of clays for making ceramic pots and water filters at Mukondeni Village, Limpopo Province, South Africa. *Journal of Engineering and Applied Sciences*, *8*(11), 927-932.

Dhillon, A., Nair, M., Bhargava, S. K., & Kumar, D. (2015). Excellent fluoride decontamination and antibacterial efficacy of Fe–Ca–Zr hybrid metal oxide nanomaterial. *Journal of Colloid and Interface Science, 457*, 289-297.

Duxson, P & Provis, J. L. (2008). Designing precursors for geopolymer cements. *Journal of the American Ceramic Society*, 91:3864-3869

Eissa, N. A., Sheta, N. H., Meligy, W. M. E *et al* (1994). Mossbauer effect of the gamma irradiation and heat treatment on montmorillonite. *Hyperfine Interact*, 91, 783-787.

Gitari, Petrik, L. F & Musyoka, N. M. (2016). Hydrothermal conversion of south african coal fly ash into pure phase zeolite Na-P1. *Zeolites: Useful Minerals*, 25.

© University of Venda

Gitari, M. W., Petrick, L. F & Musyoka, N. M. (2016). Hydrothermal conversion of South African coal fly ash into pure phase zeolite Na-P1. In *Metals and Non-metals 'Zeolites-Useful minerals'* Claudia Belviso (Ed). 25-42.

Gougazeh, M., & Buhl, J. C. (2014). Synthesis and characterization of zeolite A by hydrothermal transformation of natural Jordanian kaolin. *Journal of the Association of Arab Universities for Basic and Applied Sciences*, *15*, 35-42.

Gougazeh, M., & Buhl, J. C. (2014). Conversion of Natural Jordanian Kaolin into Zeolite A without Thermal Pre-activation. *Zeitschrift für anorganische und allgemeine Chemie*, *640* 8-9 1675-1679.

Grutzeck, M. W., & Siemer, D. D. (1997). Zeolites synthesised from class F fly ash and sodium aluminate slurry. *Journal of the American Ceramic Society, 80* 9 2449-2453.

Heller-Kallai, L., & Lapides, I. (2007). Reactions of kaolinites and metakaolinites with NaOH—comparison of different samples (Part 1). *Applied Clay Science*, *35* 1-2 99-107.

Hollman, G. G., Steenbruggen, G & Janssen-Jurkovicˇova, M. (1999). A two-step process for the synthesis of zeolites from coal fly ash. *Fuel,* 78 1225–1230.

Höller, H & Wirsching, U. (1985). Zeolite formation from fly ash. *Fortschritte der mineralogie, 63* 1 21-43.

Hu, Z., Srinivasan, M. P., & Ni, Y. (2001). Novel activation process for preparing highly microporous and mesoporous activated carbons. *Carbon*, *39*(6), 877-886.

Khandare, D & Mukherjee, S. (2019). A Review of Metal oxide Nanomaterials for Fluoride decontamination from Water Environment. *Materials Today: Proceedings*, *18*, 1146-1155.

Luo, H., Law, W. W., Wu, Y., Zhu, W., & Yang, E. H. (2018). Hydrothermal synthesis of needle-like nanocrystalline zeolites from metakaolin and their applications for efficient removal of organic pollutants and heavy metals. *Microporous and Mesoporous Materials*, *272*, 8-15.

Marsha, A., Heatha, A., Patureaub, P., Everndena, M & Walkera, P. (2019). Phase formation behaviour in alkali activation of clay mixtures. *Applied clay science,* 175 10-21.

Mezni, M., Hamzaoui, A., Hamdi, N., & Srasra, E. (2011). Synthesis of zeolites from the low-grade Tunisian natural illite by two different methods. *Applied Clay Science*, *52*(3), 209-218.

© University of Venda

Mikuła, A., Król, M., & Koleżyński, A. (2015). The influence of the long-range order on the vibrational spectra of structures based on sodalite cage. *Spectrochimica Acta Part A: Molecular and Biomolecular Spectroscopy*. 144 5 273-280

Mudzielwana, R., Gitari, M. W & Msagati, T. A. M. (2016). Characterisation of smectite-rich clay soil: Implication for groundwater defluoridation. *South African Journal of Science*, 112 11/12 1-8.

Mudzielwana, R., Gitari, M. W., Akinyemi, S. A., & Msagati, T. A. M. (2017). Synthesis and physicochemical characterization of MnO2 coated Na-bentonite for groundwater defluoridation: Adsorption modelling and mechanistic aspect. *Applied Surface Science*, *422*, 745-753.

Mudzielwana, R., Gitari, W. M., & Ndungu, P. (2019). Evaluation of the adsorptive properties of locally available alumino-silicate clay in As (III) and As (V) remediation from groundwater. *Physics and Chemistry of the Earth, Parts A/B/C*, *112*, 28-35.

Mudzielwana, R., Gitari, M. W., Akinyemi, S. A., & Msagati, T. A. (2018). Performance of Mn 2+-modified bentonite clay for the removal of fluoride from aqueous solution. *South African Journal of Chemistry*, *71*, 15-23.

Mudzielwana, R., Gitari, M. W., & Ndungu, P. (2019). Enhanced As (III) and As (V) adsorption from aqueous solution by a clay based hybrid sorbent. *Frontiers in Chemistry*, *7*.

Mudzielwana, R., Gitari, M. W., & Ndungu, P. (2019). Uptake of As (V) from Groundwater Using Fe-Mn Oxides Modified Kaolin Clay: Physicochemical Characterisation and Adsorption Data Modeling. *Water*, *11*(6), 1245.

Mudzielwana, R., Gitari, M. W., & Ndungu, P. (2019). Performance evaluation of surfactant modified kaolin clay in As (III) and As (V) adsorption from groundwater: adsorption kinetics, isotherms and thermodynamics. *Heliyon*, *5*(11), e02756.

Mudzielwana, R., Gitari, W. M., & Ndungu, P. (2019). Removal of As (III) from Synthetic Groundwater Using Fe-Mn Bimetal Modified Kaolin Clay: Adsorption Kinetics, Isotherm and Thermodynamics Studies. *Environmental Processes*, *6*(4), 1005-1018.

Musyoka, N. (2009). *Hydrothermal synthesis and optimisation of zeolite Na-P1 from South African coal fly ash.* (Doctoral thesis, University of Western Cape, South Africa).

Musyoka, N. M., Petrik, L. F., Hums, E., Baser, H & Schwieger, W. (2012). In situ ultrasonic monitoring of zeolite-A crystallisation from coal fly ash. *Catalysis today*, 190 38–46

© University of Venda

Nicholas, M. Musyoka., Leslie, F. Petrik., Wilson, M. Gitari., Gillian Balfour & Eric Hums. (2012). Optimisation of hydrothermal synthesis of pure phase zeolite Na-P1 from South African coal fly ashes Optimisation of hydrothermal synthesis of pure phase zeolite Na-P1 from South African coal fly ashes. *Journal of Environmental Science and Health, Part A* 47, 337–350

Nikolov, A., Rostovsky, I & Nugteren, H. (2017). Geopolymer materials based on natural zeolite. *Case Studies in Construction Materials,* 6 198-205

Obijole, O. A., Gitari, M. W., Ndungu, P. G., & Samie, A. (2019). Mechanochemically-activated aluminosilicate clay soils and their application to defluoridation and pathogen removal from groundwater. *International Journal of Environmental Research and Public Health, 16*(4), 654.

Petrik, L., White, R., Klink, M., Somerset, V., Key, D.L., Iwuoha, E., Burgers, C & Fey, M. V. (2005). Utilization of fly ash for acid mine drainage remediation. Water Research Commission Report No. 1242/1/05, Pretoria, South Africa.

Soulé, M. Z., Fernández, M. A., Montes, M. L., Suárez-García, F., Sánchez, R. T., & Tascón, J. M. D. (2020). Montmorillonite-hydrothermal carbon nanocomposites: Synthesis, characterization and evaluation of pesticides retention for potential treatment of agricultural wastewater. *Colloids and Surfaces A: Physicochemical and Engineering Aspects*, *586*, 124192.

Toor, M., Jin, B., Dai, S & Vimonoses, V. (2014). Activating natural bentonite as cost effective adsorbent for removal of Congo red in wastewater. *Journal of Industrial Engineering Chemistry*, 1979 1–9.

Xu, Hua., & Deventer Van, J. S. J (2000). The geopolymerisation of alumino-silicate minerals. *International journal of mineral processing,* 59 247–266.

Yao, Z., Ma, X., & Lin, Y. (2016). Effects of hydrothermal treatment temperature and residence time on characteristics and combustion behaviors of green waste. *Applied Thermal Engineering*, *104*, 678-686.

Yoshimura, M., & Byrappa, K. (2008). Hydrothermal processing of materials: past, present and future. *Journal of Materials Science*, *43*(7), 2085-2103.

© University of Venda

CHAPTER FIVE: HYDROTHERMALLY-TREATED ALUMINOSILICATE CLAY (HTAC) AND THEIR APPLICATION IN FLUORIDE AND PATHOGEN REMOVAL FROM GROUNDWATER

5 Abstract

In this study mechanochemically-activated clay was hydrothermally-treated and applied for defluoridation and pathogen removal from groundwater. Fourier transform infrared (FTIR), Brunauer-Emmett-Teller method (BET), X-ray diffraction spectroscopy (XRD) and Scanning electron microscopy-energy dispersion spectroscopy (SEM-EDS) and X-ray fluorescence (XRF) spectroscopy were employed in characterisation of the hydrothermally-treated aluminosilicate clay (HTAC). Batch defluoridation experiments were used to evaluate the fluoride adsorption capacity while well diffusion method was used to evaluate the antibacterial efficacy. The BET results showed increase in surface area from 17 m^2/g to 33.56 mg^2/g after treatment. FTIR results revealed an increase in transmittance bands 950, 650 cm^{-1}, 3000 and 1400 - 1500 cm^{-1} while disappearance of bands at 3000 and 3600 - 3700 cm^{-1} was noted in the treated materials. The transmittance of the fluoride-loaded clay after fluoride removal revealed a decrease in specific bands intensity at 3700 - 3500, 2850, 1490, 950 cm^{-1} and around 650 cm^{-1}, which indicated that the created available sites in the treated clay had been occupied by fluoride as a result of ion exchange during defluoridation. SEM micrographs of the treated material showed transformation from platy-like amorphous nature in MAC to geopolymeric gels with microspheres particulate morphology of different thicknesses as hydrothermal treatment progressed. The observation of intense characteristic peaks for the mineral phases in the treated material are confirmed by SEM images which showed geopolymer gel-like materials with aggregated microsphere particles compared with the untreated material having platy-like non-crystalline amorphous nature. This was corroborated by the BET results obtained earlier. The XRD results revealed changes in the mineral phase, in which there was appearance of new mineral phases, disappearance of some phases, increase and decrease of some phases in the treated material (HTAC) compared with the untreated (MAC). This result was corroborated by strong, intense and sharp characteristic FTIR peaks observed in the treated material. SEM micrographs of the treated material showed transformation from platy-like amorphous nature in MAC to geopolymeric gels with microspheres particulate morphology. Batch defluoridation showed maximum adsorption capacity of 1.75 mg/g with 53% fluoride removal

© University of Venda

from initial fluoride concentration of 6.0 mg/L using 0.8 g/40 mL dosage, initial pH 5.8 and contact time of 5 min at room temperature. The adsorption kinetics data better fitted well to pseudo-second-order models, while the adsorption data were best described by Freundlich adsorption model. The regeneration and recyclability potential studies with 0.1 M KCl as a regenerant showed the adsorbent could be used for up to six times. Antibacterial activities of the optimised HTAC adsorbent towards *Escherichia coli* (*E. coli*) strains indicated some potency against the strains. The outcome of this study showed the developed HTAC has a strong potential for application in groundwater defluoridation and pathogen removal.

Keywords: aluminosilicate clay, adsorbent characterisation, groundwater defluoridation, hydrothermal treatment, pathogen.

5.1 Introduction

Water is an essential resource for life sustenance and access to safe potable water have been linked to increased economic productivity, sound health and improvement in life quality (Oke *et al.,* 2014). About 1 billion (844 million) people worldwide (1 in 9) lack access to safe potable water (WHO 2015; 2017). Over 159 million people are dependent on surface water that may have been contaminated (WHO 2015; 2017). According to World Health Organization (2017) report, over 5 million deaths occur yearly due to drinking of unsafe water that has been contaminated from anthropogenic and artificial sources. Most rural dwellers, where piped-borne water is lacking depend mainly on groundwater. Some groundwater and aquifers have fluoride levels above the WHO threshold limits of 1.5 mg/L (WHO, 2017). Prolonged exposure to drinking of fluoride rich water has resulted in medical conditions such as dental and skeletal fluorosis. Fluorosis is pandemic in about 26 countries with over 30 million people affected and about 200 million at risk worldwide and the number is increasing daily (Momba & Brouckaert, 2005; WHO, 2015). Countries such as Ethiopia, Kenya, Uganda, Tanzania, Egypt, South Africa, Mexico, China, Sir Lanka and India are mostly endemic with fluorosis (McCaffrey & Willis, 2001; Ncube & Schutte, 2005: Kimambo *et al.,* 2019: Chandrajith *et al.,* 2020).

Waterborne pathogens are also major public health concerns worldwide due to high morbidity and mortality arising from numerous waterborne and water related diseases which are responsible for an estimated 3.5 million deaths per year. Globally, reports have shown that about 2 billion people are exposed to water sources that have been contaminated with faeces (Bitton,

© University of Venda

2014). Water-related deaths in the developing world account for about 98%. Worldwide, a child dies due to water-related disease, every 2 min, hence, there is urgent need to develop suitable affordable technology to address the global menace (WHO/UNICEF, 2016).

Defluoridation is a widely used method for remediation of fluoride-rich water. Various techniques and materials have been used worldwide for water defluoridation. This include adsorption (Ghorai & Pant, 2004; Mondal & George, 2015; Gitari *et al.*, 2016; Mudzielwana *et al.*, 2016; Pandi *et al.*, 2019), ion exchange (Pan *et al.*, 2018), precipitation (Saha, 1993), electro-chemical (Loganathan *et al.*, 2013), electrocoagulation (Luna *et al.*, 2018) and reverse osmosis (Khairnar *et al.*, 2018).

Amongst the Sustainable Development Goals (SDG's) set by the United Nations, Goal 6.1 aims at providing clean, safe and affordable water to everyone across the globe by 2030. This calls for development of affordable, easy to use and effective technologies for water treatment. Adsorption technology is the most widely used due to its ease of operation, universality and cost effectiveness. Materials such as clay (Gitari *et al.*, 2015, Mudzielwana *et al.*, 2016), diatomaceous earth (Izuagie *et al.*, 2016), porous nanohydoxyapatite (Wimalasiri *et al.*, 2020); activated carbon (Chen *et al.*, 2019) and activated alumina (Samrat *et al.*, 2020) have been developed for fluoride removal and have proven to be effective. By far, majority of the reported adsorbents are more effective towards fluoride alone. The occurrence of fluoride and patogens in drinking water due to geogenic and anthropogenic activities respectively, necessitated the need to develop multifunctional adsorbents capable of removing fluoride and pathogens from water. Multifunctional adsorbents such as Fe-Ca-Ze hybrid metal oxides (Dhillon *et al.*, 2015) and mechanochemically-activated clays (Obijole *et al.*, 2019) have already been reported for simultaneous removal of fluoride and pathogens. Ayinde *et al.* (2018) developed Ag/MgO nanoparticle modified nanohydroxyapatite adsorbent for fluoride and pathogen removal and found it to be effective towards both contaminants. However, these materials have not been totally effective in simultaneous defluoridation and pathogen removal from water. Furthermore, high fluoride levels are known to be associated with groundwater while pathogens are commonly found in surface water around the world (Huang *et al.*, 2018; Zhang *et al.*, 2017; Marwa *et al.*, 2018). Studies carried out on Siloam groundwater in Limpopo, South Africa revealed the presence of pathogens in some groundwater particularly in areas where the sunk boreholes were not far from the septic tanks (Denga, 2017). This was due to sipping of pathogens through the underground

© University of Venda

rocks and soils along with the underground waters or aquifers (Odiyo & Makungo, 2018), hence, the need to develop an efficient multifunctional adsorbent for application in simultaneous defluoridation and pathogen removal from groundwater.

Hydrothermal treatment is the reaction of heterogeneous clay minerals in aqueous alkaline solutions under high temperature and pressure in a closed system in order to dissolve and recrystallise new minerals that are relatively insoluble under ordinary conditions (Yoshimura & Byrappa, 2008). This process provides an excellent processing of the clay materials with a view to modifying the surface morphology by increasing the surface area to obtain desired physicochemical properties for enhanced defluoridation and pathogen removal (Hollman *et al.*, 1999). Luo *et al.* (2018) indicated that hydrothermal treatment process improves the surface porosity of the material following the recrystallisation, nucleation and re-precipitation of the dissolved Si and Al minerals at alkali conditions. In this study, locally available aluminosilicate clay was treated hydrothermally using NaOH solutions in order to modify and increase its surface adsorption properties for enhanced defluoridation, pathogen detoxification and removal from groundwater. The physicochemical characteristics of the treated clay materials were evaluated using FTIR, BET, SEM-EDS, XRD and XRF. The fluoride removal efficiency of the treated clay was evaluated using batch experiments while the antibacterial efficacy was assessed using well diffusion assay method. The adsorption kinetics and isotherms models were employed to elucidate the sorption kinetics and nature of the adsorbent. Lastly, the effect of co-existing ions on fluoride sorption and regeneration potential of the adsorbent was evaluated.

5.2 Materials and methods

5.2.1 Materials

The clay samples from the previous studies observed to be rich in aluminosilicate materials (Mudzielwana *et al.*, 2016; Gitari *et al.*, 2016; Obijole *et al.*, 2019) were obtained from Mukondeni village in Vhembe district, Limpopo, South Africa. The samples were separated from impurities, ground, washed, centrifuged and oven-dried to constant weight at 110 °C and packaged into sealable plastic bags until needed for use. All chemicals and reagents including NaOH pellets-anhydrous > 98%, Na_2CO_3 > 99%, NaF > 99%, HCl, NaCl > 99%, KCl and TISAB III solution were bought from Sigma Aldrich and they were of analytical grade.

© University of Venda

5.2.2 Hydrothermal treatment of aluminosilicate clay (HTAC) adsorbents

Prior to hydrothermal treatment, the clay was activated mechanochemically by milling at A speed of 700 rpm using a RS200 milling machine (Retch, Green Bay, WI, USA) for 30-min optimum contact time (Obijole *et al.*, 2019). This was followed by hydrothermal treatment of the clay powder at the optimised conditions obtained in the preceding studies, as follows: 100 mL of 1.5 M NaOH solution were pipetted into 250 mL heat resistant, high density plastic bottles, then 2 g of the activated clay were added. The mixture was stirred on a magnetic stirrer at a temperature of 47 °C at 800 rpm stirring speed for an optimum time of 2 h in accordance to the experimental protocol used in subsection 4.2.2.1 and 4.2.2.2 respectively. Thereafter, 20 mL of the clay/NaOH slurry obtained in the ageing step above were mixed with a desired volume of water (9 mL) and transferred into a 45 mL Parr bomb vessel, which was sealed and placed in the furnace at an optimum temperature of 140 °C and 48-h contact time respectively. Thereafter, the solid products formed after hydrothermal treatment were dispersed in 500 mL of Milli-Q water to reduce the effect of high alkalinity of solution on the aluminosilicate clay adsorbent formed. The suspensions were passed through 0.45 µm pore polypropylene membrane filters in order to recover the solid. The solids were washed further with Milli-Q water until near neutral pH. Recovered residues were then oven-dried at 110 °C for 6 h and then allowed to cool down in a desiccator. Furthermore, the obtained residues (HTAC) were milled, passed through < 250 µm sieve and then stored in plastic bottles to prevent moisture ingress (Wang *et al.*, 2017).

5.2.3 Physicochemical and mineralogical characterisation

The developed hydrothermally-treated clay (HTAC) adsorbents were evaluated for functional groups using Fourier Transform Infrared spectroscopy (Bruker, Germany: ATR-Diamond FT-IR spectrophotometer). The treated clay surface and specific area, pore volumes and pore sizes were measured with Micromeritics TriStar II Surface Area and porosity unit instrument (Micromeritics, Norcross, GA, USA) using Brunauer-Emmett-Teller (BET) method. Scanning electron microscopy was used to investigate the clays' morphology by using JEOL - 2100 Electron Microscope. Examination of the qualitative and quantitative mineral phase composition was done by employing a D8 advance X-ray diffraction (Bruker, Germany) equipped with Cu- Kα source radiation wavelength (λ1 = 1.54056 Å, λ2 = 1.54439 Å, Ni-Kβ filter) and a LynxEye 1D detector with 192 measuring channels and axial Soller slits on both sides. Titration methods using 0.001 M, 0.01 M and 0.1 M KCl solutions were employed in pH at point-of-zero charge (pH_{pzc})

© University of Venda

determination of the treated clay (HTAC) (Eggleston & Jordan, 1998). Elemental composition of the hydrothermally treated material was evaluated using a PANanalytical Axios X-ray fluorescence spectrometer equipped with a 4 kW Rh tube.

5.2.4 Batch adsorption experiments

Batch fluoride adsorption experiments were conducted to evaluate effect of contact time, adsorbent dosage, pH and adsorbate concentration using HTAC. The effect of contact time on fluoride removal and adsorption kinetics was evaluated by varying the contact time from1 to 80 min at 200 rpm agitation using 0.8 g/40 mL adsorbent dosage and initial fluoride concentration of 10 mg/L with pH of 6 ± 0.5. The obtained mixtures were centrifuged for about 30 min at 4000 rpm after agitating and the supernatants analysed for residual fluoride concentrations by the use of ORION Ion-Selective Electrode (ISE, 9609BNWP) with detection limit of 0.01 mg/L. The electrode was calibrated using 0.1, 1, 10 and 100 mg/L standards. TISAB III solution was added to both standards and samples at volume ratio of 1:10 to de-complex fluoride ions. The effect of adsorbent dosage in fluoride removal was evaluated by introducing 40 mL volume of simulated 10 mg/L fluoride solution into 250 mL plastic bottles, followed by addition of 0.1, 0.2, 0.4, 0.6, 0.8 and 1.0 g of HTAC into the bottles. The mixtures were agitated for optimum contact time of 5 min. The adsorption isotherms were studied by varying the initial concentration of the fluoride ions from 1 to 100 mg/L and the optimum adsorbent dosage of 0.8 g/40 mL was weighed into the bottles and the mixtures agitated for 5 min optimum contact time. To evaluate the effect of pH influoride removal, the mixtures' pH was adjusted between 2 and 12 using 0.1 M NaOH and 0.1 M HCl respectively. Optimum adsorbent dosage of 0.8 g/40 mL of HTAC was used. To evaluate the effect of fluoride ion concentration, 100 mL volume of between 1 to 100 mg/L fluoride solution was measured into polythene bottles. Zero point eight gramme of the samples was weighed into the bottles and the pH adjusted to the optimum pH 5.8, by adding 0.1 M HCl or 0.1 M NaOH. The mixtures equilibrated for the optimum contact time of 5 min. After the equilibration time, the suspensions were filtered. The fluoride ion concentration in each solution was determined. The effect of co-existing ions on defluoridation in the presence of 10 mg/L of chloride, nitrate, phosphate and sulphate separately was evaluated at initial fluoride concentration each of 10 mg/L using 0.8 g/40 mL adsorbent dosage at initial pH 6.9 ± 0.1 and the mixtures agitated for 5 min. All the experiments were done in duplicates and the mean values were reported for accuracy.

© University of Venda

5.2.4.1 Calculation of the per cent fluoride removal and adsorption capacity

The per cent fluoride removal and adsorption capacity were determined from equation 5.1 and 5.2, respectively.

$$\text{Per cent fluoride removal} = \frac{(C_o - C_e)}{C_o} \times 100 \quad (5.1)$$

$$\text{Adsorption capacity}, q = (C_o - C_e) \times \frac{V}{m} \quad (5.2)$$

Where q is the mass of fluoride adsorbed in mg/g of adsorbent, C_0 *and* C_e are the initial and equilibrium concentrations of fluoride respectively, V is the volume of the solution in liters and m is the mass in gram of the developed HTAC.

5.2.5 Regeneration potential experiments

Fluoride-loaded HTAC was regenerated by agitating 0.8 g of fluoride loaded HTAC separately with 100 mL of 0.1 M NaOH and 0.1M KCl on a mechanical shaker for 30 min. Thereafter, the mixtures were filtered using a 0.45 µm pore membrane filter and then the resulting filtrate diluted to 100 mL and analysed for fluoride desorbed. The resulting HTAC residues were thoroughly washed on the filter paper with deionised water and oven-dried at 110 °C for 4 h. Batch fluoride adsorption was carried out on the regenerated HTAC adsorbent. The regenerated-reuse cycle experiments were repeated for up to five times.

5.2.6 Antibacterial studies

Antibacterial efficacy of the HTAC materials for pathogen removal was tested with gram-negative *Escherichia coli* (*E. coli*) (ATCC 35218) strains by utilising the method of well diffusion assay. The inhibition zone was measured and recorded. The bacterial suspensions with 0.5 McFarland turbidity were prepared. Mueller-Hinton agar was also prepared by methods earlier described in the previous work (Obijole *et al.*, 2019) and placed into plates which were inoculated with the strains of *E. coli*. Wells with a diameter of 6 mm were cut with a cork borer and then filled with 30 µL solution of the best modified-hydrothermally-treated aluminosilicate clay (HTAC) materials on a single plate against the bacterial strains. The plate were incubated for 24 h at 37 °C. Thereafter, the growth inhibition zone diameters were measured. The agar plate and sample used in this study were carefully packaged in disposable plastic bags, sealed and sent for immediate destruction as soon as measurements were concluded.

© University of Venda

5.3 Results and discussions

5.3.1 Physicochemical characterisation

5.3.1.1 Fourier transform infra-red (FTIR) analysis

Figure 5.1 presents the FTIR spectra and functional groups of the mechanochemically-activated clay (MAC) (untreated), HTAC (treated) and HTAC after fluoride removal. The spectra of the treated clay are characteristically different from the untreated. The silica and aluminium fingerprints of the treated clay showed more intense transmittance. An increase in transmittance bands observed around 950 and 650 cm^{-1} were due to increased presence of Si-O and Al-O bands resulting from moisture loss as hydrothermal treatment temperature increased (Luo *et al.*, 2018). The increased appearance of transmittance bands around 3000 and 1400 - 1500 cm^{-1} in the treated material is suggestive of strong presence of O-H and Na-O due to the clay surfaces modification. The disappearance of transmittance bands 3000 and 3600 - 3700 cm^{-1} was due to the breakdown of O-H bonds and strong transmittance appearance around 600 cm^{-1} as a result of Al-O and Si-O bonds formation during surface modification. The disappearance of these bands could be due to dehydroxylation that occurs during hydrothermal treatment. Dehydroxylation involves the heating process during hydrothermal treatment in which the hydroxyl groups (OH) is released to form water molecules (Frost & Vassallo, 1996: Sperinck *et al.*, 2011). The transmittance of the fluoride-loaded clay after fluoride removal revealed a decrease in specific bands intensity at 3700 - 3500, 2850, 1490 and 950 cm^{-1} and around 650 cm^{-1}. The reduction in the transmittance values suggested that the created available sites in the treated clay had been occupied by fluoride as a result of ion exchange during defluoridation, which is indicative of fluoride sorption due to transmittance bands attributable to Al-F and Si-F bonds around 600 cm^{-1}. Thus, fluoride sorption is suspected to occur via electrostatic attraction owing to strong attraction of fluoride ions to the Al and Si on the synthesised adsorbent surfaces (Ghasemi *et al.*, 2014). Studies have shown that Al-OH, Si-OH and Na-O groups on the adsorbent surface tends to serve as adsorption sites, which readily combine with F^- in solutions. Fluoride adsorption mechanism for the material could involve the contribution of OH^- to hydrogen bonding with fluoride ion on the material's surface in aqueous solutions. Furthermore, the metal species such as Al, Si and Na, which are strongly positive are attracted to F^- via hydroxyl transition (Huang *et al.*, 2020). Based on the behaviour of the Si-O, Al-O and Na-O bonds in the treated clay and the fluoride-loaded treated clay, schematic presentation of the

© University of Venda

fluoride adsorption mechanism of the synthesised clay could be summarised in the following equations in accordance with the postulates of Huang *et al.* (2020):

$TO + H_2O \leftrightarrow T(OH)_2$ (5.3)

$T(OH)_2 + F^- \leftrightarrow T(OH)_2F + OH^-$ (5.4)

$TOH + HF \leftrightarrow TOHHF$ (5.5)

$TOHHF \leftrightarrow TF + H_2O$ (5.6)

T represents Al, Si and Na etc.

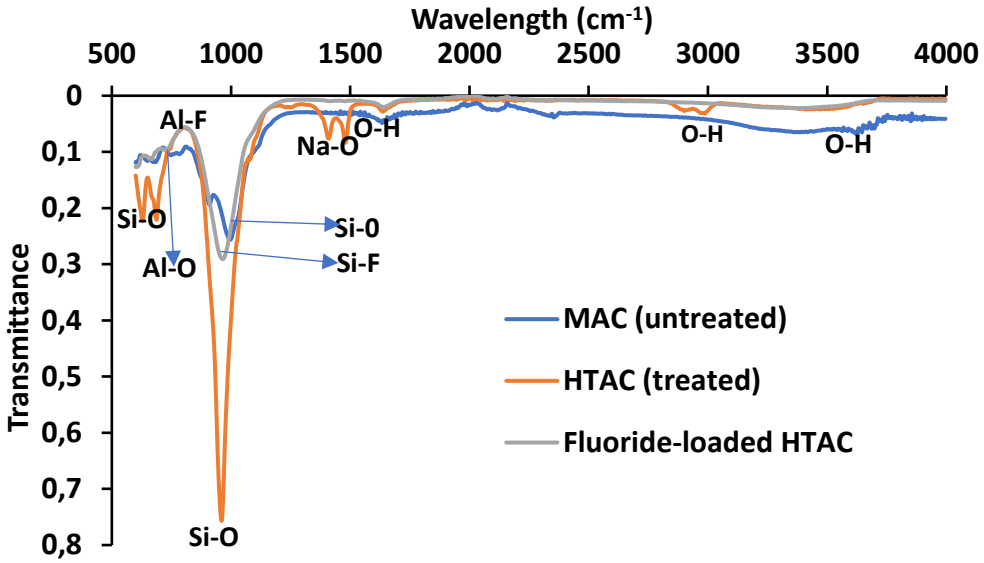

Figure 5.1: FTIR spectra of untreated clay (MAC), treated clay (HTAC) and fluoride-loaded hydrothermally treated alumiosilicate clay (F-HTAC).

5.3.1.2 Surface area determination by Brunauer-Emmett-Teller (BET)

Table 5.1 depicts the BET surface area and single point surface area. BET analysis showed a significant increase in the surface area of untreated clay (MAC) from 17 m^2/g to 33.56 m^2/g in the treated clay (HTAC) material. The increase in surface area of the HTAC) was attributable to processing and crystallisation of the clay materials during hydrothermal treatment to form gel-like geopolymers with crystalline microspheres structures. During treatment at the optimised temperature and time, there was kinetic mobility of the microsphere gels leading to breakdown, producing smaller microsphere gels with a large surface area culminating in increased adsorption sites on the surface of HTAC (Casci, 2005; Gitari *et al.*, 2016; Obijole *et al.*, 2019). Average pore diameters of 14.93 nm and 14.87 nm were obtained for the untreated and treated clays respectively

© University of Venda

(Table 5.1). Figure 5.2 a and 5.2 b depict pore distribution curves of untreated and treated clay materials respectively. The pore diameter of bulk of the pores are distributed within 0 - 50 nm range, hence, indicating that both the untreated and treated clay materials are mesoporous in nature (Figure 5.2 a and 5.2 b). Also, the nitrogen adsorption-desorption isotherm curves for raw MAC and HTAC are shown in Figure 5.2 c and 5.2 d. The adsorption-desorption curves for the untreated and treated materials are similar but quantity (volume) of adsorbed particles are higher in the treated material which is indicative of increased mesoporosity consequent upon hydrothermal treatment at elevated temperatures.

Table 5.1: The BET surface area, and surface area single point of hydrothermally-treated aluminosilicate clay (HTAC) and untreated aluminosilicate clay (MAC).

Sample	BET surface area (m^2/g)	Surface area single point (m^2/g)
Untreated clay (MAC)	17.19	16.66
Hydrothermally-treated clay (HTAC)	33.56	32.09

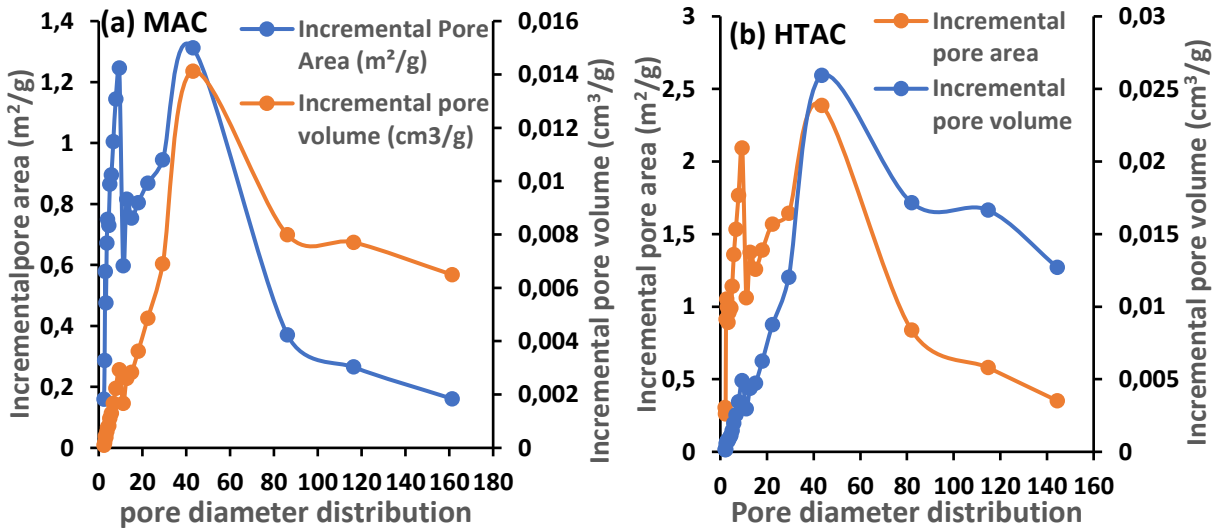

© University of Venda

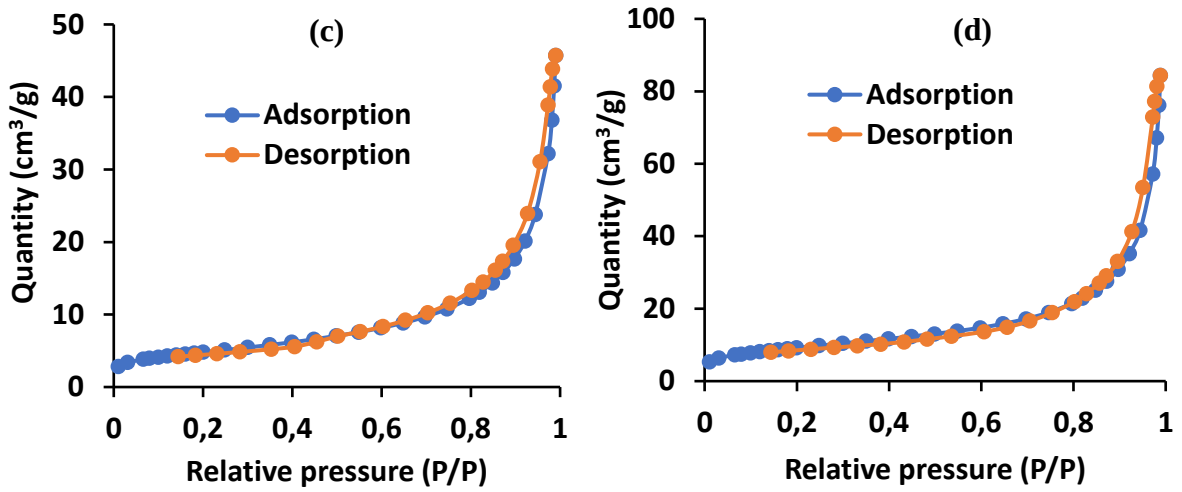

Figure 5.2: Pore distribution curves for (a) untreated clay (MAC) and (b) treated clay (HTAC); nitrogen adsorption-desorption curves for (c) untreated clay (MAC) and (d) treated clay (HTAC). BET = Brunauer-Emmett-Teller; n = number of samples; Pore volume = dose dispersion and or distribution in one unit mass; Pore volume is opposite to density.

5.3.1.3 Morphology of hydrothermally-treated clay

The surface morphology of the hydrothermally-treated clay was probed with SEM-EDS. The SEM images (a) and (b) of the untreated (MAC) and treated clay (HTAC) respectively are presented in Figure 5.3 a and 5.3 b. The images show changes in morphology, appearance and sizes of the untreated and the treated clay material. The SEM image (a) shows expanded arrays of smooth, irregular poorly defined flared corn flakes structures with non-crystalline particles and platy-like texture, (Figure 5.3 a) which changed to irregular shapes and sizes on the external surface with needle rod-like crystalline geopolymer gel microsphere structures of different thicknesses after treatment. The needle-like structures appear protruding from gel-like structures, indicating they initially grew from these structures as hydrothermal treatment progressed (Figure 5.3 b). The transformation of the structural morphology is caused by the formation of new crystalline mineral phases of zeolite type following the alkali dissolution of Si and Al containing minerals and subsequent re-precipitation of sodium on the surface (Luo *et al.*, 2018). The formed structures resembles those of hydroxy sodalite mineral phase reported by Luo *et al.* (2018). Moreover, the morphology of HTAC appears to be crystalline and porous which is corroborated by the BET results which showed an increase in the surface area after treatment (Table 5.1). The results of the elemental analysis of the untreated clay (MAC) and hydrothermally-treated (HTAC) are presented in Figre 5.3 c and 5.3 d. Both spectra's showed Silicon, Aluminium, Magnesium,

© University of Venda

Iron, Sodium and Calcium on the surface of the materials. The elemental concentrations of silicon, iron, aluminium, sodium, magnesium, potassium and calcium in the hydrothermally-treated clays were observed to increase. During hydrothermal treatment of the clay slurry which initially dissolved the aluminosilicates to give aluminium, silicon and other species in solution, recrystallisation occurred forming new chemical species such as potassium and titanium while the concentrations of species such as aluminium, silicon, sodium, magnesium, and calcium were observed to increase in HTAC. The increased concentration of the aluminosilicates species and exchangeable base cations caused increase in positively charged species, which were responsible for increased fluoride sorption onto HTAC surfaces when compared to MAC.

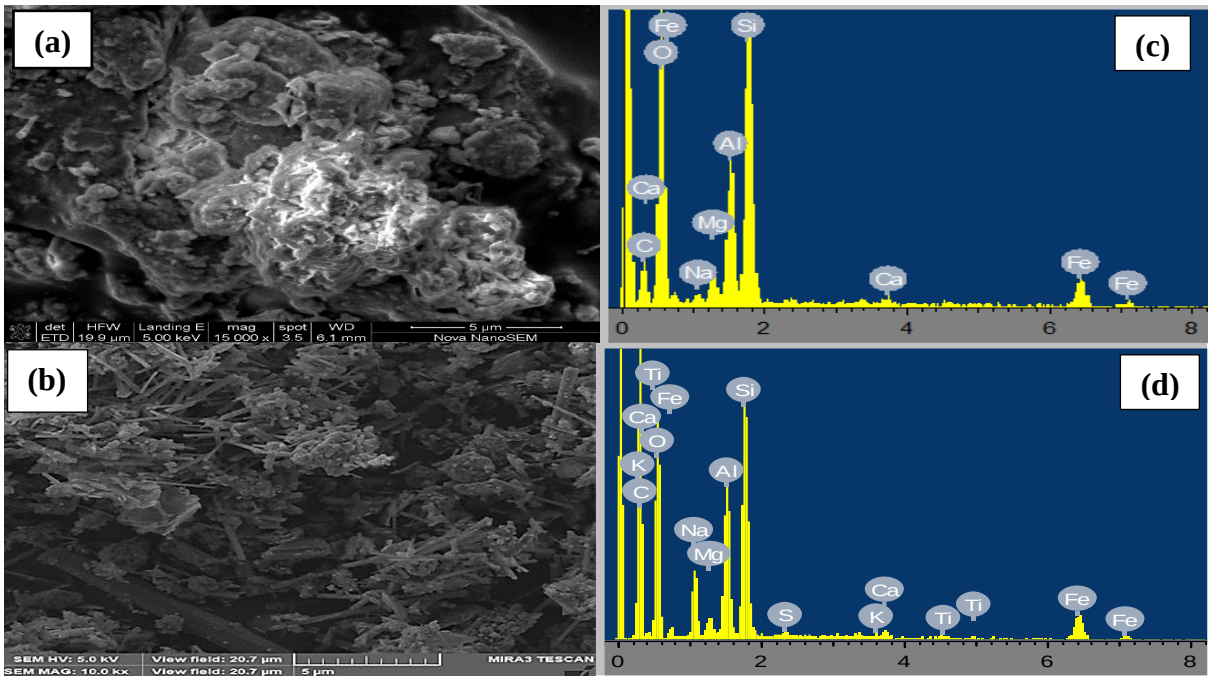

Figure 5.3: Scanning electron microscopy (SEM) micrographs of (a) untreated clay (MAC), (b) treated clay (HTAC), (c) energy dispersion spectroscopy (EDS) of (c) untreated clay (MAC) and (d) treated clay (HTAC).

5.3.1.4 X-ray diffraction (XRD)

X-ray diffraction qualitative results are presented in Figure 5.4. The results revealed the changes in the mineral phase of the treated clay (HTAC) compared to the untreated clay (MAC). The prominent peak of montmorillonite would indicate the dominance of this mineral in the clay soils. There was appearance of new mineral phases, disappearance of some phases, increase and decrease of some phases in the treated material (HTAC). Dacosta *et al* (2013) reported

© University of Venda

concentrations ranging from 38 - 55 weight % of smectite in these mukondeni clay soils. Montmorillonite was identified through its prominent peaks at 6.5°, 12°, 18° and 28° two theta. After hydrothermal treatment, there was appearance of some new peaks which were matched to the formation of new zeolitic phases including hydroxy sodalite (HS), phillipsite (Ph) and chlorite (Ch) minerals (Gougazeh *et al.*, 2014). The new prominent mineral phase are closely linked to zeolite mineral phases and were matched with hydroxy sodalite (HS) which could be attributed to dissolution and transformation of Si and Al containing minerals. It could be deduced that the absence of any impurity peaks in the products, indicates the zeolites product were highly pure. Moreover, peaks appears to be having stronger intensity as compared to the peaks in the MAC particularly at the two theta region of 15 to 35 degrees. The stronger intensity is linked to higher crystallinity nature of the HTAC as observed in SEM micrographs. The observed changes in the mineral phases were due to the occurrence of chemical transformation brought about by recrystallisation process during hydrothermal treatment, leading to the formation of some new mineral phases and breaking down of some others. The reaction mechanism includes the dissolution of aluminosilicates material in the parent material under alkali treatment to release Si and Al which is followed by re-precipitation, nucleation and recrystallisation during hydrothermal treatment. This process of recrystallisation and nucleation lead to formation of needle-like structure as determined by SEM micrographs (Figure 5.3 b and d). This result was corroborated by strong, intense and sharp characteristic FTIR peaks observed in the treated material. The FTIR showed the stronger intensity for Si-O and Al-O bands as well as the formation of new bonds related to Na-O which confirms the formation of new mineral phases as indicated from XRD results. In addition the surface area analysis also confirmed the formation of new highly porous materials which is the nature of crystalline material. SEM micrographs of the treated material showed transformation from platy-like amorphous nature in MAC to geopolymeric gels with microspheres particulate morphology. Studies reported that materials' morphology is affected by the mediums' characteristic environment and the chemical species which acted as templates around which the aluminosilicate polymerises to produce the microspheres interlaced with pores (Öztop & Shahwan, 2006). Recent studies by Mudzielwana *et al.* (2016) and Obijole *et al.* (2019) on smectite clay showed similar characteristic peaks and presence of these mineral phase in the same proportions for the untreated clay. The X-ray results indicated that the dominant minerals in the treated material are hydroxyl sodalite. The observation of intense characteristic peaks for the

© University of Venda

mineral phases in the treated material are confirmed by SEM images (Figure 5.3 b) which showed geopolymer gel-like materials with aggregated microsphere particles compared with the untreated material having platy-like non-crystalline amorphous nature. This results further corroborate the qualitative results. The chemical transformation with increased surface area impacted positively on the treated (HTAC) materials defluoridation potentials.

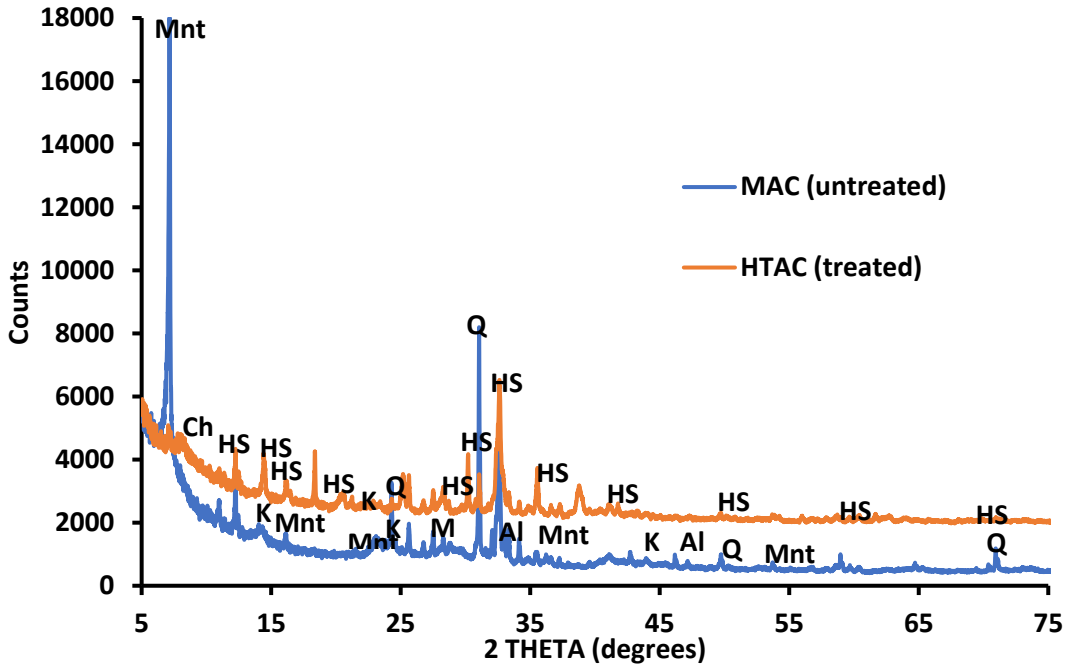

Figure 5.4: X-ray diffraction spectra of mechanochemically-activated clay (MAC) soils and hydrothermally-treated aluminosilicate clay (HTAC) soils. (Mnt - montmorillonite, Al - albite, M - muscovite, Q - quartz, A - zeolite, HS - Hydroxy sodalite hydrate).

5.3.1.5: X-ray fluorescence (XRF) analysis

Table 5.2 presents the XRF results of the elemental compositions of mechanochemically-activated clay (MAC) and the hydrothermally-treated aluminosilicate clay (HTAC). As shown below, MAC is mainly composed of SiO_2 (52.48%) and Al_2O_3 (24.62%). After hydrothermal treatment, the composition in the HTAC changed to SiO_2 (45.92%), Al_2O_3 (21.23%), and Na_2O (5.45%) which indicated that Na in NaOH solution was chemically incorporated into silica and alumina matrix of the hydrothermally-treated product which led to decreased Si and Al oxides and substantially increased the Na oxides content (Luo *et al.*, 2018).

© University of Venda

Table 5.2: Chemical composition of MAC and HTAC.

Oxides	Content (%)	
	MAC	HTAC
SiO_2	52.48	45.92
Al_2O_3	24.62	21.23
Fe_2O_3	6.64	7.56
MgO	2.985	4.56
CaO	1.53	3.21
K_2O	1.24	1.32
Na_2O	0.707	5.45
TiO_2	0.627	1.23
MnO	0.125	0.261
P_2O_3	0.034	0.045
SO_3	0.023	0.026

5.3.2 Batch defluoridation results

5.3.2.1 Contact time and adsorption kinetics

Figure 5.5 depicts the variation of percent fluoride removal with contact time. There was a sharp increase in fluoride removal rate with increase in contact time from 1 - 5 min up to 40% (Figure 5.5). The observed increase which was due to availability of sorption sites on the adsorbent was noted in similar studies carried out by Mudzielwana *et al.* (2016) and Obijole *et al.* (2019). After 5 min, the rate of fluoride removal was stabilised, indicating that the system had been saturated and equilibrium attained. Hence, 5 min were adopted as the optimum contact time and applied in subsequent experiments.

© University of Venda

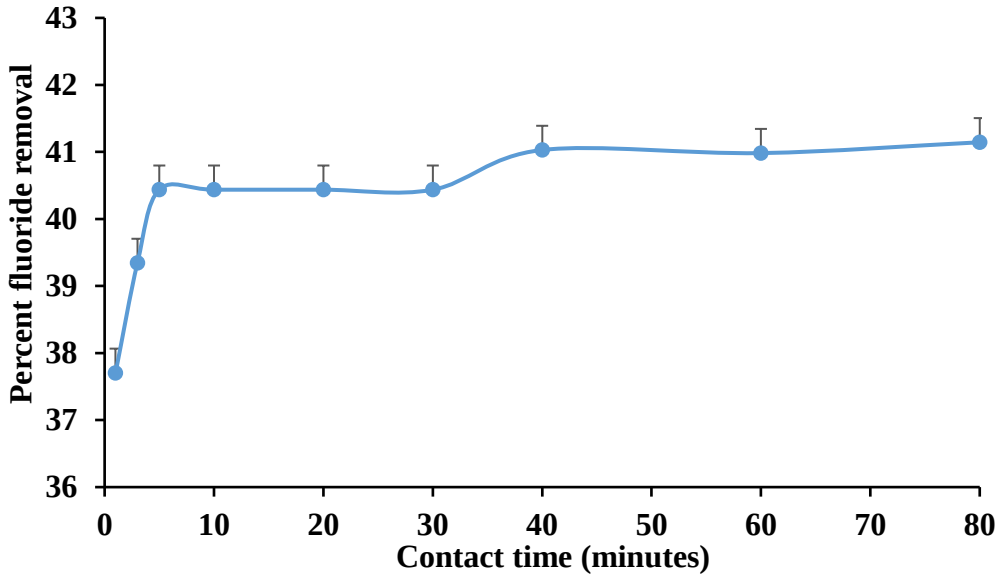

Figure 5.5: Variation of percent fluoride removal with contact time (initial fluoride concentration = 10 mg/L, initial pH = 6.0, adsorbent dosage = 0.8 g/40 mL, temperature = 298 K and 250 rpm shaking speed).

The adsorption kinetics data at different contact times fitted into the non-linear equations of pseudo-first-order (PFO) and pseudo-second-order (PSO) of reaction kinetics models as well as the Weber-Morris intra-particle diffusion model in order to establish possible sorption mechanism and fluoride removal adsorption rate as well as the rate determining factors for fluoride adsorption onto the surface of the synthesised HTAC (Lagergren, 1898: Qureshi *et al.*, 1995: Ho *et al.*, 2000: Gupta & Bhattacharyya, 2011: Yoon *et al.*, 2017: Ngulube *et al.*, 2017: Denga *et al.*, 2018). The pseudo-first-order and second-order models are expressed by the non-linearised mathematical equations 5.7 and 5.8 respectively:

$$q_t = q_e\,(1 - e^{-K_{ad}t}) \qquad (5.7)$$

$$q_t = \frac{q_e^2\,K_{2ads}\,t}{1 + K_2 q_e^2\,t} \qquad (5.8)$$

Where q_e and q_t are the adsorbed fluoride per unit mass (mg/g) at equilibrium and time, t (min), K_{ad} (min^{-1}) and K_{2ads} ($g.mg^{-1}/min$) are rate constants for pseudo-first-order and pseudo-second-order respectively. Figure 5.6 depicts pseudo-first-order and pseudo-second-order plots respectively while Table 5.3 presents the derived adsorption constants modelling parameters values values of pseudo-first-order and pseudo-second-order kinetics respectively.

© University of Venda

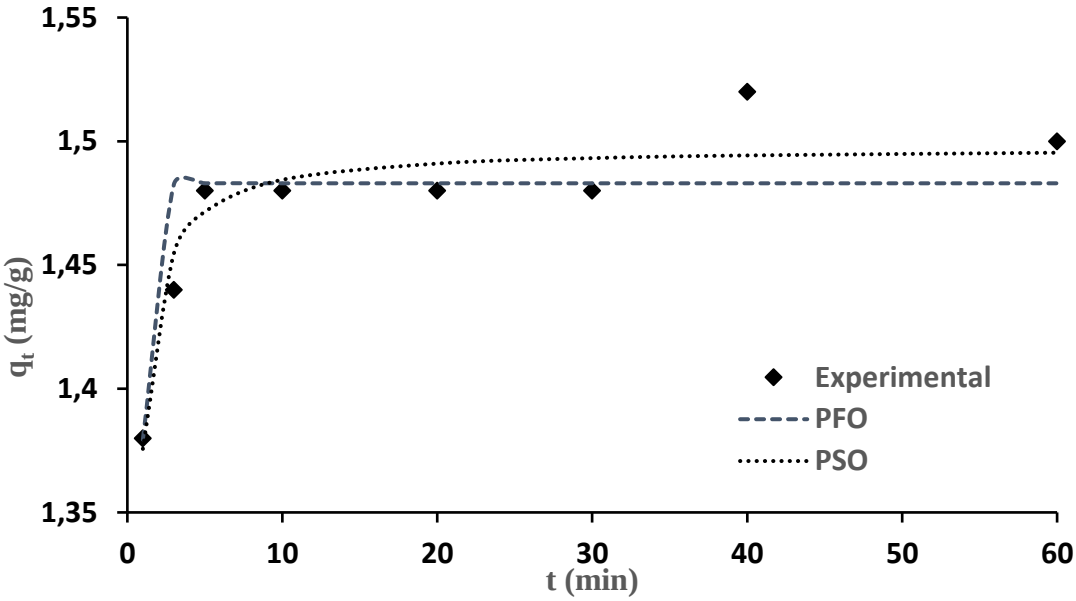

Figure 5.6: Pseudo-first-order (PFO) and Pseudo-second-order (PSO) kinetic model plot of fluoride uptake by the HTAC (initial fluoride concentration = 10 mg/L, adsorbent dosage = 0.8 g/40 mL, temperature = 298 K and shaking speed = 250 rpm).

Table 5.3: The kinetic parameters for pseudo-first-order, pseudo-second-order and intra-particle diffusion models.

Models	Values
Pseudo-first-order (PFO)	
q_{cal} (mg/g)	2.66
K_{1ad} (min^{-1})	1.48
R^2	0.73
RMSE	0.02236
X^2	0.00029
Pseudo-second-order (PSO)	
q_{cal} (mg/g)	1.49
K_{2ads} (g min^{-1} mg)	7.53
R^2	0.89
RMSE	0.01363
X^2	0.00011
Intra-particle diffusion	
C_1 (mg/g)	1.3
k_1	0.187
C_p (mg/g)	1.5
k_p	0.016
R_1^2	0.99
R_2^2	0.61

© University of Venda

Adsorption kinetics data in Table 5.3 shows the higher co-efficient of determination (R^2) value for pseudo-second-order (PSO) (R^2 = 0.89) compared to pseudo-first-order (PFO) (R^2 = 0.73) and low values of residual root mean square error (RMSE) = 0.013 and X^2 = 0.0001 in pseudo-second-order model, suggesting that adsorption of fluoride onto the HTAC interface occurred via surface interaction between the active binding sites across the HTAC and the fluoride ions depended on chemisorption. Specifically, the fluoride ions interacts with the functional groups on the surface of HTAC leading to the formation of new chemical bonds such as Al-O-F and Si-F as a results of ion exchange between OH^- group in the metal hydroxides and fluoride ions (Yoon *et al.,* 2017: Ngulube *et al.,* 2017: Denga *et al.,* 2018: Ayinde *et al.,* 2020). Furthermore, lower RMSE and X^2 values in pseudo-second-order model confirm the reaction kinetics to be more feasible. Similar trends were observed and postulated in similar studies (Ngulube *et al.,* 2017; Denga *et al.,* 2018: Ayinde *et al.,* 2020). Chemisorption is defined as an adsorption process which involves a chemical reaction between the surface of the materials and the adsorbate**.** New chemical bonds are generated at the adsorbent surface, hence the adsorbed substance (fluoride) is held by chemical bonds on the materials' surface.

The adsorption process involves steps such as the transport of adsorbate from bulk solution to the external layer of the adsorbent, diffusion of the adsorbate onto the pores of the adsorbent and subsequently interaction of the adsorbate molecules with the atoms within the pores of the adsorbent leading to chemisorption. In order to extrapolate these steps during fluoride removal by HTAC, the commonly used Weber-Morris intra-particle diffusion model (Equation 5.9) was used applied (Weber & Morris, 1963; 1964).

$$q_t = k_i t^{0.5} + C \qquad (5.9)$$

Where k_i (mg/g $min^{0.5}$) is the intra-particle diffusion rate constant and is derived from the slope of $t^{0.5}$ versus q_t while q_t (mg/g) is amount adsorbed per unit mass at a time, t ($min^{0.5}$) and C (mg/g) that gives an idea about the thickness of the boundary layer. Figure 5.7 represents represents the plot for intra-particle diffusion model. The plot of q_t versus $t^{0.5}$ showed two clear phases indicating that two adsorption mechanisms were involved in the sorption process namely, boundary layer adsorption (phase 1) wherein fluoride ions are attracted to the outer layer of the adsorbent via electrostatic attraction and intra-particle diffusion (phase 2). The initial plot is the rate-determining step and signifies the attraction of fluoride onto the adsorbents' surface and subsequent adsorbate molecules' diffusion from exterior of the adsorbent into the adsorbents' pores or along the pore-

© University of Venda

wall surfaces indicating particle diffusion (phase 1) (Figure 5.7) while the second plot is the rapid adsorption attachment of the adsorbate molecules with the atoms within the pores (phase 2) (Figure 5.7) where in fluoride ions are diffusing into the mesopores of adsorbent and interact with the atoms within the pores leading to chemisorption.

The rate constant i.e., the slope (Table 5.3) in phase 1 is higher than the value in phase 2 indicating that the boundary layer occurred faster than the diffusion step (Karthikeyan *et al.*, 2005: Gupta *et al.*, 2011; Ghasemi *et al.*, 2014; Tran *et al.*, 2017).

The intercept, *C* in the plots correspond to the boundary layer thickness. The value of *C*, determined from the intercept in the plots correspond to the boundary layer thickness is higher in phase 2 than phase 1 suggesting the stronger effect of the boundary layer limiting the diffusion of fluoride ion onto the pores of the adsorbent. The intercept values for the two plots are given in Table 5.3 and Figure 5.7. The higher the intercept the stronger the effect of boundary layer.

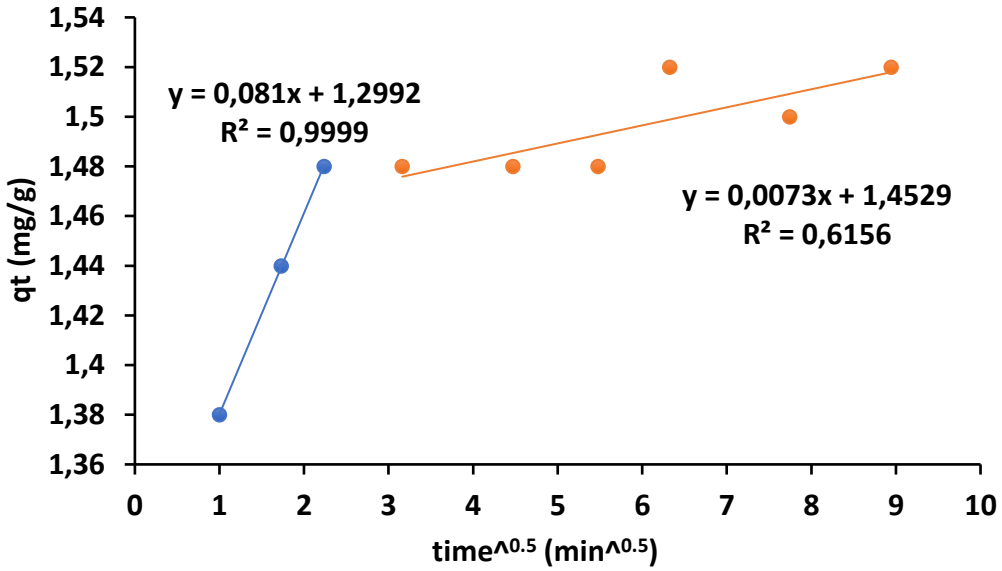

Figure 5.7: Intra-particle diffusion plot of fluoride sorption on the HTAC (dosage: 0.8 g/40 mL, initial fluoride concentration: 10 mg/L, temperature: 298 K and shaking speed: 250 rpm).

5.3.2.2 Effect of adsorbent dosage

Figure 5.8 depicts variation of percent fluoride removal and adsorption capacity with adsorbent dosage. The fluoride sorption increased steadily (from 41 to 52%) at adsorbent dosage of 0.1 to 0.8 g and thereafter stabilised. (Figure 5.8). As adsorbent dosage increased, more sites and surfaces became readily available for fluoride sorption, hence, there was increase in percent fluoride removal. Further increase in adsorbent dosage from 0.8 - 1.0 g resulted in equilibration as

© University of Venda

it became difficult for the adsorbate species to access the adsorption sites due to reduction in available sites as a result of fluoride occupation. Further additional increase in adsorbent dosage did not lead to considerable increase in adsorption capacity due to overlapping of the active sites at higher adsorbent dosage, thus reducing the net surface area (Karthikeyan *et al.*, 2005). Therefore, optimum dosage of 0.8 g/40 mL was adopted and used for subsequent experiments.

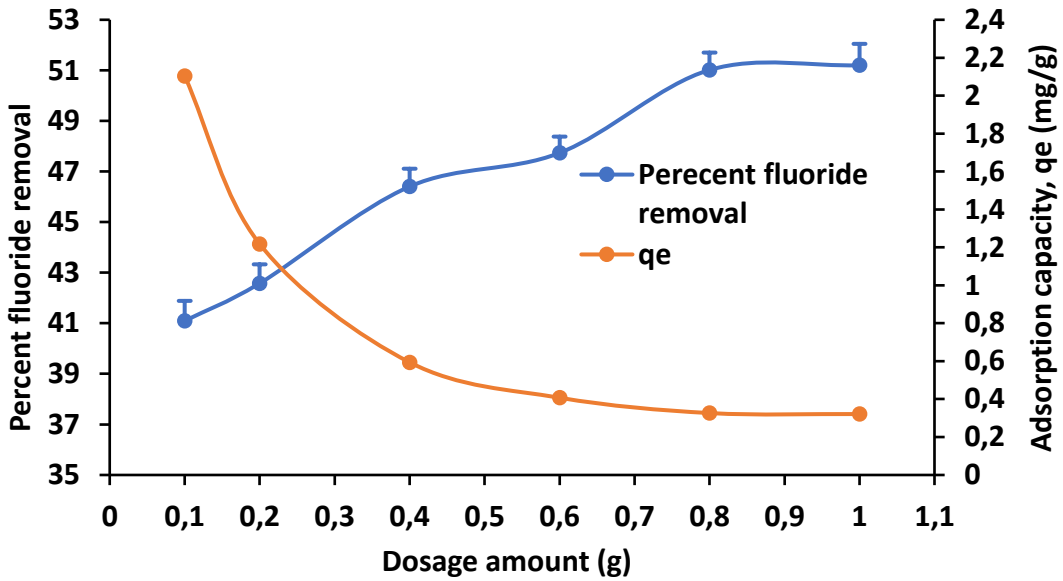

Figure 5.8: Variation of percent fluoride removal and adsorption capacity with adsorbent dosage (initial fluoride concentration = 10 mg/L, volume of solution = 40 mL, optimum contact time = 5 min, Initial pH = 6.0, temperature = 298 K and shaking speed = 250 rpm).

5.3.2.3 Effect of pH

Figure 5.9 shows the pH effect on fluoride removal. The initial pH effect on fluoride removal was assessed by varying the initial pH of the mixtures from 2 to 12, utilising 0.1 M HCl and 0.1 M NaOH. The percent fluoride removal was observed to increase as the pH increased from 2 to 6 and thereafter sharply decreased to stabilise at pH 8 - 12. Fluoride removal of about 58% was observed at optimum pH of ≈ 6.85 and decreased to about 40% at pH 8 - 12 (Figure 5.9). The pH of the solution ultimately changed the surface charges of the adsorbent and consequently this affected the behaviour of fluoride adsorption at different pH levels. To establish the behaviour of fluoride at different pH levels, the pH at point-of-zero charge (pH_{pzc}) (i.e., point at which the clay has zero net surface charges) of the adsorbent was evaluated using titration method and the results are presented in Figure 5.10. The results showed that the pH_{pzc} of HTAC was 8.1. This suggests

© University of Venda

that at pH above 8.1, the surface of the clay is negatively charged and OH^- charges dominate the surface of the adsorbent while at pH below 8.1, the surface is positively charged and the H^+ dominates the surface of the material. Therefore, the reduction in fluoride removal at pH 8.1 and above could be attributed to electrostatic repulsion between the negatively charged surface and fluoride ions in the solution. At strong acid pH, H^+ dominates the solution and hence reacts with fluoride ions in the solution, leading to formation of weak hydrofluoric acid. During fluoride sorption, the final pH was observed to be generally higher than the corresponding initial pH. The increased pH at pH below pH_{pzc} was due to H^+ released from the surface of the adsorbent due to formation of weak HF while the increased pH above pH_{pzc} was due to OH^- released as a result of ion exchange at pH above pH_{pzc}.

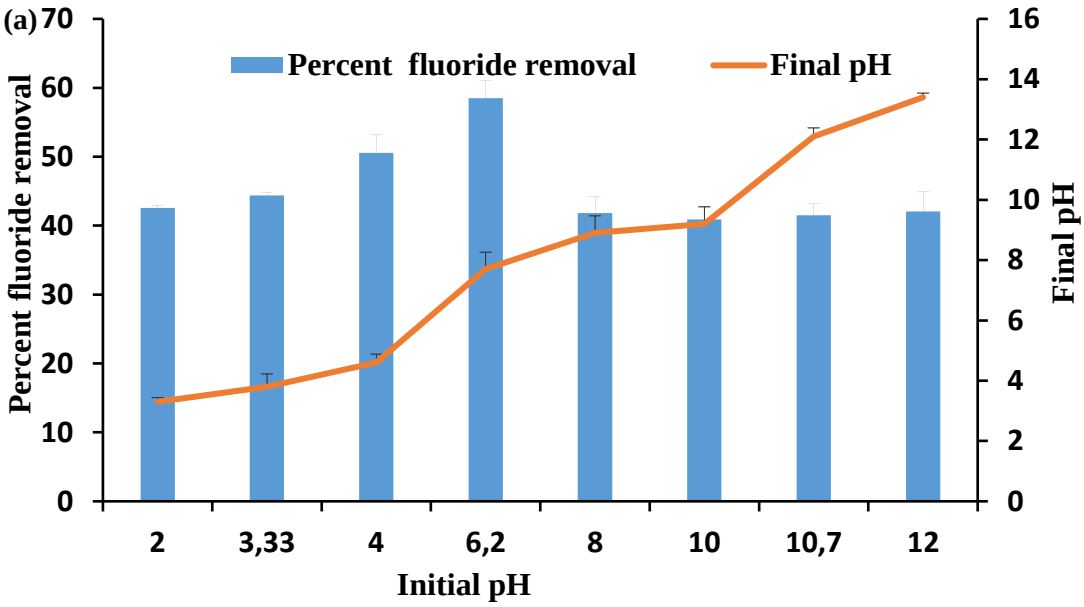

Figure 5.9: Percent fluoride removal variation and equilibrium pH with initial pH (initial fluoride concentration = 10 mg/L, volume of solution = 40 mL, optimum adsorbent dosage = 0.8 g, optimum contact time = 5 min, temperature = 298 K and shaking speed = 250 rpm. The pH was varied between 2 and 12).

© University of Venda

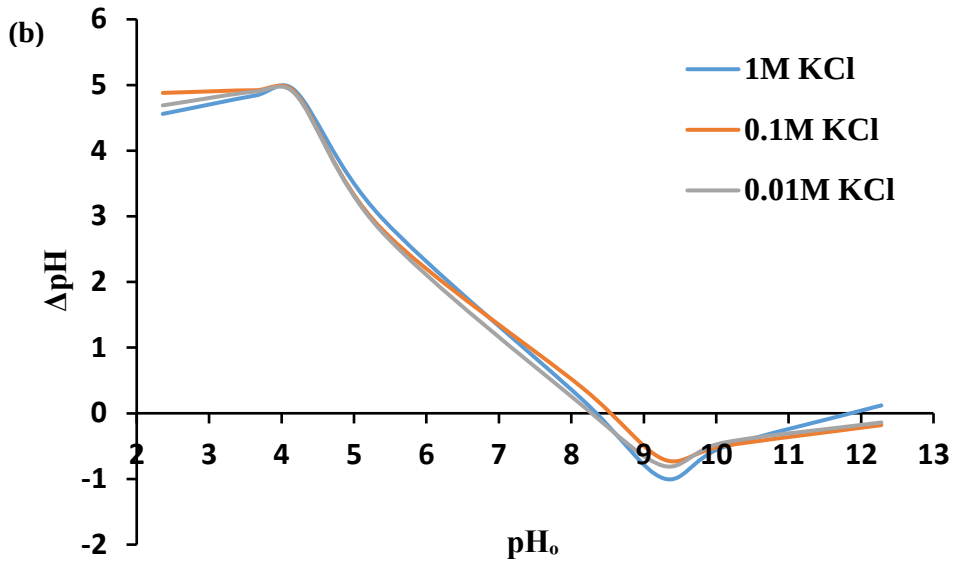

Figure 5.10: pH at point-of-zero charge (pH_{pzc}) of HTAC (adsorbent dosage = 0.8 g/40 mL, contact time = 24 h, agitation speed = 200 rpm and temperature = 298 K).

To summarise the fluoride removal mechanism, at low pH, the surface of HTAC has positive charges (Equation 5.10), the fluoride sorption decreases as pH decreases due to positively charged surfaces and since the solution has more H^+ ions at lower pH, the formation of weak HF acid becomes inevitable at this strong acid pH (Equation 5.11) while fluoride may be removed via electrostatic attraction (Equation 5.12). This is due to strong electrostatic attraction of the fluoride to the adsorbent's surface followed by a strong complexation of the inner sphere at equilibrium (Ghasemi *et al.*, 2014), while at higher pH, fluoride uptake slows down as the surface has more negatively charged ions owing to increasing hydroxyl ions on the HTAC surface and hence, a repulsion between the surface and fluoride ions (Equation 5.13). At pH equals to pH_{pzc} (point-of-zero charge), the surface of the HTAC clay has no charge (neutral) and therefore ion exchange could take place between OH^- on the neutral HTAC clay surface and the F^- in solution as illustrated in equation 5.14.

$$\equiv \mathrm{HTAC(OH)_2} + \mathrm{H^+} \leftrightarrow \equiv \mathrm{HTACOH^+} + \mathrm{H_2O} \quad (5.10)$$

$$\mathrm{H^+} + \mathrm{F^-} \leftrightarrow \mathrm{HF} \quad (5.11)$$

$$\equiv \mathrm{HTACOH^+} + \mathrm{F^-} \leftrightarrow \equiv \mathrm{HTACOHF} \quad (5.12)$$

$$\equiv \mathrm{HTAC(OH)_3^-} + \mathrm{F^-} \leftrightarrow \equiv \mathrm{HTAC(OH)_2F^-} + \mathrm{OH^-} \quad (5.13)$$

$$\equiv \mathrm{HTAC(OH)_2} + \mathrm{F^-} \leftrightarrow \equiv \mathrm{HTACOHF} + \mathrm{OH^-} \quad (5.14)$$

© University of Venda

5.3.2.4 Effect of fluoride concentrations

Figure 5.11 depicts the initial fluoride concentration effect on fluoride removal. There was a sharp increase in percent fluoride removal from about 32 to 52% as the initial fluoride concentration increased from 0.1 to 6.0 mg/L and thereafter decreased steadily as initial fluoride concentration increased further from 6 to 100 mg/L (Figure 5.11). The rapid increase in fluoride removal at low initial fluoride concentrations was attributable to availability of more binding sites on HTAC surfaces. The rapid increase peaked at 52% fluoride removal at 6.0 mg/L. Further increase in fluoride concentration led to a steady reduction in fluoride sorption due to increased fluoride ions at higher fluoride concentrations, competing for a fixed number of (reduced) binding sites on the treated clay surfaces. Hence, an initial optimum fluoride concentration of 6.0 mg/L was used for subsequent experiments. The adsorption capacity increased steadily with increasing fluoride concentration from 0.1 to 100 mg/L. However, stabilisation was observed between 40 - 50 mg/L fluoride concentrations.

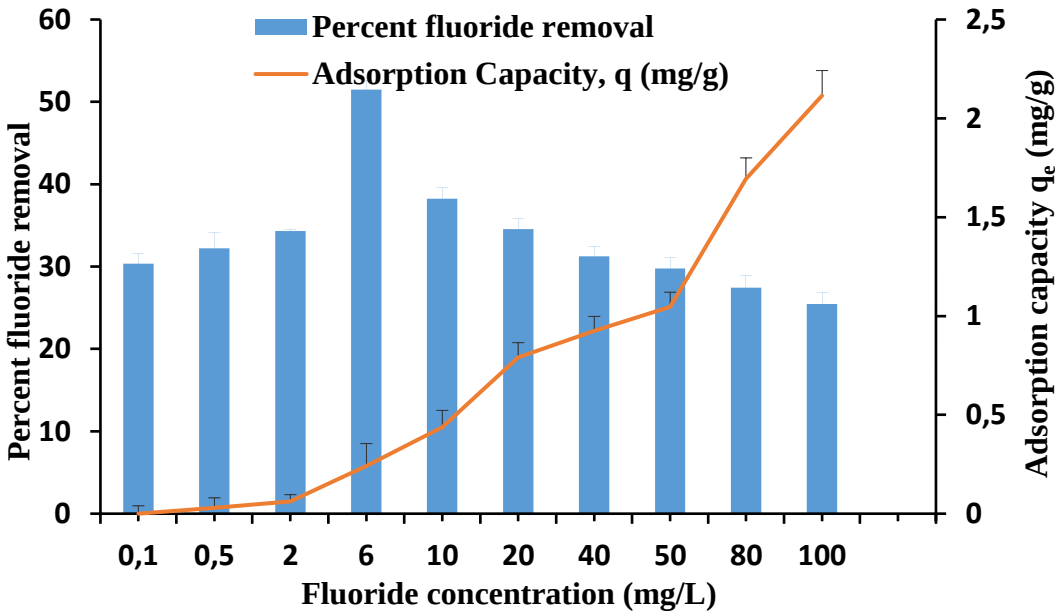

Figure 5.11: Variation of percent fluoride removal and adsorption capacity with initial fluoride concentration (adsorbent dosage = 0.8 g/40 mL, optimum contact time = 5 min, pH = 6.8, temperature = 298 K and shaking speed = 250 rpm. Variation of initial fluoride concentrations was between 0.1 mg/L and 100 mg/L).

Langmuir and Freundlich adsorption isotherm models were used to describe the fluoride sorption behavior onto HTAC adsorbent under the evaluated experimental conditions. Langmuir isotherm models the adsorption surfaces to be monolayer and assumes sorption to take place

© University of Venda

structurally on adsorbents' homogenous surface. Sorption isotherm parameters were obtained by using 0.8 g of HTAC adsorbent per 40 mL of fluoride solution (1 - 80 mg/L) for 5 min at 298 K.

Langmuir model non-linearised form, which applies to homogeneous adsorption medium describing monolayer systems in a sorbent-sorbate interface is given as (Langmuir, 1916: Karthikeyan *et al.*, 2005: Lee & Tiwari, 2015; Tran *et al.*, 2017: Sahu & Singh, 2019: Al-Ghouti & Daana, 2020):

$$q_e = \frac{Q_m K_L C_e}{1 + K_L C_e} \quad (5.15)$$

where C_e is fluoride equilibrium concentration in the solution, q_e (mg/g) is the adsorption capacity or the amount of fluoride ion adsorbed per unit mass of HTAC adsorbent at equilibrium, Q_{max} (mg/g) is maximum adsorbents' monolayer capacity and K_L (L/mg) is Langmiur adsorption equilibrium constant related to the affinity of binding sites.

Furthermore, the fundamental characteristics of Langmuir isotherm can be determined using a dimensionless constant separation factor for the fluoride equilibrium parameter, R_L (Equation 5.16) (Weber & Chakravorti, 1974: Sahu & Singh, 2019: Al-Ghouti & Daana, 2020). given as:

$$R_L = \frac{1}{1 + K_L C_i} \quad (5.16)$$

where C_i (mg/L) is the initial fluoride concentration and K_L is the Langmuir equilibrium constant The R_L value is vital in determining if an sorption process is favourable ($0 < R_L < 1$), unfavourable ($R_L > 1$), linear ($R_L = 1$) or irreversible ($R_L = 0$).

The non-linear Freundlich adsorption isotherm is used to describe multilayer sorption on heterogeneous surfaces. Freundlich non-linearised equation is expressed as in Equation 5.17 (Freundlich, 1906: Foo & Hameed, 2010: Sahu & Singh, 2019: Al-Ghouti & Daana, 2020):

$$q_e = K_F C_e^{1/n} \quad (5.17)$$

where C_e (mg/L) is equilibrium concentration of the fluoride, q_e (mg/g) is adsorption equilibrium capacity of the adsorbent, k_F (mg/g) is empirical Freundlich constant related to capacity of minimum adsorption and 1/n is the dimensionless parameter for Freundlich adsorption isotherm related to the intensity of adsorption which is adsorption driving forces' magnitude or the heterogeneity surface. Adsorption is favourable when $1/n < 1$, unfavourable when $1/n > 1$, linear

© University of Venda

when 1/n = 1 and irreversible when 1/n = 0 (Foo & Hameed, 2010: Al-Ghouti & Daana, 2020). The values of k_F and 1/n are derived from slope and intercept of log q_e versus log C_e.

Figure 5.12 depicts the non-linear plots for Langmuir and Freundlich adsorption isotherms, respectively while Table 5.4 shows the respective obtained model parameters for fluoride sorption by the hydrothermally-treated aluminosilicate clay (HTAC) adsorbent at 298 K.

The generated data described by the adsorption isotherms in Figure 5.12 revealed increased adsorption capacities with increasing fluoride concentration, characterised by saturation at high concentration. Based on the high co-efficient of determination (R^2) values and low chi-square (X^2) values in Table 5.4, the adsorption data fitted better to Freundlich adsorption isotherm model (R^2 = 0.997 and X^2 = 0.0095) than Langmuir adsorption isotherm model (R^2 = 0.995 and X^2 = 0.0194) at 298 K (Table 5.4). This suggests that adsorption of fluoride onto HTAC occurred on a heterogeneous surface.

Furthermore, the feasibility of fluoride uptake by Langmuir and Freundlich models were confirmed by the calculated values of both the dimensionless constant, (R_L) and adsorption intensity (n). Both values range between 0 and 1, thereby affirming the favourable conditions for fluoride sorption by the synthesised HTAC.

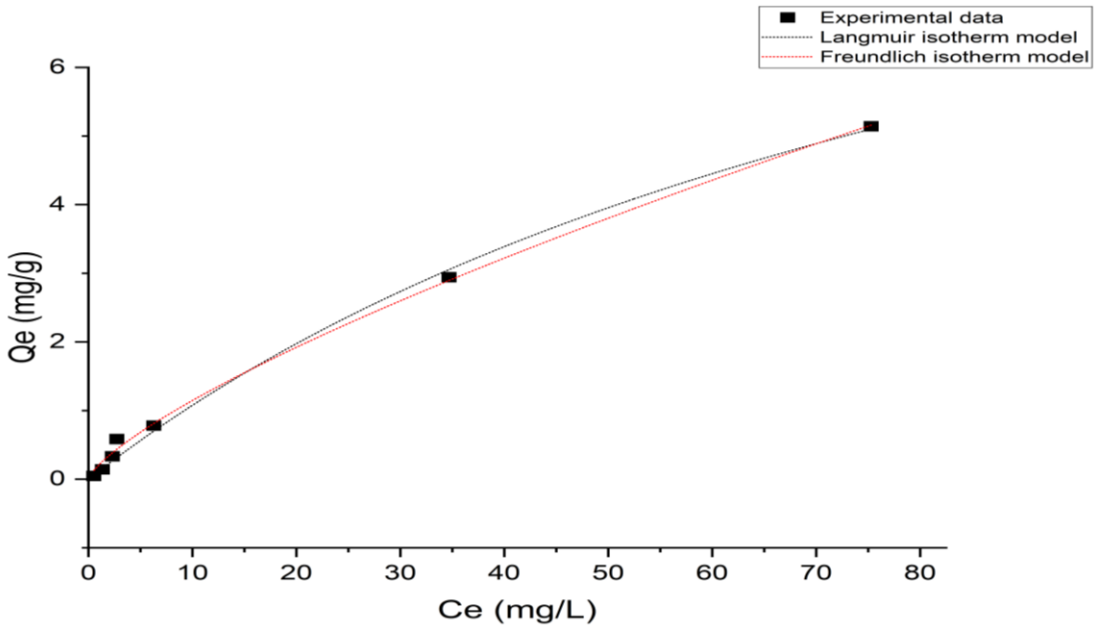

Figure 5.12: Langmuir and Freundlich adsorption isotherm plots of fluoride onto HTAC adsorbent. (adsorbent dosage = 0.8 g/40 mL, contact time = 5 min and shaking speed = 200 rpm. Fluoride concentration was varied from 1 to 80 mg/L).

© University of Venda

Table 5.4: Langmuir and Freundlich isotherm parameters for fluoride sorption onto HTAC

Model	Langmuir	Freundlich
Equation	$(Q_m*K*C_e)(1+(K*C_e)$	$(K_f*(C_e*(1/n)$
Plot	Q_e	Q_e
Q_m	11.9464 ± 1.9851	-
K	0.0099 ± 0.00261	0.2060 ± 0.0239
N	-	1.3418 ± 0.0518
Reduced chi-square (RCS) (X^2)	0.0194	0.0095
COD (R-Square) (R^2)	0.9955	0.9978
Adjusted R-Square (R^2)	0.9947	0.9973

The comparison of the maximum adsorption capacity for HTAC with other adsorbents reported in the literature is reported in Table 5.5 together with the experimental conditions. The developed HTAC adsorbent showed higher adsorption capacity at natural pH of water than other adsorbents. Further studies and surface modifications would be required to improve the efficiency of HTAC.

© University of Venda

University of Venda
Creating Future Leaders

Table 5.5: Comparison of the HTAC adsorption capacities with reported adsorbents.

Adsorbent	Concentrations and pH	Adsorption Capacity (mg/g)	References
Granular acid treated bentonite	2.8 mg/L; pH 4.9	0.09	Ma *et al.*, 2011
Zeolite	3.5 mg/L; pH 6.5	0.47	Gómez-Hortigüela *et al.*, 2013
Vermiculite functionalised cationic surfactant	8.0 mg/L; pH 6.5	2.37	Ologundudu *et al.*, 2016
Smectite-rich clay soil adsorbent	3.0 mg/L; pH 2	0.21	Mudzielwana *et al.*, 2016
Mixed (black and brown) clay soils	9.0 mg/L; pH 2	0.08	Ngulube *et al.*, 2017
Clay composite (clay, grog, bone char & sawdust)	9.12mg/L; pH 6.7	0.08	Gidi *et al.*, 2019
Mechanochemically-activated aluminosilicate clay	3.2 mg/L; pH 5	1.87	Obijole *et al.*, 2019
Hydrothermally-treated aluminosilicate rich clay	6.0 mg/L; pH 6.8	1.75	This study

© University of Venda

5.3.2.5 Effect of co-existing ions

Groundwater is known to generally contain other anions in addition to F^- that may interfere with the removal of fluoride. Figure 5.13 presents the effect of some co-existing anions on fluoride uptake by the HTAC. Fluoride sorption was very much influenced by the Cl^- ions, as there was an appreciable reduction in percent fluoride removal from the blank, hence, suggesting Cl^- ions were competing with fluoride removal during defluoridation. This was probably due to relatively smaller and similar size with F^- ions while SO_4^{2-}, PO_4^{2-}, NO_3^- and CO_3^{2-} ions gave similar decrease in per cent fluoride removal respectively. The attraction strength is dependent on charge magnitude and hydrated ion radius (size) hence, SO_4^{2-}, PO_4^{2-} and CO_3^{2-} have high charge magnitude which was probably responsible for the observed similar trends in their negative impact on percent fluoride removal. CO_3^{2-} and NO_3^- have close ionic radii, which are 178 pm and 179 pm respectively (Jenkins & Thakur, 1979). This might be why the two ions had nearly the same effect on fluoride removal (Figure 5.13). The increasing order of the negative effect of co-existing ions on fluoride uptake from water was $CO_3^{2-} < NO_3^- < PO_4^{2-} < SO_4^{2-} < Cl^-$.

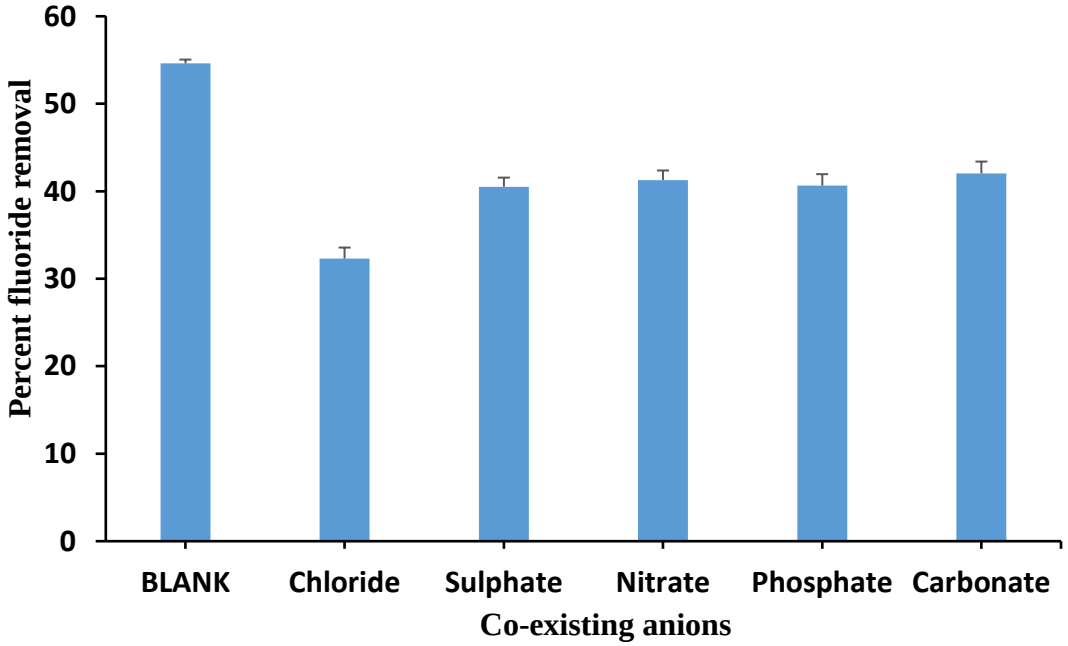

Figure 5.13: The effect of fluoride uptake in the presence of other co-existing anions (Contact time = 30 min; pH = 6.5; initial fluoride concentration = 10 mg/L; initial anion concentration = 10 mg/L; adsorbent dosage = 0.8 g; solution volume = 40 mL; shaking speed = 250 rpm; temperature = 298 K).

© University of Venda

5.3.3 Regeneration studies and life cycle of the HTAC.

The regeneration and recyclability potential of the HTAC were carried out in six successive adsorption and desorption cycles at an initial fluoride concentration of 6.0 mg/L, pH 5.85 at 5 min contact time using 0.1 M NaOH and 0.1M KCl respectively. The results are presented in Figure 5.14. The percent fluoride uptake using 0.1M NaOH as regenerant decreased from 56% at first cycle until it reached 30% at the fifth cycle. This could be due to inadequate regeneration or loss of metal oxides during regeneration. The trend observed in this study followed the same pattern reported by (Mudzielwana *et al.*, 2016; Zhang *et al.*, 2011; Jia *et al.*, 2015; Mudzielwana *et al.*, 2017). However, the percent fluoride removal using 0.1 M KCl as regenerant slightly decreased from 60% at the first cycle until about 48% at the sixth cycle, showing some promising regeneration abilities. Hence, 0.1 M KCl is a better regenerant for the developed HTAC adsorbent and therefore recommended for future use.

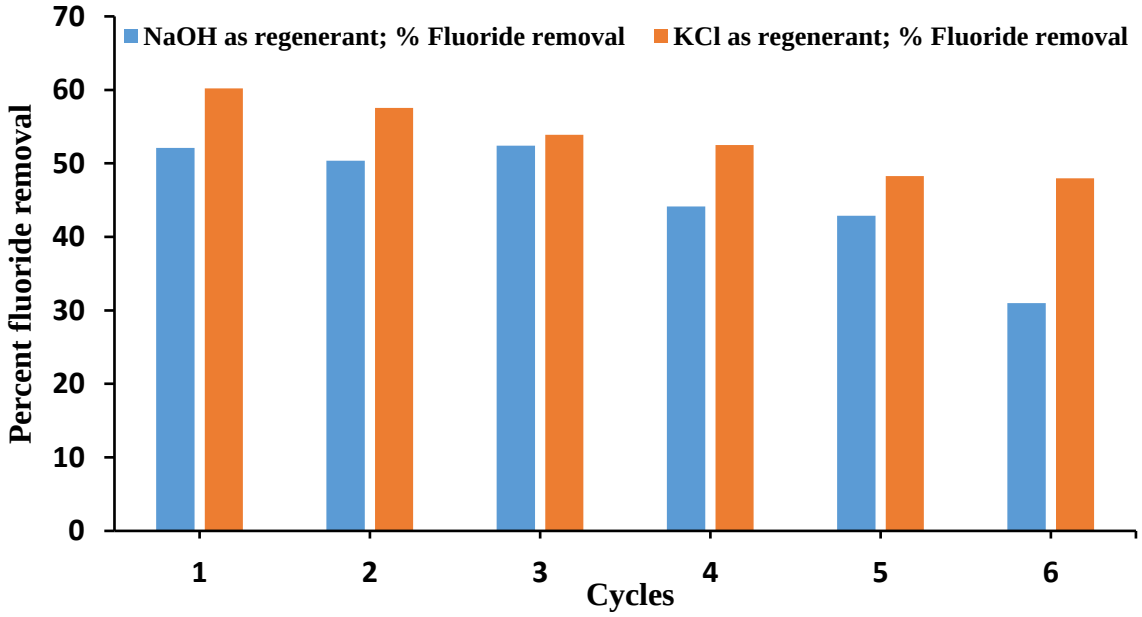

Figure 5.14: Percent fluoride removal by HTAC in successive cycles (using 0.1 M NaOH and 0.1 M KCl at ≈ 6.0 mg/L fluoride, contact time = 5 min, pH = 5.85 and shaking speed = 250 rpm).

5.3.4 Defluoridation tests of field (Siloam) groundwater

To assess the fluoride removal efficiency of HTAC in the field water samples (physicochemical composition presented in Table 5.6, water samples collected from Siloam community borehole were treated at their natural pH and at optimum pH of 6.5 using adsorbent dosage of 0.8 g/40 mL. Mixtures were agitated for 5 min optimum contact time at 250 rpm on a

© University of Venda

mechanical shaker. The results are presented in Table 5.6 along with the WHO guideline values for drinking water quality. The fluoride levels in raw Siloam water after treatments at pH 6.5 and 8.5 were found to be lower due to fluoride uptake onto the HTAC surface. A decrease in F^- concentration from 6.93 to 2.89 mg/L and 3.48 mg/L at p H 6.5 and 8.5 respectively was observed. This was attributed to the presence of more OH^- at higher pH which interfered with fluoride uptake during defluoridation. Siloam water showed a lower percent fluoride removal (49%) compared to 51% in simulated water, owing to competition of other ions with fluoride uptake during defluoridation. There was a reduction in Cl^-, CO_3^{2-} and SO_4^{2-} concentrations after treatment (Table 5.6). The lower efficiency in field water may therefore be attributed to the competition between fluoride and the co-existing ions for adsorption sites. The concentrations of Na^+ and Mg^{2+} cations were slightly higher after treatment due to exchanges of cationic species into the media. However, they remained within WHO recommended threshold (WHO, 2017). In conclusion, the developed HTAC materials are safe and have potential for application in fluoride remediation in drinking water. However, it should be applied to water with initial concentration below 6 mg/L F^- in order to attain fluoride concentration within the WHO permissible limit. Furthermore, the HTAC's defluoridation efficiency and antibacterial potency could be further enhanced by increasing its pore network, surface area and loading with bioactive anti-bacterial metal oxides respectively.

Table 5.6: Physicochemical parameters of raw and treated Siloam fluoride rich groundwater.

Parameters	Field water	Treated at optimum initial pH	Treated at initial natural pH	WHO guidelines
pH	8.4	6.5	8.4	6.0-8.5
F^-	6.93	2.89	3.48	1-1.5
Br^-	0.41	0.28	0.34	200
Cl^-	5.65	5.2	5.5	250
PO_4^{2-}	4.97	2.30	2.28	20-50
SO_4^{2-}	13.30	13.34	13.34	200-400
Na^+	68.5	90.3	87.1	200-250
K^+	3.1	0.5	0.7	200-250
Ca^{2+}	1.4	0.2	< LOD	75
Mg^{2+}	< LOD	0.3	0.1	50

Footnote: < LOD = below limit of detection. All concentrations are in mg/L.

© University of Venda

5.3.5 Antibacterial studies

Antibacterial potency of the hydrothermally-treated aluminosilicate clay (HTAC) and three untreated MAC samples were evaluated with the well assay diffusion method. Figure 5.15 shows the photographs of the zone of inhibition of the four samples investigated. The treated sample (HTAC) and three untreated samples (MACs) were tested for their antibacterial activities (Figure 5.18) by using gram negative *E. coli* strains. However, only the treated clay (HTAC) have a zone of inhibition of about 15 mm, an indication of promising antibacterial potency against the *E. coli* (ATCC 35218) strains (Figure 5.15). In the previous study, all the untreated clay (MAC) did not show antibacterial potency against the bacterial strains used (Obijole *et al.*, 2019). This results further confirmed the outcome of the previous study. The potency of the developed HTAC may be due to the release of intra-cellular reactive oxygen species on exposure of bacterial cells to the surface of synthesised hydrothermally-treated aluminosilicate clays (Horie *et al.*, 2012), among other factors.

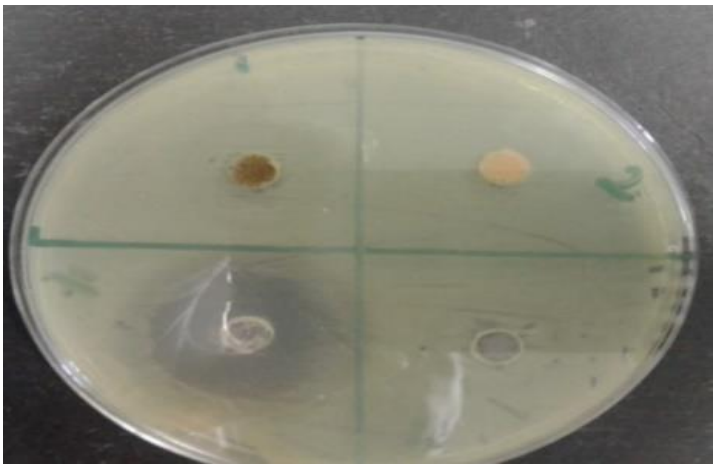

Figure 5.15: Pictorial view of the hydrothermally-treated aluminosilicate clay (HTAC) and three untreated MAC samples showing the zone of inhibition on a single plate.

5.4 Conclusions and recommendations

In this study, mechanochemically-activated clay was hydrothermally treated to enhance its performance towards defluoridation and pathogen removal from groundwater. The maximum sorption capacity of the developed hydrothermally-treated aluminosilicate clay in simulated fluoride water at pH 6.8 was 1.75 mg/g while the maximum percent fluoride removal was 53% (initial fluoride concentration: 6.0 mg/L, adsorbent dosage: 0.8 g/40 mL, contact time: 5 min, shaking speed: 250 rpm and temperature: 298 K). The kinetic studies showed fluoride sorption

© University of Venda

fitted well to pseudo-second-order thereby confirming the sorption process occurred via chemisorption. Adsorption isotherm data were better described by Freundlich isotherm model, which confirmed a multi-site heterogeneous sorption. All co-existing anions inhibited fluoride uptake, however, chloride ions exerted the greatest inhibition of the evaluated anions. The developed HTAC revealed a promising regeneration and recyclability potential when 0.1 M KCl was used as regenerant compared to 0.1 M NaOH.

The synthesised HTAC's surface is characterised by Si-OH and Al-OH groups. The mechanism of fluoride removal from solution was governed by pH of solution. At pH ≥ pH_{pzc}, fluoride removal occurred via exchange of the hydroxyl groups on the surface of the treated clay with fluoride ions in solution leading to formation of new bonds such as Al-F and Si-F. Also, the sorbent's surface was positively charged at low pH (pH < pH_{pzc}), hence, fluoride ions were adsorbed electrostatically unto the synthesised material's surface owing to stronger attractive forces between the fluoride and material's surface.

The fluoride adsorption capacity of the synthesised HTAC (0.8 g/40 mL) was evaluated for fluoride removal using Siloam groundwater at initial pH 6.5, initial fluoride concentration of 6.93 mg/L at 298 K. The percent fluoride removal was 51%. While keeping the adsorption conditions constant, the same dosage of synthesised HTAC yielded 49% fluoride removal from Siloam water at pH 8.5. Antibacterial studies showed that the developed HTAC adsorbent has potent antibacterial activities against the gram-negative *E. coli* bacterial strains. The slight reduction of percent fluoride removal in Siloam groundwater compared to simulated water was due to the presence of co-existing ions which competed for fluoride uptake in Siloam water. The HTAC adsorbent's defluoridation efficiency and antibacterial potency could be further enhanced by increasing its pore network, surface area and loading with bioactive anti-bacterial metal oxides respectively.

© University of Venda

REFERENCES

Al-Ghouti, M. A & Da'ana, D. A. (2020). Guidelines for the use and interpretation of adsorption isotherm models: A review. *Journal of Hazardous Materials*, 122383.

Arami, M., Limaee, N. Y., Mahmoodi, N. M., & Tabrizi, N. S. (2005). Removal of dyes from colored textile wastewater by orange peel adsorbent: equilibrium and kinetic studies. *Journal of Colloid and Interface Science*, *288*, 2, 371-376.

Ayinde, W. B., Gitari, W. M., Munkombwe, M., Samie, A., & Smith, J. A. (2020). Green synthesis of AgMgOnHaP nanoparticles supported on chitosan matrix: defluoridation and antibacterial effects in groundwater. *Journal of Environmental Chemical Engineering*, *8*(5), 104026.

Bitton, G. (2014). Microbiology of drinking water production and distribution: Wiley Online Library.

Chandrajith, R., Diyabalanage, S & Dissanayake, C. B. (2020). Geogenic fluoride and arsenic in groundwater of Sri Lanka and its implications to community health. *Groundwater for Sustainable Development*, 100359.

Casci, J. L. (2005). Zeolite molecular sieve: Preparation and scale up. *Microporous and Mesoporous Materials,* 2005, 82, 217–226.

Chen, N., Zhang, Z., Feng, C., Li, M., Zhu, D & Sugiura, N. (2011). Studies on fluoride adsorption of iron-impregnated granular ceramics from aqueous solution. *Materials Chemistry and Physics*, *125* (1-2), 293-298.

Chen, C. L., Park, S. W., Su, J. F., Yu, Y. H., Heo, J. E., Kim, K. D., & Huang, C. P. (2019). The adsorption characteristics of fluoride on commercial activated carbon treated with quaternary ammonium salts (Quats). *Science of The Total Environment*, *693*, 133605.

Dacosta, F. A., Muzerengi, C., Mhlongo, S. E., & Mukwevho, G. F. (2013). Characterisation of clays for making ceramic pots and water filters at Mukondeni Village, Limpopo Province, South Africa. *Journal of Engineering and Applied Science*, *8*, 11, 927-932.

Denga, M. E. (2017). *Fabrication of metal-oxide modified porous ceramic granules from aluminosilicate clay soils for defluoridation of groundwater* (Doctoral dissertation).

Denga, M. E., Gitari, W. M., Izuagie, A. A., & Akinyemi, S. A. (2018). Defluoridation of groundwater using mechanochemically-activated clay soil. *Water Practice and Technology*, *13*, 3, 599-611.

© University of Venda

Dhillon, A., Nair, M., Bhargava, S. K., & Kumar, D. (2015). Excellent fluoride decontamination and antibacterial efficacy of Fe–Ca–Zr hybrid metal oxide nanomaterial. *Journal of Colloid and Interface Science, 457*, 289-297.

Eggleston, C & Jordan, G. (1998). A new approach to pH of point of zero charge measurement: Crystal-face specificity by scanning force microscopy (SFM). *Geochimica et Cosmochimica Acta*, *62* 11, 1919-1923.

Fard, A. K., Mckay, G., Manawi, Y., Malaibari, Z., & Hussien, M. A. (2016). Outstanding adsorption performance of high aspect ratio and super-hydrophobic carbon nanotubes for oil removal. *Chemosphere, 164*, 142-155.

Foo, K. Y., & Hameed, B. H. (2010). Insights into the modeling of adsorption isotherm systems. *Chemical Engineering Journal, 156*, 1, 2-10.

Freundlich, H. (1906). *Über die Adsorption in Lösungen. Habilitationsschrift durch welche... zu haltenden Probevorlesung" Kapillarchemie und Physiologie" einladet* Dr. Herbert Freundlich: W. Engelmann.

Frost, R. L & Vassallo, A. M. (1996). The dehydroxylation of the kaolinite clay minerals using infrared emission spectroscopy. *Clays and Clay Minerals*, *44*, 5, 635-651.

Ghasemi, M., Naushad, M., Ghasemi, N., & Khosravi-Fard, Y. (2014). A novel agricultural waste-based adsorbent for the removal of Pb (II) from aqueous solution: kinetics, equilibrium and thermodynamic studies. *Journal of Industrial and Engineering Chemistry*, *20*, 2, 454-461.

Ghorai, S., & Pant, K. (2004). Investigations on the column performance of fluoride adsorption by activated alumina in a fixed bed. *Chemical Engineering Journal, 98* (1-2), 165-173.

Gidi, L. D., Amare, E. Z., Murthy, H. A., & Abebe, B. (2019). Application of Novel Clay Composite Adsorbent for Fluoride Removal. *Material Science Research India, 16*, 2.

Gitari, Ngulube, T., Masindi, V., & Gumbo, J. (2013). Natural clay-based adsorbent for defluoridation of groundwater: optimisation of adsorption conditions. 36th WEDC International Conference, Nakuru, Kenya, 2013. Delivering water, sanitation and hygiene services in an uncertain environment.

Gitari, W. M., Ngulube, T., Masindi, V & Gumbo, J. R. (2015). Defluoridation of groundwater using Fe3+-modified bentonite clay: optimisation of adsorption conditions. *Desalination and Water Treatment*, *53* 6, 1578-1590.

© University of Venda

Gitari, Petrik, L. F., & Musyoka, N. M. (2016). Hydrothermal conversion of South African coal fly ash into pure phase zeolite Na-P1. *Zeolites: Useful Minerals*, 25-42.

Gómez-Hortigüela, L., Pérez-Pariente, J., García, R., Chebude, Y., & Díaz, I. (2013). Natural zeolites from Ethiopia for elimination of fluoride from drinking water. *Separation and Purification Technology*, *120*, 224-229.

Gougazeh, M., & Buhl, J. C. (2014). Synthesis and characterisation of zeolite A by hydrothermal transformation of natural Jordanian kaolin. *Journal of the Association of Arab Universities for Basic and Applied Sciences*, *15*, 35-42.

Gupta, S. S., & Bhattacharyya, K. G. (2011). Kinetics of adsorption of metal ions on inorganic materials: a review. *Advances in Colloid and Interface Science*, *162*(1-2), 39-58.

Ho, Y. S., Ng, J. C. Y and G. McKay (2000). Kinetics of pollutant sorption by biosorbents: review, *Separation and Purification Methods*, 29 189–232.

Hollman, Steenbruggen, G., & Janssen-Jurkovičová, M. (1999). A two-step process for the synthesis of zeolites from coal fly ash. *Fuel*, *78*(10), 1225-1230.

Horie, M., Fujita, K., Kato, H., Endoh, S., Nishio, K., Komaba, L. K., Hagihara, Y. (2012). Association of the physical and chemical properties and the cytotoxicity of metal oxide nanoparticles: metal ion release, adsorption ability and specific surface area. *Metallomics*, *4*, 4, 350-360.

Huang, K., Wang, A., Zhao, Z., Zhang, H., Feng, Y. E., & Huang, W. (2018). Investigation on the status and prevention of drinking-water-borne endemic fluorosis in the disease affected areas in Yunnan Province. *Chinese Journal of Endemiology*, *37*, 10, 802-80.

Huang, L., Yang, Z., He, Y., Chai, L., Yang, W., Deng, H., ... & Crittenden, J. (2020). Adsorption mechanism for removing different species of fluoride by designing of core-shell boehmite. *Journal of Hazardous Materials*, 122555.

Izuagie, A. A., Gitari, W. M. & Gumbo, J. R., (2016). Defluoridation of groundwater using diatomaceous earth: optimisation of adsorption conditions, kinetics and leached metals risk assessment. *Desalination and Water Treatment*, *57* 36 16745-16757.

Jenkins, H. D. B. & Thakur, K. P. (1979). Reappraisal of thermochemical radii for complex ions. *Journal of Chemical Education*, *56*(9), 576, DOI: 10.1021/ed056p576.

© University of Venda

Jia, Y., Zhu, B. S., Zhang, K. S., Jin, Z., Sun, B., Luo, T & Liu, J. H. (2015). Porous 2-line ferrihydrite/bayerite composites (LFBC): fluoride removal performance and mechanism. *Chemical Engineering Journal, 268*, 325-336.

Karthikeyan, G., Pius, A & Alagmuthu, G (2005). Fluoride adsorption studies of montmorillonite clay. *Indian Journal of Chemical Technology*, 12 263-272

Khairnar, M. R., Jain, V. M., Wadgave, U., Dhole, R. I., Patil, S. J., & Chopade, S. R. (2018). Effect of different reverse osmosis water filters on fluoride content of drinking water. *Journal of Indian Association of Public Health Dentistry, 16*(2), 165.

Kimambo, V., Bhattacharya, P., Mtalo, F., Mtamba, J. & Ahmad, A. (2019). Fluoride occurrence in groundwater systems at global scale and status of defluoridation–state of the art. *Groundwater for Sustainable Development*. *9* 100223.

Lagergren, S (1898). Zur Theorie der sogenannten adsorption geloster stoffe, K. Sven, K. *Handlingar Tidskr*. 24 1–39.

Loganathan, P., Vigneswaran, S., Kandasamy, J., & Naidu, R. (2013). Defluoridation of drinking water using adsorption processes. *Journal of Hazardous Materials*, *248*, 1-19.

Langmuir, I. (1916). The constitution and fundamental properties of solids and liquids. Part I. Solids. *Journal of the American Chemical Society, 38*(11), 2221-2295.

Lee, S. M., & Tiwari, D. (2015). Porous hybrid materials in the remediation of water contaminated with As (III) and As (V). *Chemical Engineering Journal, 270*, 496-507.

Luna, J., Martinez, J., Montero, C., Muñiz, C., Ortiz, J., Gonzalez, G. & Equihua, F. (2018). Defluoridation of groundwater in central Mexico by electrocoagulation. *Fluoride*, *51*(1), 34-43.

Luo, H., Law, W. W., Wu, Y., Zhu, W., & Yang, E. H. (2018). Hydrothermal synthesis of needle-like nanocrystalline zeolites from metakaolin and their applications for efficient removal of organic pollutants and heavy metals. *Microporous and Mesoporous Materials*, *272*, 8-15.

Ma, Y., Shi, F., Zheng, X., Ma, J., & Gao, C. (2011). Removal of fluoride from aqueous solution using granular acid-treated bentonite (GHB): Batch and column studies. *Journal of Hazardous Materials, 185*(2-3), 1073-1080.

Maity, J. P., Hsu, C. M., Lin, T. J., Lee, W. C., Bhattacharya, P., Bundschuh, J., & Chen, C. Y. (2018). Removal of fluoride from water through bacterial-surfactin mediated novel

© University of Venda

hydroxyapatite nanoparticle and its efficiency assessment: Adsorption isotherm, adsorption kinetic and adsorption Thermodynamics. *Environmental Nanotechnology, Monitoring and Management, 9*, 18-28.

Marwa, J., Lufingo, M., Noubactep, C., & Machunda, R. (2018). Defeating fluorosis in the East African Rift Valley: Transforming the Kilimanjaro into a rainwater harvesting park. *Sustainability*, *10*, 11, 4194.

McCaffrey, L. P., & Willis, J. P. (2001). Distribution of fluoride-rich groundwater in the eastern and Mogwase regions of the Northern and North-West Provinces. Pretoria: Water Research Commission.

Momba, M. N. B., & Brouckaert M. B. (2005). Guidelines for ensuring sustainable effective disinfection in small water supply systems. WRC Report No. TT 249/05. Water Research Commission, Pretoria, South Africa.

Mondal, P., & George, S. (2015). A review on adsorbents used for defluoridation of drinking water. *Reviews in Environmental Science and Bio/Technology, 14*(2), 195-210.

Mudzielwana, R., Gitari, M. W., & Msagati, T. A. (2016). Characterisation of smectite-rich clay soil: Implication for groundwater defluoridation. *South African Journal of Science, 112* (11-12), 1-8.

Mudzielwana, R., Gitari, W. M., Akinyemi, S. A., & Msagati, T. A. (2017). Synthesis, characterisation, and potential application of Mn 2+-intercalated bentonite in fluoride removal: adsorption modeling and mechanism evaluation. *Applied Water Science, 7*(8), 4549-4561.

Ncube, E. J., & Schutte, C. F. (2005). The occurrence of fluoride in South African groundwater: A water quality and health problem. *Water South Africa*, 31 1 35-40.

Ngulube, T., Gitari, M. W., & Tutu, H. (2017). Defluoridation of groundwater using mixed Mukondeni clay soils. *Water Science and Technology: Water Supply*, *17*(2), 480-492.

Obijole, O. A., Gitari, M. W., Ndungu, P. G., & Samie, A. (2019). Mechanochemically-activated aluminosilicate clay soils and their application for defluoridation and pathogen removal from groundwater. *International Journal of Environmental Research and Public Health, 16*(4), 654.

© University of Venda

Odiyo, J. O., & Makungo, R. (2018). Chemical and microbial quality of groundwater in siloam village, implications to human health and sources of contamination. *International Journal of Environmental Research and Public Health*, *15*(2), 317.

Oke, I., Fasuyi-Enang, O., Obijole, H., Fehintola, E., & Amoko, J. (2014). Adsorption kinetics of Pb^{2+}, Ni^{2+} and Cd^{2+} onto powdered eggshells. *Ife Journal of Science, 16*(2), 273-290.

Ologundudu, T., Odiyo, J., & Ekosse, G.-I. (2016). Fluoride sorption efficiency of vermiculite functionalised with cationic surfactant: Isotherm and kinetics. *Applied sciences*, *6*(10), 277.

Öztop, B., & Shahwan, T. (2006). Modification of a montmorillonite–illite clay using alkaline hydrothermal treatment and its application for the removal of aqueous Cs+ ions. *Journal of Colloid and Interface Science*, *295*(2), 303-309.

Pan, J., Zheng, Y., Ding, J., Gao, C., Van der Bruggen, B., & Shen, J. (2018). Fluoride removal from water by membrane capacitive deionization with a monovalent anion selective membrane. *Industrial and Engineering Chemistry Research*, *57*(20), 7048-7053.

Pandi, K., Viswanathan, N., & Meenakshi, S. (2019). Hydrothermal synthesis of magnetic iron oxide encrusted hydrocalumite-chitosan composite for defluoridation studies. *International Journal of Biological Macromolecules*, *132*, 600-605.

Qureshi, S. Z., Khan, M. A., & Rahman, N. (1995). Synthesis and ion-exchange behavior of a new three-component ion-exchange material: Zirconium (IV) arsenate vanadate. *Bulletin of the Chemical Society of Japan*, *68*(6), 1613-1617.

Saha, S. (1993). Treatment of aqueous effluent for fluoride removal. *Water Research, 27*(8), 1347-1350.

Sahu, O & Singh, N. (2019). Significance of bioadsorption process on textile industry wastewater. In *The Impact and Prospects of Green Chemistry for Textile Technology*, (367 - 416). Woodhead Publishing.

Samrat, M. N., Gandhi, K. S. & Rao, K. K. (2020). Modelling the adsorption of fluoride onto activated alumina in the presence of other ions. *Journal of Environmental Chemical Engineering*, 103934.

Sperinck, S., Raiteri, P., Marks, N., & Wright, K. (2011). Dehydroxylation of kaolinite to metakaolin—a molecular dynamics study. *Journal of Materials Chemistry*, *21*, 7, 2118-2125.

© University of Venda

Tran, H. N., You, S.-J., Hosseini-Bandegharaei, A., & Chao, H. P (2017). Mistakes and inconsistencies regarding adsorption of contaminants from aqueous solutions: a critical review. *Water Research, 120,* 88-116.

Vhahangwele, M., Mugera, G. W., & Tholiso, N. (2014). Defluoridation of drinking water using Al^{3+}-modified bentonite clay: optimisation of fluoride adsorption conditions. *Toxicological and Environmental Chemistry, 96*(9), 1294-1309.

Wang, H., Feng, Q., Liu, K., Li, Z., Tang, X., & Li, G. (2017). Highly efficient fluoride adsorption from aqueous solution by nepheline prepared from kaolinite through alkali-hydrothermal process. *Journal of Environmental Management, 196,* 72-79.

Weber, W. J., & Morris, J. C. (1963). Kinetics of adsorption on carbon from solution. *Journal of the Sanitary Engineering division, 89*(2), 31-60.

Weber, W. J., & Morris, J. C. (1964). Equilibria and capacities for adsorption on carbon. *Journal of the Sanitary Engineering division, 90*(3), 79-108.

Weber, T. W., & Chakravorti, R. K. (1974). Pore and solid diffusion models for fixed-bed adsorbers. *American Institute of Chemical Engineering* (*AIChE*) *Journal*, *20*(2), 228-238.

Wimalasiri, A. V. K., Fernando, M. S., Williams, G. R., Dissanayake, D. P., de Silva, K. N. & de Silva, R. M. (2020). Microwave assisted accelerated fluoride adsorption by porous nanohydroxyapatite. *Materials Chemistry and Physics*. 123712.

World Health Organization (WHO). Water Sanitation and Health. (2015). Available online: http://www.who.int/water_sanitation_health/diseases.

World Health Organization (WHO) and United Nations International Children Education Fund (UNICEF). (2016). Safely managed drinking water services-thematic report on drinking water.

WRC, Distribution of Fluoride-Rich Groundwater in the Eastern and Mogwase Regions of the Northern and North-West Province (2005). WRC Report No. 526/1/01 1.1-9.85 Pretoria, 2001, as cited in: Ncube, E. J., and Schutte, C. F., The occurrence of fluoride in South African groundwater: A water quality and health problem, *Water South Africa,* 31 1 35–40.

World Health Organization (WHO), (2017). Guidelines for drinking water quality. Fluoride in drinking water. Guidelines for drinking water quality, Geneva.

© University of Venda

http://www.who.int/topics/millennium_development_goals/en/ . Accessed on 24th September, 2019.

World Health Organization (WHO) and UNICEF Joint Monitoring Programme. (2017). Progress on drinking water and sanitation 2017 update and MDG assessment.

Yao, Z., Ma, X., & Lin, Y. (2016). Effects of hydrothermal treatment temperature and residence time on characteristics and combustion behaviors of green waste. *Applied Thermal Engineering*, *104*, 678-686.

Yoon, Y., Zheng, M., Ahn, Y. T., Park, W. K., Yang, W. S., & Kang, J. W. (2017). Synthesis of magnetite/non-oxidative graphene composites and their application for arsenic removal. *Separation and Purification Technology, 178*, 40-48.

Yoshimura, M., & Byrappa, K. (2008). Hydrothermal processing of materials: past, present and future. *Journal of Materials Science, 43*(7), 2085-2103.

Zhang, B., Mingjian, L. I., Dai, X., & Zhou, S. (2017). Control status quo of drinking-water-borne endemic fluorosis in the disease affected areas in Hubei Province in 2015: an analysis of survey results. *Chinese Journal of Endemiology, 36*, 5, 346-349.

Zhang, Z., Tan, Y., & Zhong, M. (2011). Defluoridation of wastewater by calcium chloride modified natural zeolite. *Desalination, 276*(1-3), 246-252.

© University of Venda

CHAPTER SIX: PORE-FORMING-AGENT-ASSISTED (POROUS) HYDROTHERMALLY-TREATED ALUMINOSILICATE CLAYS (PHTAC): EVALUATION OF OPTIMUM CONDITIONS FOR SYNTHESIS AND PHYSICOCHEMICAL CHARACTERISATION

6 Abstract

In the previous chapter, mechanochemically-activated clay (MAC) was hydrothermally treated successfully and applied to fluoride and pathogen removal from groundwater. The maximum fluoride removal increased from 32% in MAC to 53% in HTAC. The antibacterial studies showed an improved potency from zero in MAC to 15 mm in the synthesised HTAC. Although, defluoridation and antibacterial potency improved in HTAC, further modification of the materials via surface and pore enhancement for higher fluoride removal is recommended. This chapter focusses on the optimisation of operational parameters to increase surface area and pores of HTAC through introduction of $NaClO_3$ as a pore-forming agent to synthesise porous-hydrothermally-treated aluminosilicate clays (PHTACs) and the implication on their physiochemical properties. Operational parameters such as pore-forming agent mass, hydrothermal treatment temperature and time were considered for their synthesis. Prior to addition of pore-forming agent, dissolution of silica and alumina was carried out using 1.5 M NaOH for 2 h at 298 K. Thereafter, the slurry obtained was hydrothermally treated while varying treatment time, water content, and $NaClO_3$. The samples were characterised using BET, FT-IR, SEM-EDS and XRD to study the effect of pore forming agent on the clay surface properties. Preliminary batch fluoride adsorption experiments were conducted to determine optimally synthesised samples. The results showed $NaClO_3$, treatment time and water content are critical in the modification of the synthesised materials. Several new mineral phases corresponding to hydroxy sodalite were observed and confirmed by characteristic sharp intense peaks around at 2-degree θ = 15, 25, 32 and 35, while SEM micrographs showed changes in morphology from platy-like structure to fine piston needle-like particles interlaced with pores as synthesis conditions were varied. This was confirmed by XRD, FTIR and SEM analyses. The BET results showed increasing surface area from 47.37 m^2/g to 52.56 m^2/g in the best optimised products. The introduction of $NaClO_3$ during treatment impacted on the surface area and defluoridation potential of synthesised PHTACs. The adsorption capacity of PHTAC products improved to between 1.55 and 3.45 mg/g. The best synthesised PHTAC-18 product, which was obtained by using 1.0 g/100 mL adsorbent

© University of Venda

dosage, 0.20 g/100 mL pore formers, 9 mL water content at 300 °C and 6 h hydrothermal treatment temperature and time respectively gave the highest defluoridation potential and was therefore selected for use in batch defluoridation experiment- presented in Chapter Seven.

Keywords: Adsorption, Defluoridation, Fluoride, Hydrothermal treatment, Groundwater, Mechanochemical activation, Pathogens, Pore-forming agent.

6.1 Introduction

In the preceding chapter, hydrothermally-treated aluminosilicate clay (HTAC) was successfully synthesised through hydrothermal treatment processes and further tested for its efficiency towards fluoride and pathogen removal from groundwater. The results showed that the synthesised materials performed better in fluoride and pathogen removal over mechanochemically-activated clay (MAC). However, the quest for improved fluoride removal performance led to the modification of the HTAC materials via the introduction of pore formers ($NaClO_3$).

Even though hydrothermal treatment techniques have been used to improve the surface area and crystallinity of aluminosilicate materials for better adsorptive performance such as reported in several research works (Holler & Wirsching 1985; Cundy & Cox, 2005; Byrappa *et al.*, 2006; Byrappa & Yoshimura, 2006; Yoshimura & Byrappa, 2008; Byrappa & Yoshimura, 2012; Luo *et al.*, 2018), there is the need for further improvement for better efficiency. Hydrothermal techniques have also been used to synthesise zeolites from parent aluminosilicate materials for enhanced defluoridation. Hollman *et al.* (1999) synthesised zeolite Na-P1 through direct hydrothermal treatment from coal fly ash (CFA) and NaOH solution. Musyoka *et al.* (2009), Nicholas *et al.* (2012) and Gitari *et al.* (2016) also used a two-step process involving aluminosilicate dissolution followed by hydrothermal treatment to synthesise different types of zeolites and other crystalline materials from CFA. In addition, various materials have been previously developed through some pore-forming-agent-assisted-hydrothermal treatment of alumunosilicate materials and further applied in water defluoridation (Cundy & Cox, 2005; Dhillon *et al.*, 2015; Yao *et al.*, 2018; Khandare & Mukherjee, 2019). These materials showed better performance in defluoridation than the parent materials but at elevated temperatures.

To date, studies on the multifunctionality of pore-forming agent such as $NaClO_3$-assisted-hydrothermally treated aluminosilicate rich (smectite) clays towards fluoride and pathogen

© University of Venda

removal from groundwater have not been reported, therefore, this chapter focuses on optimising conditions for enhancing the pores of hydrothermally-treated aluminosilicate clay synthesised in the previous chapter with the aim of improving its multifunctionality towards fluoride removal from groundwater. The porous-hydrothermally-treated aluminosilicate clay (PHTAC) was synthesised following the stepwise process which involves briefly, i) addition of varying amounts pore formers - $NaClO_3$ (0.05 - 0.2 g/100 mL) to the clay/NaOH slurry earlier obtained in the preceding chapter followed by ii) concurrent variation of the hydrothermal treatment time, and water content at temperature of 300 °C, iii) characterising the products obtained using FTIR, BET, SEM-EDS and XRD in order to determine the effect of pore-forming agent on physicochemical properties, iv) carrying out batch defluoridation experiments to determine the best synthesised product based on its fluoride adsorption capacity.

6.2 Materials and methods

6.2.1 Sample collection and preparation

Aluminosilicate clay samples were collected from Mukondeni village, Vhembe District in Limpopo Province, South Africa. Samples were collected and stored in a polyethylene plastic bags. Prior to experiment, clays soil sample were prepared according to the procedures described in Chapter Four (subsection 4.2.1). All analytical grade reagents used in this study included NaOH pellets-anhydrous > 98% (Sigma Aldrich), NaF > 99% (Sigma Aldrich), $NaClO_3$ (Sigma Aldrich), HCl, Na_2CO_3 > 99% (Sigma Aldrich), $NaNO_3$ > 99% (Sigma Aldrich), NaCl > 99% (Sigma Aldrich), Na_2PO_4 > 99% (Sigma Aldrich), Na_2SO_4, TISAB III solution (Sigma Aldrich).

6.2.2 Optimisation of conditions for synthesis of PHTAC adsorbents

In order to synthesise PHTAC, finely ground mechanochemically-activated clay (MAC) was subjected to dissolution using NaOH and then hydrothermally treated with addition of sodium chlorate ($NaClO_3$) as pore-forming agent while concurrently varying the hydrothermal treatment time and amount of pore-forming agent at predetermined hydrothermal temperature.

6.2.3 Dissolution of aluminosilicate clay

A two-step process adopted from Hollman *et al.* (1999) and Musyoka *et al.* (2009) and Gitari *et al.* (2016) was used for the synthesis of PHTAC. Firstly, the synthesis process involved dissolution of finely ground MAC in NaOH solution at predetermined clay/NaOH ratio and

© University of Venda

concentration followed by hydrothermal treatment of the slurry mixture in varying amount of $NaClO_3$ at predetermined temperature of about 300 °C. For hydrothermal treatment, the hydrothermal time, amount of $NaClO_3$ and water content were optimised. Solution of 1.5 M NaOH was prepared according to procedures in subsection 4.2.2.1 Thereafter, 5 g clay was dispersed into 1.5 M NaOH solution and the slurry mixtures were aged. Thereafter, mixture was filtered, residue washed, dried and then weighed following the experimental protocol in subsection 4.2.2.1. Furthermore, evaluation of the effect of contact time on dissolution of Si and Al in 1.5 M NaOH concentration was conducted according to procedures in subsections 4.2.2.1 and 4.2.2.2 respectively, to determine the optimum time for Si and Al dissolution from the clay.

6.2.4 Evaluation of optimum condition for synthesis of porous-hydrothermally-treated aluminosilicate clay (PHTAC)

In order to prepare PHTAC, the mixture obtained in subsection 6.2.3 was subjected to hydrothermal treatment while concurrently varying amount of $NaClO_3$, hydrothermal treatment time, and water/silica ratio at predetermined temperature of 300 °C (decomposition temperature of $NaClO_3$). Table 6.1 presents a summary of experimental runs conducted to optimise the conditions. Briefly, 20 mL of optimised clay/NaOH slurry mixture and a predetermined (fixed) volume of 9 mL water were measured into a parr bomb vessel followed by addition of 0.05 g mass of $NaClO_3$. Thereafter, the slurry mixture was placed in an oven at temperature of about 300 °C at hydrothermal treatment time of 1 h. The experimental runs was repeated by concurrently varying the mass of $NaClO_3$ between 0.05 and 0.2 g and hydrothermal treatment time between 1 and 18 h. Massive destruction of the materials and explosion were experienced when attempts were made to further increase the treatment time beyond 18 h at about 300 °C decomposition temperature of the pore-forming agent ($NaClO_3$). Hydrothermal treatment time, amount of pore forming agent and water content were varied concurrently in order to obtain optimal conditions for PHTAC synthesis. After treatment, the recovered solid residues of PHTAC were dispersed in 500 mL of Milli-Q water to reduce the effect of high alkalinity of solution on the PHTAC adsorbent formed. The suspensions were then passed through 0.45 µm pore polypropylene filter membrane. The residues were further rinsed with Milli-Q water until near neutral pH. Thereafter, they were oven dried at 110 °C for 6 h and milled to pass through 250 µm test sieve using a mortar and pestle and then stored in plastic bottles to prevent moisture ingress (Wang *et al.,* 2017).

© University of Venda

University of Venda
Creating Future Leaders

Table 6.1: Experimental conditions for synthesis of PHTAC.

Note: Hydrothermal treatment time, pore-forming agent amount and water content were varied concurrently in order to obtain optimum conditions for the synthesis of PHTAC adsorbent (Adapted from Musyoka, 1999; 2012).

Parameter investigated	Runs	Ageing H_2O content (mL)	Hydrothermal treatment time (h)	Hydrothermal treatment temperature (°C)	Pore-forming agent ($NaClO_3$)	Sample
Hydrothermal	1	9	1	285	0.05	PHTAC-1
treatment time	2	9	3	285	0.05	PHTAC-2
and amount of	3*	9	6	285	0.05	PHTAC-3
pore-forming	4	9	12	285	0.05	PHTAC-4
agent added to	5*	9	18	285	0.05	PHTAC-5
HTACs	6	9	1	285	0.10	PHTAC-6
	7	9	3	285	0.10	PHTAC-7
	8*	9	6	285	0.10	PHTAC-8
	9	9	12	285	0.10	PHTAC-9
	10	9	18	285	0.10	PHTAC-10
	11	9	1	285	0.15	PHTAC-11
	12	9	3	285	0.15	PHTAC-12
	13	9	6	285	0.15	PHTAC-13
	14	9	12	285	0.15	PHTAC-14
	15*	9	18	285	0.15	PHTAC-15
	16	9	1	285	0.20	PHTAC-16
	17*	9	3	285	0.20	PHTAC-17

© University of Venda

University of Venda
Creating Future Leaders

	18*	9	6	285	0.20	PHTAC-18
	19	9	12	285	0.20	PHTAC-19
	20	9	18	285	0.20	PHTAC-20
Addition of	21	0	6	285	0.20	PHTAC-21
water content	22	3	6	285	0.20	PHTAC-22
	23	6	6	285	0.20	PHTAC-23
	24	9	6	285	0.20	PHTAC-24
	25	12	6	285	0.20	PHTAC-25

Footnote**:** * selected porous-hydrothermally-treated aluminosilicate clay (PHTAC) samples.

© University of Venda

6.2.5 Physicochemical and mineralogical characterisations

The synthesised porous-hydrothermally-treated aluminosilicate clays (PHTACs) were evaluated for functional groups using Fourier Transform Infrared spectroscopy (Bruker, Germany: ATR-Diamond FT-IR spectrophotometer) in the range of 4500 - 500 cm^{-1}. The PHTAC surface and specific area, pore volumes and pore sizes were measured with Micromeritics TriStar II Surface Area and porosity unit instrument (Micromeritics, Norcross, GA, USA) using Brunauer-Emmett-Teller (BET) method. Scanning electron microscopy was conducted using JEOL - 2100 Electron Microscope TESCAN, Vega 3XMU (TESCAN, Brno, Czech Republic) to evaluate the morphology of the samples. Examination of the qualitative and quantitative mineral phase composition was done by employing a D8 advance X-ray diffraction (Bruker, Germany) equipped with Cu- Kα source radiation. The mineralogy was determined by selecting the best–fitting pattern from the ICSD database to the measured diffraction pattern, using X'Pert Highscore plus software. The relative phase amounts (weight percent of crystalline portion) were estimated using the Rietveld method (X'Pert Highscore Program).

6.2.6 Defluoridation process

Defluoridation adsorption experiments were conducted on all the PHTAC products obtained. Evaluation was carried out using 1.0 g/100 mL PHTAC dosage, 5 mg/L fluoride solution in 250 mL bottles at initial pH of 4.2. The mixtures were shaken for 30 min at 250 rpm and 298 K. Thereafter, equilibrium pH were measured. The mixtures were centrifuged for about 30 min at 4000 rpm and the supernatants analysed for residual fluoride by using a four-standard calibrated ORION fluoride ion-selective electrode. TISAB III solution was added to both standards and samples at volume ratio of 1:10 to de-complex fluoride ions. All the experiments were done in duplicates and the mean values were reported.

6.3 Results and discussion

6.3.1 Porous-hydrothermally-treated aluminosilicate clay (PHTAC) products

Figure 6.1 presents the images of sample [PHTAC-1 to PHTAC-25] obtained at different experimental runs with colour variations. From the figure 6.1, synthesised products obtained showed various shades of colour which is an indication of varying degrees of modification during the hydrothermal treatments in the presence of varying amounts of pore-forming agents ($NaClO_3$). There was a progressive change in the colours of the PHTAC products from light brown colour to

© University of Venda

dark brown and brownish-black colouration as the hydrothermal conditions such as amount of pore formers ($NaClO_3$), temperature, reaction time and water/silica ratio were varied respectively. The difference in the colours of the different products could be due to the transformation or transition in the structural oxidation state of iron within the products matrix and hydroxylation, which takes place at elevated temperature (Eissa *et al.,* 1994; Soulé *et al.,* 2020). All the PHTAC products obtained were evaluated for fluoride removal potential with the best six preforming products selected for further characterisation and surface properties.

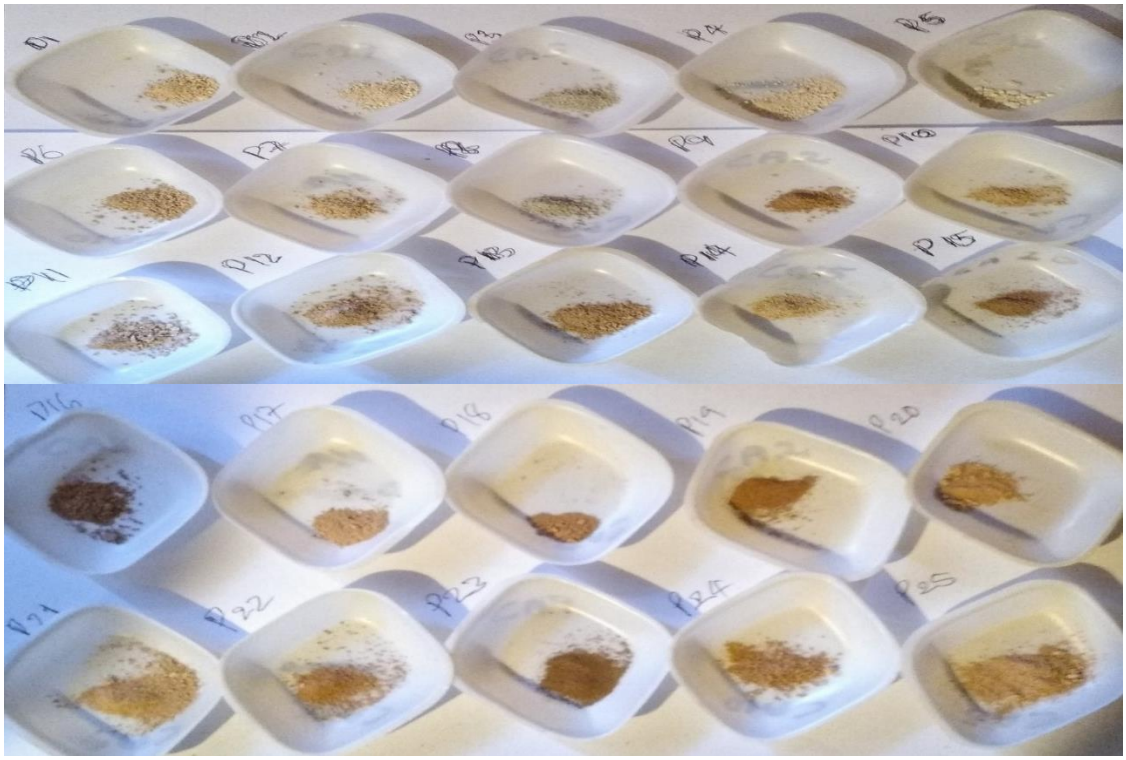

Figure 6.1: Images of all the synthesised porous-hydrothermally-treated aluminosilicate clay samples [PHTAC-1 to PHTAC-25] respectively obtained at different experimental conditions.

6.3.2 Defluoridation of simulated fluoride solutions with synthesised PHTACs

Table 6.2 presents the percent fluoride removal and adsorption capacities of all the synthesised porous-hydrothermally-treated aluminosilicate clays (PHTACs). The results from Figure 6.1 and Table 6.2 showed samples of PHTAC-1, PHTAC-2, PHTAC-3, PHTAC-4 and PHTAC-13 to have light brown colouration and thus gave lower per cent fluoride (30 - 39%) removal, hence, suggesting mild modification. Samples of PHTAC-5, PHTAC-6, PHTAC-7, PHTAC-9, PHTAC-10, PHTAC-11, PHTAC-12, PHTAC-14, PHTAC-20, PHTAC-21 and PHTAC-22 showed between 40 and 49% fluoride removal, with dark brown colourations is

© University of Venda

suggestive of moderate influence of hydrothermal treatment conditions in the presence of the added pore formers. Samples PHTAC-15, PHTAC-16, PHTAC-17, PHTAC-19, PHTAC-20, PHTAC-23 and PHTAC-25 are brownish-black in colour and have percent fluoride removal between 50 - 59%. Products PHTAC-18 and PHTAC-24 synthesised under same conditions gave highest percent fluoride removal of 63.26 and adsorption capacity of 3.24 mg/g (Table 6.2). The optimised conditions influenced the degree of modification. Hence, increase in the amount of pore formers led to increase in materials' surface area, which resulted in increasing per cent fluoride removal. The six best synthesised products were selected based on the results of preliminary defluoridation and further characterised using FTIR, BET, SEM-EDS and XRD techniques for better understanding of their surface chemistry.

Table 6.2: Adsorption capacities and percent fluoride removal of the PHTAC samples.

Sample	Percent fluoride	Adsorption capacity, q (mg/g)
PHTAC-1	32.25	1.25
PHTAC-2	34.19	1.43
PHTAC-3*	39.27	1.77
PHTAC-4	38.30	1.85
PHTAC-5*	49.98	2.93
PHTAC-6	49.12	2.81
PHTAC-7	41.20	2.44
PHTAC-8*	49.87	2.89
PHTAC-9	40.56	2.34
PHTAC-10	49.11	2.67
PHTAC-11	42.58	2.42
PHTAC-12	41.45	1.99
PHTAC-13	39.9	1.97
PHTAC-14	40.24	2.32
PHTAC-15*	55.05	3.10
PHTAC-16	57.2	3.19
PHTAC-17*	59.33	3.23
PHTAC-18*	63.26	3.45

© University of Venda

PHTAC-19	57.0	3.19
PHTAC-20	58.6	3.23
PHTAC-21	46.6	2.65
PHTAC-22	49.45	2.73
PHTAC-23	57.0	3.19
PHTAC-24	62.22	3.43
PHTAC-25	52.75	3.05

Note: Products PHTAC-18 and PHTAC-24 are the same since they were prepared under the same experimental conditions.
Footnote: * represents the selected synthesised PHTAC materials.

6.3.3 Physicochemical characterisation

6.3.3.1 Fourier transform infra-red (FTIR)

Figure 6.2 presents the FTIR spectra and functional groups of MAC, HTAC and selected porous-hydrothermally-treated aluminosilicate clay (PHTAC) samples scanned between the range 4000 and 500 cm^{-1}. Three main transmittance regions of 3000 - 3800 cm^{-1}, 1300 - 1800 cm^{-1} and 500 - 1200 cm^{-1} were observed. The OH^- stretching mode is observed around 3400 and 3700 cm^{-1}. The band observed at 1600 - 1650 cm^{-1} was attributed to H-O-H bending of water. The main functional groups of Si-O-Si and Al-O-Al were observed around 950 - 1050 cm^{-1} and 500 - 650 cm^{-1} regions respectively (Kim *et al.,* 2010; Luo *et al.,* 2018). The results showed the spectra changes in the peak intensities and bands as the hydrothermal/pore formers treatment progressed from MAC to PHTACs. The transmittance intensities for Al-O and Si-O at around 960 and 650 cm^{-1} increased in the PHTAC products owing to formation of strong Al-O-Al and Si-O-Si bonds as hydrothermal temperature increased (Luo *et al.,* 2018). The spectral band at 1650 cm^{-1} in the PHTAC products was attributed to the bending O-H bond of water molecules retained in the silica matrix during treatment (Gougazeh & Buhl, 2014). The mechanochemically-activated clay (MAC) slurry containing dissolved aluminosilcates obtained during ageing process, on reacting with NaOH and the pore former ($NaClO_3$) resulted in the vibration bands being replaced by a strong single band around 950 cm^{-1}, characteristic of Si-O-Al bonds in SiO_4 or AlO_4 tetrahedron in the synthesised PHTAC structure (Kim *et al.,* 2010; Luo *et al.,* 2018). The hydroxyl peaks were observed to decrease in the hydrothermally-treated materials as hydrothermal treatment temperature increased owing to evaporation (Figure 6.2). The gradual disappearance of

© University of Venda

transmittance bands 3000 and 3600 - 3700 cm^{-1} as treatment conditions were varied might be due to O-H bonds breakdown and very intense and strong transmittance appearance around 600 cm^{-1} resulting from moisture loss, following hydrothermal treatment and subsequent formation of Al-O and Si-O bonds during surface alteration (Luo *et al.*, 2018). The optimised HTAC-18 was observed to have the most intense transmission bands and incidentally corresponds to the material with the highest fluoride removal from groundwater.

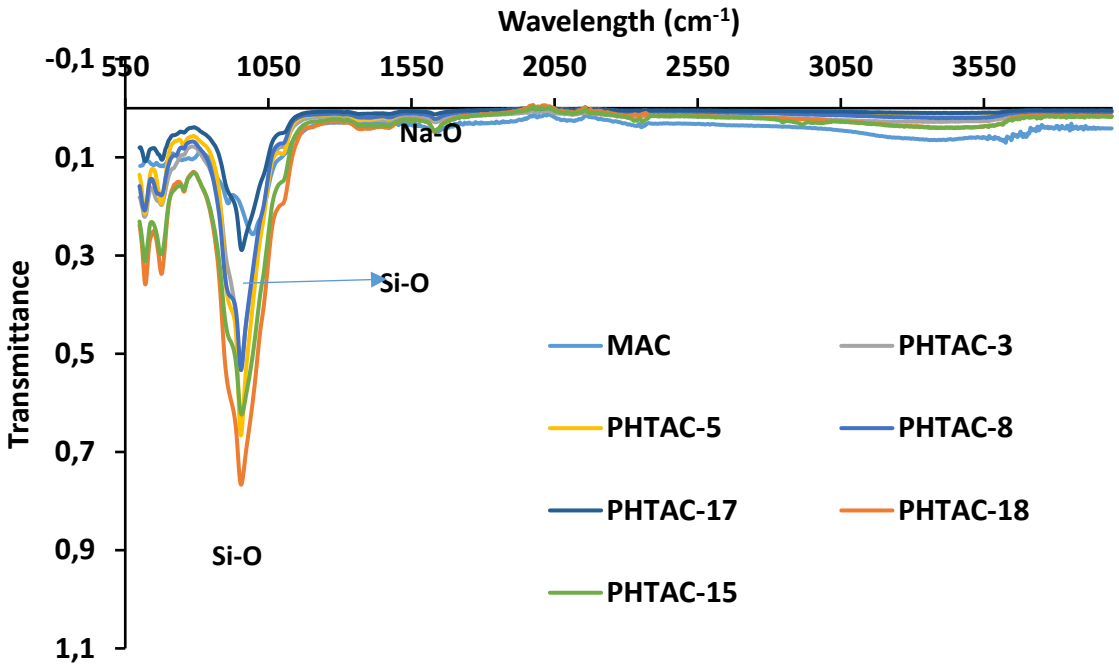

Figure 6.2: FTIR spectra of MAC, HTAC and the selected porous-hydrothermally-treated aluminosilicate clay (PHTAC) samples.

6.3.3.2 Surface area by Brunauer-Emmett-Teller (BET) method

Table 6.3 presents the surface area, pore volume and pore size of mechanochemically-activated clay (MAC), hydrothermally-treated aluminosilicate clay (HTAC) and selected porous-hydrothermally-treated aluminosilicate clays (PHTAC) based on the results of preliminary defluoridation of all the synthesised products.

BET analysis showed a significant increase in the surface area of MAC from about 17 m^2/g to 52.83 m^2/g in PHTAC. There was also an increase in the surface areas of all the PHTACs with PHTAC-18 having the highest surface area while a modest change was observed in their pore sizes

© University of Venda

and volumes respectively. The observed increase in surface area could be due to increasing amount of $NaClO_3$ introduced, which led to surface alteration and formation of pores from the oxygen released from the pore formers at pore formers' melting point temperature range. The average pore diameters of about 10.5 nm and 14.5 nm were obtained for the MAC, HTAC and all the PHTAC adsorbents, hence, suggesting that the pore formers did not have any significant effect on the pore diameters of synthesised products at the hydrothermal treatment time and temperatures. The pore diameter of bulk of the pores were distributed within 0 - 50 nm range, suggesting that all the materials were mesoporous (Table 6.3). The surface area of the products increased with increase in the amount of pore-forming agent. During hydrothermal treatment at elevated temperatures, the pore-forming agent ($NaClO_3$) thermally decompose to yield sodium chloride (Na^+Cl^-) and oxygen (O_2) (Equation 6.1). The O_2 is introduced into the products' matrix creating pores while Na^+ forms part of the exchangeable cations on the synthesised products' surface thus increasing positive charges on the materials' surface. Furthermore, there was increased in products' kinetic mobility leading to particle breakdown into smaller particles at elevated temperatures, with particles recrystallising to form gel-like, fine crystalline piston-like morphologies (Casci, 2005; Musyoka *et al.,* 2012). The fine crystals could lead to an increase in surface area and hence, an increase in the number of sorption sites and thus, higher defluoridation potentials of the synthesised PHTAC products.

$$2NaClO_3 \rightarrow 2NaCl + 3O_2 \qquad (6.1)$$

Table 6.3: The surface area, pore volume and pore size of MAC, HTAC and the selected porous-hydrothermally-treated aluminosilicate clays (PHTACs).

Sample	BET surface area (m^2/g)	Surface area single point (m^2/g)	Pore volume (cm^3/g)	Pore size (nm)
MAC	17.19	16.66	10.06	14.93
HTAC	33.56	32.09	10.20	14.87
PHTAC-3	47.37	46.67	10.36	14.82
PHTAC-5	46.79	45.56	10.32	14.54
PHTAC-8	49.35	48.23	10.75	14.37
PHTAC-15	47.93	46 89	10.69	14.22
PHTAC-17	49.48	48.87	10.78	14.25
PHTAC-18	52.83	51 45	10.95	14.54

© University of Venda

6.3.3.3 X-ray diffraction (XRD)

X-ray diffraction results are presented in Figure 6.3. The results showed progressive changes and trends in the mineral phase of MAC compared to other modified clay adsorbents. There were changes from weak and broad peaks in the precursor materials of MAC and HTAC to characteristic strong and sharp peak intensities and formation of new mineral phases as pore formers were gradually increased from 0.05 g to 0.2 g during hydrothermal treatment. The pore formers gradually introduced oxygen into clay matrix, leading to surface alteration and enhancement of pores leading to disappearance of peaks and formation of new mineral phases when compared to MAC and HTAC, which were synthesised without pore formers (Figure 6.3). The strong presence of plagioclase (albite), quartz and montmorillonite which was identified through its prominent peaks at 6.5°, 12°, 18° and 28° two theta, in MAC was chemically transformed via recrystallisation processes into zeolitic materials containing mainly hydroxy sodalite in the HTAC during hydrothermal treatment (without pore formers) (Figure 6.4). The change observed in the course of both hydrothermal treatment and addition of pore formers led to the chemical transformation of mineral phases in HTAC into hydroxy sodalite mineral phases in the formed geopolymeric zeolitic PHTAC products (Figure 6.3). Recent studies by (Mudzielwana *et al.* (2016; 2017), Obijole *et al.* (2019) and Gitari *et al.* (2020) on smectite clay showed similar characteristic peaks and presence of these mineral phase in the same proportions for MAC adsorbent. Optimum amount of 0.2 g of $NaClO_3$ was observed to correspond to optimum synthesised PHTAC-18 sample.

© University of Venda

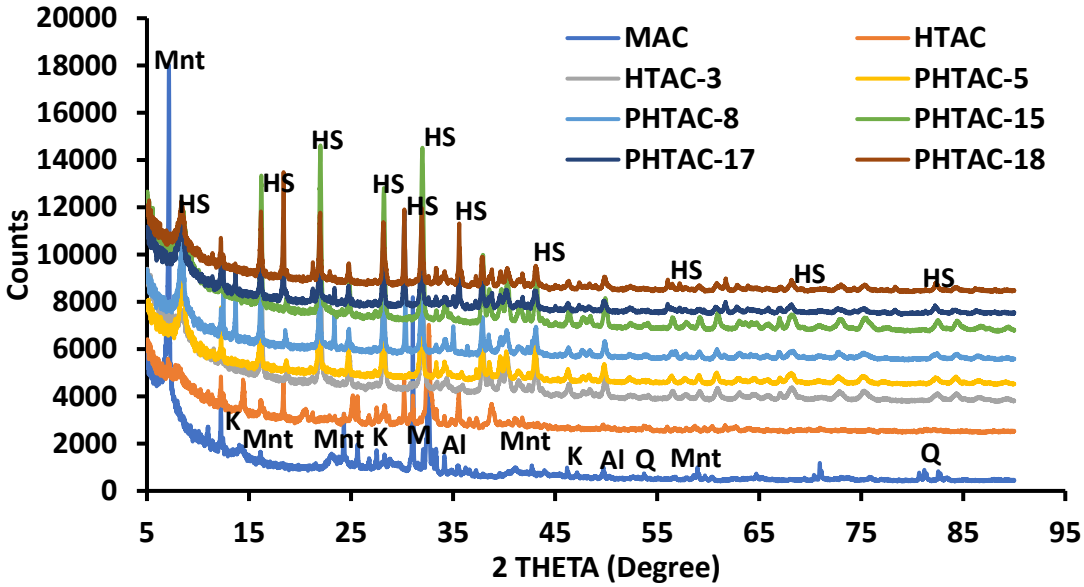

Figure 6.3: X-ray diffraction spectra of MAC, HTAC and selected porous-hydrothermally-treated aluminosilicate clay (PHTAC) samples. (Mnt - montmorillonite, Al - albite, M - muscovite, Q - quartz, A - zeolite, HS - Hydroxy sodalite hydrate)

6.3.3.4 Surface morphology analysis

Figure 6.4 a - h presents the micrographs of MAC, HTAC and the selected PHTACs samples. The images show progressive changes in morphology, appearance and surface area from MAC through HTAC to all the PHTACs. The expanded arrays of irregular flared corn flakes structures with non-crystalline platy-like particles observed in MAC (Figure 6.4 a) gradually changed to irregular shapes and sizes with formation of crystalline geopolymer gel microsphere structure of different thicknesses. Increasing the amount of pore-forming agent had profound influence on the morphologies of the HTAC as observed in Figure 6.4 b. where the irregular flared corn flakes structure and non-crystalline platy-like structures in MAC gradually gave way to long crystalline geopolymeric gel with prismatic needle-like particles in the PHTAC products (Figure 6.4 c - h). The crystalline microspheres structure in HTAC was gradually converted into long prismatic crystalline particles which indicated successful synthesis conditions for conversion in the various PHTAC products. The smooth irregular crystalline microspheric geopolymer gel structures observed in HTAC (without pore-forming agent) gave way to geopolymer gel having piston needle like crystalline particles interlaced with pores in PHTAC (with pore-forming agent). Maximum effect was noticed in PHTAC-18 where optimum amount of 0.20 g of pore formers was introduced.

© University of Venda

Elemental analysis (EDS) revealed increased concentrations of base cations of sodium, magnesium and potassium particularly in HTAC and the PHTAC-3, PHTAC-5, PHTAC-8 and PHTAC-18 (Figure 6.4 b - h). These elevated exchangeable base cations concentrations are responsible for increased positive charges on the treated clay surfaces (Horie *et al.*, 2012), this could be responsible for enhanced fluoride sorption capacity of treated clay materials.

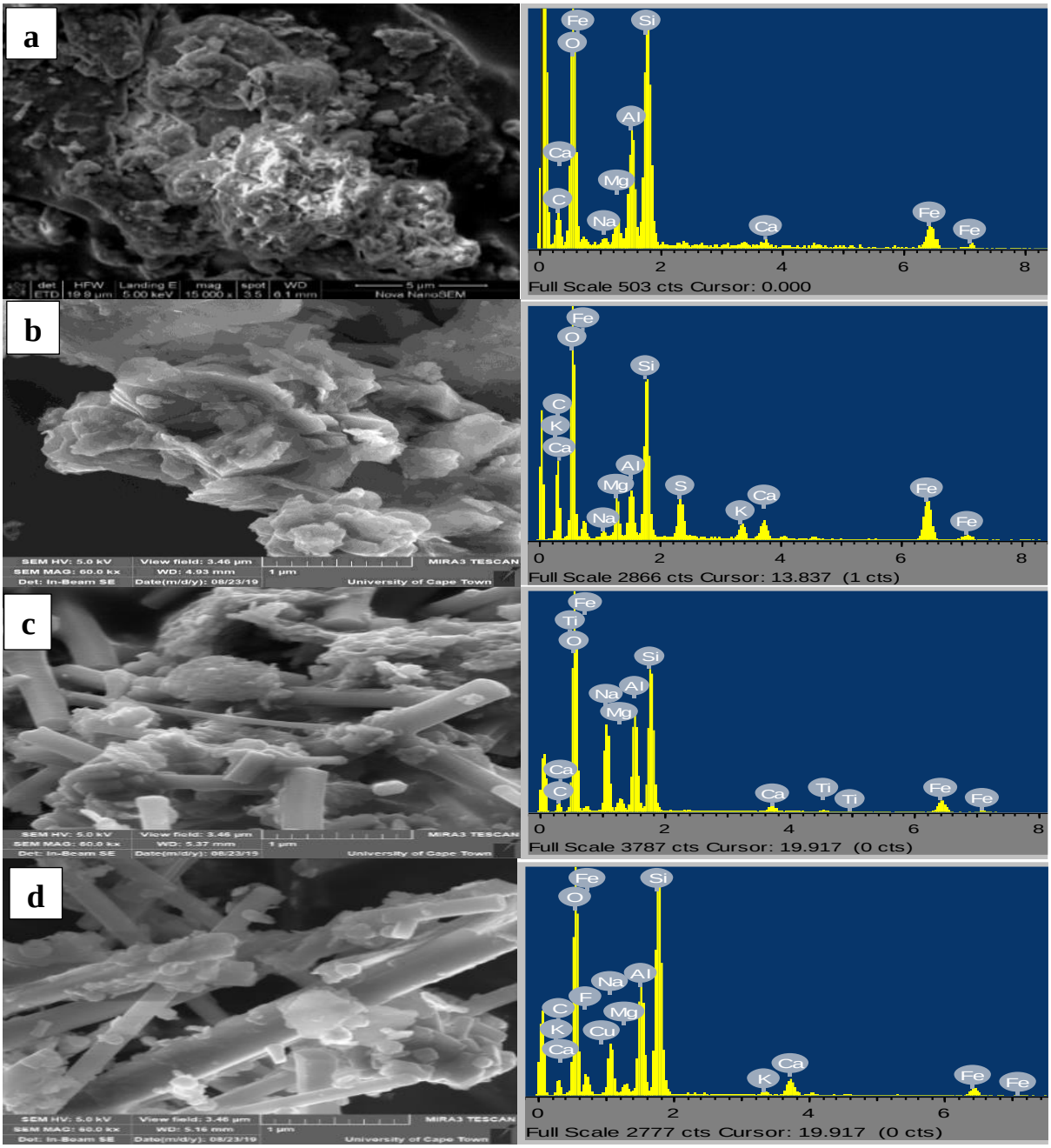

© University of Venda

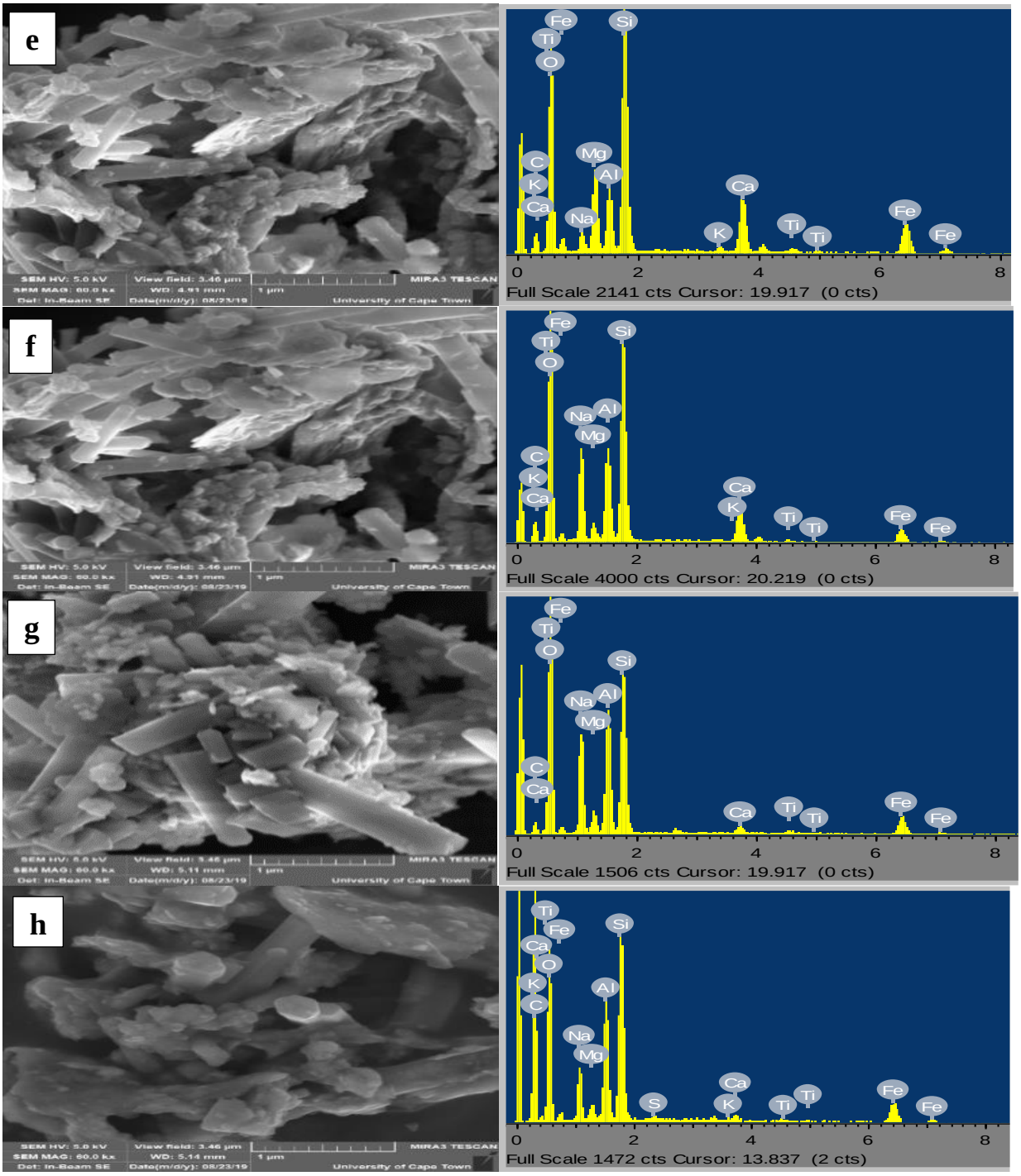

Figure 6.4: SEM-EDS micrographs of **a.** MAC, **b.** HTAC, **c.** PHTAC-3, **d.** PHTAC-5, **e.** PHTAC-8, **f.** PHTAC-15, **g.** PHTAC-17 and **h.** PHTAC-18 samples respectively.
Appendix 6.5: SEM-EDS micrographs of Figure 6.5

6.3.3.5 Defluoridation

Table 6.4 presents the adsorption capacities and percent fluoride removal of MAC, HTAC and the selected porous-hydrothermally-treated aluminosilicate clays (PHTACs). The results in

© University of Venda

the table reveal an increase in percent fluoride removal from MAC to HTAC, which is an indication of successful modification and treatment. The addition of pore formers led to alteration in the surface properties which could be linked to increasing defluoridation capacities of the PHTACs. However, lower adsorption capacities observed in PHTAC-3 and PHTAC-5 could be due to lower amount of pore-forming agent (0.05 g) used, resulting in reduced alteration. Adsorption capacity was observed to increase with increased amount of pore former, which suggests the pore formers may have enhanced pore formation and surface area upon which fluoride was adsorbed.

Generally, the introduction of pore formers was observed to lead to surface alteration leading to larger surface area resulting in higher fluoride sorption noted in the porous-hydrothermally-treated aluminosilicate (PHTAC) products. PHTAC-18 gave the highest adsorption capacity owing to the highest amount of pore-forming agent which resulted to increased crystalline morphology and pronounced surface alteration, leading to larger surface area. Therefore, PHTAC with the highest adsorption capacity of 3.45 mg/g was selected as optimal product for application in batch defluoridation and pathogen removal in chapter seven.

Table 6.4: Percent fluoride removal and adsorption capacities of MAC, HTAC and six best synthesised porous-hydrothermally-treated aluminosilicate clay (PHTAC) adsorbents.

Sample	Percent fluoride removal	Adsorption capacity, q (mg/g)
MAC	32	1.87
HTAC	53	1.75
PHTAC-3	49	1.55
PHTAC-5	49	1.58
PHTAC-8	59	2.23
PHTAC-15	55	1.98
PHTAC-17	59	2.26
PHTAC-18	63	3.45

6.4 Conclusions and recommendations

In this study, operational parameters to synthesise porous-hydrothermally-treated aluminosilicate clay (PHTAC) adsorbents from mechanochemically-activated clay (MAC) adsorbents through the addition of pore formers during hydrothermal treatment process were

© University of Venda

evaluated. PHTAC-18 product was synthesised at optimum conditions of 6 h treatment time, 0.20 g $NaClO_3$ and 9 mL volume of water content at 298 K. BET results showed that the surface area of the materials increased with increasing amount of pore-forming agent ($NaClO_3$). Increase in water content brought about an increase in molecular species of the mixtures and purity of products formed. Increasing water content also led to change in degree of supersaturation of ionic species, which increased the crystal growth until equilibration was reached after which the degree of supersaturation was slowed down. Crystallisation kinetics was therefore slowed down, thus, restricting product formation. Increasing amount of $NaClO_3$ altered the surface morphology of the synthesized products as the decomposition of pore former at elevated temperature releases oxygen which is incorporated into the clay mixture matrix, thereby increasing the surface area and alteration of the pores, and thus, impacting positively on the material's defluoridation potential. The results of the preliminary defluoridation indicated that optimally-altered sample (PHTAC-18) fared better in defluoridation compared to other modified materials. The best modified synthesised PHTAC-18 sample had the highest adsorption capacity of 3.45 mg/g. Hence, it was selected for application in more detailed batch defluoridation and antibacterial potency evaluation in chapter seven.

© University of Venda

REFERENCES

Byrappa, K., Subramani, A. K., Ananda, S., Rai, K. L., Sunitha, M. H., Basavalingu, B., & Soga, K. (2006). Impregnation of ZnO onto activated carbon under hydrothermal conditions and its photocatalytic properties. *Journal of Materials Science*, 41(5), 1355-1362.

Byrappa, K. & Yoshimura, M. (2006). A novel method of advanced materials processing. *Journal of material science* 41, 1294–1682.

Byrappa, K., & Yoshimura, M. (2012). *Handbook of hydrothermal technology*. William Andrew Publications, NJ, USA.

Casci, J. L (2005). Zeolite molecular sieve: Preparation and scale up. *Microporous and Mesoporous Materials*, 82, 217–226.

Cundy, C. S & Cox, P. A (2005). The hydrothermal synthesis of zeolites: precursors, intermediates and reaction mechanism. *Microporous and Mesoporous Materials*, 82, 1–78.

Dhillon, A., Nair, M., Bhargava, S. K., & Kumar, D. (2015). Excellent fluoride decontamination and antibacterial efficacy of Fe–Ca–Zr hybrid metal oxide nanomaterial. *Journal of Colloid and Interface Science, 457*, 289-297.

Eissa, N. A., Sheta, N. H., El Meligy, W. M., & Sallam, H. A. (1994). Mössbauer effect study of the effect of gamma irradiation and heat treatment on montmorillonite. *Hyperfine Interactions*, *91*(1), 783-787.

Gitari, Ngulube, T., Masindi, V., & Gumbo, J. (2013). Natural clay based adsorbent for defluoridation of groundwater: optimisation of adsorption conditions. 36th WEDC International Conference Nakuru, Kenya. 1-6

Gitari, Petrik, L. F., & Musyoka, N. M. (2016). Hydrothermal conversion of south african coal fly ash into pure phase zeolite Na-P1. *Zeolites: Useful Minerals*, 25.

Gitari, W. M., Izuagie, A. A., & Gumbo, J. R. (2020). Synthesis, characterisation and batch assessment of groundwater fluoride removal capacity of trimetal Mg/Ce/Mn oxide-modified diatomaceous earth. *Arabian Journal of Chemistry*, *13*(1), 1-16.

Gougazeh, M & Buhl, J. C (2014). Synthesis and characterisation of zeolite A by hydrothermal transformation of natural Jordanian kaolin, *Journal of the Association of Arab Universities for Basic and Applied Sciences*, 15 35–42.

Hollman, G. G., Steenbruggen, G., & Janssen-Jurkovicˇova, M. (1999). A two-step process for the synthesis of zeolites from coal fly ash. *Fuel*, 78 1225–1230.

© University of Venda

Höller, H., & Wirsching, U. (1985). Zeolite formation from fly ash. *Fortschritte der mineralogie*, *63* 1 21-43.

Horie, M., Fujita, K., Kato, H., Endoh, S., Nishio, K., Komaba, L. K., & Hagihara, Y. (2012). Association of the physical and chemical properties and the cytotoxicity of metal oxide nanoparticles: metal ion release, adsorption ability and specific surface area. *Metallomics*, *4*(4), 350-360.

Khandare, D., & Mukherjee, S. (2019). A Review of Metal oxide Nanomaterials for Fluoride decontamination from Water Environment. *Materials Today: Proceedings*, *18*, 1146-1155.

Kim, W., Choi, D & Kim, S (2010). Sonochemical synthesis of zeolite A from metakaolinite in NaOH solution, *Materials Transactions*, 51 1694–1698.

Luo, H., Law, W. W., Wu, Y., Zhu, W., & Yang, E. H. (2018). Hydrothermal synthesis of needle-like nanocrystalline zeolites from metakaolin and their applications for efficient removal of organic pollutants and heavy metals. *Microporous and Mesoporous Materials*, *272*, 8-15.

Nicholas, M. Musyoka., Leslie, F. Petrik., Wilson, M. Gitari., Gillian Balfour & Eric Hums (2012). Optimisation of hydrothermal synthesis of pure phase zeolite Na-P1 from South African coal fly ashes Optimisation of hydrothermal synthesis of pure phase zeolite Na-P1 from South African coal fly ashes. *Journal of Environmental Science and Health, Part A* 47, 337–350.

Mudzielwana, R., Gitari, M. W & Msagati, T. A. M. (2016). Characterisation of smectite-rich clay soil: Implication for groundwater defluoridation. *South African Journal of Science.* 112 11/12 1-8.

Mudzielwana, R., Gitari, W. M., Akinyemi, S. A., & Msagati, T. A. (2017). Synthesis, characterisation, and potential application of Mn 2^{+}-intercalated bentonite in fluoride removal: adsorption modeling and mechanism evaluation. *Applied Water Science*, *7*(8), 4549-4561.

Musyoka, N. (2009). *Hydrothermal synthesis and optimisation of zeolite Na-P1 from South African coal fly ash.* (Doctoral thesis, University of Western Cape, South Africa).

Musyoka, N. M., Petrik, L. F., Hums, E., Baser, H & Schwieger, W. (2012). In situ ultrasonic monitoring of zeolite-A crystallization from coal fly ash. *Catalysis Today.* 190 38–46

© University of Venda

Obijole, O. A., Gitari, M. W., Ndungu, P. G., & Samie, A. (2019). Mechanochemically Activated Aluminosilicate Clay Soils and their Application for Defluoridation and Pathogen Removal from Groundwater. *International Journal of Environmental Research and Public Health, 16*(4), 654.

Soulé, M. Z., Fernández, M. A., Montes, M. L., Suárez-García, F., Sánchez, R. T., & Tascón, J. M. D. (2020). Montmorillonite-hydrothermal carbon nanocomposites: Synthesis, characterisation and evaluation of pesticides retention for potential treatment of agricultural wastewater. *Colloids and Surfaces A: Physicochemical and Engineering Aspects*, *586*, 124192.

Wang, H., Feng, Q., Liu, K., Li, Z., Tang, X., & Li, G. (2017). Highly efficient fluoride adsorption from aqueous solution by nepheline prepared from kaolinite through alkali-hydrothermal process. *Journal of Environmental Management, 196*, 72-79.

Yao, G., Lei, J., Zhang, X., Sun, Z., & Zheng, S. (2018). One-step hydrothermal synthesis of zeolite X powder from natural low-grade diatomite. *Materials, 11*(6), 906.

Yoshimura, M., & Byrappa, K. (2008). Hydrothermal processing of materials: past, present and future. *Journal of Materials Science*, *43*(7), 2085-2103.

© University of Venda

University of Venda
Creating Future Leaders

CHAPTER SEVEN: APPLICATION OF POROUS-HYDROTHERMALLY-TREATED ALUMINOSILICATE CLAY (PHTAC) IN DEFLUORIDATION AND PATHOGEN REMOVAL FROM GROUNDWATER

7 Abstract

This chapter presents the performance of porous-hydrothermally-treated aluminosilicate clay (PHTAC) synthesised from hydrothermally-treated aluminosilicate clay (HTAC) in fluoride removal from groundwater and its potency towards pathogens. The physicochemical characterisation of PHTAC was carried out using FTIR, SEM-EDS, BET and XRD. Batch defluoridation studies were conducted to determine the optimum conditions for fluoride removal. The effect of competing ions and regeneration potential were also evaluated. Antibacterial studies were conducted using well assay diffusion method. The batch adsorption studies of PHTAC showed optimum 68% fluoride removal and adsorption capacity of 3.45 mg/g at 10 min contact time, 0.9 g /100 mL adsorbent dosage, 4.0 mg/L initial fluoride concentration, pH ≈ 4.0 and 250 rpm shaking speed at a temperature of 298 K. The adsorption isotherm modelling showed a good fit to both Langmuir and Freundlich isotherm models, thereby confirming both homogeneous and heterogeneous multi-site adsorption processes. The adsorption kinetics data also showed a good fit to both pseudo-first-order and pseudo-second-order models implying that fluoride sorption proceeded via both physiosorption and chemisorption respectively. Chloride and carbonate as co-existing ions in solution reduced the fluoride removal efficiency of the adsorbent material. The adsorbent was successfully reused for up to 8 regeneration-reuse cycles using 0.1 M KCl as regenerant. The PHTAC showed minimum inhibition zone towards *E. coli* strain of 15 mm, indicating its potency towards *E. coli*. The percent growth inhibition of the *E. coli* bacterial cell was 89 which is very close to 90 - 95% obtained in most government water treatment plants. The test of efficiency of PHTAC in field groundwater containing 3.94 mg/L initial fluoride concentration using 0.9 g/100 L adsorbent dosage at 10 min contact time showed its capability to reduce fluoride concentration from 3.94 mg/L to 1.35 mg/L, which is within the permissible WHO limits (1.5 mg/L). In conclusion, the adsorption efficiency and antibacterial potency of the synthesised PHTAC for fluoride and pathogen removal from groundwater improved over those of mechanochemically-activated clay (MAC) and HTAC synthesised in the preceding chapters.

© University of Venda

Keywords: Adsorbent, Aluminosilicate Clay soils, Defluoridation, Fluoride, Groundwater, Hydrothermal treatment, Pathogens, Pore-forming agent.

7.1 Introduction

Groundwater contamination by fluoride and pathogens, traced to natural and anthropogenic sources has been a great threat to human health worldwide, particularly in rural communities where potable treated pipe-borne water are not easily accessible (WHO, 2017; 2019). This has resulted in medical condition of dental, skeletal fluorosis (Mudzielwana *et al.*, 2017) and various forms of waterborne diseases. Several technologies have been proposed for water defluoridation among which are ion exchange (Pan *et al.*, 2018), chemical precipitation (Aldaco *et al.*, 2005), membrane filtration process (Kumar *et al.*, 2017), nanofiltration (Waghmare & Arfin, 2015), reverse osmosis (Bennajah *et al.*, 2009), electrocoagulation (Luna *et al.*, 2018) and adsorption (Gitari *et al.*, 2017). Adsorption technology is the most preferred due to environmental and economic advantages (Ghorai & Pant 2004; Mudzielwana *et al.*, 2016; Gitari *et al.*, 2013; 2016). In the preceding chapter, optimum conditions for synthesis of (porous) pore-forming-agent-modified-hydrothermally-treated aluminosilicate clay (PHTAC) from MAC and HTAC through introduction of pore-forming agent during hydrothermal treatment was successfully achieved. Characterisation and preliminary studies of all the synthesised products led to the selection of the optimum PHTAC synthesised. The optimised material exhibited enhanced morphology, increased surface area and alteration of crystalline particle sizes which promoted improved performance in preliminary defluoridation studies. In the quest to further evaluate the optimised material, batch defluoridation and pathogen removal efficacy were conducted, thus, the main objective of this chapter was to apply the optimally synthesised PHTAC adsorbent to batch defluoridation and disinfection of harmful pathogen from groundwater. This was achieved by (i) characterisation of the optimised PHTAC adsorbent synthesised, using FTIR, BET, SEM-EDS, XRD and XRF. (ii) batch adsorption experiments to evaluate the synthesised material defluoridation capabilities (iii) The adsorption kinetics and isotherms models were employed to elucidate the sorption kinetics and nature of the synthesised adsorbent. (iv) assessment of effect of co-existing ions (v) evaluation of its regeneration potential (vi) evaluation of the antibacterial efficacy of the synthesised PHTACadsorbent.

© University of Venda

7.2 Methods and materials

7.2.1 Sample collection, material and reagent preparation

Aluminosilicate clay samples were collected from Mukondeni village, Vhembe District in Limpopo Province, South Africa. Samples were collected and stored in polyethylene plastic bags. Prior to experiment, clays soil were prepared according to the procedures described in subsection 4.2.1. All the chemicals and reagents used in this study were analytical grade, produced by Sigma Aldrich. The list is as follows: NaOH pellets-anhydrous > 98%, NaF > 99%, $NaClO_3$, HCl, Na_2CO_3 > 99%, $NaNO_3$ > 99%, NaCl > 99%, Na_2PO_4 > 99%, Na_2SO_4, TISAB III solution. Volumes of 250 mL each of 0.5, 1, 1.5 and 2 M sodium hydroxide (NaOH) solutions were prepared in four separate 250 mL volumetric flasks according to procedures described in subsection 4.2.2.1 The solutions were kept in 250 mL plastic bottles with lid until when needed.

7.2.2 Synthesis of porous-hydrothermally-treated aluminosilicate clay (PHTAC) adsorbents

Prior to hydrothermal treatment of clay/NaOH/$NaClO_3$ slurry mixture, the raw clay was activated mechanochemically by milling at 700 rpm using a RS200 milling machine (Retch, Green Bay, WI, USA) for 30 min optimum contact time (Obijole *et al.*, 2019). Thereafter, clay powder was hydrothermally treated in the presence of pore-forming agent ($NaClO_3$) as follows: 100 mL of 1.5 M NaOH solution were pipetted into 250 mL heat resistant, high density plastic bottles followed by addition of 2 g of the activated clay. The slurry was aged by observing experimental protocol in subsection 4.2.2.1 and 4.2.2.2 respectively (Gitari *et al.*, 2016; Musyoka, 2009; Musyoka, Petrik & Hums, 2011). Thereafter, an optimum amount of 0.20 g $NaClO_3$ was added to 100 mL clay/NaOH slurry and thoroughly shaken together. Aliquots of 20 mL of the clay/NaOH/$NaClO_3$ slurry were transferred into a 45 mL Parr bomb vessels which were sealed and placed in the furnace at a predetermined temperature of 300 °C and 6 h optimum hydrothermal treatment time respectively. Thereafter, the solid products formed were dispersed in 500 mL of Milli-Q water to reduce the effect of high alkalinity of solution on the aluminosilicate clay adsorbent formed. The suspensions were passed through 0.45 µm pore polypropylene membrane filters in order to recover the solid. The solids were washed further with Milli-Q water until near neutral pH. Recovered residues were then oven dried at 110 °C for 6 h and then allowed to cool in a desiccator. Thereafter, residues (PHTAC) were milled to pass through < 250 µm sieve and then stored in plastic bottles to prevent moisture ingress (Wang *et al.*, 2017). The physicochemical,

© University of Venda

mineralogical characterisation as well as fluoride and pathogen removal efficiency of the optimised PHTAC product were conducted.

7.2.3 Physicochemical and mineralogical characterisation

The infrared spectrum of the developed PHTAC and fluoride-loaded adsorbent were investigated for functional groups using Alpha FTIR spectrometer (Bruker, Germany: ATR-Diamond FTIR spectrophotometer) in the range of 4500 - 500 cm^{-1}. The PHTAC surface and specific area, pore volumes and sizes were measured with Micromeritics TriStar II surface area and porosity unit instrument (Micromeritics, Norcross, GA, USA). Scanning electron microscope was used to characterise the synthesised PHTAC and fluoride-loaded PHTAC to understand their surface properties responsible for fluoride sorption. SEM was conducted using JEOL - 2100 Electron microscope TESCAN, Vega 3XMU (TESCAN, Brno, Czech Republic). XRD qualitative and quantitative (mineralogy) analysis was conducted via standardised Pan-analytical backloading system, which provided nearly random distribution of the particles. Examination of qualitative and quantitative mineral phase composition was conducted using a D8 advance X-ray diffraction (Bruker, Germany) equipped with Cu- Kα source radiation. The mineralogy was determined by selecting the best–fitting pattern from the ICSD database to the measured diffraction pattern, using X'Pert Highscore plus software. The relative phase amounts (weight% of crystalline portion) were estimated using Rietveld method (X'Pert High score Program).

7.2.4 Batch defluoridation experiments

Batch adsorption experiments were conducted to evaluate the effects of contact time, adsorbent dosage, pH and adsorbate concentration on fluoride removal by PHTAC. Evaluation of the effect of contact time was carried out using 1.0 g/100 mL adsorbent dosage, 4.0 mg/L initial fluoride concentration and initial pH of ≈ 4.0. The mixtures were shaken at 250 rpm while varying the contact time from 1 to 80 min at 298 K. After equilibration, mixtures were centrifuged for about 30 min at 4000 rpm and the supernatants analysed for residual fluoride by using a four-standard calibrated ORION fluoride ion-selective electrode. TISAB III solution was added to both standards and samples at volume ratio of 1:10 to de-complex fluoride ions. The effect of adsorbent dosage was evaluated using initial concentration of ≈ 4 mg/L and varying adsorbent dosage from 0.1 to 1.5 g/100 mL. Mixtures were agitated for optimum contact time of 10 min at 250 rpm. The adsorption isotherms were studied by varying the initial concentration of the fluoride ions from 1

© University of Venda

to 100 mg/L while the optimum adsorbent dosage of 1.0 g/100 mL was added and the mixtures agitated for 10 min optimum contact time. To evaluate the effect of pH, the mixtures' pH was adjusted between 2 and 12 using 0.1 M NaOH and 0.1 M HCl respectively. Optimum adsorbent dosage of 0.9 g/100 mL, 10 min contact time and 4 mg/L initial fluoride concentration were used. The effect of co-existing ions on defluoridation in the presence of separate 10 mg/L of chloride, nitrate, phosphate, carbonate and sulphate was evaluated at initial fluoride concentration of 10 mg/L using 1.0 g/100 mL adsorbent dosage at initial pH 6.9 ± 0.1 with the mixtures agitated for 30 min. All the experiments were carried out in duplicates and the mean values reported.

The percent fluoride removal and adsorption capacity were derived from equations 7.1 and 7.2, respectively.

$$\text{Percent fluoride removal} = \frac{(C_o - C_e)}{C_o} \times 100 \quad (7.1)$$

$$\text{Adsorption capacity, } q = (C_o - C_e) \times \frac{V}{m} \quad (7.2)$$

Where q is the mass of fluoride adsorbed in mg/g of adsorbent, C_o *and* C_e are the initial and equilibrium concentrations of fluoride respectively, *V i*s the volume of the solution in litres and m is the mass in gramme of the developed PHTAC

7.2.5 Regeneration potential experiment

Fluoride-loaded PHTAC was regenerated by agitating 1.0 g of loaded PHTAC separately with 100 mL of 0.1 M NaOH and 0.1 M KCl on a mechanical shaker for 30 min. Thereafter, the mixtures were filtered using a 0.45-µm pore membrane filter and then the resulting filtrate diluted to 100 mL and analysed for fluoride desorbed. The resulting PHTAC residues were thoroughly washed on the filter paper with deionised water and oven-dried at 110 °C for 4 h. Batch experiments were carried out on the regenerated PHTAC adsorbent. The regenerated-reuse experiments were repeated up to eight times.

7.2.6 Antibacterial studies

Antibacterial activities of the synthesised PHTAC adsorbent were evaluated with *Escherichia coli* (*E. coli*) strains by using well diffusion assay method. The well diffusion assay method is a simple and standard antibacterial testing procedures worldwide. The zone of inhibitions was recorded in millimeter (mm). The bacterial suspensions were prepared with the turbidity of 0.5 McFarland. Muller-Hinton agar was also prepared by methods earlier described in

© University of Venda

subsection 5.2.6 and placed into plates, which were inoculated with the strains of *E. coli*. Wells with 6 mm diameter were bored with a cork borer and filled with 30 µL of four of the PHTAC slurry on a plate against the bacterial strain. The plates were incubated for 24 h at 37 °C. Thereafter, the growth inhibition zone diameters were measured. The agar plates and PHTAC sample used in this study were carefully packaged in disposable plastic bags, sealed and sent for immediate destruction as soon as measurements were concluded.

Furthermore, the antibacterial potency of the synthesised PHTAC sorbent against *E. coli* in water was further tested using a modified liquid culture technique and UV-visible spectrophotometry (Adeeyo *et al.,* 2015). For the test, 0.9 g of the PHTAC sorbent was introduced into fluoride-rich raw Siloam groundwater with standardised *E. coli* cells. Bacteria subculture was made in broth and washed aseptically (Pritchard *et al.,* 2008). Resuspension was made in 1000 mL of natural fluoride-rich raw Siloam groundwater as final working culture suspension. The preparation was confirmed using gram staining techniques and API-20E bacteria identification test kit. The count per 100 mL working solution was adjusted to 30,000 ($3x10^4$) colony-forming unit (cfu) by plate count technique. It has been reported that most surface and groundwater hold about $3x10^4$ cfu of *E.coli* per 100 mL of water (Pritchard *et al.,* 2008). The control sample consist of the bacterial suspension without the addition of the treatment (PHTAC). The sorption experiment was set up at optimised parameters obtained in the study (synthesis of PHTAC) in replicates. The treatment potential of synthesised PHTAC against the bacterial strains in water suspension was considered as the optical density (OD) at 600 nm and the percent growth inhibition was calculated.

Percent (%) $growth\ inhibition = \frac{(AbsControl - AbsTest)}{AbsControl} \times 100$

where Abs is absorbance reading.

7.3 Results and discussions

7.3.1 Physicochemical characterisation

7.3.1.1 Fourier transform infra-red (FTIR) analysis

Figure 7.1 presents the FTIR spectra and functional groups of the MAC, HTAC, PHTAC and fluoride-loaded PHTAC samples, which were scanned between 550 and 4000 cm^{-1} range.

The spectra of the porous-hydrothermally-treated aluminosilicate clay (PHTAC) are different from MAC, HTAC and fluoride-loaded PHTAC. The major transmittance bands were

© University of Venda

observed around 3000 - 3800 cm^{-1}, 1300 - 1800 cm^{-1} and 500 - 1200 cm^{-1}. The bands around 3400 and 3700 cm^{-1} were due to OH stretching mode while bands at 1600 - 1650 cm^{-1} were attributed to H-O-H bending of water. The main functional groups of Si-O-Si and Al-O-Al and dominant bands of MAC, HTAC, PHTAC and fluoride-loaded PHTAC were observed around 950 - 1050 cm^{-1} and 500 - 650 cm^{-1} region respectively (Kim *et al.,* 2010; Mikuła *et al.,* 2015; Marsha *et al.,* 2019).

The transmittance bands at around 650 and 950 cm^{-1} became sharper and intense in HTAC at elevated hydrothermal temperature owing to formation of strong Al-O-Al, Al-O-Si and Si-O-Si bonds. The disappearance of transmittance bands around 3000 to 3600 and 2100 to 2300 cm^{-1} ascribed to stretching and vibration of the OH groups is indicative of moisture and hydroxyl group lost from within the hydrothermally-treated clay interlayers at elevated temperatures (Toor *et al*., 2014). The disappearance of transmittance bands around 3000 - 3600 and 2100 cm^{-1} observed in the hydrothermally-treated clay samples is suggestive of absence of O-H bands at elevated temperature while the observed bands around 1500 - 1800 cm^{-1} in the treated samples suggest the formation of Na-O bands from the sodium aluminosilicate precursor, NaOH and $NaClO_3$ used in the ageing and hydrothermal treatment processes. The alkaline activation and introduction of $NaClO_3$ (pore formers) at elevated temperatures played a major role in the treated material surfaces alteration. The disappearance of transmittance bands around 750 - 850 and 2000 - 3700 cm^{-1} was due to the breakdown of O-H bonds while strong transmittance appearance around 600 - 650 cm^{-1} and 950 cm^{-1} was due to strong Al-O and Si-O bonds formation during treatment. The characteristic transmittance bands of the fluoride-loaded PHTAC showed a slight decrease in specific bands intensity at 3700 - 3500, 2850, 1490 and 950 cm^{-1} and around 650 cm^{-1} when compared with others. The observed transmittance reduction indicated that the created available sites in the modified products had been occupied by fluoride as fluoride removal progresses which is suggestive of fluoride uptake due to transmittance bands attributable to Al-F and Si-F bonds around 600 - 650 cm^{-1}.

© University of Venda

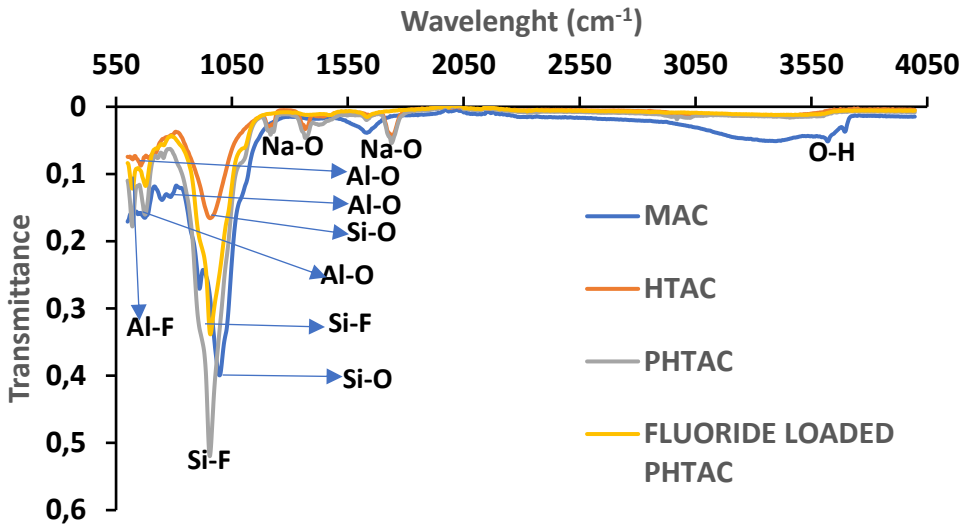

Figure 7.1: FTIR spectra of (a) MAC (b) HTAC (c) PHTAC (d) Fluoride-loaded PHTAC.

7.3.1.2 Surface area by Brunauer-Emmett-Teller (BET)

Brunauer-Emmett-Teller (BET) surface area results of PHTAC, HTAC and MAC is summarised in Table 7.1. There was an increase in the surface area from 17.19 m^2/g in MAC to 33.25 m^2/g in HTAC, which further increased to 52.83 m^2/g in PHTAC while there was no significant change in the pore volumes and sizes. The progressive increase observed in surface area is an indication of surface alteration during modification process. This could be due to the pop up of the aluminosilicate clay interlayer structure during the hydrothermal treatments and introduction of the pore former ($NaClO_3$.). The average pore distribution (bulk) of the precursor materials and the PHTAC is within the mesoporous range (Figure 7.2 a, b, and c). Also, the nitrogen adsorption-desorption isotherm curves for raw MAC, HTAC and PHTAC are shown in Figure 7.2 d, e and f. The adsorption-desorption curves for all the materials are similar, but quantity (volume) of adsorbed paticles is higher in HTAC and PHTAC, which is suggestive of increasing mesoporosity consequent upon hydrothermal treatment and introduction of pore formers respectively at elevated temperatures.

© University of Venda

Table 7.1: BET surface area, surface area single point, pore volumes and sizes of MAC, HTAC and PHTAC

Samples	BET surface area (m^2/g)	Surface area single point (m^2/g)	Pore volume (cm^3/g)	Pore size (nm)
MAC	17.19	16.66	10.06	14.92
HTAC	33.25	32.02	10.12	15.27
PHTAC	52.83	49.14	10.13	15.90

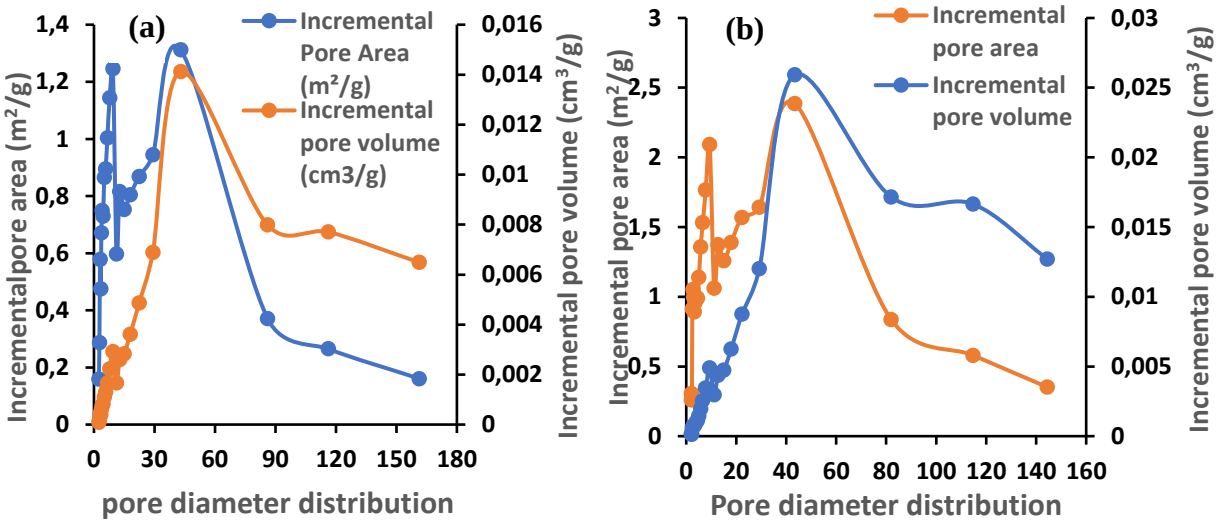

© University of Venda

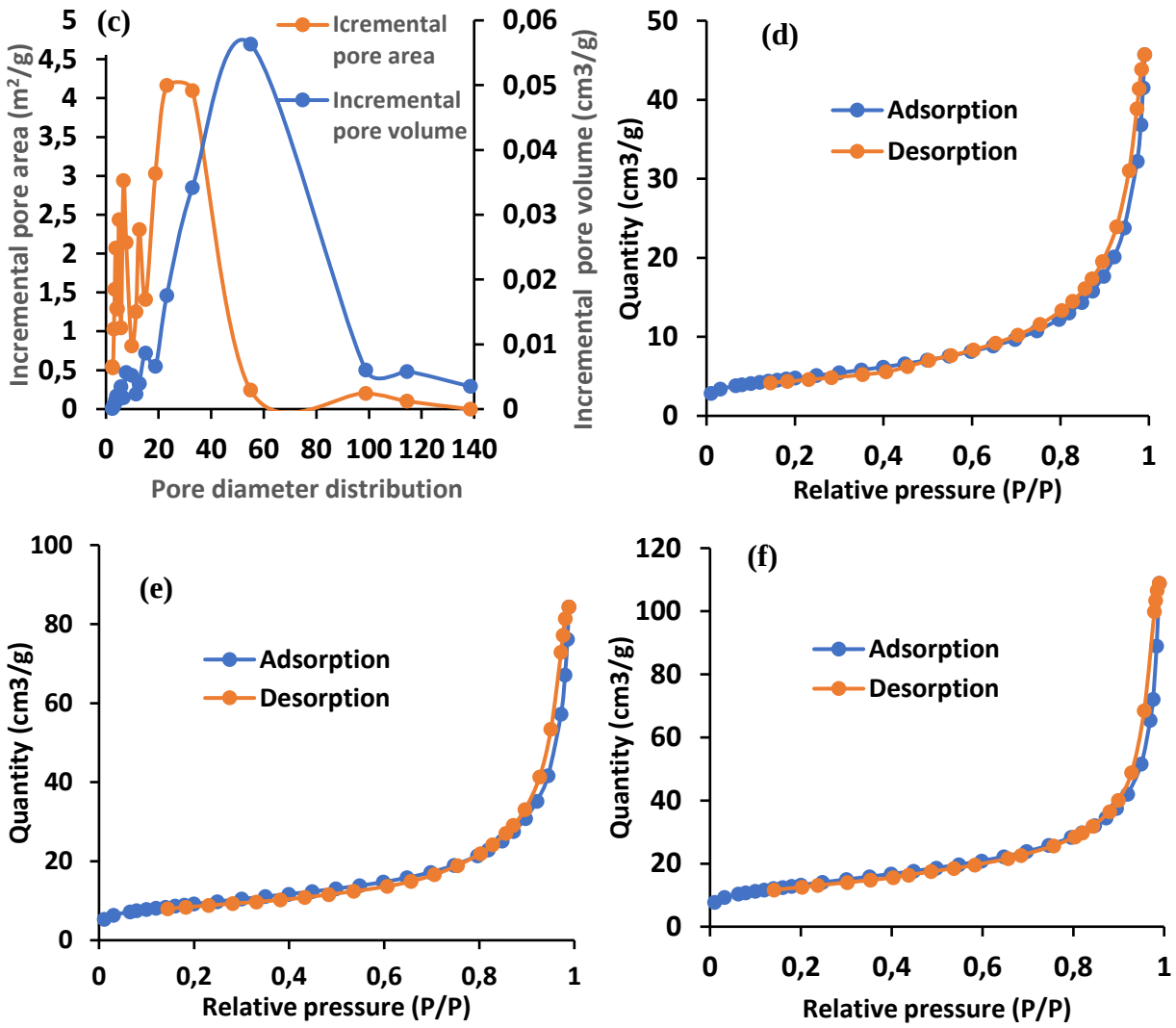

Figure 7.2: Pore distribution curves for (a) MAC (b) HTAC and (c) PHTAC; Nitrogen adsorption-desorption curves for (d) MAC (e) HTAC and (f) PHTAC.

7.3.1.3 Morphology analysis

Figure 7.3 presents the SEM-EDS micrographs of MAC, HTAC and PHTAC. The micrograph of MAC shows expanded arrays of irregular, flared, corn flakes and platy-like structures (Figure 7.3 a) which changed to irregular shapes and sizes particles on the external surface with porous crystalline microspheric geopolymer gel structure, HTAC (Figure 7.3 b) while further chemical transformation in the PHTACs products in the course of treatment produced porous geopolymeric gels with fine crystalline, long prismatic needle-like textures interlaced with pores (Figure 7.3 c).The images revealed nano-sized particles for all the micrographs as confirmed by their BET particle size analysis results. Elemental analysis is presented in Figure 7.3 (a - c).

© University of Venda

EDS revealed elements such as silicon, aluminium, sodium, magnesium, iron, calcium etc increased progressively from MAC to HTAC and PHTAC as hydrothermal treatment progressed. The increased in the levels of Na cations observed in PHTAC might be due to Na ions introduced from the decomposition of pore-forming agent ($NaClO_3$). The increase in concentrations of some of the exchangeable base cations such as magnesium iron, calcium, potassium, titanium and sodium during hydrothermal treatment in the presence of pore formers led to increase in positive charges on the PHTAC surfaces and hence, increase in fluoride adsorption via electrostatic attraction of the fluoride ions onto the highly positive surfaces of the material (Konta, 1995; Byrappa & Yoshimura, 2006, 2012).

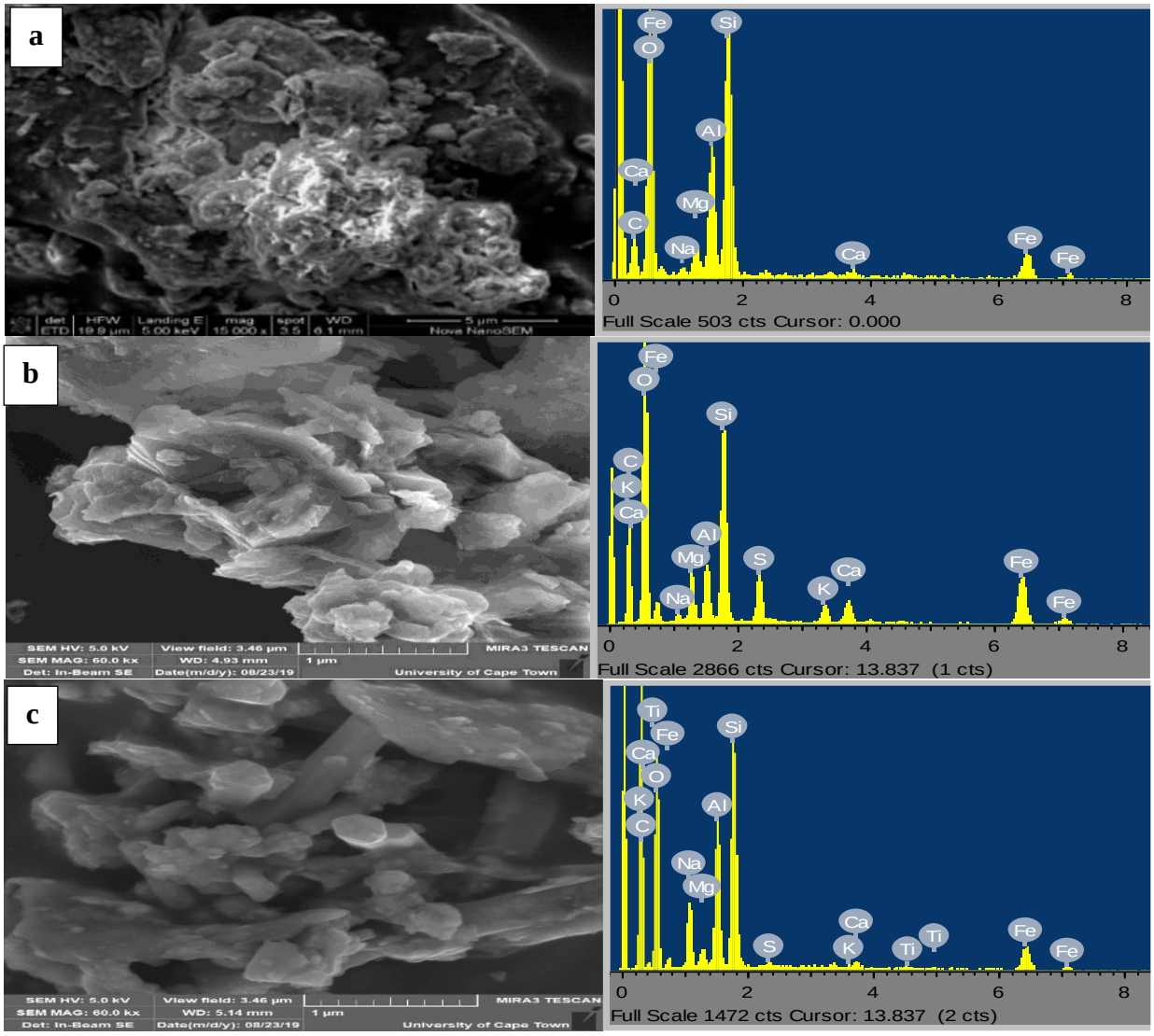

Figure 7.3 SEM-EDS Micrographs of (a) MAC (b) HTAC and (c) PHTAC.

© University of Venda

7.3.1.4 X-ray diffraction (XRD)

The XRD qualitative results of MAC, HTAC and PHTAC are presented in Figure 7.4. There was an appearance of new mineral phases, disappearance of some phases, increase and decrease of some phases in the MAC, HTAC (without pore formers) and PHTAC (with pore formers) as hydrothermal treatment progressed at different syntheses conditions. New phases observed in the HTAC (without pore formers) are new zeolitic phases such as hydroxy sodalite (HS) with traces of phillipsite (Ph) and chlorite (Ch) (Gougazeh *et al.*, 2014) while chabazite, microcline montmoronollite which was identified through prominent peaks at 6.5°, 12°, 18° and 28° two theta, which were present in MAC disappeared in HTAC. PHTAC (with pore formers) had the following new phases: zeolite, hydroxy sodalite and hydroxy sodalite hydrate while albite and quartz mineral, which were present in HTAC disappeared in PHTAC. The most important of these changes are the transformation to hydroxy sodalite hydrate (HS) and cancrinite, which are critical to enhancement of surface properties responsible for high fluoride sorption in PHTAC when compared to other materials. The changes observed in the mineral composition during treatment (with or without pore formers) were due to chemical transformation, which occurred via recrystallisation process. This result was further confirmed by the changes in the FTIR characteristic peak intensities as one moves from HTAC to PHTAC. SEM micrographs of HTAC materials showed transformation from geopolymeric gel structure with microspheres to fine geopolymer gel with crystalline piston-like morphology interlaced with pores. Studies showed that morphology of the geopolymeric gel materials are affected by the mediums' characteristics and the chemical species which acted as templates around which the aluminosilicate polymerises to produce the microspheres and long crystalline prismatic particles interlaced with pores in both HTAC and PHTAC. The SEM (Öztop & Shahwan, 2006). Studies by Obijole *et al.* (2019) on smectite clay showed similar characteristic peaks and mineral phases for the MAC sample. The change observed in the characteristic peak intensities in the HTAC and PHTAC are confirmed by SEM images, which showed geopolymer gel-like materials with aggregated microsphere particles in HTAC transformed into geopolymeric crystalline long piston-like particles interlaced with pores. These results further corroborate the qualitative results. The trend of morphological changes corresponds to the chemical transformation, which led to increased surface area in PHTAC, thus, having a more positive impact on defluoridation potentials compared to MAC and HTAC.

© University of Venda

Hydrothermal treatment was observed to bring about complete dissolution of the slurry and the partial dissolution of quartz led to the release of free aluminium and silicon species (Esaifan *et al.*, 2019). Also, the dominant appearance of XRD transmittance bands assigned to cancrinite and hydroxy-sodalite indicated the crystallisation of released aluminium and silicon species and reaction with calcite to form cancrinite. Once the calcite was consumed, hydroxy-sodalite started to crystallise. This observation is confirmed by the studies conducted by Esaifan *et al.* (2019). Furthermore, the high adsorption capacity-synthesised hydroxy-sodalite and canrinite-rich geolitic PHTAC material is a confirmation of a successful synthesis.

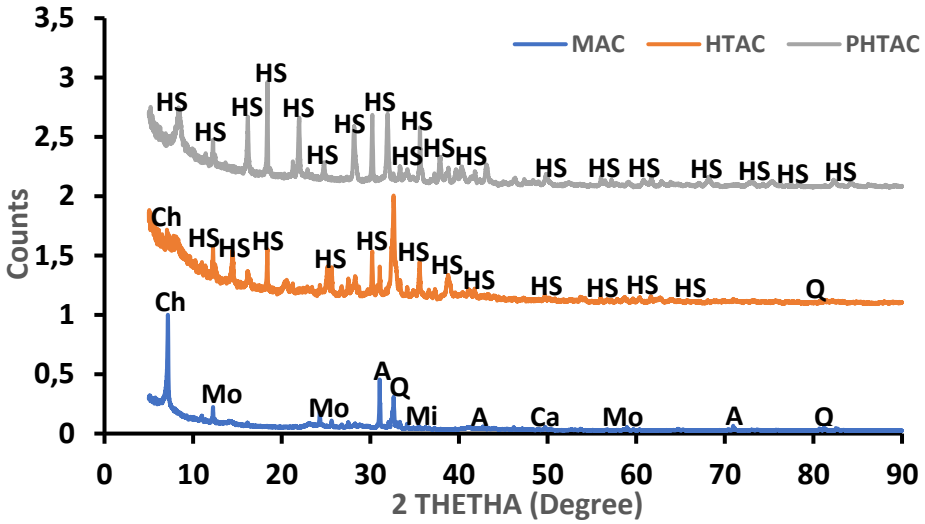

Figure 7.4: The X-ray diffraction (XRD) spectra of MAC, HTAC and PHTAC.
Footnote: (Mnt - montmorillonite, Al - albite, M - muscovite, Q - quartz, A - zeolite, HS - Hydroxy sodalite hydrate).

7.3.1.5: X-ray fluorescence analysis (XRF)

Table 7.2 presents the elemental composition of the raw MAC, HTAC and PHTAC products. From the table, all the products are aluminosilicate materials since silica (SiO_2) and alumina (Al_2O_3) were observed to be the major composition. After the hydrothermal treatment, the SiO_2 and Al_2O_3 content were observed to decrease progressively from MAC to HTAC and PHTAC respectively, while the Na_2O content increased in the order MAC (0.7%) < HTAC (5%) < PHTAC (12%). This observation indicates that Na^+ was substantially incorporated into the precursor material during hydrothermal treatment, while further addition of pore-forming agent ($NaClO_3$) resulted in higher Na_2O content in PHTAC. Even though, the excess NaOH in the reaction products was washed by repeated centrifugation using deionised water until the solution pH reached ≈ 8. Hence, the XRF results indicates Na was chemically incorporated into SiO_2 and Al_2O_3 in the clay

© University of Venda

matrix leading to the decrease SiO_2 and Al_2O_3 and increase Na_2O contents in the HTAC and PHTAC products (Luo *et al.*, 2018).

Table 7.2: Elemental composition of MAC, HTAC and PHTAC

	Content (%)		
Oxides	MAC	HTAC	PHTAC
SiO_2	52.48	45.92	42.34
Al_2O_3	24.62	24.23	21.42
Fe_2O_3	6.64	7.56	7.89
MgO	2.985	4.56	6.24
CaO	1.53	3.21	3.56
K_2O	1.24	1.32	1.43
Na_2O	0.707	5.45	12.21
TiO_2	0.627	1.23	1.76
MnO	0.125	0.261	0.231
P_2O_3	0.034	0.0425	0.327
SO_3	0.023	0.026	0.054

7.3.2 Batch defluoridation

7.3.2.1 Contact time and adsorption kinetics

The effect of contact time on fluoride removal is presented in Figure 7.5. An increase in fluoride removal from 46% to 68% was observed from 5 - 10 min and thereafter stabilised with further increase in contact time. The increase was due to availability of sorption sites on the adsorbent surfaces while stabilisation observed at about 10 min was due to saturation at the surfaces, which suggests that equilibrium had been reached (Obijole *et al.*, 2019). Therefore, 10 min contact time was taken as the optimum equilibration time for subsequent experiments.

© University of Venda

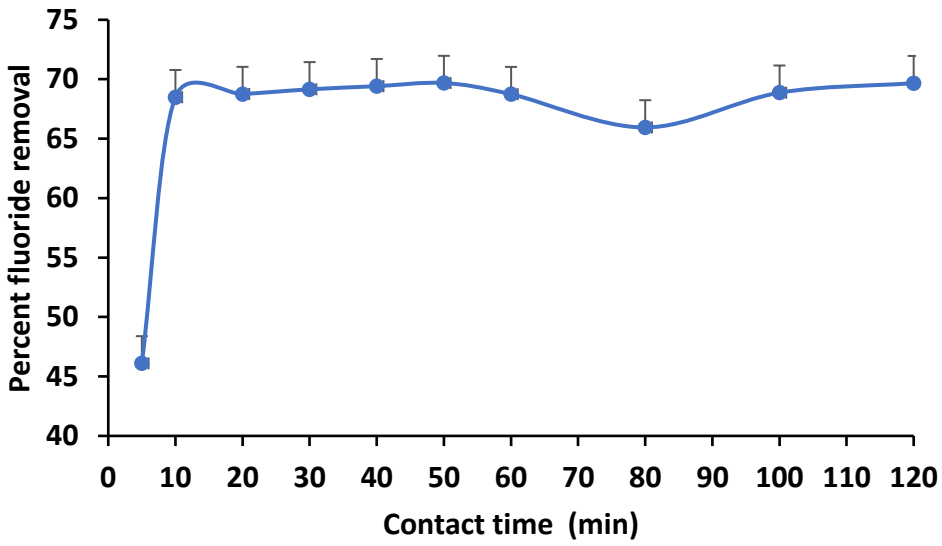

Figure 7.5: Variation of percent fluoride removal with contact time **(**at 10 min contact time, 0.9 g/100 mL dosage, 4.0 mg/L initial fluoride concentration, pH ≈ 4.0, 250 rpm shaking speed and temperature of 298 K).

To elucidate the possible fluoride adsorption mechanism and the rate limiting factors, the non-linear equations of pseudo-first-order and pseudo-second-order models as well as Weber-Morris intra-particle diffusion models (Yoon *et al.*, 2017) were applied. The adsorption kinetics studies were carried out using pseudo-first-order (PFO) and pseudo-second-order (PSO) models to establish the sorption mechanism and fluoride removal adsorption rate of the synthesised PHTAC (Lagergren, 1898: Qureshi *et al.*, 1995: Ho *et al.*, 2000: Yoon *et al.*, 2017: Ngulube *et al.*, 2017: Denga *et al.*, 2018). The pseudo-first and second-order models are expressed by the non-linearised mathematical equations 7.3 and 7.4 respectively:

$$q_t = q_e\,(1 - e^{-K_{ad}t}) \qquad (7.3)$$

$$q_t = \frac{q_e^2\,K_{2ads}\,t}{1 + K_2 q_e^2\,t} \qquad (7.4)$$

Where q_e and q_t are the adsorbed fluoride per unit mass (mg/g) at equilibrium and time, t (min), K_{ad} (min^{-1}) and K_{2ads} ($g.mg^{-1}/min$) are rate constants for pseudo-first-order and pseudo-second-order respectively. Figure 7.6 depicts pseudo-first-order and second-order plots respectively while Table 7.3 presents the derived adsorption modelling parameters values values of pseudo-first-order and pseudo-second-order kinetics respectively.

© University of Venda

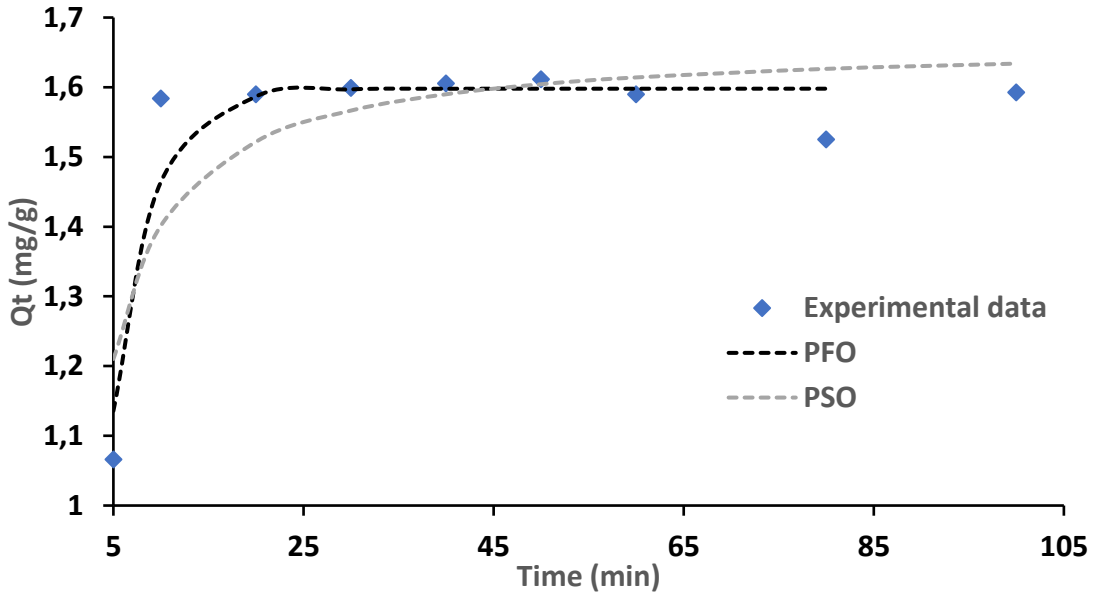

Figure 7.6: Pseudo-first-order (PFO) and Pseudo-second-order (PSO) kinetic model plot of fluoride uptake by the PHTAC (initial fluoride concentration = 4.0 mg/L, adsorbent dosage = 0.9 g/100 mL, temperature = 298 K and shaking speed of 250 rpm).

Table 7.3: The kinetic parameters for pseudo-first-order and pseudo-second-order models.

Models	Values
Pseudo-first-order (PFO)	
q_{cal} (mg/g)	1.59
K_{1ad} (min^{-1})	0.24
R^2	0.99
RMSE	0.055
X^2	0.001
Pseudo-second-order (PSO)	
q_{cal} (mg/g)	1.66
K_{2ads} (g min^{-1} mg)	0.32
R^2	0.99
RMSE	0.0952
X^2	0.0052

Adsorption kinetics data in Table 7.3 shows high co-efficient of determination (R^2) value for both pseudo-first-order (PSO) (R^2 = 0.99) and pseudo-second-order (PFO) (R^2 = 0.99) and low values of residual root mean square error (RMSE) of 0.05 and 0.09 for pseudo-first-order and pseudo-second-order kinetics respectively while X^2 gives a low values of 0.001 and 0.005 for pseudo-first-order and pseudo-second-order models respectively, hence indicating that adsorption

© University of Venda

of fluoride onto the PHTAC depended on both physiosorption and chemisorption (Yoon *et al.*, 2017: Ayinde., 2020). Similar trends were observed and postulated in similar studies (Qureshi *et al.*, 1995: Ho *et al.*, 2000: Yoon *et al.*, 2017; Ayinde *et al.*, 2020).

The intra-particle diffusion model (Figure 7.7) showed two distinct phases. The first phase (phase 1) could be attributable to boundary layer adsorption in which the fluoride ions are transferred from the bulk solution into the boundary layer of the PHTAC adsorbents' surface via physical attraction. The second phase (phase 2) represents the intra-particle diffusion where we have the fluoride ions being diffused into the PHTACs micropores and mesopores and interact with molecules within the particles resulting in chemisorption. The rate constants of adsorption k_{1ad} determined from the slope were found to be higher during phase 1, suggesting faster adsorption compared to intra-particle diffusion phase 2 which is slower as equilibrium is attained. The constant, *C*, related to the boundary layer thickness showed an increase from phase 1 to 2, suggestive of increase in boundary layer of the adsorbent particles (Table 7.4).

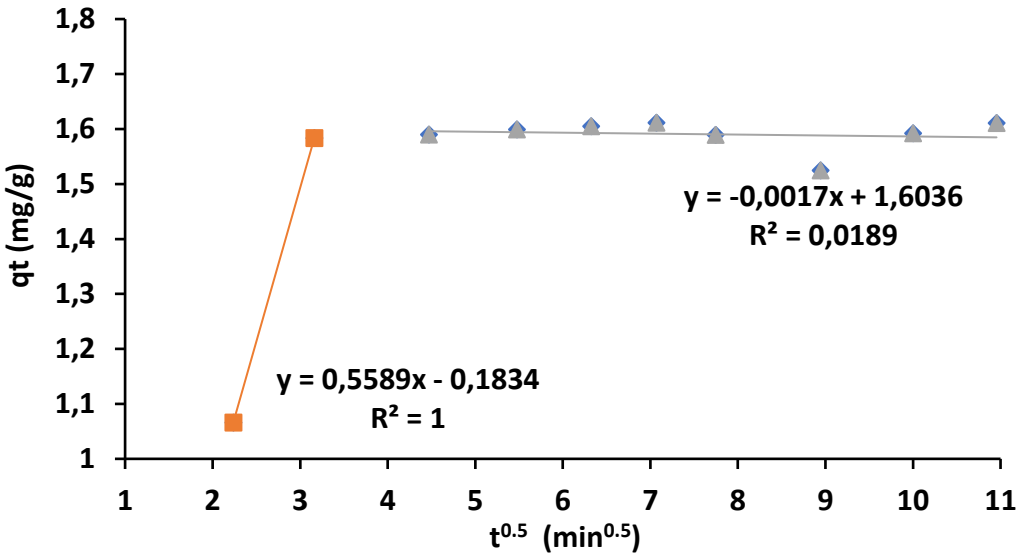

Figure 7.7: Intra-particle diffusion plot of fluoride sorption on the PHTAC (adsorbent dosage = 1.0 g/100 mL, initial fluoride concentration = 10 mg/L, temperature = 298 K and shaking speed = 250 rpm).

Table 7.4: Parameters for intra-particle diffusion model

Intra-particle diffusion					
k_i	k_p	C_i (mg/g)	C_p (mg/g)	R_1^2	R_2^2
1.28	3.94×10^{-4}	1.8×10^{-1}	1.6	1	0.02

© University of Venda

7.3.2.2 Effect of adsorbent dosage

The effect of adsorbent dosage on percent fluoride removal and adsorption capacity is presented in Figure 7.8. The percent fluoride removal was observed to increase gradually from 0.1 to 0.9 g/100 mL where maximum uptake of 69% was reached. Thereafter, slight changes were observed as the dosage increased to 1.5 g/100 mL, indicating that the system had reached equilibrium. A general increase in percent fluoride removal could be ascribed to more adsorption active sites for fluoride sorption leading to higher fluoride uptake. The optimum dosage of 0.9 g/100 mL was therefore selected for subsequent experiments.

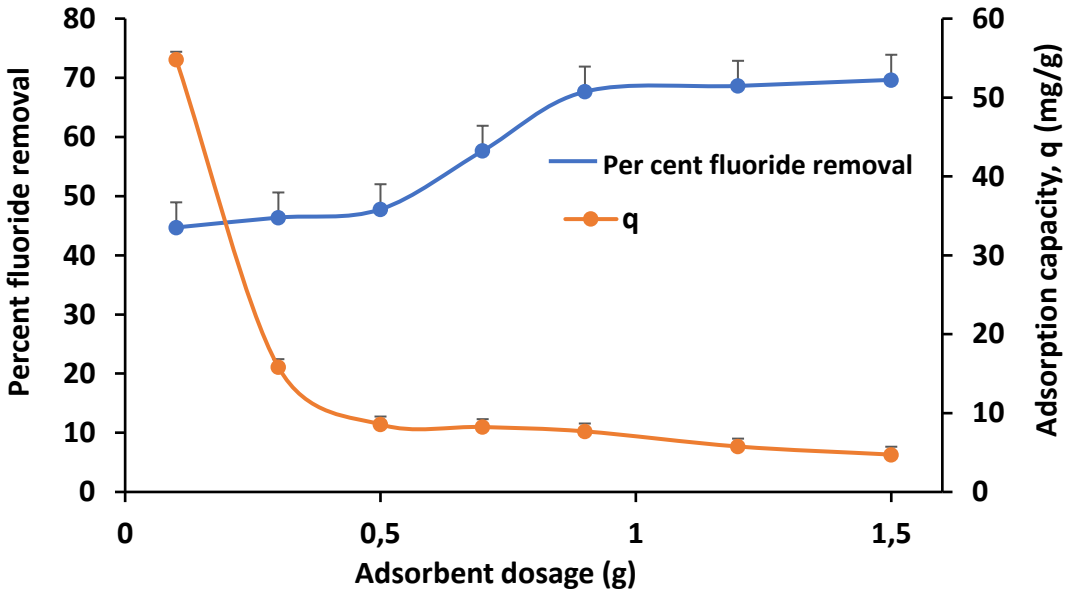

Figure 7.8: Variation of percent fluoride removal and adsorption capacity with adsorbent dosage (initial fluoride concentration = 4.0 mg/L, volume of solution = 100 mL, optimum contact time = 10 min, initial pH ≈ 4.0, temperature = 298 K and shaking speed = 250 rpm).

7.3.2.3 Effect of pH

The effect of initial pH on percent fluoride removal is presented in Figure 7.9. The effect of initial pH on fluoride removal was evaluated by varying the initial pH of the mixtures from 2 to 12, using 0.1 M HCl and 0.1 M NaOH. The per cent fluoride removal was observed to be optimum at 60% at low pH ≈ 3, due to increase in surface area consequent upon hydrothermal treatment in the presence of pore formers and thereafter decreased to about 40% and stabilises at pH ≈ 4 - 6 after which a gradual decrease to about 30% was observed from pH 7 - 12 (Figure 7.9). Figure 7.10 presents the pH at point-of-zero charge (pH_{pzc}) of optimised between PHTAC. The point-of-

© University of Venda

zero charge was assessed to be 4.5 ± 0.5. This suggests that at pH below 4.5 ± 0.5 the surface is positively charged while above this pH the surface is negatively charged. Therefore, higher fluoride removal at pH below pH_{pzc} is ascribed to electrostatic attraction onto the positively charged surface of the material and negatively charged fluoride ion while the reduction could be ascribed to the repulsion forces between the fluoride ion and negatively charged surface. Hence, optimum pH of 4.5 was selected.

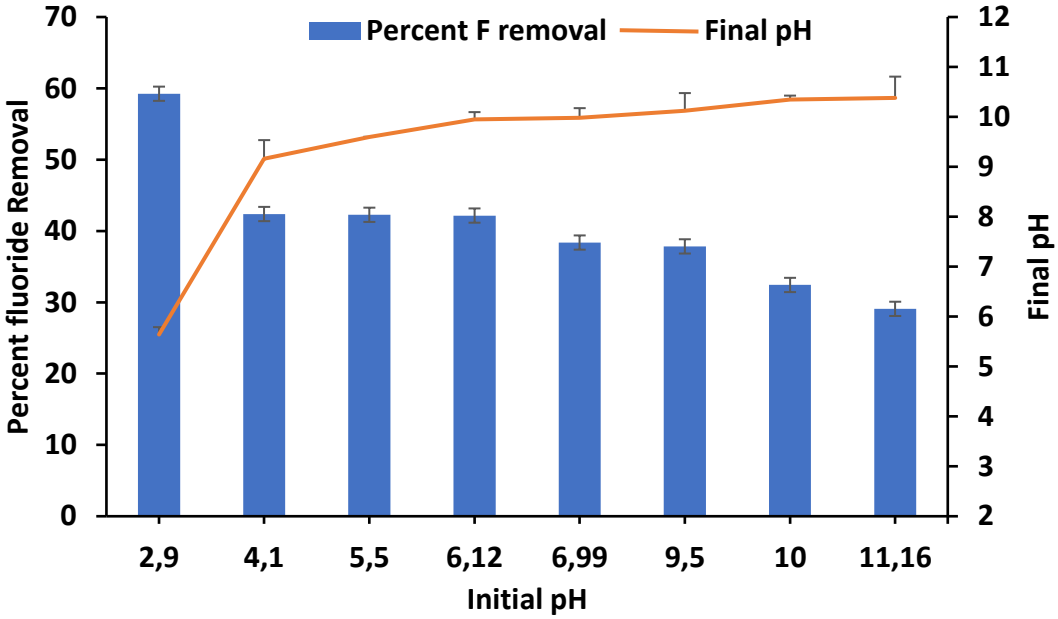

Figure 7.9: Variation of percent fluoride removal and final pH with initial pH (initial fluoride concentration = 4.0 mg/L, volume of solution = 100 mL, optimum dosage = 0.9 g, optimum contact time = 10 min, temperature = 298 K and shaking speed = 250 rpm. The was varied between 2 and 12).

© University of Venda

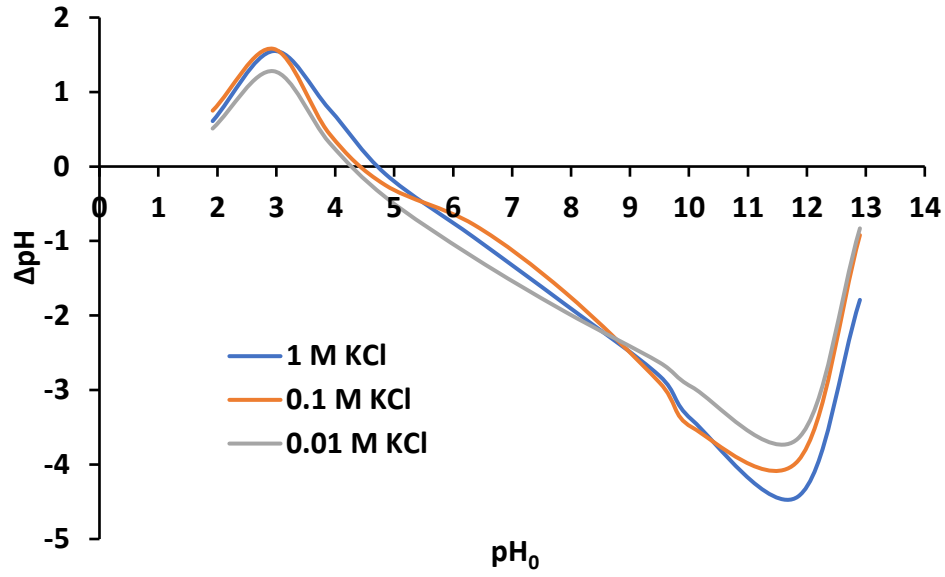

Figure 7.10: Point-of-zero charge (pH_{pzc}) of PHTAC adsorbent using 1 M KCl, 0.1 M KCl and 0.01 M KCl (adsorbent dosage = 4.0 g/100 mL, contact time = 24 h, agitation/shaking speed = 250 rpm and temperature = 298 K).

The mechanism of fluoride removal is governed by the pH of solution. At pH below 4.5 ± 0.5 where PHTAC surface is positively charged, fluoride ions were removed via electrostatic attraction (Equation 7.5) as well as ligands exchange mechanism where fluoride ions forms strong complexes in the inner sphere of the adsorbent (Equation 7.6). At pH between 4 and 6 where the surface is circum neutral and also at pH > 7 where negative charges dominate the surface of the materials; fluoride ions were removed through ion exchange (Equation 7.7).

$$\equiv \mathrm{PHTACOH^+} + \mathrm{F^-} \leftrightarrow \equiv \mathrm{PHTACOHF} \quad (7.5)$$

$$\equiv \mathrm{PHTAC(OH)_3^-} + \mathrm{F^-} \leftrightarrow \equiv \mathrm{PHTAC(OH)_2F^-} + \mathrm{OH^-} \quad (7.6)$$

$$\equiv \mathrm{PHTAC(OH)_2} + \mathrm{F^-} \leftrightarrow \equiv \mathrm{PHTACOHF} + \mathrm{OH^-} \quad (7.7)$$

7.3.2.4 Effect of fluoride concentrations

The effect of initial fluoride ion concentration on percent fluoride removal is presented in Figure 7.11. There was a sharp increase in per cent fluoride removal (from 43 to 58%) as the initial fluoride concentration increased from 1 - 5 mg/L and thereafter steadily decreased (from 58 to 30%) with a further increase in the initial fluoride concentration from 5 to100 mg/L (Figure 7.11). The increase in fluoride uptake at low initial fluoride concentration was due to availability of positive/binding sites at lower fluoride ions in solution This peaked at 5 mg/L and thereafter slowly decreases with increasing initial fluoride concentration, competing for fewer positive/binding sites

© University of Venda

on the PHTAC adsorbent surfaces. Hence, an initial fluoride concentration of 5 mg/L was taken as the optimum concentration for subsequent experiments.

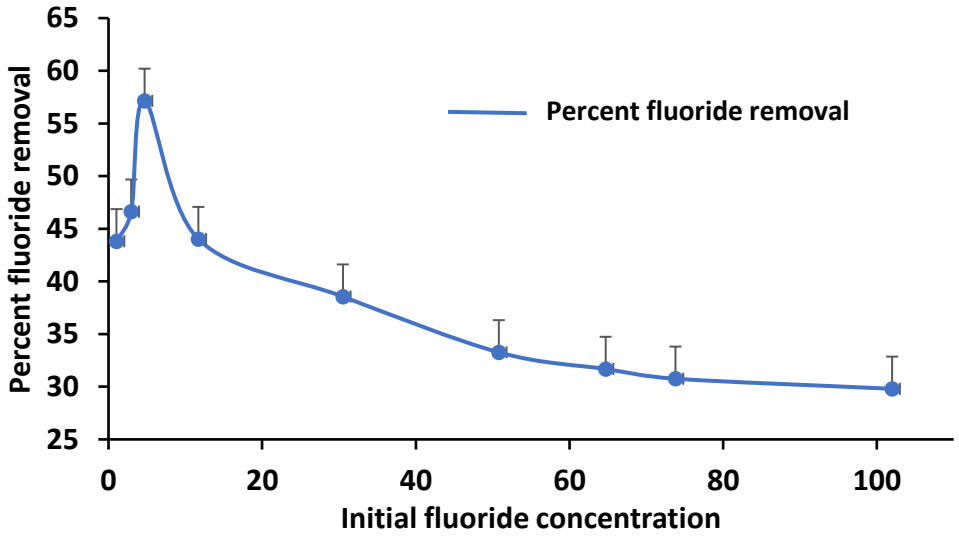

Figure 7.11: Variation of percent fluoride removal with initial fluoride concentration (adsorbent dosage = 0.9 g/100 mL, optimum contact time = 10 min, pH ≈ 4.0, temperature = 298 K and shaking speed = 250 rpm. Initial fluoride concentration was varied between 0.1 mg/L and 100 mg/L).

7.3.3 Adsorption isotherms

Langmuir and Freundlich adsorption isotherm models were used to describe the fluoride sorption behavior onto PHTAC sorbent under the evaluated experimental conditions. Langmuir isotherm models the adsorption surfaces to be monolayer and assumes sorption to take place structurally on adsorbents homogenous surface. The sorption isotherms parameters were obtained by using 1.0 g of PHTAC adsorbent per 100 mL of fluoride solution (1 - 100 mg/L) for 60 min at 298 K.

Langmuir model non-linearised form, which applies to homogeneous adsorption medium describing monolayer systems in a sorbent-sorbate interface is given as (Langmuir, 1916: Karthikeyan *et al.*, 2005: Lee & Tiwari, 2015; Tran *et al.*, 2017: Sahu & Singh, 2019):

$$q_e = \frac{Q_m K_L C_e}{1 + K_L C_e} \qquad (7.8)$$

where C_e is fluoride equilibrium concentration in the solution, q_e (mg/g) is the adsorption capacity or the amount of fluoride ion adsorbed per unit mass of HTAC adsorbent at equilibrium, Q_{max}

© University of Venda

(mg/g) is maximum adsorbents' monolayer capacity and K_L (L/mg) is Langmiur adsorption equilibrium constant related to the affinity of binding sites.

Furthermore, the fundamental characteristics of Langmuir isotherm can be determined using a dimensionless constant separation factor for the fluoride equilibrium parameter, R_L (Equation 7.9) (Weber & Chakravorti, 1974: Sahu & Singh, 2019) given as:

$$R_L = \frac{1}{1 + K_L C_i} \quad (7.9)$$

where C_i (mg/L) is the initial fluoride concentration and K_L is the Langmuir equilibrium constant The R_L value is vital in determining if an sorption process is favourable ($0 < R_L < 1$), unfavourable ($R_L > 1$), linear ($R_L = 1$) or irreversible ($R_L = 0$).

The non-linear Freundlich adsorption isotherm is used to describe multilayer sorption on heterogeneous surfaces. Freundlich non-linearised equation is expressed as in Equation 7.10 (Freundlich, 1906: Foo & Hameed, 2010: Sahu & Singh, 2019):

$$q_e = K_F C_e^{1/n} \quad (7.10)$$

where C_e (mg/L) is equilibrium concentration of the fluoride, q_e (mg/g) is adsorption equilibrium capacity of the adsorbent, k_F (mg/g) is empirical Freundlich constant related to capacity of minimum adsorption and 1/n is the dimensionless parameter for Freundlich adsorption isotherm related to the intensity of adsorption which is adsorption driving forces' magnitude or the heterogeneity surface. Adsorption is favourable when 1/n < 1, unfavourable when 1/n >1, linear when 1/n = 1 and irreversible when 1/n = 0 (Ghorai & Pant, 2004: Foo & Hameed, 2010). The values of k_F and 1/n are derived from slope and intercept of log q_e versus log C_e.

Figure 7.12 depicts the non-linear plots for Langmuir and Freundlich adsorption isotherms, respectively while Table 7.5 shows the respective obtained model parameters for fluoride sorption by the porous hydrothermally-treated aluminosilicate clay (PHTAC) adsorbent at 298 K.

The generated data described by the adsorption isotherms in Figure 7.13 revealed increased adsorption capacities with increasing fluoride concentration, characterised by saturation at high concentration. Based on the high correlation co-efficient (R^2) values and low chi-square (X^2) values for both Langmuir and Freundlich models in Table 7.5, the adsorption data had a good fit to both Langmuir (R^2 = 0.99 and X^2 = 0.061) and Freundlich adsorption isotherm models (R^2 = 0.99 and X^2 = 0.071) at 298 K (Table 7.5). This suggests that adsorption of fluoride onto HTAC occurred on a both homogeneous and heterogeneous surfaces.

© University of Venda

Furthermore, the feasibility of fluoride uptake by Langmuir and Freundlich models were confirmed by the calculated values of both the dimensionless constant, (R_L) and adsorption intensity (n). Both values range between 0 and 1, thereby affirming the favourable conditions for fluoride sorption by the synthesised PHTAC.

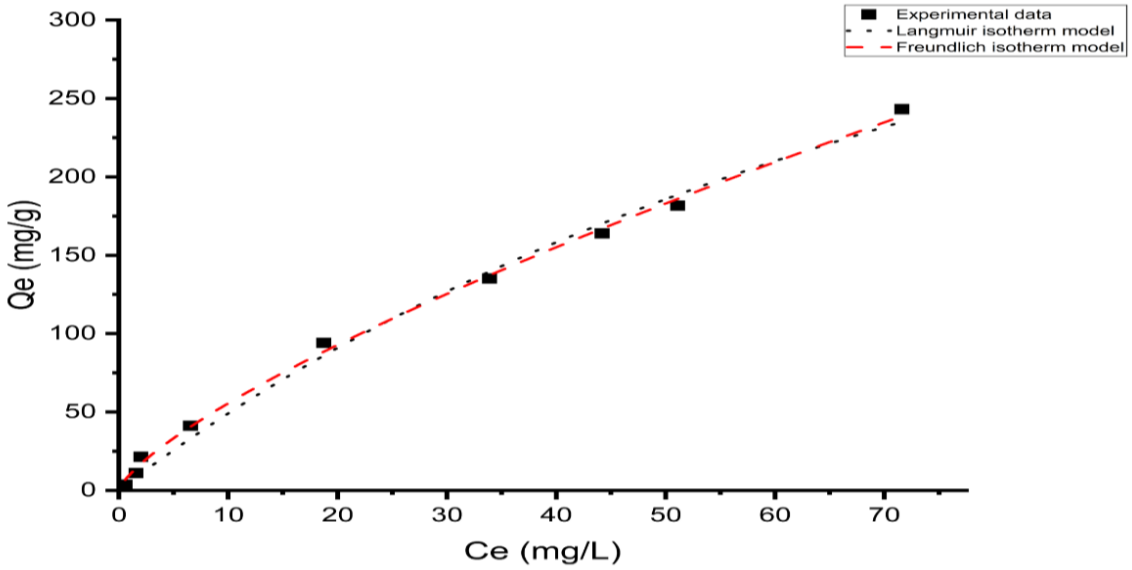

Figure 7.12: Langmuir and Freundlich isotherm plot of fluoride adsorption on the PHTAC (1.0 g PHTAC, 60 min contact time, agitation speed of 250 rpm at 298 K. Fluoride concentration was varied from 1 to 100 mg/L).

Table 7.5: Langmuir and Freundlich isotherm parameters for fluoride sorption onto PHTAC.

Model	Langmuir	Freundlich
Equation	$(Q_m*K*C_e)(1+(K*C_e)$	$(K_f*(C_e*(1/n)$
Plot	Q_e	Q_e
Q_m	610.5 ± 119.31	-
K	0.008 ± 0.0024	10.09 ± 0.95
N	-	1.35 ± 0.044
Reduced chi-square (RCS) (X^2)	0.061	0.017
COD (R-Square) (R^2)	0.99	0.99
Adjusted R-Square (R^2)	0.99	0.99

© University of Venda

7.3.4 Effect of co-existing ions on the defluoridation

Groundwater may contain other co-existing ions that may hinder the fluoride adsorption. Figure 7.13 presents the effect of co-existing ions on fluoride adsorption. In the presence of Cl^-, fluoride removal reduced from 68 to 30% while in the presence of CO_3^{2-}, it reduced from 68 to 36%, indicating that Cl^- and CO_3^{2-} competed with fluoride for adsorption sites. This could be due to relatively similar and smaller sizes of Cl^- and CO_3^{2-} compared to other anions which only showed slight reduction. The order of F^- uptake in the presence of other co-existing anions was as follows: $Cl^- < CO_3^{2-} < PO_4^{2-} < SO_4^{2-} < NO_3^-$. Hence, the synthesised PHTAC adsorbent may not be suitable for defluoridation in chloride and carbonate ions-rich groundwater.

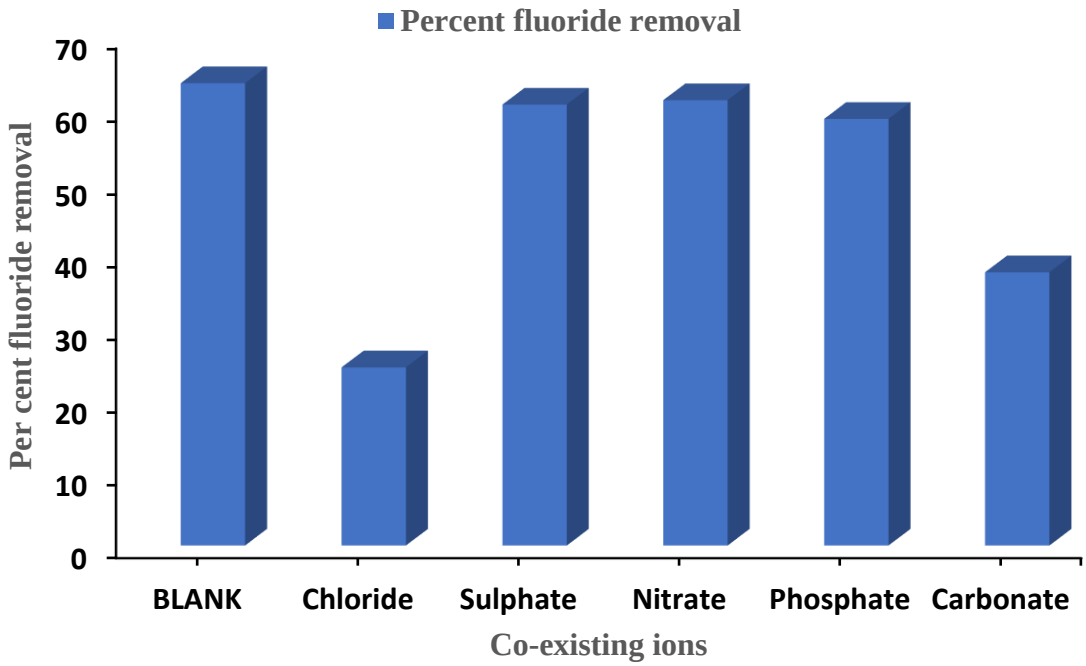

Figure 7.13: The effect of fluoride uptake in the presence of co-existing ions (Contact time = 30 min; pH ≈ 4.0; initial fluoride concentration = 10 mg/L; initial anion concentration = 10 mg/L; Adsorbent dosage = 1.0 g/100 mL; shaking speed = 250 rpm; temperature = 298 K).

7.3.5 Regeneration studies and life cycle of the PHTAC

Figure 7.14 presents the per cent fluoride removal by PHTAC in successive cycles using 0.1 M NaOH and 0.1 M KCl as regenerants. The regeneration and recyclability potential of PHTAC were carried out for up to eight successive adsorption and desorption cycles at an initial fluoride concentration of 4.0 mg/L, pH ≈ 4.0 at 10 min contact time. It was observed that the per cent fluoride removal decreased with increasing adsorption cycles from 60% to 15% when NaOH

© University of Venda

was used as regenerant while the decrease observed when KCl was used as regenerant was from 60% to about 55%. Desorption of fluoride could be due to ion exchange between fluoride and the anions present. Therefore, KCl is a more suitable solution for regeneration of PHTAC as the material regenerated yielded higher fluoride removal even at the 8th cycle.

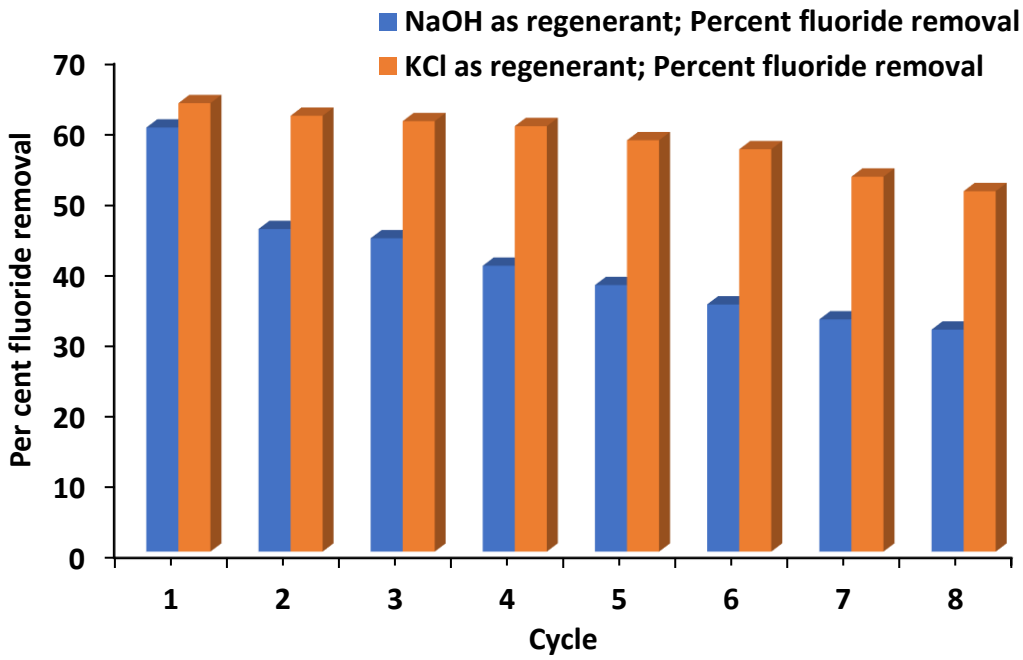

Figure 7.14: Percent fluoride removal by PHTAC in successive cycles (using 0.1 M NaOH and 0.1 M KCl at 4.0 mg/L fluoride, contact time of 10 min and pH ≈ 4.0 at 250 rpm).

7.3.6 Comparison of adsorption capacity of the synthesised PHTAC with other reported adsorbents

The adsorption capacities for the various hydrothermally-altered clay and similar adsorbents with their experimental conditions reported in literature were compared with the synthesised PHTAC adsorbent (Table 7.6). The synthesised PHTAC adsorbent showed higher adsorption capacity at pH of ≈ 4.0. Some of the adsorbent materials reported in the literature showed lower adsorption capacities both within and outside the natural pH range. Further studies and surface modifications are therefore recommended to improve fluoride sorption efficiencies particularly at natural water pH.

© University of Venda

University of Venda
Creating Future Leaders

Table 7.6: Comparison of the adsorption capacities of some adsorbents with synthesised PHTAC adsorbent

Adsorbent	Concentrations and pH	Adsorption Capacity (mg/g)	References
Granular acid treated bentonite	2.8 mg/L; pH 4.9	0.09	Ma *et al.*, 2011
Hydrothermally-modified limestone (HML)	0.9 mg/L; pH 3.0	6.45	Gogoi *et al.*, 2016
La-Al loaded hydrothermal palygorskite composite	0.5 mg/L; pH 5	1.30	Lyu *et al.*, 2016
Smectite-rich clay soil adsorbent	3.0 mg/L; pH 2	0.21	Mudzielwana *et al.*, 2016
Nepheline formed via alkali-hydrothermal pathway	6.0 mg/L; pH 5.25	1.8	Wang *et al.*, 2017
Clay composite (clay, grog, bone char & sawdust)	9.12mg/L; pH 6.7	0.08	Gidi *et al.*, 2019
Mechanochemically-activated aluminosilicate clay (MAC)	3.2 mg/L; pH 5	1.87	Obijole *et al.*, 2019
Hydrothermally-treated aluminosilicate clay (HTAC)	6.0 mg/L; pH 6.8	1.75	Obijole *et al.*, 2021
Porous-hydrothermally-treated aluminosilicate clay (PHTAC)	4.6 mg/L; pH 4.0	3.45	This study

© University of Venda

7.3.7 Field testing of Siloam field groundwater

The efficiency of PHTAC was further tested in field water collected from Siloam borehole containing 3.94 mg/L initial fluoride concentration using 0.9 g/100 L adsorbent dosage at 10 min contact time. Table 7.7 presents the physicochemical properties of Siloam field groundwater before and after treatment at natural pH of 8 in comparison with SANS and WHO permissible limits. The synthesised porous-hydrothermally-treated aluminosilicate clay (PHTAC) adsorbent showed the capability to remove fluoride from initial fluoride concentration of 3.94 mg/L to 1.35 mg/L, which is within the permissible WHO limits (1.5 mg/L). There was no major change in the concentrations of the Br^- and SO_4^{2-} before and after treatment, indicating that these co-existing anions did not compete in defluoridation process. PO_4^{2-}, Ca^{2+} and Mg^{2+} concentrations decreased, indicating that the material has potential to remove other contaminants in water. The concentrations of Na^+ and Cl^- were slightly higher after treatments. This could be due to the leaching from the adsorbent or due to some cationic exchanges into the media, but are still within SANS and WHO permissible limits. Therefore, the synthesised porous-hydrothermally-treated aluminosilicate clay (PHTAC) adsorbent is safe and can be recommended for remediation of fluoride in drinking water since it has shown potential to bring fluoride to less than 1.5 mg/L.

Table 7.7: Physicochemical properties of raw and treated field (Siloam) fluoride-rich groundwater

Parameters	Ion concentration in raw field water before treatment at pH 8 (mg/L)	Ion concentration in treated field water at pH 8 (mg/L)	SANS/WHO guidelines
F^-	2.84	1.35	1.0 - 1.5
Br^-	0.33	0.24	200
Cl^-	5.46	5.66	250
PO_4^{2-}	4.67	2.34	20 - 50
SO_4^{2-}	13.23	13.64	200 - 240
Na^+	81.1	147.8	200 - 250
Ca^{2+}	1.0	LOD	75
Mg^{2+}	0.2	LOD	50

Footnote: LOD means limit of detection.

7.3.8 Antibacterial studies

Antibacterial activities of the synthesised porous-hydrothermally-treated aluminosilicate clay adsorbent were evaluated by using the well diffusion assay method. Figure

© University of Venda

7.15 shows pictorial view of the plates and the bored holes containing the mixture of the MAC, HTAC, PHTAC and the *E. coli* strains that were being investigated for antibacterial activities via zone of inhibition measurements respectively. From pictures (b) and (c) in Figure 7.15, it can be observed that the HTAC and PHTAC samples inhibited the bacterial strains with the zone of inhibition measured as 15 mm, hence indicating some measure of potent activities against the *E. coli* strains used in this study. Meanwhile, MAC did not show any zone of inhibition (Figure 7.15 a and b) while HTAC and PHTAC (Figure 7.15 b and c) exhibited some potency against the bacterial strains. The exhibition of potency in HTAC and PHTAC respectively could be due to release of intra-cellular reactive oxygen species generated during hydrothermal treatment and introduction of pore formers ($NaClO_3$), which are exposed to bacterial cells on the synthesised materials surface (Horie *et al.,* 2012).

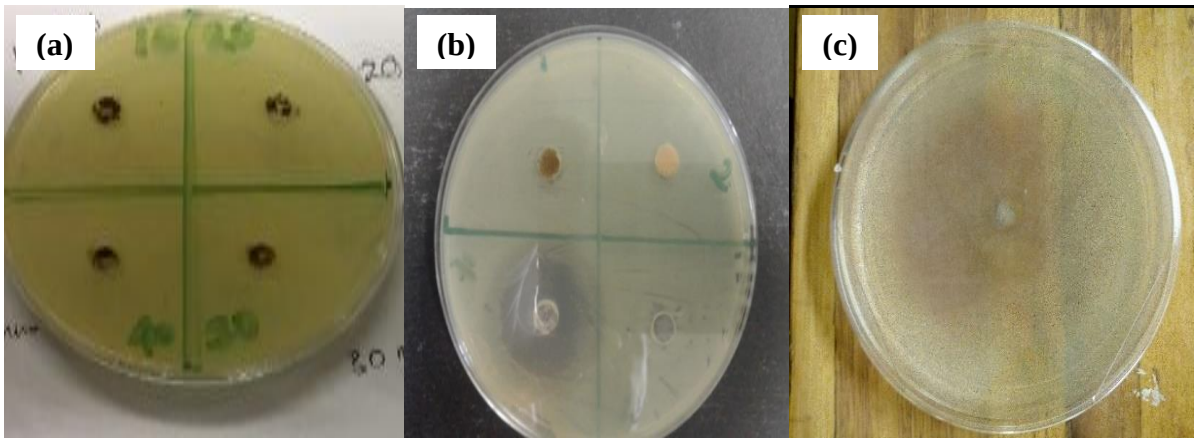

Figure 7.15: Pictorial view of the plate showing the zone of inhibition of (a) MAC (b) HTAC and (c) PHTAC samples when *E. coli* strains were used.

In addition, the minimum inhibition zone of the fluoride-loaded groundwater, HTAC and PHTAC observed towards *E. coli* strain was about 13 - 14 mm (a little lower than when fluoride free water was used). This is presented in Figure 7.16. The interaction between the synthesised material and the fluoride in water which led to the the sorption of fluoride unto the surface and pores of the materials may be responsible for the observed minimal reduction in the bacterial potency against the materials as the trapped bacterial cells competed with fluoride uptake onto the surface and pores of the synthesised material.

© University of Venda

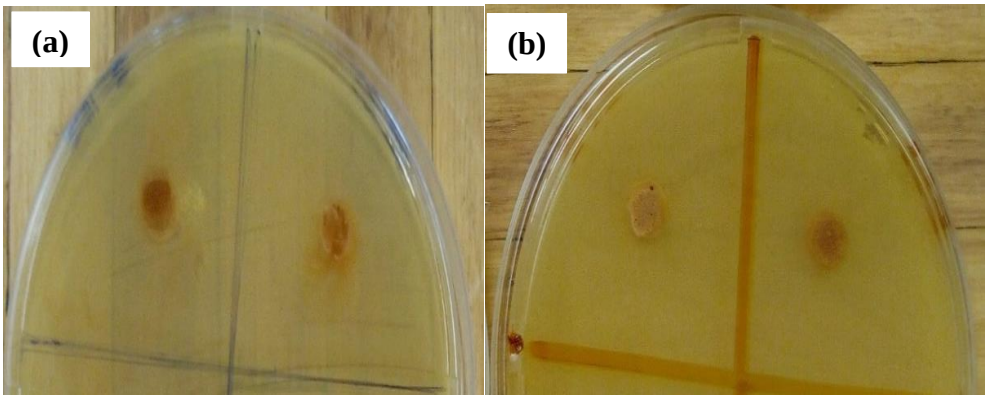

Figure 7.16: Pictorial view of the plate showing the zone of inhibition of (a) HTAC, Fluoride loaded groundwater (b) PHTAC, Fluoride-loaded groundwater samples when *E. coli* strains were used.

Antibacterial activities of the synthesised porous-hydrothermally-treated aluminosilicate clay (PHTAC) adsorbent were further evaluated using modified liquid culture technique and UV-visible spectrophotometry. From the results, percent growth inhibition or reduction in the bacterial cells was 89% (Table 7.8). This could be due to some bactericidal effects (killing of the bacterial cells) or entrapment of the bacterial cells into the pores of the PHTAC adsorbent. It can also be through the inactivation or killing of the bacteria as noted in the zone of inhibition measurements. Most government water treatment plants succeeded in having percent growth inhibition or reduction in the bacterial cells to between 90% to 95%. Thus, PHTAC is a promising adsorbent capable of removing pathogen from water to safe levels. It should also be noted that mechanism of the detailed study is beyond the scope of this work. However, the high point of this research is the materials ability to inactivate as well as trap the bacterial cells within the synthesised material pores.

In addition, a "rule of thumb" based upon generations of light and electron microscopy measurements for the dimensions of an *Escherichia coli* (*E. coli*) cell, showed it is a gram negative facultative, anaerobic, rod-shaped bacteria with a diameter (width) of 1.1 - 1.5 µm, a length of 2 - 6 µm and a cell volume of about 1.3 μm^3 (Molenaar *et al.*, 2009; Amir, 2014). Bacterial shapes are approximated as a spherocylinder, i.e. a cylinder with hemispherical caps. The synthesised materials' pore volume of 10 cm^3/g is a further confirmation of entrapment of the *E. coli* cells occurred within the synthesised materials' pores as the pore volumes are wide enough to accommodate and trap as many bacterial cells within the pores. In conclusion, the high point of this research work is the materials' ability to inactivate as well as trap the bacterial cells within the pores of the synthesised multifunctional porous-hydrothermally-treated aluminosilicate clay (PHTAC) adsorbent materials.

© University of Venda

Table 7.8: Absorbance measurements of the treated PHTAC material in bacterial suspension in water

Sample	Absorbance measurements (nm)
Synthesised PHTAC absorbent + bacterial suspension in water	0.075
Control (bacterial suspension in water without the addition of the material)	0.682
Activity (%)	89

7.4 Conclusions and recommendations

A porous-hydrothermally-treated aluminosilicate clay (PHTAC) adsorbent was successfully synthesised from hydrothermally-treated aluminosilicate clay (HTAC) and further tested in defluoridation and pathogen removal from groundwater. The PHTAC showed a maximum per cent fluoride removal of 68% and adsorption capacity of 3.45 mg/g at 10 min contact time, 0.9 g dosage/100 mL, 4.0 mg/L initial fluoride concentration, pH ≈ 4.0 and shaking speed of 250 rpm at 298 K (simulated fluoride-rich water). Good point of this research work is the adsorbents' ability to reduce fluoride at natural pH of water, particularly when compared with similar materials found in the literature. Main thrust of this research work is the high adsorption capacity of the synthesized material which is an indication of high potency of the material in defluoridation when put side by side with other similar adsorbents in literature. The adsorption isotherm data fitted well to both Langmuir and Freundlich isotherm models which is suggestive of the sorption process occurring on both homogeneous and heterogeneous surfaces. The adsorption kinetics data also showed a good fit to both pseudo-first-order and pseudo-second-order models respectively, implying that the fluoride sorption proceeded via both physiosorption and chemisorption respectively. Chloride and carbonate reduced the fluoride removal efficiency of the adsorbent. The synthesised PHTAC adsorbent was successfully reused for up to 8 regeneration-reuse cycles, hence, better than MAC and HTAC in recyclability and reuse.

The minimum inhibition zone observed towards *E. coli* strain was about 15 mm. This could be through the inactivation or killing of the bacteria. The percent growth inhibition of the bacterial cell was 89 which is very close to 90 - 95% obtained in most government water treatment plants. This could also be due to some bactericidal effects (killing of the bacterial cells) or entrapment of the bacterial cells into the pores of the PHTAC adsorbent. Thus PHTAC

© University of Venda

is a promising material for pathogen remediation in water. Hence, the synthesised multifunctional PHTAC was able to remove fluoride and pathogen from water reasonably well.

The efficiency of PHTAC, when further tested in field groundwater containing 3.94 mg/L initial fluoride concentration using 0.9 g/100 L adsorbent dosage at 10 min contact time, showed its capability to reduce fluoride from initial concentration of 3.94 mg/L to 1.35 mg/L, which is within the permissible WHO limits (1.5 mg/L). The adsorption efficiency and antibacterial potency of the synthesised PHTAC for fluoride and pathogen removal from groundwater improved over those of MAC and HTAC.

In addition, efficiency of PHTAC when tested in field groundwater containing 3.98 mg/L initial fluoride and *E. coli* strains using 0.9 g/ 100 L sorbent dosage at 10 min contact time, was still able to reduce fluoride from initial conc of 3.98 mg/L to 1.43 mg/L. The synthesised multifunctional porous-hydrothermally treated aluminosilicate clay (PHTAC) was able to remove fluoride and pathogen from water reasonably well. Therefore the synthesised material could be deployed for groundwater defluoridation anywhere in the world where the fluoride levels is equal to or less than 4.0 mg/L thereby contributing to reducing the incidence of fluorosis in endemic rural communities worldwide.

Amongst the Sustainable Development Goals (SDG's) set by the United Nations, Goal 6.1 aims at providing clean, safe and affordable water to everyone across the globe by 2030. Hence, the study succeeded at synthesising an affordable, easy to use and effective technologies targeted at fluorosis endemic rural households communities where fluoride levels in water is equal to or less than 4.0 mg/L. However, it is recommended that its adsorption surfaces are further treated sonochemically and loaded with suitable antibacterial metal oxides to increase particles' crystallinity, surface area and pores for excellent defluoridation and increased pathogen activity against *E. coli* strains.

© University of Venda

REFERENCES

Adeeyo A.O (2014). Multi-Step strain improvement of L. edodes for exopolysaccharide production. Master's Thesis submitted to Ladoke Akintola University of Technology, Nigeria. 1-312.

Aldaco, R., Irabien, A., & Luis, P. (2005). Fluidised bed reactor for fluoride removal. *Chemical Engineering Journal*, *107*(1-3), 113-117.

Ayinde, W. B., Gitari, W. M., Munkombwe, M., Samie, A., & Smith, J. A. (2020). Green synthesis of AgMgOnHaP nanoparticles supported on chitosan matrix: defluoridation and antibacterial effects in groundwater. *Journal of Environmental Chemical Engineering*, *8*(5), 104026.

Bennajah, M., Gourich, B., Essadki, A. H., Vial, C. H & Delmas, H. (2009). Defluoridation of Morocco drinking water by Electrocoagolation and Electroflotation in an electrochemical external-loop airlift reactor. *Chemical Engineering Journal,* 148 122-131.

Bia, G., De Pauli, C. P., & Borgnino, L. (2012). The role of Fe (III) modified montmorillonite on fluoride mobility: adsorption experiments and competition with phosphate. *Journal of Environmental Management, 100,* 1-9.

Byrappa, K., Subramani, A. K., Ananda, S., Rai, K. L., Sunitha, M. H., Basavalingu, B., & Soga, K. (2006). Impregnation of ZnO onto activated carbon under hydrothermal conditions and its photocatalytic properties. *Journal of Materials Science*, *41*(5), 1355-1362.

Byrappa, K., & Yoshimura, M. (2012). *Handbook of hydrothermal technology*. William Andrew Publications, NJ, USA.

Cuthbertson, A. A., Kimura, S. Y., Liberatore, H. K., Summers, R. S., Knappe, D. R., Stanford, B. D., & Richardson, S. D. (2019). Does granular activated carbon with chlorination produce safer drinking water? From disinfection byproducts and total organic halogen to calculated toxicity. *Environmental Science and Technology*, *53*(10), 5987-5999.

Coetzee, P. P., Coetzee, L. L., Puka, R., & Mubenga, S. (2003). Fluoride adsorption modelling and characterisation of clays for defluoridation of natural clays. *Water South Africa,* 29 3 331-338.

Denga, M. E., Gitari, W. M., Izuagie, A. A., & Akinyemi, S. A. (2018). Defluoridation of groundwater using mechanochemically-activated clay soil. *Water Practice and Technology, 13,* 3, 599-611.

© University of Venda

Dhillon, A., Nair, M., Bhargava, S. K., & Kumar, D. (2015). Excellent fluoride decontamination and antibacterial efficacy of Fe–Ca–Zr hybrid metal oxide nanomaterial. *Journal of Colloid and Interface Science*, *457*, 289-297.

Esaifan, M., Warr, L. N., Grathoff, G., Meyer, T., Schafmeister, M. T., Kruth, A., & Testrich, H. (2019). Synthesis of hydroxy-sodalite/cancrinite zeolites from calcite-bearing kaolin for the removal of heavy metal ions in aqueous media. *Minerals*, *9*(8), 484.

Foo, K. Y., & Hameed, B. H. (2010). Insights into the modeling of adsorption isotherm systems. *Chemical Engineering Journal*, *156*, 1, 2-10.

Freundlich, H. M. F. (1906). Uber die adsorption in losungen. *Journal of Physical Chemistry*, Leipzig. 57A 385-470.

Ghasemi, M., Naushad, M., Ghasemi, N & Khosravi-fard, Y. (2014). A novel agricultural waste-based adsorbent for the removal of Pb (II) from aqueous solution: kinetics, equilibrium and thermodynamic studies. *Journal of Industrial Engineering and Chemistry*, 20 2 454-461. 06/01/19.

Ghorai, S. & Pant, K. K. (2004). Investigations on the column performance of fluoride adsorption by activated alumina in a fixed-bed, *Chemical Engineering Journal*. 98 165–173.

Gitari, Ngulube, T., Masindi, V., & Gumbo, J. (2013). Natural clay based adsorbent for defluoridation of groundwater: optimisation of adsorption conditions. 36th WEDC International Conference, Nakuru, Kenya. 2013**.** Delivering water, sanitation and hygiene services in an uncertain environment.

Gidi, L. D., Amare, E. Z., Murthy, H. A., & Abebe, B. (2019). Application of Novel Clay Composite Adsorbent for Fluoride Removal. *Material Science Research India*, *16*(2), 164-173.

Gitari, W. M., Petrik, L. F., & Musyoka, N. M. (2016). Hydrothermal conversion of South African coal fly ash into pure phase zeolite Na-P1. *Zeolites: Useful Minerals*, 25.

Gitari, W. M., Izuagie, A. A., & Gumbo, J. R. (2020). Synthesis, characterisation and batch assessment of groundwater fluoride removal capacity of trimetal Mg/Ce/Mn oxide-modified diatomaceous earth. *Arabian Journal of Chemistry*, *13*(1), 1-16.

Gogoi, S., & Dutta, R. K. (2016). Fluoride removal by hydrothermally modified limestone powder using phosphoric acid. *Journal of Environmental Chemical Engineering*, 4 1 1040-1049.

Ho, Y. S., Ng, J. C. Y and G. McKay (2000). Kinetics of pollutant sorption by biosorbents: review, *Separation and Purification Methods*, 29 189-232.

© University of Venda

Horie, M., Fujita, K., Kato, H., Endoh, S., Nishio, K., Komaba, L. K & Hagihara, Y. (2012). Association of the physical and chemical properties and the cytotoxicity of metal oxide nanoparticles: metal ion release, adsorption ability and specific surface area. *Metallomics*, *4*(4), 350-360.

Karthikeyan, T., Rajgopal, S., & Miranda, L. R. (2005). Chromium (VI) adsorption from aqueous solution by Hevea Brasilinesis sawdust activated carbon. *Journal of Hazardous Materials*, *124*(1-3), 192-199.

Kaygusuz, H., Çoşkunırmak, M. H., Kahya, N., & Erim, F. B. (2015). Aluminum alginate–montmorillonite composite beads for defluoridation of water. *Water, Air and Soil Pollution*, *226*(1), 2257.

Kim, W., Choi, D., & Kim, S. (2010). Sonochemical synthesis of zeolite A from metakaolinite in NaOH solution. *Materials transactions*, 51 (1694-1698) 1008171153-1008171153.

Konta, J. (1995). Clay and Man: Clay raw materials in the service of man. *Applied Clay Science*, 10 275–335.

Kumar, M. S., Dhakate, R., Yadagiri, G., & Reddy, K. S. (2017). Principal component and multivariate statistical approach for evaluation of hydrochemical characterisation of fluoride-rich groundwater of Shaslar Vagu watershed, Nalgonda District, India. *Arabian Journal of Geosciences*, *10*(4), 83.

Kunduru, K. R., Nazarkovsky, M., Farah, S., Pawar, R. P., Basu, A., & Domb, A. J. (2017). Nanotechnology for water purification: applications of nanotechnology methods in wastewater treatment. In *Water Purification*, (pp. 33-74). Academic Press.

Lagergren, S (1898). Zur Theorie der sogenannten adsorption geloster stoffe, K. Sven, K. *Handlingar Tidskr.* 24 1–39.

Langmuir, J. (1916). The properties of solids and liquids. *Journal of America Chemical Society.* 38 2221-2295.

Lee, S. M., & Tiwari, D. (2015). Porous hybrid materials in the remediation of water contaminated with As (III) and As (V). *Chemical Engineering Journal*, *270*, 496-507.

Luna, J., Martinez, J., Montero, C., Muñiz, C., Ortiz, J., Gonzalez, G., . . . Equihua, F. (2018). Defluoridation of groundwater in central Mexico by electrocoagulation. *Fluoride*, *51*(1), 34-43.

Lyu, Y., Su, X., Zhang, S., & Zhang, Y. (2016). Preparation and characterisation of La (III)-Al (III) co-loaded hydrothermal palygorskite adsorbent for fluoride removal from groundwater. *Water, Air, and Soil Pollution*, 227 12 454.

© University of Venda

Ma, Y., Shi, F., Zheng, X., Ma, J., & Gao, C. (2011). Removal of fluoride from aqueous solution using granular acid-treated bentonite (GHB): Batch and column studies. *Journal of Hazardous Materials, 185*(2-3), 1073-1080.

Maity, J. P., Hsu, C. M., Lin, T. J., Lee, W. C., Bhattacharya, P., Bundschuh, J., & Chen, C. Y. (2018). Removal of fluoride from water through bacterial-surfactin mediated novel hydroxyapatite nanoparticle and its efficiency assessment: Adsorption isotherm, adsorption kinetic and adsorption Thermodynamics. *Environmental Nanotechnology, Monitoring and Management, 9*, 18-28.

Marsha, A., Heatha, A., Patureaub, P., Everndena, M & Walkera, P (2019). Phase formation behaviour in alkali activation of clay mixtures. *Applied Clay Science,* 175 10-21.

Mikuła, A., Król, M., & Koleżyński, A. (2015). The influence of the long-range order on the vibrational spectra of structures based on sodalite cage. *Spectrochimica Acta Part A: Molecular and Biomolecular Spectroscopy*, 144 5 273-280

Meenakshi, S., Sairam Sundaram, C. & Sukumar, R. (2008). Enhanced fluoride sorption by mechanochemically activated kaolinites, *Journal of Hazard Materials,*153 164–172.

Momba, M. N. B., & Brouckaert, M. B. (2005). Guidelines for ensuring sustainable effective disinfection in small water supply systems. WRC Report No. TT 249/05. Water Research Commission, Pretoria, South Africa.

Mudzielwana, R., Gitari, M. W., & Msagati, T. A. (2016). Characterisation of smectite-rich clay soil: Implication for groundwater defluoridation. *South African Journal of Science, 112*(11-12), 1-8.

Mudzielwana, R., Gitari, W. M., Akinyemi, S. A., & Msagati, T. A. (2017). Synthesis, characterisation, and potential application of Mn 2+-intercalated bentonite in fluoride removal: adsorption modeling and mechanism evaluation. *Applied Water Science, 7*(8), 4549-4561.

Musyoka, N. (2009). *Hydrothermal synthesis and optimisation of zeolite Na-P1 from South African coal fly ash.* (Doctoral thesis, University of Western Cape, South Africa).

Musyoka, N., Petrik, L., & Hums, E. (2011). Ultrasonic assisted synthesis of zeolite A from coal fly ash using mine waters (acid mine drainage and circumneutral mine water) as a substitute for ultrapure water. *Proceedings of International Mineral Water Association, Aachen, Germany*, 423-428.

Ngulube, T., Gitari, M. W., & Tutu, H. (2017). Defluoridation of groundwater using mixed Mukondeni clay soils. *Water Science and Technology: Water Supply*, *17*(2), 480-492.

© University of Venda

Obijole, O. A., Gitari, M. W., Ndungu, P. G., & Samie, A. (2019). Mechanochemically Activated Aluminosilicate Clay Soils and their Application for Defluoridation and Pathogen Removal from Groundwater. *International Journal of Environmental Research and Public Health, 16*(4), 654.

Pan, J., Zheng, Y., Ding, J., Gao, C., Van der Bruggen, B., & Shen, J. (2018). Fluoride removal from water by membrane capacitive deionization with a monovalent anion selective membrane. *Industrial & Engineering Chemistry Research, 57*(20), 7048-7053.

Pritchard, M., Mkandawire, T., & O'neill, J. G. (2008). Assessment of groundwater quality in shallow wells within the southern districts of Malawi. *Physics and Chemistry of the Earth, Parts A/B/C, 33*(8-13), 812-823.

Qureshi, S. Z., Khan, M. A., & Rahman, N. (1995). Synthesis and ion-exchange behavior of a new three-component ion-exchange material: Zirconium (IV) arsenate vanadate. *Bulletin of the Chemical Society of Japan, 68*(6), 1613-1617.

Sahu, O., & Singh, N. (2019). Significance of bioadsorption process on textile industry wastewater. In *The Impact and Prospects of Green Chemistry for Textile Technology* (pp. 367-416): Elsevier.

SANS 241. South African National Standard (SANS) 241 (2006). Drinking Water Specification. South African Bureau of Standards (SABS) SANS 241. Pretoria, South Africa. 187-205.

Tran, H. N., You, S. J., Hosseini-Bandegharaei, A., & Chao, H. P. (2017). Mistakes and inconsistencies regarding adsorption of contaminants from aqueous solutions: a critical review. *Water Research, 120*, 88-116.

Toor, M., Jin, B., Dai, S & Vimonoses, V. (2014). Activating natural bentonite as cost effective adsorbent for removal of Congo red in wastewater. *Journal of Industrial Engineering Chemistry*, 1979 1–9.

Waghmare, S. S., & Arfin, T. (2015). Fluoride removal by clays, geomaterials, minerals, low cost materials and zeolites by adsorption: a review. *International Journal of Science, Engineering and Technology Research, 4*(11), 3663-3676.

Wang, H., Feng, Q., Liu, K., Li, Z., Tang, X., & Li, G. (2017). Highly efficient fluoride adsorption from aqueous solution by nepheline prepared from kaolinite through alkali-hydrothermal process. *Journal of Environmental Management, 196*, 72-79.

Weber, W. J. & Morris, J. C. (1964). Equilibria and capacities for adsorption on carbon, *Journal of Sanitary Engineering Division*, 90 79–107.

© University of Venda

Weber, T. W., & Chakravorti, R. K. (1974). Pore and solid diffusion models for fixed-bed adsorbers. *AIChE Journal*, *20*(2), 228-238.

World Health Organization (WHO), (2017). Guidelines for Drinking Water Quality. Fluoride in drinking water. Guidelines for Drinking Water Quality, Geneva. http://www.who.int/topics/millennium_development_goals/en/

World Health Organization. (2019). *Preventing disease through healthy environments: inadequate or excess fluoride: a major public health concern* (No. WHO/CED/PHE/EPE/19.4. 5). World Health Organization.

Yoon, Y., Zheng, M., Ahn, Y. T., Park, W. K., Yang, W. S., & Kang, J. W. (2017). Synthesis of magnetite/non-oxidative graphene composites and their application for arsenic removal. *Separation and Purification Technology*, *178*, 40-48.

Yoshimura, M., & Byrappa, K. (2008). Hydrothermal processing of materials: past, present and future. *Journal of Materials Science*, *43*(7), 2085-2103.

© University of Venda

CHAPTER EIGHT: CONCLUSION AND RECOMMENDATIONS

8 Conclusion

This research work was conceptualised with the main objective to develop a porous-hydrothermally-treated aluminosilicate clay (PHTAC) adsorbents from aluminosilicate-rich clay soils, through hydrothermal treatment for application in defluoridation and pathogen removal from groundwater.

The specific objectives were to:

- mechanochemically activate raw aluminosilicate clay soils (MAC) and evaluate their physicochemical and mineralogical characteristics and their application for defluoridation and pathogen removal from groundwater;
- optimise the operational parameters for synthesis of hydrothermally-treated aluminosilicate clays (HTAC), evaluate their physicochemical properties and potential for fluoride and pathogen removal from groundwater;
- hydrothermally treat the mechanochemically-activated clay (MAC) at previously established optimum operational parameters and evaluate their adsorptive capacities for fluoride removal in groundwater and further evaluate their antibacterial efficacy towards selected bacterial strains;
- optimise the operational parameters for modification of MAC through hydrothermal treatment in presence of a pore-forming agent, and evaluation of their physicochemical properties and potential for fluoride and pathogen removal from groundwater;
- synthesise a pore forming-agent-modified-hydrothermally-treated aluminosilicate clay (PHTAC) at previously optimised conditions and evaluation of its fluoride adsorptive capacities in groundwater and antibacterial efficacy towards selected strains.

All the above objectives were successfully accomplished with the forgoing conclusions made from each specific objective:

The first objective focused on the physicochemical characterisation of clay soils sourced from Mukondeni village, Limpopo Province, South Africa, mechanochemical treatment of the clay and application to fluoride and pathogen removal from groundwater. The clay soil was found to be rich in aluminosilicate, moderate in cation exchange capacity and mesoporous in nature. The raw clay was mechanochemically treated at different contact times and subjected to characterisation using Brunauer-Emmett-Teller (BET) method, Fourier transform infra red (FTIR) spectroscopy, scanning electron microscopy-energy dispersal

© University of Venda

spectroscopy (SEM-EDS), X-ray diffraction (XRD) and X-ray fluorescence (XRF). The optimised materials were applied in batch adsorption defluoridation.

(i) It was found that the maximum fluoride sorption capacity of mechanically-activated clay (MAC) was 1.87 mg/g with 32% fluoride removal at 2 g/100 mL adsorbent dosage, initial fluoride concentration of 3.2 mg/L, pH 6.0, 60 min contact time, shaking speed of 250 rpm and temperature of 298 K;

(ii) Fluoride uptake reduced slightly in the presence of Cl^- and increased slightly in the presence of SO_4^{2-}, NO_3^- and PO_4^{2-} while CO_3^{2-} significantly competed with fluoride uptake in the adsorption process as the per cent fluoride removal was substantially reduced;

(iii) Freundlich isotherm gave a better fit to the sorption data, thereby confirming heterogeneous adsorption process for the MAC materials when linearised model was used;

(iv) Langmuir and Freundlich isotherms both fitted well when non-linear model were employed, hence confirming adsorption occurred on both monolayer and multilayer surfaces;

(v) The kinetic studies showed fluoride sorption could better be described with the pseudo-second-order model when linearised modelling were used, indicating the dominance of chemisorption mechanism;

(vi) Adsorption kinetics data fitted well to both pseudo-first order and pseudo-second order reaction kinetics,thus indicating adsorption mechanisms to be both physiosorption and chemosorption respectively.

(vii) The activated clay did not show any activity against the *E. coli* strains used, hence, suggesting absence or very low antibacterial properties on the activated clays' surfaces.

The following recommendations were made from this objective:

- The adsorption efficiency and antibacterial potency of MAC could be improved by modification of the clays' surfaces via hydrothermal treatment with a view to improving the sorption capacity of the adsorbent materials.

The second objective focused on optimisation of synthesis conditions for hydrothermal treatment of MAC for fluoride and pathogen removal from groundwater and physicochemical characterisation.

(i) Here, MAC was aged at different NaOH concentrations and contact times at a predetermined temperature (47 ^{O}C). The inductly coupled plasma-mass spectroscopy (ICP-MS) results of the filtrates showed the most dissolved Al and Si occurred at 1.5 M concentration and 2 hour contact time;

(ii) Hydrothermal treatment was conducted on the optimally aged slurry mixture by concurrently varying hydrothermal treatment temperature, contact time and water to obtain the

© University of Venda

most crystalline clay with the highest surface area. Preliminary defluoridation of products was carried out;

(iii) The hydrothermally-treated aluminosilicate clays (HTACs) were characterised using FTIR, BET, SEM-EDS and XRD. Furthermore, comparative studies of the synthesised materials for defluoridation were undertaken;

(iv) The study concluded that the optimised parameters such as hydrothermal treatment temperature, time and water content played critical roles in the modification process.

The following recommendation was made from this objective:

Optimally-synthesised HTAC-8 fared better in preliminary defluoridation compared with other modified materials and hence, selected for application in fluoride removal from groundwater.

The third objective focused on application of the optimally-synthesised HTAC from MAC, for fluoride and pathogen removal from groundwater and physicochemical characterisations.

(i) It was found that maximum sorption capacity of the optimally synthesised HTAC was 1.75 mg/g and 52% fluoride removal at 0.8 g/40 mL adsorbent dosage, 6.0 mg/L initial fluoride concentration, pH 6.8, 5 min contact time, shaking speed of 250 rpm and temperature of 298 K;

(ii) The kinetic studies showed fluoride sorption data fitted well to pseudo-second-order thereby confirming that sorption process occurred via chemisorption and a multi-site heterogeneous sorption;

(iii) All co-existing anions reduced fluoride uptake, however, Cl^- exerted greater reduction.

(iv) HTAC performed better when 0.1 M KCl was used as regenerant compared to 0.1 M NaOH;

(v) Fluoride sorption occurred via ion exchange;

(vi) Siloam groundwater at initial pH 6.5 and natural pH 8.5, initial fluoride concentration of 6.93 mg/L with 0.8 g/40 mL of the HTAC gave 51% and 49% fluoride removals respectively;

(vii) Antibacterial studies showed HTAC had potent antibacterial activities against *E. coli* strains.

The following recommendation was made from this objective:

- The HTAC defluoridation efficiency and antibacterial potency could be further enhanced by loading its surfaces with pore formers such as sodium chlorate ($NaClO_3$).

The fourth objective focused on modifying the surface properties of the HTAC by conducting hydrothermal treatment of MAC in the presence of a pore-forming agent ($NaClO_3$) [product designated as “porous-hydrothermally-treated aluminosilicate clay” (PHTAC)].

© University of Venda

(i) In this objective, operational parameters were optimised for synthesis of PHTAC and products characterised using BET, FT-IR, SEM-EDS and XRD;

(ii) Preliminary defluoridation experiments were conducted;

(iii) The results showed operational parameters such as pore former ($NaClO_3$), contact time and temperature are critical in the materials modification and fluoride removal potential;

(iv) The study concluded that pore-forming agent, temperature, time and water content introduced during the hydrothermal treatment increased the surface area, which impacted positively on the defluoridation and antibacterial performance of the synthesised materials.

The following recommendation was made from this objective:

(i) Optimally-synthesised HTAC performed better in preliminary fluoride removal compared to other modified materials and hence, selected for application in fluoride removal from groundwater.

The **fifth objective** focused on the synthesis of porous-hydrothermally-treated aluminosilicate clay (PHTAC) from the hydrothermally-treated aluminosilicate clay (HTAC), characterisation and batch defluoridation and antibacterial evaluation. PHTAC absorbent was successfully synthesised from HTAC for further application in fluoride and pathogen removal from groundwater. The optimised PHTAC was characterised by using BET, FT-IR, SEM-EDS, XRD and XRF. Batch adsorption experiments, effect of competing ions and regeneration potential were investigated. From the objective, the following were concluded:

(i) evaluation of the adsorptive capacities of the PHTAC showed optimum defluoridation capacity of 3.45 mg/g and 68% fluoride removal at 10 min contact time, 0.9 g dosage/100 mL, 4.0 mg/L initial fluoride concentration, pH ≈ 4.0, shaking speed of 250 rpm and temperature 298 K.

(ii) the fluoride sorption uptake data fitted well to both Langmuir and Freundlich isotherm models, thereby confirming both homogeneous and heterogeneous adsorption processes respectively for the PHTAC materials;

(iii) the kinetic studies showed fluoride sorption data fitted well to both pseudo-first-order and pseudo-second-order models respectively, implying that the fluoride sorption proceeded via both physiosorption and chemisorption respectively;

(iv) the fluoride removal efficiency reduced in the presence of Cl^- and CO_3^{2-} ions;

(v) the synthesised PHTAC adsorbent performed better in regeneration and recyclability than the MAC and HTAC;

(vi) the synthesised PHTAC adsorbent performed much better than MAC and HTAC earlier developed, thus indicating successful modification via introduction of pore formers ($NaClO_3$).

© University of Venda

(vii) The minimum inhibition zone observed towards *E. coli* strain was about 15 mm.

(viii) The percent growth inhibition of the bacterial cell was 89 which is very close to 90 - 95% obtained in most government water treatment plants.

(ix) PHTAC is a promising adsorbent for pathogen remediation in water.

(x) The efficiency of PHTAC, when further tested in field groundwater containing 3.94 mg/L initial fluoride concentration using 0.9 g/100 L adsorbent dosage at 10 min contact time showed its capability to reduce fluoride from initial concentration of 3.94 mg/L to 1.35 mg/L, which is within the permissible WHO limits (1.5 mg/L).

(xi) In addition, efficiency of PHTAC when tested in field groundwater containing 3.98 mg/L initial fluoride and *E. coli* strains using 0.9 g/ 100 L sorbent dosage at 10 min contact time was still able to reduce fluoride from initial conc of 3.98 mg/L to 1.43 mg/L.

(xii) The synthesised multifunctional PHTAC was able to remove fluoride and pathogen from water reasonably well anywhere in the world where the twin problems of fluorosis and waterborne diseases are prevalent.

(vii) The synthesised material could be deployed for groundwater defluoridation anywhere in the world where the fluoride levels is equal to or less than 4.0 mg/L, thereby contributing to reducing the incidence of fluorosis in endemic rural communities worldwide.

© University of Venda

8.1 Recomendations for future work

The adsorption efficiency and antibacterial potency of the synthesised PHTAC for fluoride and pathogen removal from groundwater improved substantially, it still fell short of the expectation. Hence, from the conclusion in the present study, it is hereby recommended that the following studies be conducted to improve the defluoridation and antibacterial efficiency of the PHTAC adsorbent material:

- that its adsorptive surfaces can be loaded with suitable antibacterial metal oxides with a view to obtaining a high surface area, pore volumes for excellent defluoridation and increased potent activities against *E. coli* strains;
- that the PHTAC be subjected to sonochemical treatment for better crystallinity, higher surface area and excellent performance;
- design and adaptation of suitable technology for the synthesised adsorbent material for household application.

© University of Venda

APPENDIXES

Appendix 1.1: Determination of pH at point-of-zero charge of mechanochemically-activated clay (MAC) using 1 M KCl, 0.1 M KCl and 0.01 M KCl respectively.

pHo	ΔH	pHo	ΔH	pHo	ΔH
2.05	0.36	2.23	0.57	2.19	0.63
3.07	1.61	3.26	2.02	3.01	2.59
3.95	1.41	4.16	1.63	4	2.23
5.13	0.57	4.84	1.25	5.23	1.08
5.85	0.11	6.17	-0.16	5.96	0.44
7.29	-1.07	6.9	-0.59	7.25	-0.72
7.92	-1.53	7.89	-1.63	8.19	-1.41
9.06	-2.8	8.83	-2.39	9.09	-2.35
10.03	-3.68	9.86	-3.25	10.07	-3.25
11.05	-4.06	10.98	-3.99	11.06	-3.74
12.02	-0.79	12.01	-0.95	12.01	-0.81

Appendix 2.1: XRD quantitative results of MAC sample

Prepared MAC sample		
	weight%	3 σ error
Actinolite	6.56	0.81
Calcite	1.12	0.42
Chlorite	13.71	0.99
Kaolinite	11.62	0.9
Microcline	5.25	0.69
Muscovite	6.1	0.9
Plagioclase	31.09	1.53
Quartz	24.55	0.99

Appendix 3.1: The surface area, pore volume and pore size of MAC materials

Samples	Mechanochemical treatment time (mins)	BET surface area (m^2/g)	Surface area single point (m^2/g)	Pore volume (cm^3/g)	Pore size (nm)
A	5	16.27	15.56	10.03	5.93
B	10	15.67	15.20	10. 04	11.57
C	20	16.08	15.61	10.05	12.05
D	30	17.19	16.66	10.07	14.92
E	40	16.50	15.96	10.07	15.15
F	60	13.22	12.57	10.05	14.67

© University of Venda

Appendix 4.1 a-f: FTIR spectra of MAC and HTAC samples CA1 to CA21

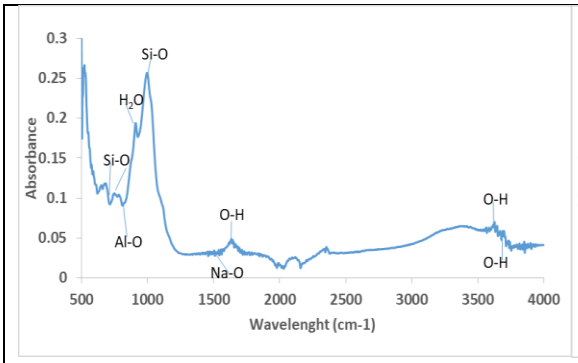

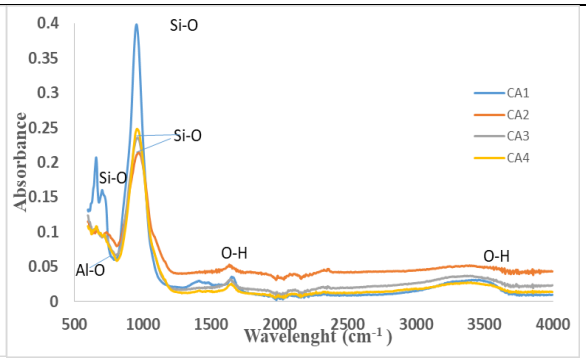

Fig 4a: FTIR spectra of MAC. **Fig 4b:** FTIR spectra of HTAC samples [CA1-CA4 (HTAC-1-HTAC-4)]

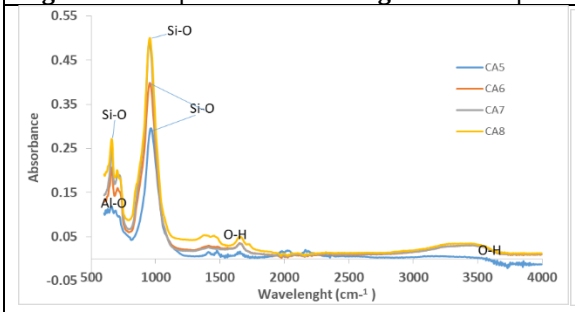

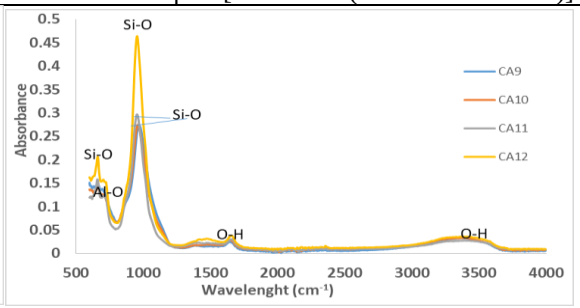

Fig 4c: FTIR spectra of HTAC samples [CA5-CA8 (HTAC-5 to HTAC-8)]. **Fig 4d:** FTIR spectra of HTAC samples [CA9-CA12 (HTAC-9 to HTAC-12)]

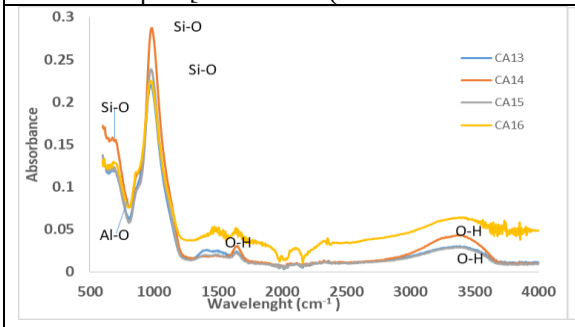

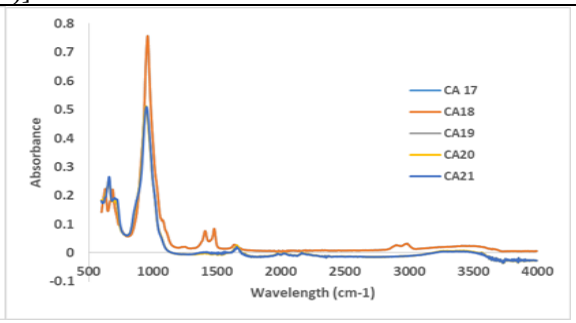

Fig 4e: FTIR spectra of HTAC samples [CA13-CA16 (HTAC-13-HTAC-16)]. **Fig 4f:** FTIR spectra of HTAC samples [CA17-CA21 (HTAC-17-HTAC-21)]

Appendix 4.2 g: FTIR Spectra of raw clay and the modified clay samples [HTAC(CA5-CA8/20), CA12, CA14 and CA18)]

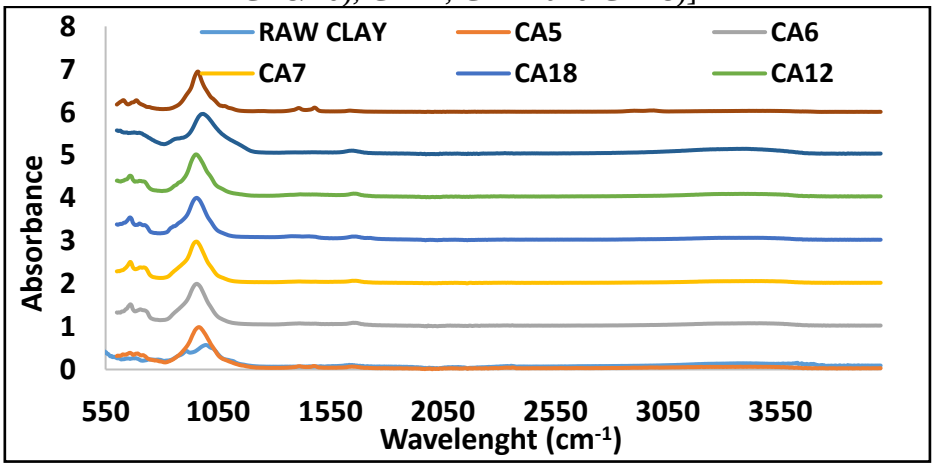

© University of Venda

Appendix 4.2 h: FTIR Spectra of raw clay and the modified clay samples [HTAC(CA5-CA8/20, CA12, CA14 and CA18)].

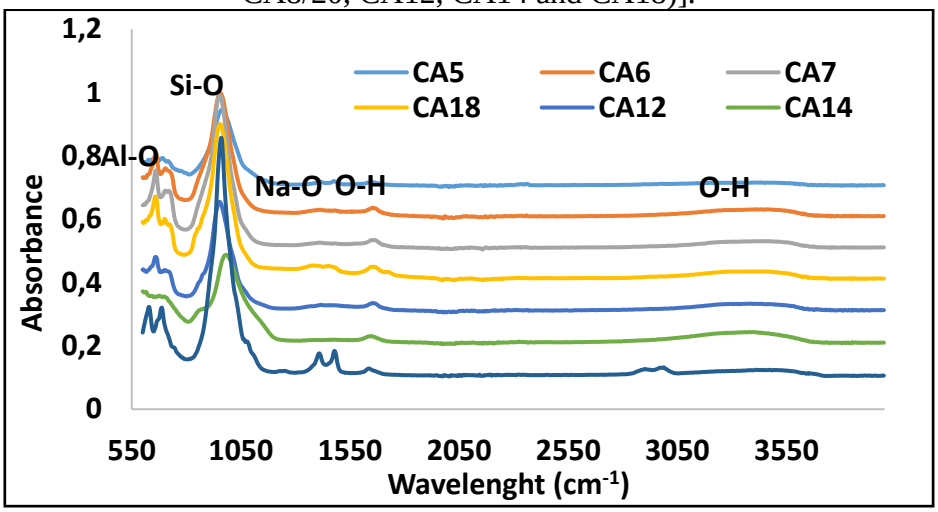

Appendix 4.3a-g: XRD spectra of the MAC and the selected HTAC products.

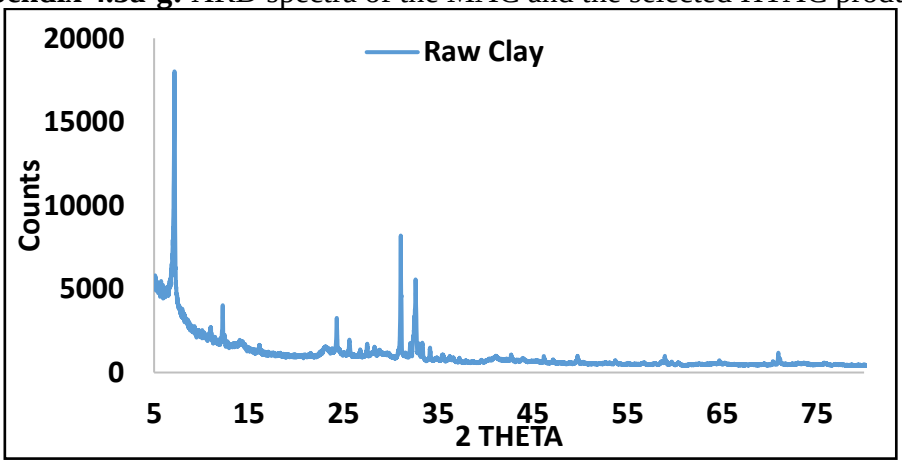

Figure 4.3a: XRD of Raw Clay (MAC)

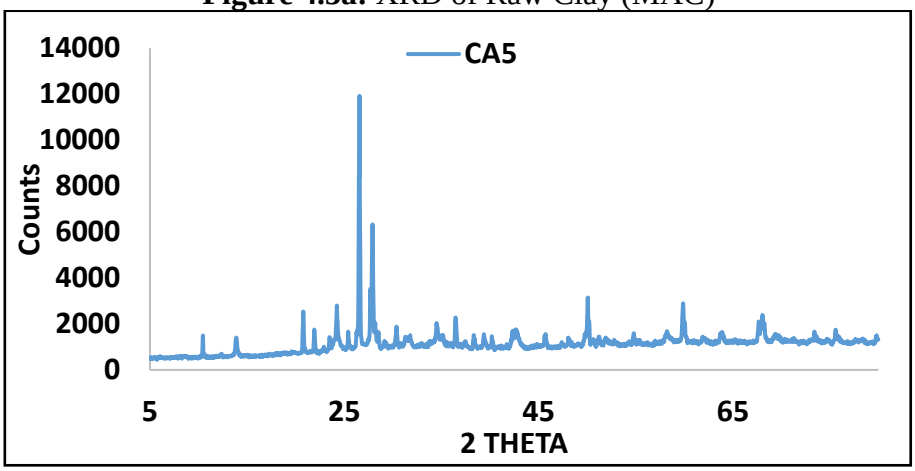

Figure 4.3b: XRD of CA5 (HTAC-5)

© University of Venda

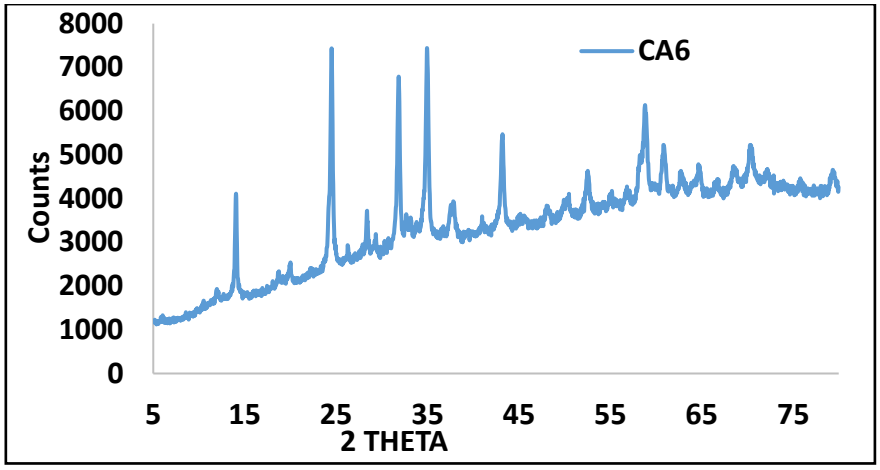

Figure 4.3c: XRD of CA6 (HTAC-6)

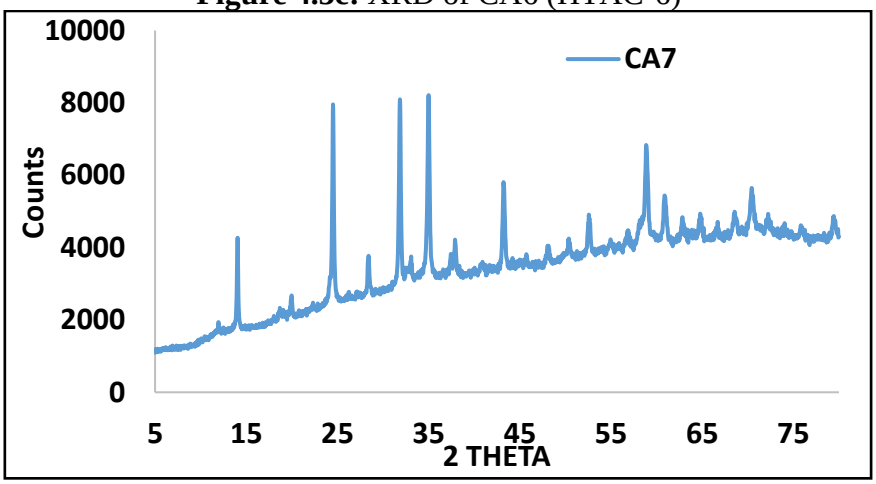

Figure 4.3d: XRD of CA7 (HTAC-7)

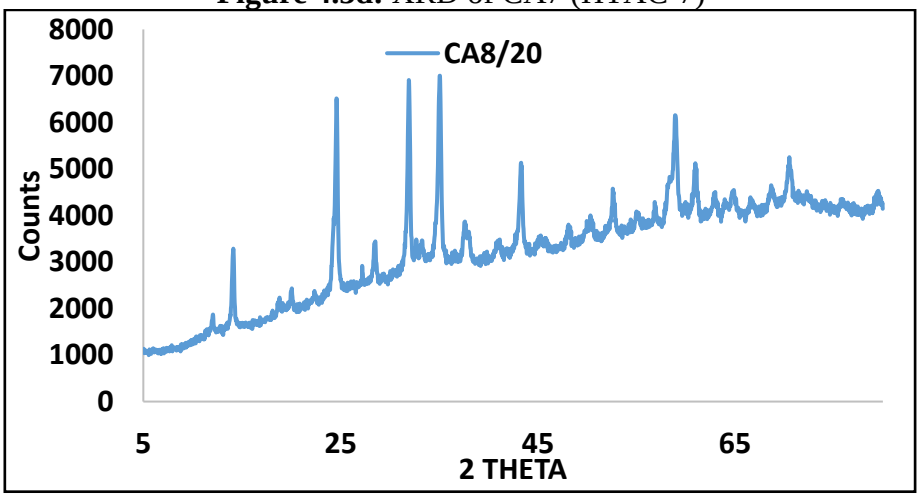

Figure 4.3e: XRD of CA8/20 (HTAC-8/20)

© University of Venda

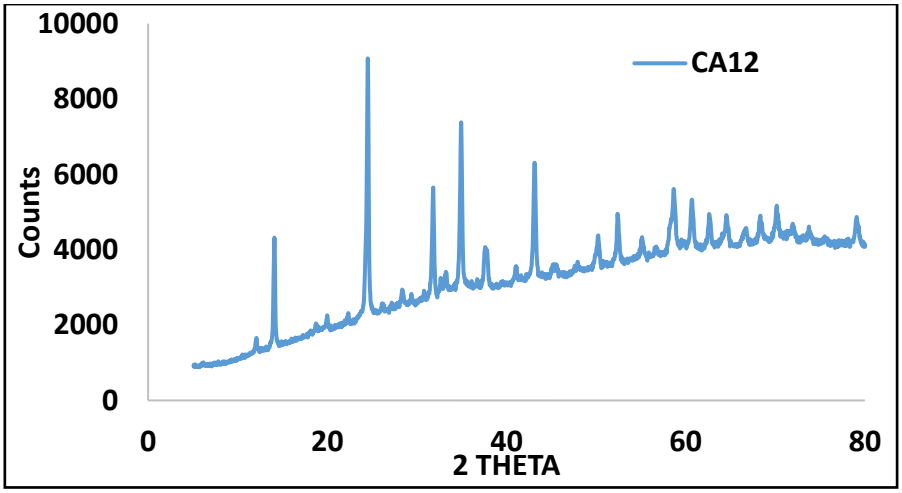

Figure 4.3f: XRD of CA12 (HTAC-12)

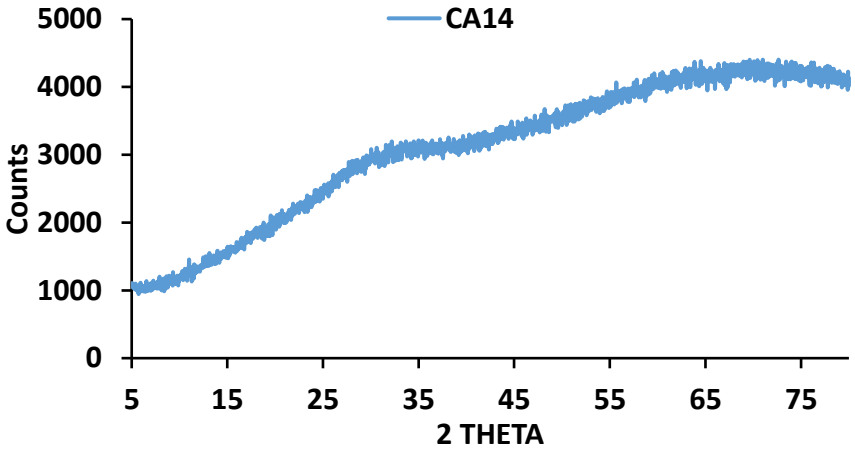

Fig 4.6g: XRD of CA14 (HTAC-14)

Appendix 6.1: X-ray diffraction (XRD) of PACs (PHTACs).

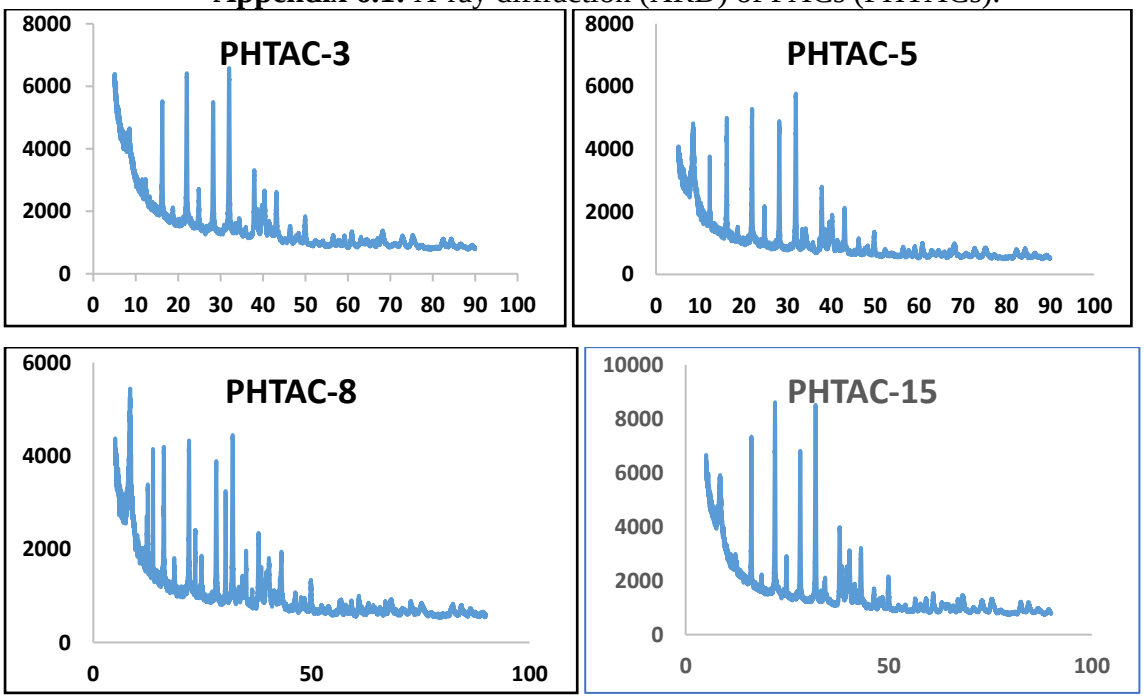

© University of Venda

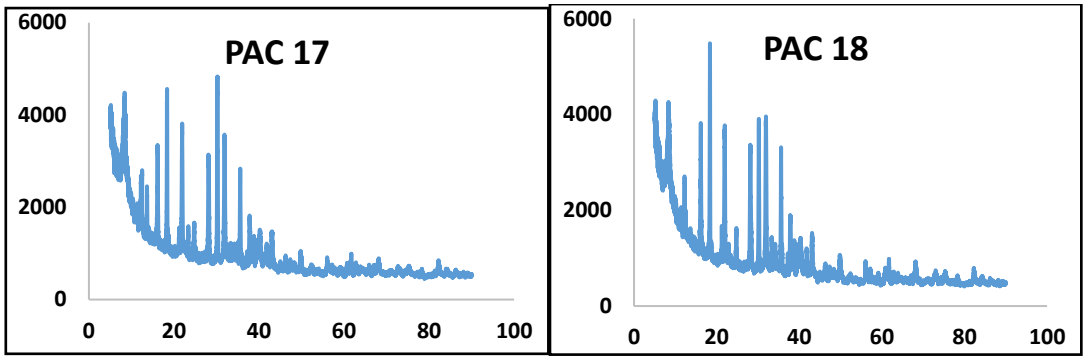

Appendix 6.2: FTIR spectra of MAC, HTAC, Fluoride loaded PHTAC, PHTAC-3, PHTAC-5, PHTAC-8, PHTAC-15, PHTAC-17 and PHTAC-18.

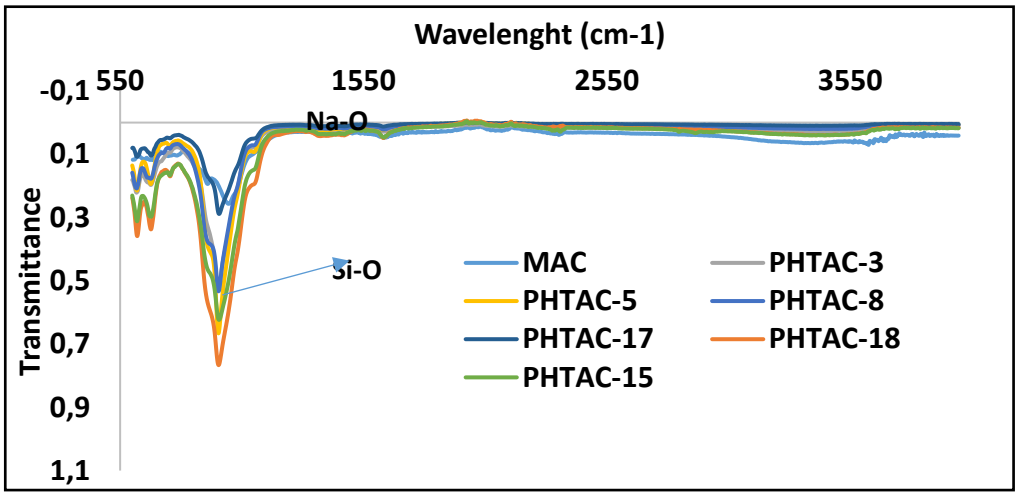

Appendix 6.3: X-ray diffraction (XRD) Spectra of MAC, HTAC, [PHTAC(PAC3, PAC5, PAC8, PAC15, PAC17 and PAC-18)].

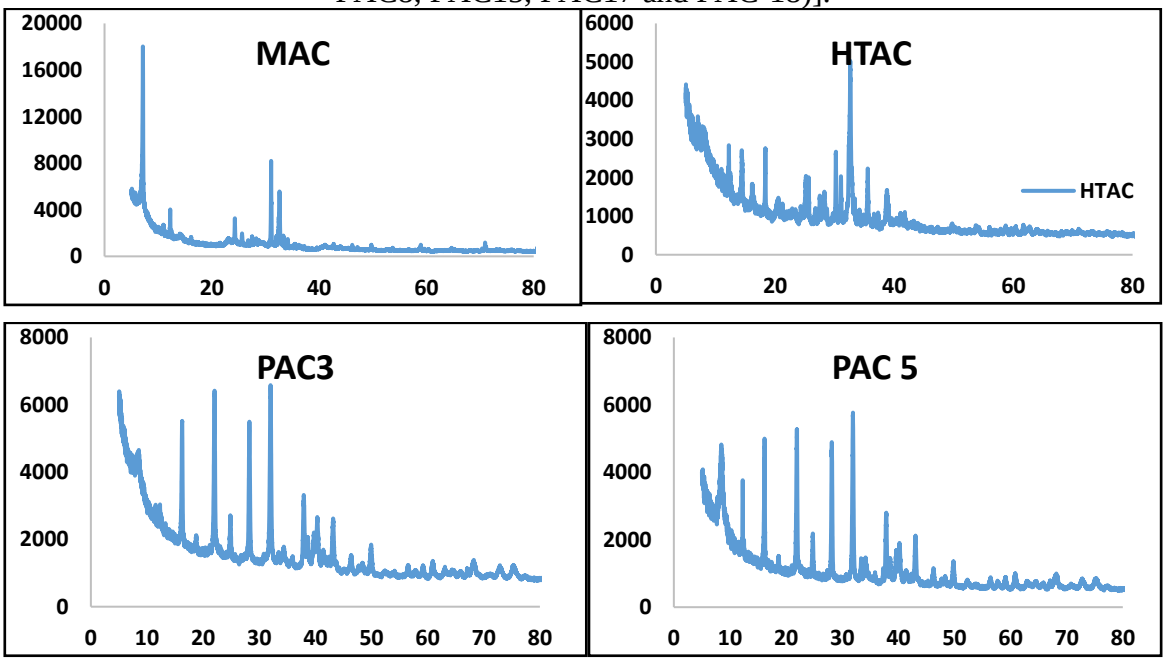

© University of Venda

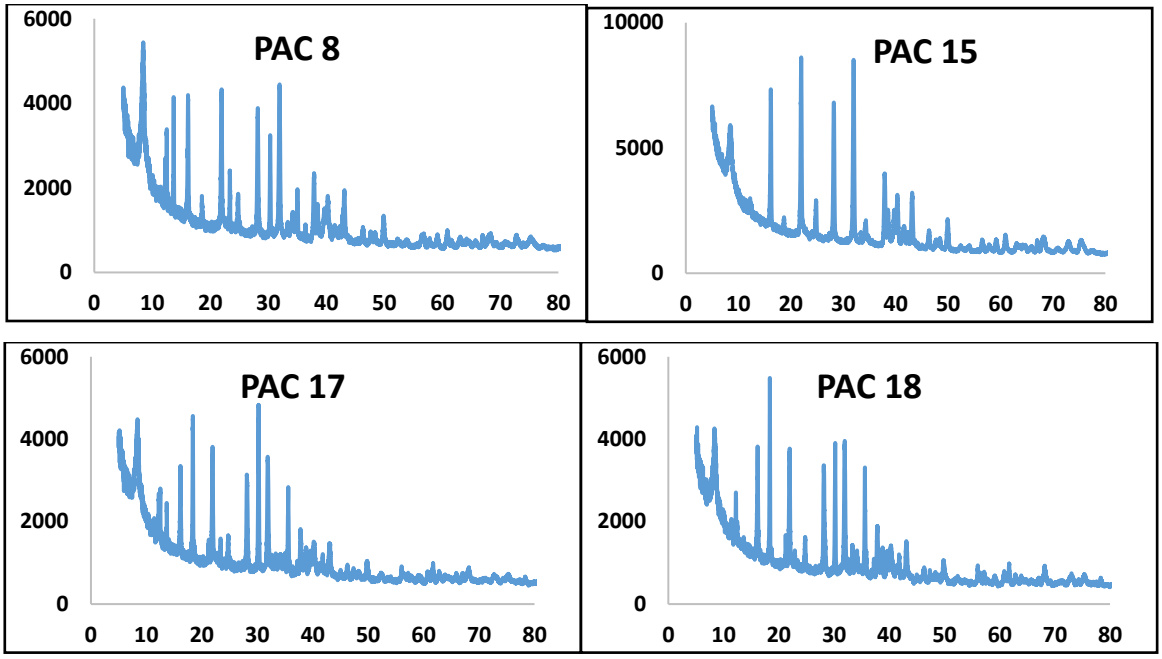

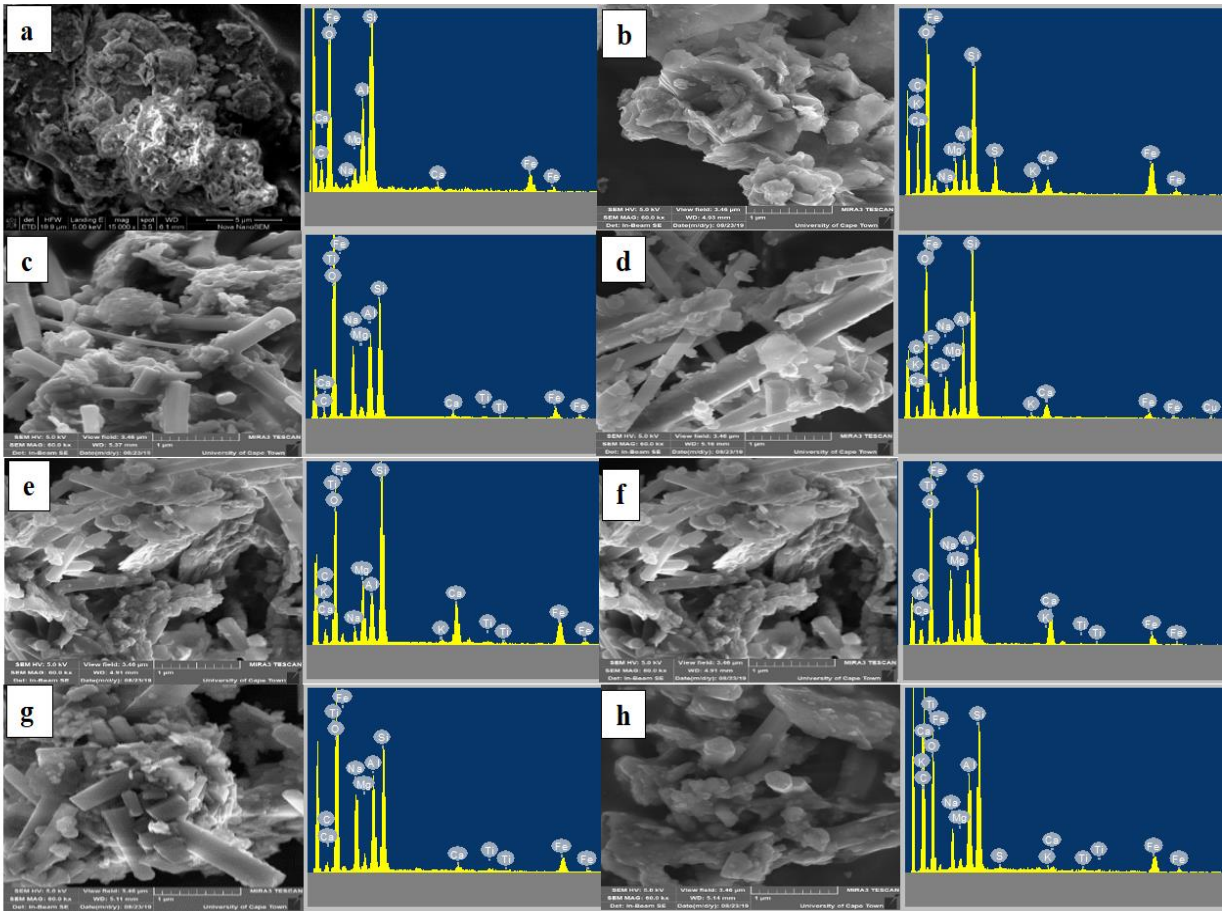

Appendix 6.4: SEM-EDS spectra of (a) MAC (b) HTAC (c) PHTAC-3 (d) PHTAC-5 (e) PHTAC-8 (f) PHTAC-15 (g) PHTAC-17 and (h) PHTAC-18 adsorbent samples.

© University of Venda

Appendix 7.1: X-ray diffraction (XRD) Spectra of (a) Untreated PHTAC alone (b) PHTAC and MAC (c) PHTAC, HTAC and MAC (UNSTACKED PLOTS).

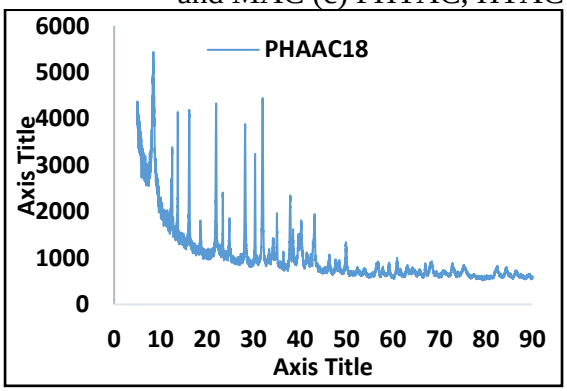

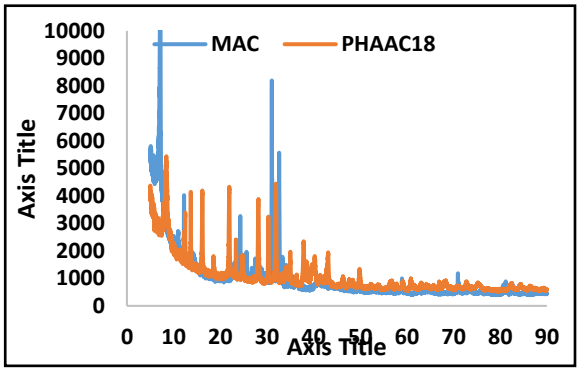

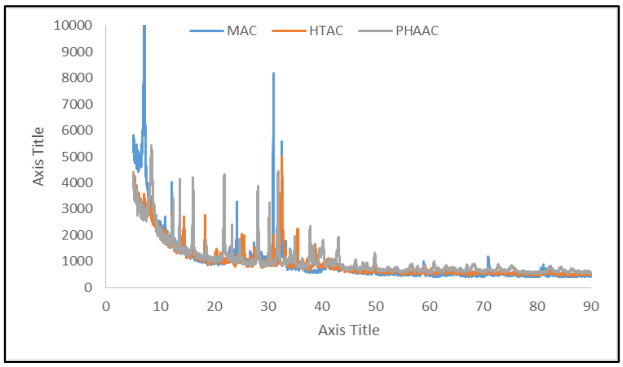

Appendix 7.2: X-ray diffraction (XRD) Spectra of (a) Untreated PHTAC alone (b) PHTAC and MAC (c) PHTAC, HTAC and MAC [STACKED PLOTS].

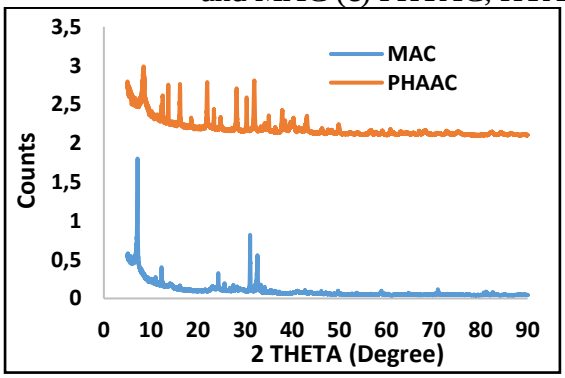

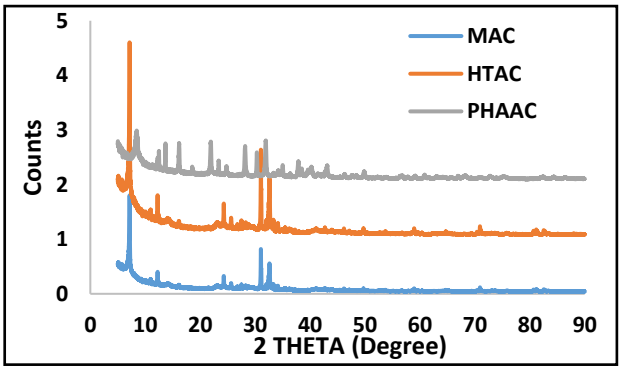

© University of Venda